Diversity in Neutrophil Biology: From Simple Foot Soldiers to Versatile Commanders of Immunity in Infectious Diseases

Inauguraldissertation

zur

Erlangung der Würde eines Doktors der Philosophie

vorgelegt der

Philosophisch-Naturwissenschaftlichen Fakultät

der Universität Basel

von

Pascal Forrer

aus Wildhaus (SG), Schweiz

Basel, 2018

Genehmigt von der Philosophisch-Naturwissenschaftlichen Fakultät

auf Antrag von

Prof. Dr. Dirk Bumann

Prof. Dr. Nina Khanna

Prof. Dr. Urs Jenal

Basel, den 22. Mai 2018

Prof. Dr. Martin Spiess

Dekan

Table of Contents

1 Abbreviations

General

APC	Antigen-presenting cell
APO	Apolipoprotein
BCA	Bicinchoninic acid
BLS	Bare lymphocyte syndrome
CCL	C-C motif ligand
CD	Cluster of differentiation
CFSE	Carboxyfluorescein succinimidyl ester
CGD	Chronic granulomatous disease
CIITA	Class II major histocompatibility complex transactivator
Cl^-	Chloride ion
CLR	C-type lectin receptor
CR	Complement receptor
CREB	cAMP response element-binding protein
CTLA	Cytotoxic T-lymphocyte-associated protein
CXC	C-X-C motif
DCs	Dendritic cells
DNA	Desoxyribonucleic acid
DPI	Diphenyleneiodonium
DPPI	Pipeptidyl peptidase I
ERK	Extracellular-signal regulated kinase
FBS	Fetal bovine serum
F_cR	F_c receptor
fMLP	N-Formylmethionine-leucyl-phenylalanine
GCP	Good clinical practice
GM-CSF	Granulocyte-macrophage colony-stimulating factor
GMP	Granulocyte-monocyte myeloid progenitor
H^+	Hydrogen ion
H_2O_2	Hydrogen peroxide
HLA	Human leukocyte antigen
HOCl	Hypochlorite
IFN-γ	Interferon gamma

IgG	Immunoglobulin G
IL	Interleukin
JAK	Janus kinase
JNK	c-Jun-N-terminal kinase
K^+	Potassium Ion
LB	Luria-Bertani
LC-MS	Liquid chromatography-mass spectrometry
LMPP	Lymphoid-primed multipotent progenitor
LN	Lymph node
LPS	Lipopolysaccharide
LTB4	Leukotriene B4
LysM	Lysozyme M gene
MAIT	Mucosa-associated invariant T cells
MAPK	Mitogen-activated protein kinase
MCP	Monocyte chemotactic protein
MDSC	Myeloid-derived suppressor cells
MEK	Kinase of mitogen-activated protein kinase
MHC	Major histocompatibility complex
MOI	Multiplicity of infection
MPO	Myeloperoxidase
MSK	Mitogen- and stress-activated protein kinase
mTOR	Mechanistic target of rapamycin
NADPH	Nicotinamide adenine dinucleotide phosphate
NETs	Neutrophil extracellular traps
NFY	Nuclear transcription factor Y
NK cells	Natural killer cells
NO	Nitric oxide
O_2	Oxygen
O_2^*	Singlet oxygen
O_2^-	Superoxide
OH^-	Hydroxyl radical
OT	Ovalbumin-specific T cells
OVA	Ovalbumin
PAMP	Pathogen-associated molecular pattern

PBMC	Peripheral blood mononuclear cell
PBS	Phosphate buffered saline
(RT)- PCR	(Reverse transcription)- Polymerase chain reaction
PD1	Programmed cell death 1
PDK	Phosphoinositide-dependent kinase
PEC	Peritoneal exudate cell
PI	Propidium iodide
PI3K	Phosphoinositide 3-kinase
PKA	Protein kinase A
PMA	Phorbol-12-myristate-13-acetate
PMN	Polymorphonuclear neutrophils
PRR	Pattern recognition receptor
qSOFA	quick Sequential organ failure assessment
RFP	Red fluorescent protein
RFX	Regulatory factor X
RFXANK	Regulatory factor X-associated ankyrin-containing protein
RFXAP	Regulatory factor X-associated protein
ROS	Reactive oxygen species
RSK	Ribosomal S6 kinase
SNAP	Synaptosomal-associated proteins
STAT	Signal transducer and activator of transcription
TAN	Tumour-associated neutrophils
TCR	T-cell receptor
TGF	Transforming growth factor
T_H1	T helper subset 1
T_H2	T helper subset 2
TIM-3	T cell molecule with immunoglobulin and mucin domain 3
TLR	Toll-like receptor
TNF-α	Tumour necrosis factor alpha
TRAIL	Tumour necrosis factor-related apoptosis-inducing ligand
T_{Reg} cells	Regulatory T cells
US	United States
VEGF	Vascular endothelial growth factor

Microbes

C. albicans	*Candida albicans*
A. fumigatus	*Aspergillus fumigatus*
E. coli	*Escherichia coli*
S. aureus	*Staphylococcus aureus*
L. monocytogenes	*Listeria monocytogenes*
M. tuberculosis	*Mycobacterium tuberculosis*
A. phagocytophilum	*Anaplasma phagocytophilum*
C. pneumoniae	*Chlamydophila pneumoniae*
S. typhimurium	*Salmonella typhimurium*

Units

CFU	Colony-forming units
h	hour
min	minute
s	second
µ	micro
n	nano

2 Summary

Pathogen clearance in infectious diseases strongly depends on a fine-tuned interplay between innate and adaptive immunity. Undoubtedly, neutrophils as first line defense against invading pathogens play a major role to recognize, phagocytose and kill the invaders. However, the diverse role of neutrophils under inflammatory conditions in infectious diseases has been largely ignored so far.

In my PhD thesis, I addressed the implications of the versatile neutrophil functions in immunity encountering pathogenic microorganisms that cause infectious diseases. In particular, experimental approaches with human neutrophils from healthy individuals and from patients suffering from various infectious diseases and immunological disorders, respectively, were combined with a mouse model of *Salmonella* infection with the help of techniques such as flow cytometry, reverse transcription- polymerase chain reaction (RT-PCR) and proteomics to reveal the so far underestimated diversity in neutrophil function.

We showed that “simple foot soldier” neutrophils are important for host defense against bacterial and fungal pathogens. With the help of the nicotinamide adenine dinucleotide phosphate (NADPH) oxidase and myeloperoxidase (MPO), neutrophils are able to produce large amounts of reactive oxygen species (ROS) that are important for pathogen destruction. We could show that neutrophils from patients receiving allogeneic hematopoietic stem cell transplantations (HSCT) have significantly impaired ROS production against *Candida (C.) albicans* and *Aspergillus (A.) fumigatus*. However, ROS can also cause detrimental damage in host tissues. We showed that MPO, one of the key enzymes in ROS production, has a protective role in the host by scavenging diffusible hydrogen peroxide (H_2O_2) at the *Salmonella* surface and converting it into highly reactive hypochlorite (HOCl) within a short reach. This sophisticated mechanism of MPO- to confine potential harmful molecules to the pathogen microenvironment- leads to both effective pathogen destruction and minimal collateral host tissue damage.

Neutrophils as “versatile commanders” are unambiguously involved in the pathogenesis of sepsis, the dysregulated host response to infection. We could observe that neutrophils and monocytes accumulate neutral lipids during *Salmonella* infection and change their lipid metabolic program in sepsis comparable to atherosclerosis. Moreover, we identified a subset of antigen-presenting cell (APC)-like neutrophils with major histocompatibility complex (MHC) class II molecule expression, which could be induced under inflammatory conditions. The inflammatory environment triggers highly specific signaling pathways in neutrophils that orchestrate intracellular protein phosphorylation cascades, finally leading to the formation of the MHC class II enhanceosome.

We could show that the MHC class II enhanceosome is responsible for the subsequent MHC class II expression on neutrophils and that targeting Janus kinase (JAK) 1/2 could be a promising therapeutic approach in sepsis to reach homeostasis. Overall, these data show that the immunological function of neutrophils in sepsis is highly versatile and goes far beyond simple pathogen destruction. Together, these data show that infectious disease control implies a specialized, but versatile immune system with diverse neutrophil functionality.

3 Introduction

3.1 Neutrophil biology

Neutrophils, also known as polymorphonuclear neutrophils (PMN) or granulocytes, are the most abundant immune cell type in the periphery making up to 70% of total leukocytes. They play a crucial role in the efficient innate immune defense against invading pathogens, but also contribute in the pathogenesis of autoimmunity, chronic inflammation and cancer [1].

To compensate the high turnover rate, neutrophils are produced in large amounts in the bone marrow. Estimated two-thirds of bone marrow space are dedicated to the formation of neutrophils and monocytes in steady-state conditions [2]. During granulopoiesis, neutrophil development starts from a common lymphoid-primed multipotent progenitor (LMPPs) and further differentiates into a granulocyte-monocyte myeloid progenitor cell (GMPs) under the influence of several transcription factors. The transition from GMP state to hyper-segmented, mature neutrophils is characterized by the full equipment of all granule subsets, which is typical for these immune cells [3]. Fully differentiated neutrophils are released from bone marrow into periphery with a relatively short lifespan compared to other immune cells [4,5]. A neutrophil has a diameter of 10-15 µm and a volume of 346 μm^3 with 3-to 5-lobe- segmented nucleus with randomly distributed chromosomes. Mitochondria are rare (1% of cell volume), thus glycolytic metabolism is preferred [Hallet MB, The Neutrophil: Cellular Biochemistry and physiology 1990; Chapter 1: *The significance of stimulus- response coupling in the neutrophil for physiology and pathology*]. Blood-circulating neutrophils are recruited to the site of infection or inflammation upon activation by a process called extravasation. Normally about 3% of total neutrophils *in vivo* are migrating into tissue upon demand and help to resolve the infection by several killing mechanisms [4]. As professional phagocytes, neutrophils ingest and degrade pathogens in the phagolysosome by using oxygen-dependent and oxygen-independent mechanisms. The oxygen-dependent mechanism generates large amounts of reactive oxygen species (ROS), ultimately leading to DNA, protein and lipid damage, whereas the oxygen-independent mechanism is using potent antimicrobial substances, which are stored in the heterogeneous cytoplasmic granules [6]. The oxygen-independent mechanism is referred to as degranulation and can lead to membrane permeabilization and hydrolysis of several biomolecules. However, the precise interplay between oxygen-dependent and oxygen-independent mechanisms in successful pathogen clearance is still unknown [7]. Recently, the dogma that neutrophils are solely simple phagocytes with restricted pro-inflammatory resources is heavily challenged. Neutrophils can contribute to chronic inflammatory conditions and regulate a vast repertoire of adaptive immune responses [5], extending the so far underestimated diversity in neutrophil biology.

3.2 The life and death of a neutrophil

Apoptosis as a special variant of cell death is an important mechanism for maintaining homeostasis of the immune system, especially for high abundant immune cells with a rapid turnover rate and potentially harmful cellular components such as neutrophils [8]. During early stages of inflammation, a prolonged neutrophil survival is desirable to control the infection, but after resolution of infection a dampened response should be triggered to prevent inflammatory disorders and tissue damage. Apoptosis in neutrophils occurs in the absence of activation [9] and is accelerated upon phagocytosis by several pathogens [10], e.g. *Escherichia coli* (*E. coli)*, *Staphylococcus aureus* (*S. aureus)*, *Listeria monocytogenes (L. monocytogenes)*, *Mycobacterium tuberculosis* (*M. tuberculosis)* [11], with exception of *Anaplasma phagocytophilum (A. phagocytophilum)* [12] and *Chlamydophila pneumoniae (C. pneumoniae)* [13] that delay neutrophil apoptosis. Furthermore, pro-inflammatory cytokines such as tumour necrosis factor (TNF)- α, interleukin (IL)-1β, IL-6, granulocyte colony-stimulating factor (G-CSF), granulocyte-macrophage colony-stimulating factor (GM-CSF) and Interferon gamma (IFN-γ) as well as some particular pathogen-associated molecular patterns (PAMPs), e.g. lipopolysaccharide, delay neutrophil apoptosis [14]. During the apoptotic process, neutrophils are impaired in many classical effector functions such as chemotaxis, adhesion, phagocytosis, ROS production, and cytokine secretion [15].

Historically, neutrophils were considered as short-lived cells with a half-life in the circulation of approximately 1.5 and 8 hours in mice and humans, respectively [5,16]. However, recent findings show that the average circulatory lifespan of neutrophils *in vivo* is much longer than previously thought with up to 12.5 hours in mice and unprecedented 5.4 days in humans [17], but these data are still heavily debated [18,19]. Nevertheless, neutrophils become activated under inflammatory conditions and their longevity increases by several fold [20,21]. It is assumed that these long-living, primed neutrophils at the site of inflammation may change their phenotype under the influence of a particular cytokine-rich milieu [14,22] and may adapt novel immune cell functions [5].

3.3 Recruitment to the site of infection

Active recruitment of neutrophils to the site of infection involves active mobilization out of peripheral blood and bone marrow, a process called extravasation. Potent host factors triggering recruitment are C-X-C motif ligand (CXCL) 8, leukotriene B4 (LTB4), CXCL1 and CXCL2 [5]. These chemokines are produced upon inflammation by monocytes, macrophages, mast cells, epithelial cells, fibroblasts and endothelial cells and specifically bind chemokine receptors C-X-C motif receptor (CXCR) 1, LTB4 receptor and CXCR2, respectively, on neutrophil surface. Further, bacteria can also produce molecules that directly attract neutrophils e.g. N-formylated peptides [23]. The neutrophil "rolling process" in blood vessels, one of the first steps in extravasation, is mediated by C-type lectin glycoproteins known as selectins [24]. E- and P-selectins are upregulated on the surface of activated endothelial cells and activated platelets [25]. Not only cytokines, but also other factors such as LTB4, histamine or complement peptide C5a are able to induce selectin expression [26]. E- and P- selectins interact with neutrophil CD162 (P-selectin glycoprotein ligand 1), thus facilitating neutrophil aggregation to endothelial tissue, a process called tethering [27]. Tethering precedes adhesion by leukocyte adhesion molecules such as β1- (very late antigen-4) and β2- integrins (macrophage-1 antigen or lymphocyte function-associated antigen 1) [28]. Transmigration into tissue after tight adhesion is mediated by neutrophil surface molecules CD31 [29], CD54 [30], CD44 [31] and CD47 [32].

3.4 Phagocytosis of microorganisms during infection

At site of infection, neutrophils bind and ingest invading microorganisms, a process called phagocytosis. Neutrophils recognize conserved pathogen-associated molecular patterns (PAMPs) unique to microbial structures via pattern recognition receptors (PRRs). PRRs in neutrophils consist out of the family of toll-like receptors (TLRs), complement receptors (CR), F_c receptors (F_cR) and C-type lectin receptors (CLR). The discovery of the germ-line encoded TLR family as key players in innate immunity brought high scientific attention and Nobel Prize in Medicine to Jules Hoffmann and Bruce Beutler in 2011 [33]. Human neutrophils express a repertoire of 9 different surface bound or soluble TLRs (TLR1, 2, 4-9 [34]), all involved in efficient uptake and engulfment of bacterial and fungal pathogens. Moreover, the efficiency of phagocytosis by neutrophils is drastically improved if microbes are opsonized with human serum proteins, such as complement components C3b, iC3b and Clq as well as antibodies.

Complement components are recognized by CR1 (CD35) [35], CR3 (CD11b/CD18) [36] and CR4 (CD11c/CD18) [37] on neutrophil surface and antibodies can be bound by $F_c\gamma R1$ (CD64, high affinity IgG receptor), $F_c\gamma R2$ (CD32, low affinity IgG receptor), $F_c\gamma R3$ (CD16, high affinity IgG receptor) [38] as well as IgE receptor $F_c\varepsilon R1$ (CD23) [39] and $F_c\alpha R$ (CD89) [40]. Altogether, TLRs, CRs, F_cRs and CLRs contribute to the phagocytic process and subsequent pathogen elimination.

3.5 Production of reactive oxygen species (ROS) as oxidative killing pathway

Followed by phagocytic uptake of microorganisms, neutrophils start to produce ROS, a process known as oxidative burst or respiratory burst. ROS production is induced by an activated membrane-bound nicotinamide adenine dinucleotide phosphate (NADPH)-dependent oxidase, which transfers electrons from cytosolic NADPH to extracellular or intraphagosomal molecular oxygen (O_2), therefore producing short-lived superoxide (O_2^-) [41]. The inactivated NADPH oxidase consists out of cytosolic p40phox, p47phox, p67phox, Rac2 [42-44] and membrane-bound flavocytochrome b_{558} (heterodimer out of gp91phox and p22phox [42,45]). During phagocytic process, the cytosolic components translocate to the phagosomal membrane and associate with flavocytochrome b_{558}, thus forming a functional NADPH oxidase capable in O_2^- generation [42]. O_2^- can dismutate into hydrogen peroxide (H_2O_2) spontaneously [46] or enzymatically by superoxide dismutase [47]. However, the process of H_2O_2 production is indispensable for neutral intraphagosomal pH maintenance [48].

Another key enzyme in neutrophils, the myeloperoxidase (MPO), is released from azurophilic granules and converts almost all O_2^- or H_2O_2 into highly toxic hypohalous acids (OCl^-, OBr^-, OF^- or OI^-). Hypochlorite (HOCl) is the predominant ROS in the neutrophil phagosome if chloride supply is not limited. HOCl is a highly reactive oxidant with potent antimicrobial efficacy [49] and supposed to be the major oxidative weapon in neutrophils. Furthermore, hydroxyl radical (OH^-) and singlet oxygen (O_2*) contribute to microbicidal activity, too [50] (Fig. 1).

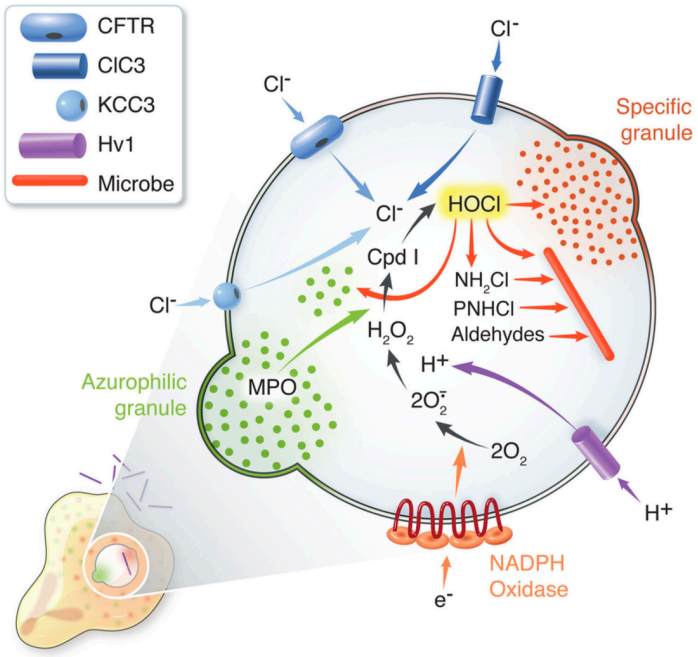

Fig. 1: **MPO-dependent events in human neutrophil phagosome**. Concomitant with phagocytosis, the NADPH oxidase generates high fluxes of ROS (O_2^-) and MPO coverts the intracellular hydrogen peroxide (H_2O_2) into hypochlorite (HOCl), which can directly attack microbial targets. O_2, oxygen; O_2^-, superoxide; Cpd1, compound 1; Cl, chloride; CFTR, cystric fibrosis conductance regulator. After Nauseef, Cell Microbiol. 2014.

The relevance of NADPH oxidase and MPO in host immunity is reflected by the clinical impact of their deficiencies. Patients suffering from NADPH oxidase deficiency develop a severe disease called chronic granulomatous disease (CGD), characterized by mostly X-linked recessive defect in the *cytochrome b (588) subunit beta* gene encoding the gp91-phox subunit of the NADPH oxidase. CGD patients suffer from severe, recurrent bacterial and fungal infections due to defective O_2^- anion generation, resulting in attenuated antimicrobial activity [51,52]. Interestingly, antimicrobial activity in CGD patients can be restored by introducing exogenous H_2O_2 *in vitro* [53]. The incidence of CGD is estimated around 1 in 200'000. On the other hand, MPO deficiency is one of the most frequent inherited phagocytic disorders with a prevalence of 1 in 2000-4000 individuals in US/ Europe [54,55] respectively 1 in 20'000-60'000 individuals in Japan [56]. Early epidemiological studies propose a correlation between MPO deficiency and cancer [57,58] and bacterial/ fungal infections, respectively [59,60]. In strong contrast, other studies could not show any particular susceptibility to cancer or severe infections in MPO deficient patients [61,62]. The reasons for these discrepancies among literature may be due to the clinical manifestation of partial and full MPO deficiency in human individuals, the follow-up and the investigated number of cases. Partial MPO deficient individuals still have residual MPO activity that might be sufficient for a protective antimicrobial immune response [54], whereas only the less prevalent, full MPO deficiency shows a clinical manifestation. This concept is in agreement with the finding that only individuals with full MPO deficiency fail to form neutrophil extracellular traps (NETs) [63] , an important antimicrobial protective response mechanism to large pathogens [64].

Rare *in vitro* studies with human MPO deficient neutrophils are inconsistent. The first case report of a full MPO deficient individual dates back to 1969. His neutrophils *in vitro* have shown impaired killing capacity to *Candida* and *Staphylococci* [65], supported later by others [49,57]. Another report could demonstrate that there have been only minor defects in *S. aureus* killing by MPO deficient neutrophils, whereas *C. albicans* killing was heavily impaired [59]. In summary, MPO deficient neutrophils are still able to kill microbes with reactive oxygen species, although less efficiently [49]. Nevertheless, the clinical consequence of MPO deficiency is not comparable with the phenotype observed in patients with NADPH oxidase deficiency. It can be speculated that MPO-independent microbicidal mechanisms increase their activity to compensate for the lack of MPO [62] or other ROS than HOCl can be produced, namely O_2^- and H_2O_2, and those can lead to antimicrobial killing [66]. It is reported that those two ROS can generate the highly reactive hydroxyl radical (OH^-) via the Fenton reaction, leading to severe DNA damage [67].

Mice deficient in MPO infected with various pathogens show conflicting results. On one hand, MPO deficient mice have been more susceptible to infections with *C. albicans* [49,68,69], *Aspergillus fumigatus (A. fumigatus)* [68], *Pseudomonas aeruginosa* [68] and *Klebsiella pneumoniae* [70] than wildtype. On the other hand, there was no difference observed between MPO deficient and wildtype mice infected with *Candida glabrata*, *S. aureus* and *Streptococcus pneumonia* [49,68].

Taken together, data from individuals lacking MPO and mice with MPO deficiency in infection are inconclusive and the role of ROS and MPO in infection control remains to be elucidated.

3.6 Degranulation as a non-oxidative killing pathway

Upon neutrophil phagocytosis of intracellular microorganisms, cytoplasmic granules are triggered to mobilize and fuse with the phagosomes [71], leading to the formation of the phagolysosome. The cytoplasmic granules are fully packed with a huge repertoire of antimicrobial peptides and proteases. The action of these antimicrobial agents constitutes to the non-oxidative killing pathway of neutrophils [72]. The signalling pathway underlying granule mobilization has not been fully elucidated, but involves calcium-mediated signal transduction, Src family tyrosine kinases Gardner-Rasheed feline sarcoma and HCK, p38 mitogen-activated protein kinases, synaptosomal-associated proteins (SNAPs) as well as SNAP receptors [73-77]. Basically, there are four different granule types in neutrophils: The azurophilic (primary), the specific (secondary), gelatinase (tertiary) and secretory granules [78].

The granule classification is based on their protein content, their temporal biosynthesis during neutrophil differentiation in the bone marrow and their ability of exocytosis after pathogen engulfment [72]. Azurophilic granules are very limited in exocytosis and contribute mainly to intracellular pathogen destruction in the phagolysosome [72]. The fusion of azurophilic granules with the phagosome leads to enrichment of the phagosome lumen with antimicrobial agents (MPO, α-defensins, cathepsins, proteinase-3, elastase and azurocidin [78]). MPO is considered to play a major role in the oxidative killing pathway, as mentioned above in details. α-defensins, a group of cationic polypeptides which interact with negatively charged surfaces [79], comprise up to 50% in azurophilic granules and are able to rupture bacterial membranes [80]. Moreover, α-defensins can modulate innate immune responses inclusive chemotaxis and histamine release [81]. Cathepsins are powerful proteases that exert protein hydrolysis. The cathepsin family consists out of serine proteases (cathepsin A and G), aspartate proteases (cathepsin D and E) and cysteine proteases [82]. Mice deficient in cathepsin G are more susceptible to infection with *S. aureus* [83]. The precise killing mechanism of cathepsin G is unclear, but *E. coli* membrane disruption could be observed *in vivo* [84]. Neutrophil proteinase 3 and elastase share many structural and functional homologies to cathepsin G. Mice deficient in elastase are more susceptible to infection with gram-negative pathogens such as *E. coli*, *Klebsiella pneumoniae* and several enterobacteria species [85,86]. It has been shown that neutrophil elastase directly cleaves microbial virulence factors in *Salmonella enterica* serovar Typhimurium, *Shigella flexneri* and *Yersinia enterocolitica* [86]. The lack of neutrophil elastase leads to phagosomal escape of bacteria, ultimately leading to prolonged survival in infected neutrophils [86].

Interestingly, patients suffering from Papillon-Lefèvre syndrome (Loss- of- function mutation in the gene encoding dipeptidyl peptidase I, DPPI) [87] have an almost total loss of functional cathepsin G and neutrophil elastase, but still show normal neutrophil microbicidal activity against *S. aureus* and *E. coli* [88]. These results highlight that efficient microbial killing does not fully rely on cathepsin G and neutrophil elastase.

Specific granules, containing flavocytochrome b_{558} [89], lactoferrin [90], cathelicidin and lysozyme [72] contribute substantially to the potent microbicidal effect observed in neutrophils. Beside direct bacterial membrane permeabilization, lactoferrin sequesters iron originated from microorganisms, thus limiting bacterial growth [91]. Lysozyme hydrolyses peptidoglycan, a major component of bacterial cell wall, especially in gram-positive bacteria [92]. In conclusion, the importance of non-oxidative killing mechanisms for infection control is not fully understood. So far, the only clinically relevant disease associated with mutations in the non-oxidative killing pathway, the Papillon-Lefèvre syndrome, is not associated with higher burden of infectious complications. Thus, the interplay between oxidative and non-oxidative killing mechanisms should be highlighted in more details.

3.7 The interlink between oxidative and non-oxidative killing pathways

Traditionally, the oxidative killing pathway by generating large quantities of ROS is thought to be responsible for the direct killing of microorganisms [72]. This view is highly supported by the fact that CGD patients (lack of NADPH oxidase) succumb to severe systemic bacterial and fungal infections. However, this view is heavily challenged by Reeves *et al.* They have demonstrated that ROS may have limited capacity for direct microbicidal activity, opposite to the hitherto accepted view. More likely, non-oxidative killing by proteases shall be primarily responsible for pathogen destruction [83,93]. According to their proposed model, the NADPH oxidase consumes O_2 and generates O_2^- anions. To compensate the negative charge accumulation in the phagolysosome, cations are pumped into the phagosome across membrane (K^+, H^+). As a consequence of the K^+ influx into the phagolysosome, serine proteases are activated, released from the sulphated proteoglycan matrix in the azurophilic granule and distributed among the lumen of the phagolysosome, thus leading to effective microbial destruction. Moreover, protonation of O_2^- anions in the phagosome generates H_2O_2. Accumulated H_2O_2 is used by MPO to produce the highly toxic HOCl. At the same time, solely by the catalytic oxidative activity of MPO, serine proteases are protected from collateral MPO-mediated inactivation and execute their deadly killing activity. In agreement with this concept, an early study by Vissers *et al*. has shown that neutrophil elastase activity is dependent on MPO-mediated H_2O_2/ Cl^- chlorinating system [94]. In contrast, another study could show that MPO is a direct oxidative inactivator of neutrophil elastase [70]. Despite this effort to synergize oxidative and non-oxidative killing mechanisms, there are still many open questions in terms of the precise interplay between oxidative and non-oxidative killing mechanisms in neutrophils. However, a recent mechanism called neutrophil extracellular trap formation (NETosis) tries to answer some of those questions.

3.8 NETosis

NETosis as a novel neutrophil killing mechanism has been described for the first time in 2004 by Brinkmann *et al* [95]. NETs are extracellular, web-like structures composed of nuclear and granular protein material with decondensed DNA or mitochondria-derived chromatin [95,96]. NETs have the capacity to entrap and kill bacteria [95], fungi [97], viruses [98], parasites [99] and prevent pathogen dissemination [64]. Moreover, NETosis occurs after pro-inflammatory cytokine (IL-8, TNF-α) priming [100].

The precise NET protein composition strongly depends on the stimulus [101]. Initial studies have revealed 24 proteins in NETs upon activation with phorbol-12-myristate-13-acetate (PMA), including histones, neutrophil elastase, MPO, calprotectin, cathelicidins, defensins and actin [102]. Studies with *Pseudomonas aeruginosa* mucoid and non-mucoid strains could induce NETosis with a composition of 33-50 different proteins, dependent on bacterial strain [103]. The difference between NETosis and other forms of cell death is the characteristic loss of intracellular membranes. Later, the integrity of the plasma membrane is compromised, too [104].

Interestingly, NETosis links intracellular oxidative and non-oxidative killing mechanisms to a novel, extracellular killing mechanism. In brief, ROS are generated by the NADPH oxidase and MPO. MPO activity leads to activation and nuclear translocation of neutrophil elastase, where it starts to proteolytically process histones and induces chromatin decondensation [105]. Neutrophils from patients with CGD and diphenyleneiodonium (DPI)-treated neutrophils from healthy individuals have shown a complete loss of NETosis in response to PMA and *S. aureus*, and exogenously added H_2O_2 could restore NETosis [104]. In addition, NADPH oxidase-deficient mice have shown abrogated NETosis during pulmonary *Aspergillosis* infection [106]. Both studies highlight the important role of NADPH oxidase-generated ROS fluxes in triggering NETosis.

Patients suffering from full MPO deficiency fail to form NETs, in contrast to patients with partial MPO deficiency, who are still able to form NETs [63]. In agreement with this finding, the pharmacological inhibition of the enzymatic activity of MPO cannot block but only delay NETosis [63]. In summary, partially MPO deficient neutrophils or incompletely abrogated MPO activity in neutrophils are still able to induce NETosis.

Mice defective in neutrophil elastase fail to form NETs in a Sendai virus infection [107] and a pulmonary *Klebsiella pneumonia* infection model [105]. Similarly, neutrophils from patients with Papillon-Lefèvre syndrome with inactive neutrophil elastase are defective in NETosis [108,109].

Mechanistically, a fraction of MPO and neutrophil elastase are bound in a complex called the azurosome, which spans granule membrane in resting neutrophil state [110]. Upon

neutrophil activation, MPO orchestrates neutrophil elastase release from azurophilic granules independent from its enzymatic activity, thereby promoting neutrophil elastase-mediated actin cytoskeleton degradation in the cytosol and chromatin decondensation in the nucleus, ultimately committing neutrophils to NETosis [101,105]. NETosis must be tightly regulated and pathogen size is one of the key factors that influence NETosis. Pathogen sensing depends on the limited access to neutrophil elastase via NETosis or phagocytosis. Small pathogens are taken up into the phagosome, fuse with azurophilic granules and use neutrophil elastase directly for antimicrobial destruction, thereby hindering neutrophil elastase from nuclear translocation and chromatin decondensation. Large pathogens (such as fungal hyphae or bacterial biofilm aggregates) cannot enter the phagosome, thus neutrophil elastase is freely available from azurophilic granules to induce NETosis [64]. Opposite to this "neutrophil elastase availability model", several other studies have revealed that the phagocytic process after NET formation in response to pathogens is not affected. Even after loss of DNA, anuclear neutrophils are still able to chase and phagocytose bacteria [111,112].

In summary, NETosis is a potent antimicrobial mechanism, especially during infections with large pathogens, and combines both oxidative and non-oxidative killing mechanisms.

3.9 The expanding repertoire of neutrophil-derived cytokines as immunomodulatory agents

Phagocytosis in neutrophils does not only trigger killing mechanisms, but also induces transcriptional activity of a huge repertoire of immunomodulatory agents including Interleukin (IL)-1α, IL-1β, IL-1ε, IL-6, IL-8, IL-10, IL-12β, IL-15, IL-18, C-C motif ligand (CCL)-2 (also macrophage inflammatory protein-1alpha), CCL3 (also macrophage inflammatory protein-1beta), CXCL1 (growth regulated oncogene-alpha), CXCL2 (macrophage inflammatory protein-2alpha), CXCL3 (macrophage inflammatory protein-2beta), CXCL12 (stromal cell-derived factor 1), CCL20 (macrophage inflammatory protein-3alpha), tumour necrosis factor (TNF)-α and vascular endothelial growth factor (VEGF) [1,113,114]. In a positive feedback manner, this cytokine response modulates additional PMNs and attracts macrophages, dendritic cells (DCs) and lymphocytes to site of infection. The secretion of cytokines is one particular way how neutrophils can modulate innate and adaptive immune responses.

3.10 Neutrophil crosstalk with the innate immune system

The first evidence that neutrophils play a regulatory role for DCs during microbial infection is dated back to 2003. Bennouna *et al.* could demonstrate that the supernatant from mouse

neutrophil cultures stimulated with *Toxoplasma gondii* induces the maturation of bone-marrow-derived DCs *in vitro*, upregulates CD40 and CD86 and triggers the production of IL-12 and TNF in DCs [115]. In line with this finding, splenic DCs from neutrophil depleted mice infected with *Toxoplasma gondii* show impaired IL-12 and TNF production [116]. Studies with human neutrophils *in vitro* could show that they can induce maturation of monocyte-derived DCs through TNF- α release [117] in a contact-dependent interaction involving CD18/ CEACAM1 and DC-SIGN [118]. The neutrophil-DC interaction could be visualized at inflammatory sites in Crohn's disease patients, where neutrophils frequently interact with DCs in the colonic mucosa [117]. These findings show that neutrophils can modulate T-cell responses indirectly through DC activation and provide a cellular link between innate and adaptive immunity. In contrary, neutrophils also bear the potential of suppressive features on DCs, as shown by Maffia *et al*. They could demonstrate that neutrophil elastase decrease the allostimulatory ability of human monocyte-derived DCs by switching immature DCs into transforming growth factor (TGF-β)-secreting cells [119]. Overall, there is accumulating evidence that neutrophils are capable to recruit and activate or inhibit DCs *in vitro* and *in vivo* [1,120].

Neutrophils can also modulate natural killer (NK) cell survival, proliferation, cytotoxic activity and IFN-γ production by ROS production and granule protein secretion [121]. Reciprocally, co-culture experiments with human neutrophils and NK cells *ex vivo* [21] or NK-cell derived soluble factors (such as GM-CSF and IFN-γ) [20] promote neutrophil survival, expression of activation marker (CD11b, CD64, CD69), elevated ROS production and cytokine synthesis (e.g. heparin-binding EGF-like growth factor) [20,21,121].

The molecular mechanism of prolonged neutrophil survival upon GM-CSF stimulation has been elucidated by several studies and involves Survivin, Bax, Bad and Mcl-1. Survivin is highly expressed in immature neutrophils, whereas strongly decreased in mature neutrophils [122]. GM-CSF promotes mature neutrophils to re-express survivin to a higher extent, thus enhance inflammation and inhibit cell death [122]. Another study has shown that GM-CSF reduces the expression of Bax, an important member of the bcl-2 family of pro-apoptotic proteins [123, 124]. Further, GM-CSF delays apoptosis via pro-apoptotic Bad phosphorylation at serine residue 99 [125]. Bad molecule is a paradigm showing activity upon dephosphorylation [126]. Furthermore, GM-CSF supports Mcl-1 expression in neutrophils and high expression of Mcl-1 protein is correlated with prolonged neutrophil survival [127].

The molecular role of IFN-γ on neutrophil survival has not been fully elaborated yet. One study has shown that IFN-γ synthesize and store tumour necrosis factor-related apoptosis-inducing ligand (TRAIL) in neutrophils [128]. TRAIL is able to interact with death receptors TRAIL1 and TRAIL2, both somehow linked in elimination of senescent neutrophils [129].

3.11 Neutrophil crosstalk with the adaptive immune system (T cells)

Neutrophil interaction with T cells can result in T-cell suppression or T-cell activation, strongly dependent on the experimental conditions. Human co-culture experiments *in vitro* with neutrophils and T lymphocytes under non-inflammatory conditions reveal that neutrophils suppress $CD4^+$ T-cell activation, proliferation and viability by the granule proteins arginase and calprotectin, but not MPO [130]. Arginase release depletes extracellular L-arginine, an essential amino acid for T-cell activation, in the T-cell environment and downregulates CD3-zeta expression [131,132]. Moreover, co-culturing neutrophils and T cells differentiates T-cell populations into a high fraction of IFN-γ and IL-17 producing T cells and decreases the percentage of IL-10 producing $CD4^+$ T cells [130], highlighting a potential modulatory role of neutrophils in T-cell subset differentiation. Moreover, activated neutrophils produce ROS such as H_2O_2 that potently inhibit T-cell activation [133] and release anti-inflammatory cytokines such as IL-10 and TGF-β that have been shown to exert inhibitory activity on T cells [1].

On the other hand, human neutrophils cultured with LPS and IFN-γ can recruit T helper subset 17 (T_H17) cells via release of chemokines (CCL2, CXCL9, CXCL10, CCL20) *in vitro* [134]. Vice versa, regulatory T (T_{Reg}) cells can attract neutrophils by releasing IL-8, a potent neutrophil chemoattractant [135]. Additionally, $CD4^+$, $CD8^+$ T cells and T_H17 cells produce pro-inflammatory cytokines such as GM-CSF, IFN-γ and TNF that modulate neutrophil survival and expression of activation markers *in vitro* [136], similarly like co-culture experiments with human neutrophils and NK cells *ex vivo* [20,21] (Fig. 2).

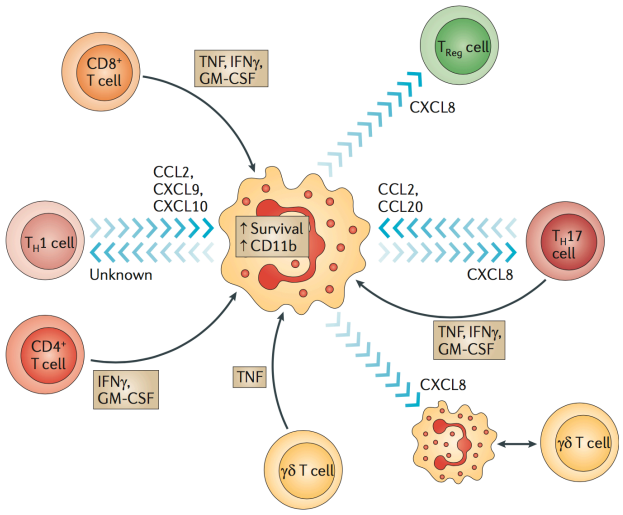

Fig. 2: **Interplay between neutrophils and T cells**. Activated neutrophils release several chemokines and cytokines that mediate the recruitment of adaptive immune responses such as T helper 1 (T_H1) cells, T_H17 cells, $CD8^+$ T cells, $CD4^+$ T cells, γδ T cells, regulatory T cells (T_{Reg}). CCL, CC-chemokine ligand; CXCL, CXC-chemokine ligand; TNF, tumour necrosis factor; IFN, interferon; GM-CSF, granulocyte-macrophage colony-stimulating factor. After Mantovani *et al.*, Nature Reviews Immunology 2011.

Recent evidence exists that neutrophils can migrate to lymph nodes following antigen capture at the periphery, as shown for *Mycobacterium bovis* Bacillus Calmette-Guerin vaccination [137], intracellular *Toxoplasma gondii* infection [138] and intradermal injection of modified vaccinia Ankara virus [139] and transport antigens to the site of T-cell activation. Similar to DC migration, the CC-chemokine receptor 7 plays an important role for neutrophil migration to the lymph nodes (LN) [140]. Those LN- residing neutrophils are able to suppress B-cell- and $CD4^+$ T-cell responses, but not the $CD8^+$ T-cell response [141]. Moreover, *ex vivo* injected antigen-pulsed neutrophils are shown to cross-prime naïve $CD8^+$ T cells, strongly supporting a neutrophils-lymphocyte interaction in draining LN [140]. The neutrophil-mediated immunosuppression is independent from ROS production, nitric oxide (NO) release or IL-10 production [141]. In contrary, a study from Hampton *et al*. could show in a mouse model of local *S. aureus* skin infection that neutrophil re-localize to draining LN only when bacteria are present in the primary lesion. A process that is dependent on CD11b and CXCR4, but not CCR7. Moreover, LN- residing neutrophils augment B-cell-, $CD4^+$- and $CD8^+$ T-cell proliferation [142]. Conclusively, neutrophils can interact with several different immune cell types in various niches in the body to modulate a huge repertoire of adaptive immune cell functions.

3.11.1 Antigen presenting cells regulate adaptive T-cell immunity

Professional antigen presenting cells (APCs) such as DCs, B cells and macrophages are pivotal for the induction of adaptive immune responses. Phenotypically, professional APCs constitutively express major histocompatibility complex (MHC) class II molecules and co-stimulatory molecules such as CD80 and CD86. Functionally, professional APCs process and present antigens to $CD4^+$ T cells thus triggering the adaptive immune system to respond to antigens in the periphery. Defects in this fine-tuned system have tremendous consequences. Patients suffering from MHC class II deficiency- also known as Bare lymphocyte syndrome (BLS) - suffer from severe and recurrent bacterial, viral, fungal and protozoan infections, leading to chronic diarrhea, malabsorption, growth retardation and death in early childhood [143]- only due to the inability of $CD4^+$ T cells to respond to antigens in the periphery.

In recent years, the dogma that professional APCs are essential to induce adaptive immune responses has been challenged by the fact that- under certain conditions- atypical APCs can replace professional APCs ([144,145], reviewed in [146]). Atypical APCs are hematopoietic cell types (mast cells, basophils, eosinophils, innate lymphoid cells) with inducible MHC class II molecule expression and antigen presenting functions, which are often limited to specific immune environments. It is controversially discussed whether they can activate naïve $CD4^+$ T cells in an antigen-specific manner.

Whether neutrophils contribute as atypical APCs in infections is heavily debated [146] and the development and function of these atypical APC-like neutrophils in inflammation and infection have still to be elucidated.

3.11.2 APC-like neutrophils in the human setting

The first report describing *de novo* MHC class II molecule expression on human neutrophils after *in vitro* stimulation with IFN-γ has appeared in 1987 [147]. Furthermore, Gosselin *et al.* could demonstrate *de novo* MHC class II induction on mRNA and protein level after stimulation with GM-CSF [148]. GM-CSF and IFN-γ stimulated human neutrophils activate superantigen-dependent T cell responses, but are not able to re-activate toxoid-specific T cells [149]. Opposite to this report, Iking-Konert *et al.* could demonstrate that MHC class II positive neutrophils express *de novo* co-stimulatory molecules such as CD86 and are able to induce proliferation of a tetanus-specific T-cell line *in vitro* [150]. These *in vitro* findings are further supported by rare clinical trial reports where IFN-γ [151] and GM-CSF [152] administration has similarly led to *de novo* MHC class II induction in human neutrophils, highlighting the *in vivo* relevance of this phenotype.

Moreover, two studies with rheumatoid arthritis patients have reported the presence of MHC class II$^+$ and CD86$^+$ neutrophils in synovial fluid, but not peripheral blood [153,154], whereas another study could show MHC class II positive and CD86$^+$ neutrophils in synovial fluid as well as peripheral blood [155]. These discrepancies can be partially explained by methodological variations. However, these findings support the idea that the local microenvironment (tissue, cell types, cytokines) shapes neutrophil phenotype.

A recent report of APC-like phenotype in human neutrophils illustrates the crosstalk between neutrophils and mucosa-associated invariant T (MAIT) cells or γδ T cells and translates their findings to patients with severe sepsis. The authors speculate about plausible cytokine influence to shape APC-like phenotype in sepsis [156]. However, it is unclear from that study whether neutrophils with APC-like phenotype can be found in peripheral blood during acute infection. Another study by Singhal *et al*. could identify a local subset of tumour-associated neutrophils (TANs) in stage I/II human lung cancer that shows granulocytes with APC-like phenotype. This particular TAN subset can cross-present tumour antigens and induces a functional anti-tumour T-cell response. Moreover, the development of these APC-like TANs from long-lived, immature bone marrow derived neutrophils requires tumour-derived factors GM-CSF and IFN-γ [157]. However, a local synapse between APC-like neutrophils and T cells has not been shown by any group so far.

To summarize, some cytokines show the potential to induce *de novo* MHC class II expression on neutrophils. It is unclear, which cytokine or cytokine combination is responsible to shape this APC-like phenotype. Moreover, the local relevance of APC-like neutrophils *in vivo* in respect to T-cell activation or T-cell suppression is still unknown. In general, the function of APC-like neutrophils in the development and manifestation of infectious and inflammatory diseases such as sepsis or rheumatoid arthritis remains undetermined. Furthermore, the understanding of cellular signalling pathways leading to APC-like phenotype and possible therapeutic approaches to interfere within this system are completely unknown.

3.11.3 APC-like neutrophils in experimental animal models

Compared to human research, there is limited knowledge available from mouse studies. Early studies could describe MHC class II expression (H-2 and I-A antigens) on peritoneal exudate (PEC)- derived neutrophils [158]. One year later, the same authors describe exogenous antigen presentation capacity of those neutrophils to antigen-primed T cells [159], a finding to be supported and extended by Fitzgerald *et al.*, who could show that PEC-derived neutrophils present ovalbumin (OVA) to OVA-specific, naïve CD4$^+$ T cells isolated from ovalbumin-specific (OT-II) T-cell receptor (TCR) transgenic mice [160].

In contrast, Abi Abdallah *et al.* could demonstrate that freshly purified PEC-derived neutrophils do not express MHC class II and CD86, but after co-culturing for 2 hours with naïve $CD4^+$ T cells, neutrophils start to express *de novo* MHC class II, CD86 and slightly CD80. Furthermore, neutrophils need a direct T-cell contact to induce APC-like phenotype [161].

However, all *ex vivo* systems are prone to artefacts and do not consider the local environment. In a mouse model of inflammatory bowel disease (chronic colitis), the authors could demonstrate APC-like phenotype in neutrophils in the colon (but not in peripheral blood, spleen or mesenteric lymph nodes). Moreover, colonic APC-like neutrophils could induce OVA-specific $CD4^+$ T-cell proliferation *ex vivo* [162]. In a mouse model of local *S. aureus* infection, it could be demonstrated that APC-like neutrophils are only induced in draining LN, but not in blood, spleen, non-draining LN or ear. Those LN-derived neutrophils induce $CD4^+$ T-cell proliferation *in vivo* [142]. However, the authors have used a potent depletion antibody to $Ly6G^+$ to measure $CD4^+$ T-cell proliferation *in vivo*, which eradicates all neutrophils instead of targeting selectively MHC class II^+ neutrophils. Very recently, another study demonstrates that neutrophils sorted from vaccine-draining LN from rhesus macaques show expression of human leukocyte antigen- antigen D related (HLA-DR). Elevated HLA-DR expression requires the co-cultivation with autologous $CD4^+$ T cells for 30 hours *ex vivo*. Moreover, those APC-like neutrophils are able to present the vaccine antigen to autologous antigen-specific memory $CD4^+$ T cell *ex vivo* [163].

All reports highlight the role of local inflammation as driving force to shape APC-like phenotype in neutrophils. However, basic questions remain unanswered such as the role of cytokines to induce APC-like phenotype *in vivo*, cellular signalling pathways leading to APC-like induction and ultimately the functional and immunological consequences of the particular APC-like neutrophil subset, not total neutrophils, during the course of infection.

3.12 The role of neutrophils in the pathology of sepsis

3.12.1 Sepsis

Sepsis is a heterogeneous host inflammatory response to severe, life-threatening infection with the manifestation of organ dysfunction [164]. Sepsis imposes a detrimental global disease associated with high mortality and morbidity, especially in the elderly population [165]. Recently, the World Health Organization has recognized sepsis as a global health priority and implemented strategies to reduce this fatal disease [166]. The global incidence of sepsis is estimated up to 50 million annually [167] with estimated deaths up to 5.3 million [168]. Current medical treatment options are vastly limited and there is a high unmet medical need for new therapies [169].

3.12.2 Pathophysiology and immune cell dysregulation

Despite huge progress in the basic understanding of the pathophysiology of sepsis, the imbalances in the host immune system leading to sepsis are incompletely understood [170,171]. Host immunity in sepsis is disturbed in a paradox way, involving excessive inflammation, immune suppression and an overall failure to return to normal homeostasis [168]. Moreover, metabolic reprogramming in immune cells is an emerging concept in sepsis, too [172].

Currently, there are two proposed controversial models of the host response in sepsis: the traditional model and the competing model. The traditional model describes the onset of sepsis with an acute hyperinflammatory phase over several days with systemic release of cytokines ("cytokine storm") [173] followed by a late immunosuppressive phase ("immunoparalysis") with persistent severe lymphopenia ("T-cell exhaustion") [169,171,174,175]. Innate immune cells, namely monocytes and neutrophils, trigger the hyperinflammatory phase by releasing high levels of proinflammatory cytokines (TNF, IL-1a, IL-6, IL-12, IL-18, IL-1β). Adaptive immune cells, namely the subset of innate activator B cells, produce IL-3, that further increases inflammation in a mouse model of sepsis [176]. Moreover, IL-3 levels in human sepsis patients correlate with increased mortality [176]. Taken together, this "cytokine storm" will lead to uncontrolled inflammation, fever, refractory shock, acidosis and hypercatabolism or even death [177]. If the disease persists, patients will undergo the immunosuppressive phase ("immunoparalysis") [172,178]. Deaths during the immunosuppressive phase can occur due to the failure to clear the primary infection or an enhanced susceptibility to secondary infections [165]. This traditional model is supported by the findings that a decreased proinflammatory cytokine profile could be found in peripheral blood mononuclear cells and whole blood in the late phase of sepsis [179,180]. Moreover, deaths in sepsis patients (post-mortem studies) in the late phase of sepsis are often accompanied by opportunistic infections, highlighting the broad defects in host immunity [181,182] associated with T-cell depletion and T-cell exhaustion [175]. Interestingly, post mortem analysis of $CD4^+$ T cells from sepsis patients reveal increased expression of programmed cell death 1 (PD1), while local macrophages and endothelial cells show increased expression of PD1 ligand 1. The inhibition of PD1-PD1 ligand 1 interaction in a septic mouse model results in improved survival [175], highlighting the PD1-PD1 ligand 1 interaction as a potential novel target for therapeutic approaches in sepsis.

Immunoparalysis in sepsis is not only caused by T-cell exhaustion, but also DCs and macrophages. Both, DCs and blood derived monocytes show reduced HLA-DR expression in the late phase of sepsis [183,184], leading to insufficient adaptive immune response activation. Moreover, DCs produce elevated levels of anti-inflammatory IL-10 during sepsis, whereas monocytes show impaired capacity to produce pro-inflammatory cytokines (TNF,

IL-1a, IL-6, IL-12) upon stimulation in the late phase of sepsis [185]. Moreover, enhanced anti-inflammatory cytokine secretion (IL-1RA, IL-10) in response to endotoxin is reported in monocytes, too [186]. The exact mechanisms leading to immunoparalysis are not fully understood, but a recent report highlights broad defects in the energy metabolism of monocytes [172]. Interestingly, IFN-γ therapy shows some partial restoration of immunometabolism and might be a potent therapeutic intervention in sepsis [172,187]. Altogether, cytokine imbalances towards an anti-inflammatory state or pro-inflammatory state and reduced HLA-DR expression are worsening patient's prognosis during sepsis. Of note, the failure of many clinical trials with anti-inflammatory agents to treat patients with sepsis strongly supports the concept of immunoparalysis as an important pathophysiological characteristic in sepsis [188]. However, the competing model agrees with the acute phase (hyperinflammatory phase), but the advocates postulate that an unremitting innate immune system inflammation persists and is ultimately responsible for organ injury and patient's death during the late phase of sepsis. This theory is supported by the fact that patients who have died from sepsis show longer duration and greater degree of organ injury, caused by innate immunity [189] (Fig. 3).

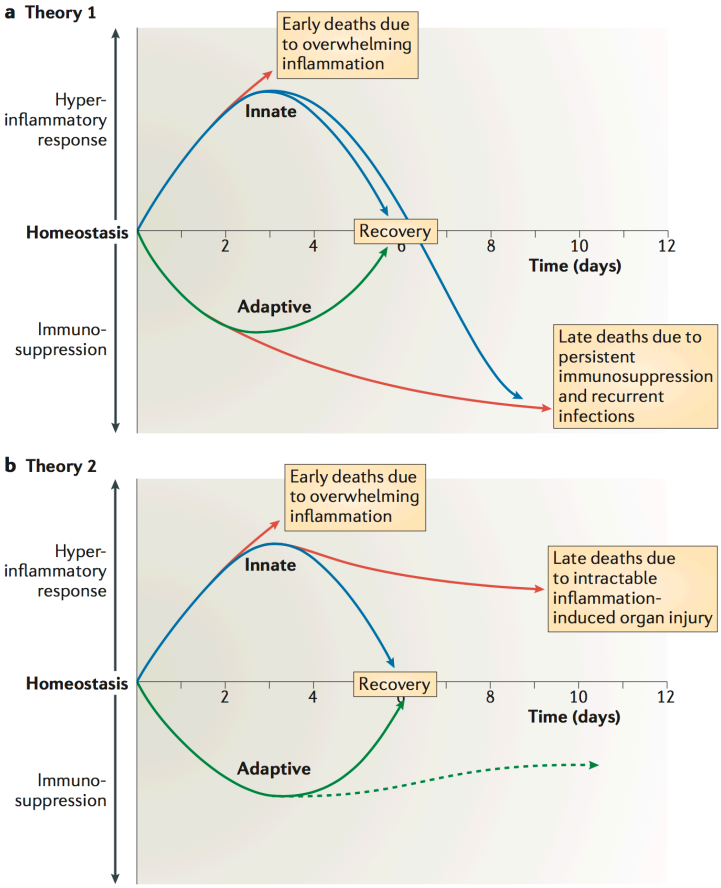

Fig. 3: **Competing theories of the host immune response in sepsis**. Theory 1: Early deaths in sepsis are due to the overwhelming cytokine-driven inflammation, whereas late deaths are explained by persistent immunosuppressive features and recurrent infections. Theory 2: In agreement with theory 1, early deaths in sepsis are explained by overwhelming cytokine-driven inflammation processes, whereas late deaths are due to inflammation-driven organ injury events. After Hotchkiss *et al.*, Nature Reviews Immunology 2013.

3.12.3 Neutrophils in sepsis

Neutrophils as first line defense against invading pathogens play a major role to recognize, phagocytose and kill pathogens. Pathogen elimination is crucially dependent on neutrophil recruitment to the site of infection [5]. Beside these classical effector functions, neutrophils contribute to the development of multiple organ failure in sepsis [190]. Several studies observe that circulating neutrophil cell counts are abnormally high and neutrophil lifespan is prolonged in sepsis patients [191]. Moreover, chemotactic activity seems to be reduced and consequently, neutrophil migration to the site of infection is impaired [191,192]. A possible explanation for this migratory defect is the internalization of CXCR2 in circulating neutrophils from mice or patients with severe sepsis [193-195]. Furthermore, IL-17 signaling could be shown to be crucial for recruitment of neutrophils to the site of infection during sepsis [196]. Interestingly, neutrophils isolated from sepsis patients show reduced migratory capacity *ex vivo,* linking to the clinical observation of patient survival: Survivors show higher neutrophil migration compared to non-survivors [197]. The migratory defect could be partially restored by IL-33 treatment [198].

NETosis is a highly efficient host defense mechanism in pathogen control [64]. Interestingly, NETosis in circulation is increased in sepsis patients, ultimately leading to organ dysfunction [199], in agreement with a previous report in a mouse model of endotoxemia that has shown platelet TLR4-mediated NETosis in sepsis [200]. NETosis formation occurs by the exposure of human neutrophils to plasma from septic patients [200] and by direct pathogen contact [201] (Fig. 4).

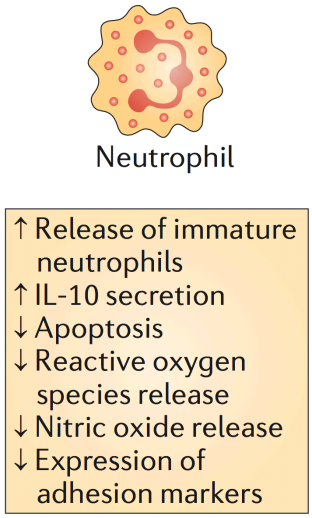

Fig. 4: **Impact of sepsis on neutrophils in sepsis**. Abnormal neutrophil counts with elevated levels of immature cells and decreased apoptosis. Neutrophil functionality in sepsis is impaired by decreased ROS production, decreased nitric oxide release and reduced expression of adhesion markers. After Hotchkiss *et al.*, Nature Reviews Immunology 2013.

Recent findings postulate neutrophil plasticity as a driving force in sepsis, ultimately leading to novel neutrophil subsets (such as PMN-myeloid-derived suppressor cells, short PMN-MDSC) with immunosuppressive features [202,203]. Human studies with sepsis depicts increased numbers of PMN-MDSCs, dominating in gram-positive cases [204,205]. The PMN-MDSC subset is associated with adverse outcome [206]. Moreover, it is shown in experimental mouse models of polymicrobial sepsis that MDSCs induce T-cell suppression, T_H2 polarization and reduce T-cell cytokine production (such as IFN-γ and IL-2) [202]. Another report could show that specific neutrophil subsets produce large amounts of IL-10 [207] and they have inhibitory effects on T-cell proliferation [208]. Since there is a correlation between gradual increase of MDSC frequency and the onset of sepsis, it is speculated that MDSCs exert an immunosuppressive effect on adaptive immunity, similarly to the situation observed in cancer [205]. So far, it is still unclear whether PMN-MDSCs influence the induction of various $CD4^+$ T-cell subpopulations (e.g. T_{Reg} cells) or contribute to T-cell exhaustion during the immunosuppressive phase in sepsis. Moreover, neutrophils and PMN-MDSCs share common cell markers and are morphologically identical, thus it is a substantial problem to distinguish both cell types from each other [3].

In conclusion, there are many ambiguities in the understanding of the role of PMN-MDSCs in sepsis and future research will hopefully address these important questions.

There are some reports supporting a role of atypical APC-like neutrophils in sepsis [209], especially in GM-CSF- rich environments [146]. Davey *et al.* could find an APC-like phenotype in neutrophils in acute human sepsis (increased levels of CD86, CD64 and CD40), a phenotype that can be induced by unconventional T cells [210]. Delano *et al.* could identify an immature Gr-1$^+$/ CD11b$^+$ population in a murine mouse model of polymicrobial sepsis, which contributes to sepsis-induced T-cell suppression and T_H2 polarization [202]. Nevertheless, it is unclear how relevant those APC-like neutrophils *in vivo* are and how they contribute in the pathophysiology of sepsis.

Another mechanism by which neutrophils might support T-cell exhaustion in sepsis is through programmed cell death ligand 1 (PD-L1) [211]. Neutrophils isolated from sepsis patients express the surface molecule PD-L1, a potent inducer of T-cell exhaustion and apoptosis [212]. Moreover, PD-L1 expression level on neutrophils is positively correlated with sepsis severity [213,214] and negatively correlated with the monocyte HLA-DR expression level [212]. It is unclear whether IFN-γ [215], GM-CSF [216] or the combination [217] induce PD-L1 expression on neutrophils. However, the PD-1– PD-L1 axis is thought to be an important mechanism in immune suppression in sepsis patients [169,218] and PD1-PD-L1 inhibition after the induction of sepsis improves survival in mice [219].

To summarize, both competing sepsis models agree that innate immunity, namely neutrophils and monocytes, plays a crucial role in the orchestration of aberrant adaptive immune responses in sepsis. However, the impact of human neutrophils and monocytes during septic immune responses are incompletely understood, mostly limited to a descriptive design and lacking in a systematic analysis [191], whereas animal studies are limited in profound reflection of human sepsis [169,191]. Of note, the role of neutrophils during sepsis is sparsely described and novel approaches to elaborate the role of neutrophils in sepsis are urgently needed. A systematic understanding of the inflammatory, dysregulated immune response in human sepsis supported with adequate sepsis mouse models will have crucial implications for the development of new therapeutic approaches in sepsis.

4 Aim of the thesis

Pathogen clearance in infectious diseases strongly depends on protective innate and adaptive host immunity. Past research has focused on the important role of neutrophils as first line defense in innate immunity against pathogens. Recent reports highlight that the immunological function of neutrophils in inflammation is highly versatile and goes far beyond simple pathogen destruction. However, the diverse role of neutrophils under inflammatory conditions in infectious diseases and their contribution in mediating adaptive immune responses has been largely neglected so far. To understand infectious diseases in more details, it is of highest interest to understand neutrophil biology under inflammatory conditions in the host. My aim was to investigate the diversity of neutrophil biology encountering pathogenic microorganisms that cause infectious diseases. To achieve this aim, I used human neutrophils from healthy individuals and from patients suffering from various infectious diseases and immunological disorders, respectively, in combination with a mouse model of *Salmonella* infection with the help of techniques such as flow cytometry, RT-PCR and proteomics to reveal the so far underestimated diversity in neutrophil function in infectious diseases.

My main questions are the following:

a. How do neutrophils protect against invading pathogens?
b. What are the versatile neutrophil functions in inflammation/ infection?
c. How do neutrophils crosstalk with other immune cells?

By answering these questions, I would like to show that infectious disease control implies a diverse neutrophil functionality ranging from simple foot soldiers to versatile commanders of immunity.

5 Results

5.1 Myeloperoxidase targets oxidative host attacks to *Salmonella* and prevents collateral tissue damage

Nura Schürmann[1#], **Pascal Forrer**[2#], Olivier Casse[1], Jiagui Li[1], Boas Felmy[3], Anne-Valérie Burgener[2], Nikolaus Ehrenfeuchter[4], Wolf-Dietrich Hardt[3], Mike Recher[2], Christoph Hess[2], Astrid Tschan-Plessl[2], Nina Khanna[2], Dirk Bumann[1*]

[1]Focal Area Infection Biology, University of Basel, CH-4056 Basel, Switzerland; [2]Department of Biomedicine and University Hospital Basel, University of Basel, CH-4056 Basel, Switzerland; [3]Institute of Microbiology, ETH Zurich, CH-8093 Zurich, Switzerland; [4]Imaging Core Facility, Biozentrum, University of Basel, CH-4056 Basel, Switzerland.

[#] These authors contributed equally to this work.

* Corresponding author

Manuscript has been published in Nature Microbiology, 2017 Jan 23;2:16268

DOI: 10.1038/nmicrobiol.2016.268

Statement of my work:

Design of experiments, Performance of experiments, Data analysis, Patient recruitment (together with A.-V.B., C.H. and M.R.), Immune cell isolation, Writing the paper (with N.S. & D.B.).

In vitro assays of H_2O_2 release (Fig. 2A; Fig. 2C; Fig. 2D; Fig. 2E; Fig. S1C; Fig. S1D; Fig. S1H, together with N.S.), HOCl detection (Fig. S1B), MPO activity (Fig. 2A; Fig. 2B; Fig. 2C; Fig. 2E; Fig. S1A; Fig. S1C; Fig. S1H; Fig. S1I), Oxygen consumption (Fig. 2A; Fig. 2D; Fig. S1D; Fig. S1E, together with N.S.), Degranulation with flow cytometry (Fig. S1F), Degranulation with ELISA (Fig. S1H), and Neutrophil viability (Fig. S1G).

Revisions done with D.B.

Note: The following part contains the final version of the manuscript published in Nature Microbiology.

nature microbiology

ARTICLES

PUBLISHED: 23 JANUARY 2017 | VOLUME: 2 | ARTICLE NUMBER: 16268

Myeloperoxidase targets oxidative host attacks to *Salmonella* and prevents collateral tissue damage

Nura Schürmann[1†], Pascal Forrer[2†], Olivier Casse[1], Jiagui Li[1], Boas Felmy[3], Anne-Valérie Burgener[2], Nikolaus Ehrenfeuchter[4], Wolf-Dietrich Hardt[3], Mike Recher[2], Christoph Hess[2], Astrid Tschan-Plessl[2], Nina Khanna[2] and Dirk Bumann[1*]

Host control of infections crucially depends on the capability to kill pathogens with reactive oxygen species (ROS). However, these toxic molecules can also readily damage host components and cause severe immunopathology. Here, we show that neutrophils use their most abundant granule protein, myeloperoxidase, to target ROS specifically to pathogens while minimizing collateral tissue damage. A computational model predicted that myeloperoxidase efficiently scavenges diffusible H_2O_2 at the surface of phagosomal *Salmonella* and converts it into highly reactive HOCl (bleach), which rapidly damages biomolecules within a radius of less than 0.1 μm. Myeloperoxidase-deficient neutrophils were predicted to accumulate large quantities of H_2O_2 that still effectively kill *Salmonella*, but most H_2O_2 would leak from the phagosome. *Salmonella* stimulation of neutrophils from normal and myeloperoxidase-deficient human donors experimentally confirmed an inverse relationship between myeloperoxidase activity and extracellular H_2O_2 release. Myeloperoxidase-deficient mice infected with *Salmonella* had elevated hydrogen peroxide tissue levels and exacerbated oxidative damage of host lipids and DNA, despite almost normal *Salmonella* control. These data show that myeloperoxidase has a major function in mitigating collateral tissue damage during antimicrobial oxidative bursts, by converting diffusible long-lived H_2O_2 into highly reactive, microbicidal and locally confined HOCl at pathogen surfaces.

When stimulated by microbes, neutrophils use the enzyme phagocyte NADPH oxidase to generate bursts of superoxide O_2^-, which spontaneously dismutates to hydrogen peroxide, H_2O_2. The enzyme myeloperoxidase (MPO) can then convert O_2^- and H_2O_2 into hypohalites (predominantly HOCl (bleach), but also HOBr)[1]. The MPO intermediate 'compound I' is the strongest two-electron oxidant generated in humans[2], and its product HOCl is a kinetically and thermodynamically highly reactive oxidant[3] with potent antimicrobial efficacy[1]. MPO can also contribute to the formation of antimicrobial neutrophil extracellular traps (NETs)[4,5]. However, MPO apparently has an only limited role in infection control in humans and mice, at least in modern hygienic environments, in marked contrast to NADPH oxidase, which is essential for controlling a wide range of infections[1]. MPO has clear detrimental effects in cardiovascular diseases[6], and MPO inhibitors are currently in clinical development for these and other indications[7]. Taken together, it is not entirely clear why neutrophils contain large quantities of MPO.

Results

Computational modelling of MPO impact on *Salmonella* killing and ROS leakage. To re-examine the role of MPO during infection, we combined a previously described computational model of oxidative bursts in neutrophil phagosomes[8] with our recent model of ROS defence in *Salmonella enterica* serovar Typhimurium[9] (Supplementary section 'Computational model parameters'). We used this model to compare conditions in neutrophils with various levels of MPO (Fig. 1).

In the absence of MPO (Fig. 1a, left), this model predicted H_2O_2 to be the dominant ROS output (Fig. 1a,b), as previously reported[8,9]. *Salmonella* could detoxify about 3% of this H_2O_2 output using its catalase KatG, while peroxidases (AhpC, Tsa, Tpx) had low saturated activities (Fig. 1c), consistent with the respective enzyme kinetics[10]. This minor detoxification had negligible impact on the *Salmonella* internal H_2O_2 concentration compared to the phagosomal lumen (Fig. 1d), resulting in lethal levels well above the toxicity threshold of ~2 μM (ref. 11) and suggesting H_2O_2-mediated *Salmonella* killing under conditions without MPO (ref. 9). At the same time, most H_2O_2 would not actually enter the *Salmonella*, but would instead leak out of the phagosome to the surrounding neutrophil cytosol (Fig. 1b), reflecting the diffusion of H_2O_2 through membranes at substantial rates ($\sim 1 \times 10^{-3}$ to 3×10^{-3} cm s^{-1} across bacterial[11] and mammalian[12] membranes), again in agreement with previous modelling results[8]. By contrast, the O_2^- concentration in *Salmonella* compartments always remained at non-toxic subnanomolar levels, in agreement with our previous results[9].

In the presence of low levels of MPO, the model suggested that H_2O_2 was partially converted to HOCl (Fig. 1a, middle, 50% conversion to HOCl at 0.13 mM MPO; Fig. 1b). The remaining H_2O_2 would still overwhelm *Salmonella* detoxification and kill *Salmonella* (Fig. 1d), but also largely leak from the phagosome (Fig. 1b). By contrast, HOCl would act locally. Based on the HOCl reaction rate constants[3], its diffusion coefficient[13] and protein concentrations in phagosomes[8], HOCl is expected to have a lifetime of 0.1 μs and a diffusion length of ~30 nm (similar to previous estimates[8]). This short reach would confine HOCl-mediated damage largely to the phagosome, consistent with recent experimental data[14]. In fact, the immunohistochemistry of *Salmonella* and MPO in infected mouse spleen showed that most MPO bound to the *Salmonella* (Fig. 1e), suggesting

[1]Focal Area Infection Biology, University of Basel, CH-4056 Basel, Switzerland. [2]Department Biomedicine and University Hospital Basel, University of Basel, CH-4056 Basel, Switzerland. [3]Institute of Microbiology, ETH Zurich, CH-8093 Zurich, Switzerland. [4]Imaging Core Facility, Biozentrum, University of Basel, CH-4056 Basel, Switzerland. †These authors contributed equally to this work. *e-mail: dirk.bumann@unibas.ch

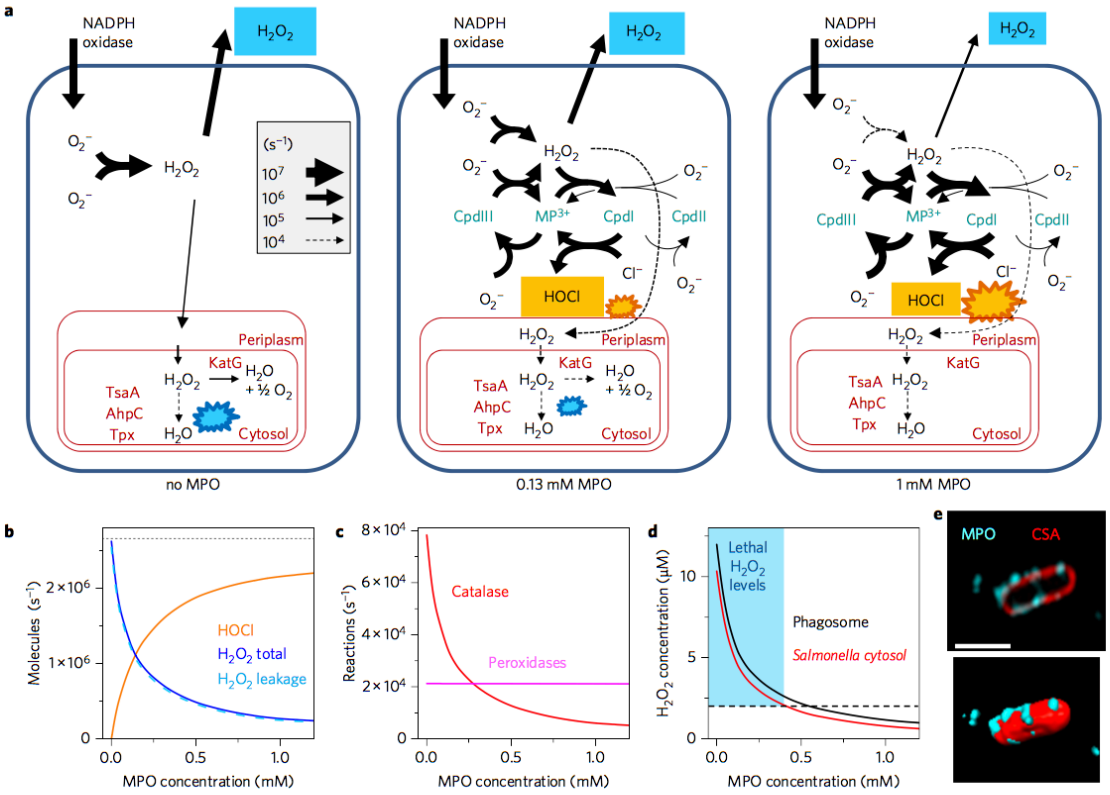

Figure 1 | Computational model of ROS generation and leakage in neutrophil phagosomes containing *Salmonella*. **a**, Schematic representation of redox reactions and diffusion in neutrophil phagosomes containing various concentrations of MPO (Cpd, compound; MP^{3+}, native MPO) and *Salmonella* expressing detoxification enzymes (red), as predicted by computational modelling. Only the most relevant reactions are shown. Thickness of arrows represents reaction rates, as shown in the inset of the left panel. The star-like patterns represent lethal *Salmonella* damage caused by H_2O_2 (blue) or HOCl (orange). **b**, Predicted generation and leakage of HOCl and H_2O_2 as final host ROS products (before damage reactions) as a function of MPO concentration. HOCl was predicted to remain confined exclusively to the phagosome. **c**, Predicted *Salmonella* detoxification of H_2O_2 through catalase (KatG) and peroxidases (AhpC, TsaA, Tpx). **d**, Impact of MPO concentration on H_2O_2 concentrations in the phagosome lumen and the *Salmonella* cytosol. The blue box and dashed line represent cytosolic concentrations above 2 μM, which are lethal for *Salmonella*. **e**, Top: Representative micrograph of *Salmonella* in infected mouse spleen stained for MPO and common *Salmonella* antigen (CSA). Bottom: Three-dimensional surface rendering of the confocal stack. Scale bar, 2 μm.

precise targeting of HOCl generation and its damaging action on the pathogen surface.

At normal MPO concentrations (around 1 mM) in the phagosome[8], the model predicted efficient conversion of O_2^- to HOCl (80% of the optimal theoretical yield of ½HOCl per O_2^-, Fig. 1a, right; Fig. 1b), consistent with previous experimental[1] and modelling results[8]. HOCl (and its reaction products, such as chloramines[14]) are probably the main bactericidal ROS under these conditions, because efficient scavenging of O_2^- and H_2O_2 by MPO would limit the concentrations of these other ROS to levels (17.4 μM and 1.2 μM) that *Salmonella* could easily detoxify with its peroxidases and catalase (internal H_2O_2 concentration of 0.77 μM, well below the toxicity threshold of ~2 μM (ref. 11), Fig. 1d). Due to its low phagosomal concentration, H_2O_2 would leak only slowly from the phagosome under these conditions (Fig. 1b).

These data suggested that the absence/presence of MPO alters the bactericidal ROS (H_2O_2 versus HOCl), but has little impact on overall *Salmonella* killing. Our results differ somewhat from previous interpretations of computational modelling results that suggested O_2^-, but not H_2O_2, to be the most important bactericidal ROS when MPO activity is low[8]. However, *Salmonella* and other pathogens have potent superoxide dismutases[15] that detoxify O_2^- at very high, diffusion-limited rates[16,17], whereas H_2O_2 in *Salmonella* compartments easily reaches micromolar concentrations, despite their catalases and peroxidases. This is sufficient for lethal damage[11], despite the observation that *in vitro* killing with bolus injections into bacterial cultures requires millimolar H_2O_2 concentrations. Under such non-physiological conditions, quick consumption of reduced free iron as the Fenton reaction catalyst and blocking of metabolism render the bacteria less vulnerable to oxidative damage[18].

Consistent with previous data[8], the model predicted a major role of MPO in the control of ROS leakage from the phagosome (Fig. 1a,b). This was the consequence of differences in reactivity and reach between the MPO substrate H_2O_2 (comparatively stable, rapid diffusion through membranes)[19] and MPO product HOCl (highly reactive, reach in the nanometre range). At normal levels of MPO, most H_2O_2 was rapidly consumed, minimizing its leakage (Fig. 1a, right; Fig. 1b), but at partial MPO deficiency (13% of normal), H_2O_2 leakage already reaches rates above 1 million H_2O_2 molecules s^{-1}, surpassing HOCl production (Fig. 1b). A major role of MPO

might thus be the confinement of ROSs and their damaging action on the neutrophil phagosome during oxidative bursts.

MPO controls H_2O_2 leakage from *Salmonella*-stimulated human neutrophils *in vitro*. H_2O_2 leaking from the phagosome can be scavenged by several detoxification systems in the neutrophil cytosol[20]. However, a substantial fraction of H_2O_2 would still escape from the phagosome through the cytosol to the extracellular space[19]. Early experimental data suggested little H_2O_2 release in the first few minutes after microbial stimulation of neutrophils, with a weak impact from MPO (refs 21,22). We revisited this issue with purified human neutrophils *in vitro* using longer observation times. Stimulation with heat-killed *Salmonella* resulted in typical neutrophil oxygen consumption kinetics and luminol chemoluminescence (a specific readout for MPO activity[23]), with peaks at 20–40 min. (Fig. 2a, left and middle). An assay using horseradish peroxidase (HRP) and Amplex Red that reports H_2O_2 in the extracellular medium indicated significant H_2O_2 leakage from neutrophils throughout the entire oxidative burst (Fig. 2a, right).

To modulate MPO activity, we used the specific inhibitor 4-aminobenzoic acid hydrazide (ABAH)[24]. MPO inhibition in intact human neutrophils required rather high ABAH concentrations (half-maximum inhibitory concentration (IC_{50}) of ~200 μM under our assay conditions) compared to the much lower inhibitory concentrations ($IC_{50} = 3$ μM) for neutrophil lysates (Supplementary Fig. 1a). IC_{50} values for MPO in intact cells that were about 60-fold higher than in freely accessible MPO are consistent with previous reports[23,24] and might reflect the low saturation of MPO with endogenously generated H_2O_2 in phagosomes and/or poor intracellular drug penetration. At such high concentrations, ABAH reduced MPO activity and enhanced extracellular H_2O_2 leakage during stimulation with live or heat-killed *Salmonella* (Fig. 2c), or with the fungal pathogen *Candida albicans* (Supplementary Fig. 1c). These data are consistent with the computational predictions of enhanced H_2O_2 leakage at low MPO activities. Another reagent to detect MPO activity and more selectively HOCl production[25], 3′-(*p*-aminophenyl) fluorescein (APF), gave similar results (Supplementary Fig. 1b). The release of H_2O_2 did not correlate with differential oxygen consumption (Fig. 2d and Supplementary Fig. 1d,e). Inhibiting NADPH oxidase with diphenylene iodonium (DPI) largely abolished luminol/APF oxidation, extracellular H_2O_2 leakage and oxygen consumption (Fig. 2c and Supplementary Fig. 1b,e), as expected. ABAH and DPI did not affect neutrophil degranulation as measured by three different assays[26] (Supplementary Fig. 1f). Neither inhibitor caused detectable toxicity under our conditions (Supplementary Fig. 1g).

We next tested neutrophils from donors with partial or severe MPO deficiency according to standard clinical cytometry (Fig. 2b). As expected, MPO-deficient neutrophils had lower MPO activities than normal donors, and this was associated with strongly increased H_2O_2 release (Fig. 2c and Supplementary Fig. 1c). MPO activity and extracellular H_2O_2 leakage had a highly significant inverse relationship (Fig. 2e), consistent with our model predictions. Similarly, the cytometry parameter for MPO, the 'mean peroxidase index' (MPXI), correlated with MPO activity but had a significant inverse correlation with H_2O_2 release (Supplementary Fig. 1h). These data demonstrate that neutrophils release H_2O_2 depending on their MPO activity.

In most experiments, we used particulate pathogen material (*Salmonella* and *Candida*) that triggers oxidative bursts at the phagosome membrane[27]. For comparison, we also stimulated neutrophils with phorbol esters (PMA) that induce oxidative bursts predominantly at the cell surface[27]. Under these conditions, partial blocking of MPO did not significantly alter H_2O_2 release (Supplementary Fig. 1i). Diffusion of reactants at the cell surface and altered activities of NADPH oxidase and the various MPO enzymatic reactions (both consuming and generating H_2O_2)[8] might result in balanced MPO-mediated H_2O_2 production and consumption under these somewhat artificial conditions. Future work might clarify this issue.

MPO controls H_2O_2 release and tissue damage in *Salmonella*-infected mice. In a mouse typhoid fever model[28], neutrophils and inflammatory monocytes provide strong, yet incomplete, control of *Salmonella*[29–32] through NADPH oxidase-mediated mechanisms[9], suggesting a key importance of oxidative bursts and ROS. In humans, neutropenia is sometimes associated with *Salmonella* bacteraemia, although endogenous pathogens are much more frequent, whereas NADPH oxidase defects are associated with severe *Salmonella* infections[33]. In contrast to the strong impact of NADPH oxidase deficiency, *S. enterica* serovar Typhimurium grows only slightly faster in MPO-deficient mice than in congenic wild-type mice (about threefold higher spleen loads at day 4 post-infection, a minor difference compared to the overall 1,000–10,000 fold increase during the same time interval)[9]. To obtain equivalent *Salmonella* spleen loads at day 4 (Fig. 3a), we infected MPO mice with a two- to threefold lower dose in this study.

To determine extracellular H_2O_2 release *in vivo*, we used a H_2O_2-specific *Salmonella* biosensor[9] carrying a transcriptional fusion of the *katGp* promoter to *gfp* in addition to constitutively expressed mCherry. *katGp* is controlled by the transcription factor OxyR, which is activated by direct reaction of cysteines with H_2O_2 (ref. 34) in the submicromolar range[35]. Biosensor *Salmonella* thus always show red fluorescence (when alive), enabling their discrimination from host debris (Fig. 3b), and additional green fluorescence when exposed to H_2O_2 at levels above 0.1 μM with up to 100-fold induction when optimally stimulated[9] (Fig. 3c). This *Salmonella* H_2O_2 biosensor showed more[9] and brighter GFP^{hi} cells in MPO-deficient mice than in congenic mice (Fig. 3d,e), suggesting an increased fraction of H_2O_2-exposed *Salmonella*, as well as higher levels of exposure.

The majority of GFP^{hi}, H_2O_2-exposed *Salmonella* in MPO-deficient mice resided in $F4/80^{hi}$ resident macrophages within the red pulp (Fig. 3f,g), the major host cell type harbouring live *Salmonella* in the spleen[9]. This was initially surprising, as neutrophils and inflammatory monocytes generate much stronger oxidative bursts than macrophages[1,36]. Moreover, neutrophils and monocytes, but not macrophages, normally express MPO (ref. 36) and would thus be primarily affected by MPO deficiency. Apparently, H_2O_2 leaking from MPO-deficient neutrophils/monocytes *in vivo* diffused through the surrounding tissue to reach resident macrophages and their intracellular biosensor *Salmonella*.

Previous studies have reported similar or altered neutrophil tissue infiltration for MPO-deficient mice in various disease models[37–44], which could affect oxidative stress levels. However, in the typhoid fever model, neutrophil recruitment as detected by an antibody to Ly-6G was similar in infected wild-type and MPO-deficient mice (Fig. 4c, left). MPO-deficient human individuals also had rather normal blood neutrophil counts compared to controls ($(3.2 \pm 0.5) \times 10^9$ ml^{-1} versus $(3.4 \pm 0.3) \times 10^9$ ml^{-1}; $N = 5, 8$; $P > 0.05$).

Although less reactive than HOCl, H_2O_2 is still a strong oxidant that can damage a large range of biomolecules, especially when in contact with metals, nitric oxide and so on[45]. Indeed, infected MPO-deficient mice that had higher H_2O_2 tissue levels also had strongly exacerbated lipid peroxidation in the spleen red pulp (where most *Salmonella* and neutrophils/monocytes resided), as detected by the reaction product 4-hydroxynonenal (4-HNE) (refs 46,47 and Fig. 4a,c), and significantly increased DNA damage based on increased levels of 8-hydroxy-2′-deoxyguanosine (8-OHdG) (ref. 47 and Fig. 4b,c) compared to infected wild-type

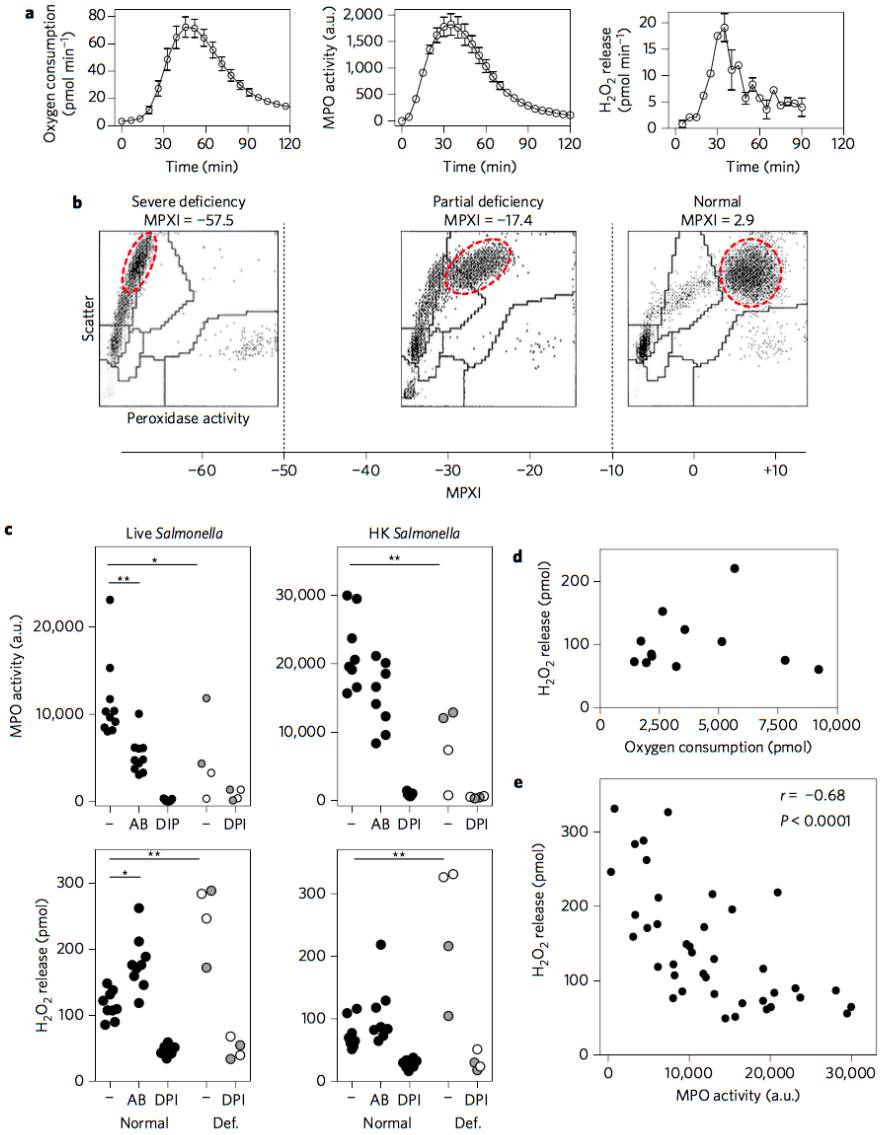

Figure 2 | ROS generation and leakage of human neutrophils *in vitro*. **a**, Kinetics of oxygen consumption, MPO activity (as measured by luminol oxidation) and extracellular H_2O_2 release during *Salmonella* stimulation of neutrophils from one representative normal human donor. Means and standard deviations of three technical replicates are shown. **b**, Representative leukograms of donors with different levels of MPO activities (MPXI, mean peroxidase index). For each donor, one leukogram was recorded. Red circles contain granulocyte populations. Dashed lines separate MPXI ranges for severe or partial deficiency and normal values. **c**, MPO activity and H_2O_2 release of neutrophils from eight different normal donors (black circles), two partially deficient donors (grey circles) and two severely deficient (def.) donors (open circles) after 75 min stimulation with live or heat-killed (HK) *Salmonella* in the presence/absence of the MPO inhibitor ABAH (AB) or the NADPH oxidase inhibitor DPI (Kruskal–Wallis multiple comparisons test; $*P < 0.05$ and $**P < 0.01$). **d**, Relationship between oxygen consumption and H_2O_2 release in neutrophils stimulated with heat-killed *Salmonella* for 75 min. Values for wells containing 100,000 neutrophils are shown. **e**, Relationship between MPO activity and H_2O_2 release after 75 min stimulation with live or heat-killed *Salmonella* (r, Spearman correlation coefficient).

mice. The oxidative damage sometimes occurred within or close to *Salmonella* (based on co-localization with an antibody to lipopolysaccharide, LPS), but most damage was to host components in the $CD11b^{hi}$ cells (neutrophils and monocytes, with potent oxidative bursts) and $CD11b^{low}$ bystander cells (Fig. 4a,b, insets), consistent with ROS leakage and diffusion through the tissue. Uninfected mice showed background staining in the spleen white pulp, but no detectable damage in the spleen red pulp (Supplementary Fig. 2). Together, these data suggest that ROS, which are generated as part of an inflammatory response to infection, are released and cause exacerbated collateral tissue damage unless MPO confines them to intracellular compartments (Fig. 4d).

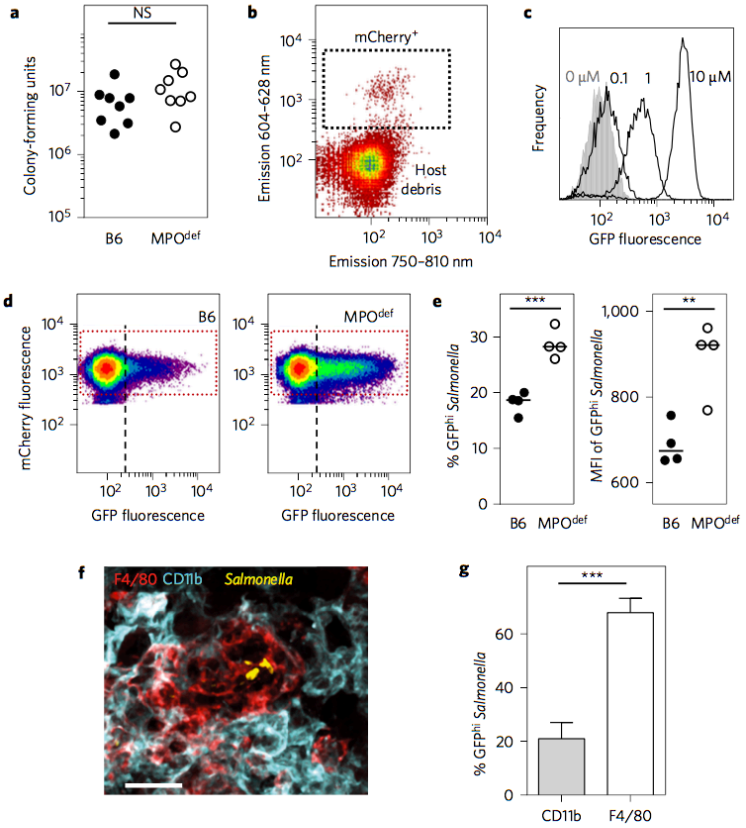

Figure 3 | H_2O_2 exposure of *Salmonella* in spleen of wild-type and MPO-deficient mice as revealed by a *Salmonella* biosensor strain. a, *Salmonella* spleen loads in wild-type (B6) and MPO-deficient (MPO^{def}) mice 4 days after infection (each dot represents one mouse; *t*-test on log-transformed data; NS, not significant). **b**, Detection of mCherry-expressing ($mCherry^+$) *Salmonella* against a background of preponderant host debris in infected mouse spleen homogenates using flow cytometry (laser excitation wavelength of 561 nm for the two channels shown). The dotted box represents the acquisition gate for monitoring GFP expression in *Salmonella*. One representative example of eight mice is shown. **c**, *In vitro* stimulation of GFP fluorescence after 30 min incubation with various concentrations of H_2O_2 (flow cytometry histograms). Representative data of one of three experiments are shown. **d**, Representative flow cytometry density plots of *Salmonella* biosensor in spleen homogenates of wild-type (B6) and MPO-deficient mice. Dotted red lines represent a more stringent gate on mCherry-positive *Salmonella*. Black dashed lines separate positive biosensor responses (GFP^{hi}, *Salmonella* subset with high GFP levels) from baseline *Salmonella* fluorescence. $mCherry^{lo}$ particles (*Salmonella* subset with low mCherry levels) were excluded during data acquisition to avoid excessively large data files. Even in MPO-deficient mice, more than 95% of *Salmonella* biosensor cells were still not stimulated at saturating levels based on *in vitro* induction dynamics (**c**). **e**, Quantification of flow cytometry data as shown in **d** (MFI, mean fluorescence intensity; $N = 4, 4$; *t*-test; $^{***}P < 0.001$ and $^{**}P < 0.01$). **f**, Localization of GFP^{hi} biosensor *Salmonella* in $F4/80^{hi}$ macrophages in the vicinity of $CD11b^{hi}$ neutrophils/inflammatory monocytes using immunohistochemistry of a spleen cryosection. Representative data for one of four MPO-deficient mice are shown. Scale bar, 10 μm. **g**, Quantification of localization data as shown in **f** (means and standard deviations; $N = 4, 4$; *t*-test; $^{***}P < 0.001$).

Discussion

Several pathogens, such as *Salmonella*, have versatile stress defence mechanisms. Killing these sturdy pathogens requires aggressive immune attacks with high local intensity, but this inevitably poses a risk of excessive self-damage in host tissues. Our data show how host immunity can solve this fundamental problem for a crucial antimicrobial mechanism, the employment of ROS. During oxidative bursts, neutrophils use NADPH oxidase to generate high fluxes of superoxide, which spontaneously dismutates to H_2O_2. The large amount of H_2O_2 that these cells generate is sufficient to kill *Salmonella*, thus achieving the primary objective—microbial target destruction. However, H_2O_2 can also readily leak to the surrounding host tissue, thus posing a risk of substantial collateral damage. Neutrophils use the highly abundant protein MPO to solve this problem by converting stable diffusible H_2O_2 into HOCl, which rapidly reacts with biomolecules within a few nanometres. MPO directly binds to the surface of various microbes, including *Salmonella* (Fig. 1e) and *Staphylococcus aureus*[1], enabling precision targeting of pathogens with intense oxidative attacks while mitigating the risk of collateral damage (Fig. 4a–c). Interestingly, MPO is largely absent in the resident tissue macrophages, which generate ROS at about tenfold lower rates than neutrophils[10], resulting in a lower risk of collateral damage.

Without self-protecting MPO, host tissues experience exacerbated oxidative tissue damage, including lipid peroxidation and DNA oxidation during infection. Increased oxidative damage during infections could have cumulative consequences over the lifetime of an individual, even though the consequences for organ function and survival during a single infection might be moderate. Repeated oxidative damage can contribute to many diseases, such as neurodegenerative and cardiovascular diseases and cancer, as well as accelerated

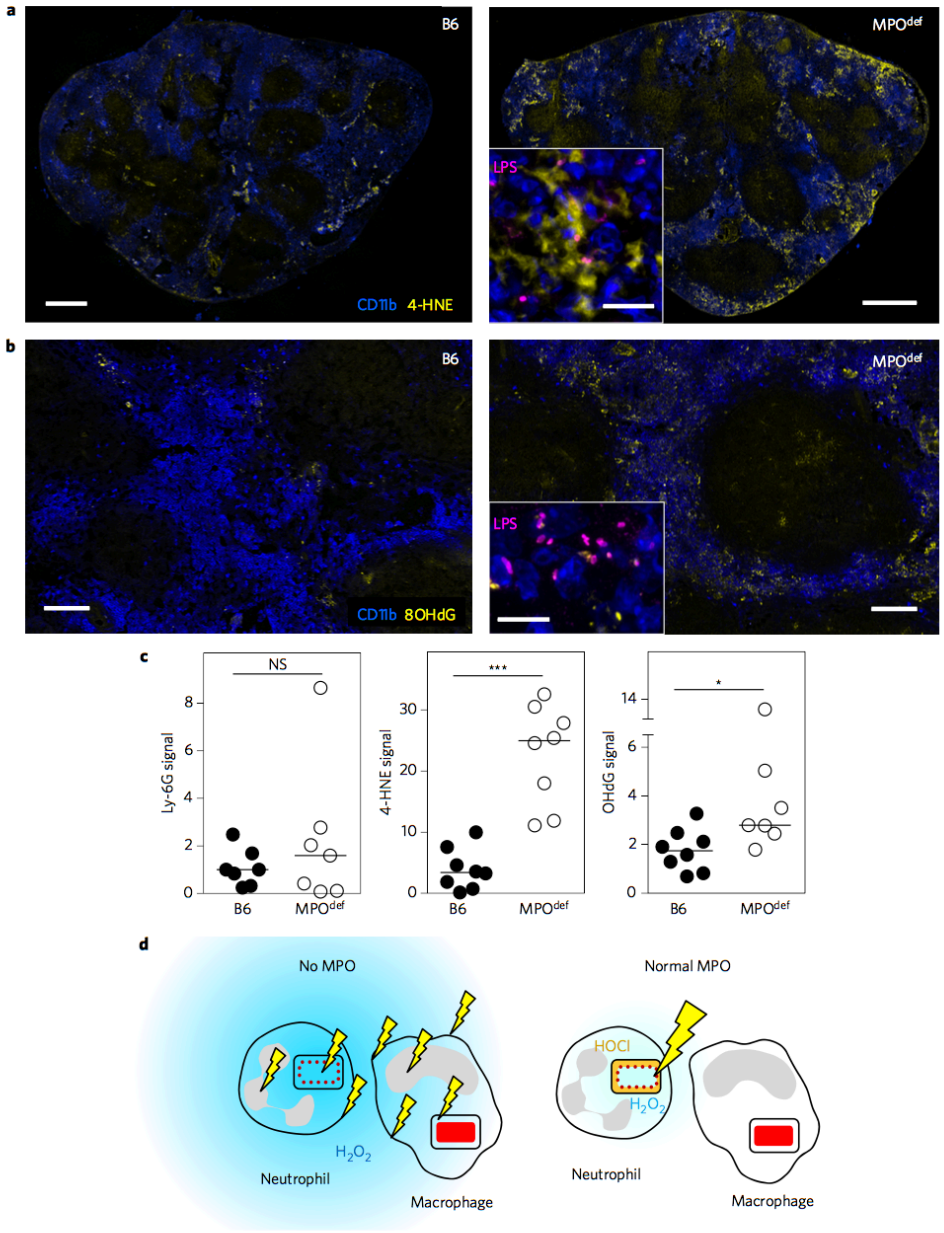

Figure 4 | Collateral tissue damage in the absence of MPO. a, Lipid peroxidation in infected spleen as detected by an antibody to 4-hydroxynonenal (4-HNE). Spleen cross-sections from wild-type (B6) and MPO-deficient mice imaged at identical microscopy settings are shown. These images are representative for eight individuals of either genotype. Scale bars, 500 µm. The inset shows a representative area at higher magnification from a different section that was also stained with an antibody to *Salmonella*-LPS (scale bar, 10 µm). **b**, Nucleoside oxidative damage as detected by an antibody to 8-hydroxy-2′-deoxyguanosine (OHdG). These images are representative of eight individuals of either genotype. Scale bars, 100 µm. Inset: A representative area at higher magnification from a different section that was also stained with an antibody to *Salmonella*-LPS (scale bar, 10 µm). **c**, Quantification of Ly-6G staining (reflecting neutrophil numbers), 4-HNE staining (reflecting lipid oxidation) and OHdG staining (reflecting DNA damage) in the red pulp (where most *Salmonella* and CD11b^{hi} host cells reside). Each dot represents one mouse (Mann–Whitney *U* test; ***$P < 0.001$ and *$P < 0.05$). **d**, Schematic model for the role of MPO. In MPO-deficient individuals (left), ROS generation in the neutrophil phagosome leads to high H_2O_2 (blue) accumulation, which kills *Salmonella* (dotted red line) in the phagosome. However, most H_2O_2 leaks out from the phagosome and diffuses through the tissue where it causes collateral damage (small lightning bolts) and is detected by live *Salmonella* (red). By contrast, in normal individuals (right), MPO at the *Salmonella* surface converts almost all generated ROS into HOCl (orange). HOCl immediately reacts with nearby biomolecules causing lethal *Salmonella* damage (large lightning bolt). Because of this efficient scavenging by MPO, little H_2O_2 leaks out from the phagosome, resulting in minimal collateral damage under these conditions.

aging[48,49]. Human data are scarce, but early studies have reported an increased cancer incidence in patients with complete MPO deficiency[50], whereas the single nucleotide polymorphisms that modulate MPO activity have weak if any impact on cancer risk[51]. Indeed, our computational model and experimental data suggest that detrimental effects should appear mostly in patients with severe/complete MPO deficiency (Figs 1b and 2c), which is rare (in contrast to partial deficiency[1]). Importantly, studies have only been carried out in industrialized countries where human infections have become greatly reduced in modern times[52], reducing the lifetime impact of inflammation, collateral damage and MPO deficiency[1]. On the other hand, long-term treatment with MPO inhibitors could exacerbate these issues and this should perhaps be considered during the current clinical development of such drugs.

Our results differ from a study of zymosan-induced peritonitis that showed that MPO actually promotes lipid peroxidation[53]. Zymosan-induced peritonitis causes extensive cell death of neutrophils within a few hours[54] and released MPO can then access and broadly damage extracellular host molecules. Extracellular MPO release might also be involved in other disease models in which MPO causes exacerbated immune pathology[1,39,41]. In contrast, detectable host cell death is rare in our mouse typhoid fever model (around 1% of all infected cells)[55], thus preserving intracellular containment of MPO and its damaging action.

MPO generates highly bactericidal agents that contribute to the control of pathogens such as *S. aureus*[1] and *Candida*[56], and can trigger NET formation. This study shows that MPO has an additional major function in mitigating collateral tissue damage during oxidative antimicrobial attacks, by converting diffusible long-lived H_2O_2 (which can leak out and cause damage in the surrounding tissue) into highly reactive, microbiocidal and locally confined HOCl at the pathogen surface (Fig. 4e). More work will be required to fully assess the impact of this protective mechanism in humans.

Methods

Modelling of oxidative bursts in neutrophil phagosomes. We built a diffusion-reaction model based on a previous neutrophil phagosome model[8] and our previous model of *Salmonella* oxidative stress defence[9], which are both based on experimentally determined parameters (Supplementary section 'Computational model parameters'). The model covers O_2^- generation by NADPH oxidase, O_2^- protonation equilibrium, spontaneous O_2^- dismutation, reactions of O_2^- catalysed by MPO or *Salmonella* superoxide dismutases SodA, SodB and SodCI, reactions of H_2O_2 catalysed by MPO or *Salmonella* catalase KatG or peroxidases AhpC, Tsa and Tpx, generation of HOCl by reaction of MPO compound I with chloride and MPO side reactions and diffusion of HO_2 and H_2O_2 across the phagosomal membrane as well as *Salmonella* outer and inner membranes. Simulations using the Simulink feature of MATLAB were run until steady-state concentrations were reached. Code is available upon request from the corresponding author.

MPO-deficient human individuals and normal volunteers. The study was approved by the responsible Ethics Committee (EKNZ 2015-187) and in compliance with the Declaration of Helsinki. Study participants signed an informed consent form.

Fresh venous blood was drawn in 2.7 ml polyethylene tubes containing 1.6 mg EDTA per ml blood (Sarsted) and analysed within 2 h on a fully automated Advia 2120 haematological analyser (Bayer) at the Hematology Routine Diagnostics Laboratory, University Hospital Basel. MPO level was determined from a Perox diagram according to cell size and peroxidase activity. The MPO Index (MPXI) was calculated according to the formula MPXI = 121.1–2.38 × *A*(deg), where *A*(deg) describes the angle through the centre of the deficient cluster and the baseline of the diagram[57].

Human neutrophil isolation. Human neutrophils were isolated as previously described[58]. In brief, human peripheral blood was collected in 7.5 ml polyethylene tubes containing 1.6 mg EDTA per ml blood (Sarsted), mixed with 3% dextran (Pharmacia)/NaCl solution supplemented with 10 μg ml^{-1} polymyxin-B (Calbiochem) in a ratio of 2:1. Erythrocyte sedimentation occurred after incubation for 30 min at 37 °C in a 5% CO_2 incubator. The leukocyte-rich plasma was then aspirated and centrifuged for 7 min at 1,400 r.p.m., 4 °C. The pellet was resuspended and transferred to a discontinuous Percoll gradient with 53% and 67% Percoll (GE Healthcare). Percoll gradient centrifugation was performed for 30 min at 1,400 r.p.m., 4 °C, with no braking. The visible ring containing neutrophil fraction was collected and washed in 0.9% NaCl, resuspended in Roswell Park Memorial Institute medium (RPMI, Invitrogen Gibco) + 10% fetal calf serum (FCS) and counted with Türk solution and an automatic cell counter system (ADAM, Digital Bio). Purity and viability was routinely >97% and >99%, respectively. If necessary, hypotonic erythrocyte lysis was performed with erythrocyte lysis buffer (Biolegend). Neutrophils were distributed and incubated for 15 min before stimulation.

Pathogen cultures. The *Salmonella* strains used in this study were derived from *Salmonella enterica* serovar Typhimurium *SL1344 hisG strAB xyl* (refs 59,60). The H_2O_2 biosensor construct p*katGp-gfpOVA* has been described previously[9]. *Salmonella* were cultured at 37 °C with aeration (200 r.p.m.) in Lennox lysogeny broth (LB) with the addition of 90 μg ml^{-1} streptomycin with or without 100 μg ml^{-1} ampicillin. For *in vitro* experiments, stationary-phase *Salmonella* were opsonized in 10% human serum in PBS for 20 min at 37 °C, washed with PBS, and diluted to a multiplicity of infection (MOI) of 30 for immediate use (live *Salmonella*). Alternatively, *Salmonella* were grown to mid-log phase, washed twice in PBS and heat-inactivated at 99 °C for 15 min. Heat-inactivated *Salmonella* were opsonized in 10% human serum in PBS for 20 min at 37 °C, washed with PBS and diluted to an MOI of 200 for immediate use (heat-inactivated *Salmonella*).

C. albicans SC5314 was grown overnight in yeast peptone dextrose (YPD, BD Difco) medium at 37 °C. A subculture was inoculated 1:100 and grown to mid-log phase. *C. albicans* was washed twice with 0.9% NaCl and heat-inactivated at 95 °C for 1 h. *C. albicans* was opsonized in 10% human serum in PBS for 20 min at 37 °C, washed with PBS and diluted to an MOI of 1 for immediate use.

MPO acitivity assays. MPO activity of neutrophils was measured using luminol-enhanced chemoluminescence or APF fluorescence. In brief, 2×10^5 cells were incubated in RPMI + 10% FCS for 1 h at 37 °C, 5% CO_2 without inhibitors, or with 500 μM ABAH or 10 μM DPI. Neutrophils were stimulated with opsonized *Salmonella*, *C. albicans* or 1 nM PMA in the presence of 10% human serum and 100 μM luminol (Fluka) in HBSS (Invitrogen, Gibco) containing 0.1% glucose (Braun). Chemiluminescence was measured at 5 min intervals at 37 °C with a luminometer (Microlumat Plus, Berthold Technologies). APF fluorescence was measured with flow cytometry. Values were corrected based on unstimulated controls and initial time points.

H_2O_2 release of human neutrophils. Extracellular H_2O_2 release was measured by the production of Resofurin from Amplex Red (Invitrogen). In brief, 1×10^5 cells per well were treated with or without inhibitors in RPMI containing 10% FCS for 1 h at 37 °C, 5% CO_2. Cells were washed once and incubated in 50 μM Amplex Red + 0.1 U ml^{-1} HRP (Sigma) in KRPG buffer (145 mM NaCl, 5.7 mM sodium phosphate, 4.86 mM KCl, 0.54 mM $CaCl_2$, 1.22 mM $MgSO_4$, 5.5 mM glucose, pH 7.35). Neutrophils were stimulated with *Salmonella* or *C. albicans* and fluorescence was measured at 5 min intervals at 37 °C with a fluorescence plate reader (490 nm excitation, 590 nm emission). Values were corrected based on negative controls without HRP and initial time points. H_2O_2 concentration was determined using standard curves obtained with defined H_2O_2 concentrations.

Oxygen consumption rate. Oxygen consumption rate was measured with a Seahorse XF-96 metabolic extracellular flux analyser (Seahorse Bioscience). Human peripheral blood-derived neutrophils pretreated or not with inhibitors were resuspended in KRPG buffer and plated onto Seahorse cell plates (3×10^5 cells per well) coated with Cell-Tak (BD Bioscience). Heat-killed *C. albicans* SC5314 (MOI = 2) or heat-killed *Salmonella* Typhimurium SL1344 (MOI = 200) was directly applied onto plated cells via the instrument's injection port. The experimental parameters were set at 3 min mixture/0 min wait/3 min measurement for 23 cycles.

Peroxidation activity of MPO in intact and lysed neutrophils. Peroxidation activity was quantified by the production of Resofurin from Amplex Red. To determine the MPO activity of neutrophil lysates, 1×10^5 cells per well were lysed with 1× lysis buffer (Cell Signaling, no. 9803) and treated with increasing ABAH concentrations (0–500 μM) in RPMI + 10% FCS. 50 μM Amplex Red + 5 μM H_2O_2 were added and fluorescence was measured after 30 min incubation at 37 °C. To determine MPO activity of intact neutrophils, 1×10^5 cells per well were washed three times with PBS after 1 h treatment of increasing ABAH concentrations (0–500 μM) in RPMI + 10% FCS and then lysed. 50 μM Amplex Red + 5 μM H_2O_2 were added and fluorescence was measured after 30 min incubation at 37 °C. MPO activity was determined using standard curves obtained with defined MPO (Sigma M6908) concentrations.

Neutrophil degranulation. MPO release in neutrophil supernatants at 75 min after stimulation was quantified with the Human MPO DuoSet ELISA kit (R&D, no. DY3174) using a MPO standard for calibration following the manufacturer's instructions. The optical density of standards and neutrophil supernatants was determined in triplicate at 450 nm using a microplate reader (Biotek, Synergy H3).

The appearance of CD63 and CD66 at the neutrophil surface following 75 min stimulation was quantified with flow cytometry. Cells were incubated for 15 min at room temperature with human TruStain FcX Blocking solution (Biolegend, no. 422302, 2 μl per test), followed by incubation with fluorescein-labelled anti-human CD66b (Biolegend, Clone G10F5, no. 305104) and APC anti-human CD63 (Biolegend, Clone H5C6, no. 353008) for 30 min at 4 °C. Samples

were analysed using a BD Accuri C6 flow cytometer using FL-1 (488 nm laser, 530/30 filter) and FL-4 (640 nm laser, 675/25 filter) channels.

Mouse infections and tissue collection. All animal experiments were approved (license 2239, Kantonales Veterinäramt Basel) and performed according to local guidelines (Tierschutz-Verordnung, Basel) and Swiss animal protection law (Tierschutz-Gesetz). Female eight- to ten-week-old B6.129X1-MPO$^{tm1Lus/J}$ as well as age- and sex-matched C57BL/6J congenic mice were infected by tail vein injection of 800–2,800 *Salmonella* in 100 µl PBS and euthanized at 4 days post-infection. Spleen tissue was collected from each mouse and dissected into several pieces. Colony-forming unit (c.f.u.) counts were determined by plating. We estimated sample size by a sequential statistical design. We first infected four mice, each based on effect sizes and variation observed in our previous study[9]. Biosensor responses and oxidative tissue damage analysis suggested that four additional mice in each group would be sufficient to determine statistical significance with sufficient power. This was indeed the case (Fig. 4a–c). We neither randomized nor blinded the experiments. However, image analysis of stained sections was carried out using an automated unbiased approach (see 'Image analysis' section).

Immunohistochemistry. Two- to three-mm-thick spleen sections were fixed with fresh 4% paraformaldehyde at 4 °C for 4 h, followed by incubating in increasing sucrose concentrations from 10 to 40% at 4 °C. After overnight incubation in 40% sucrose, tissue was rapidly frozen in embedding media (Tissue-Tek O.C.T; Sakura), left overnight at −80 °C and then stored at −20 °C. Unfixed tissue was immediately frozen in embedding media, left overnight at −80 °C and then stored at −20 °C. Cryosections (10–14 µm thick) were cut, put on coated glass coverslips (Thermo Scientific) and dried in a desiccator. After blocking with 1% blocking reagent (Invitrogen) and 2% mouse serum (Invitrogen) in PBS containing 0.05% Tween, sections were stained with primary antibodies (rat anti-CD11b, BD clone M1/70; goat anti-CSA1, KPL 01-91-99-MG, goat anti-4-HNE, Alpha Diagnostics HNE12-S, rabbit anti-myeloperoxidase, abcam 9535, goat anti-8 Hydroxyguanosine abcam 10802; rat F4/80, Serotec clone CI:A31; rat Ly-6G, BD clone 1A8). A variety of secondary antibodies were used depending on the application (Molecular Probes cat. no. A-21443; S11225, S21374; A-21206; A11096, D20698, Invitrogen A31556, Santa CruzBT sc-362245). For 4-HNE and 8-OHdG staining, we used unfixed sections and an HRP kit (Molecular Probes cat. no. T-20936) to amplify the signal. Sections were mounted in fluorescence mounting medium (Dako or Vectashield) and examined with a Zeiss LSM 700 confocal microscope using glycerol ×25, ×40 and ×63 objectives. Tiles covering an entire spleen section were stitched together. High-resolution images were obtained with a Zeiss LSM 800 using Airy Scanning.

Image analysis. For quantitative analysis of lipid peroxidation and DNA damage on antibody-stained spleen sections, we used an unbiased, automated protocol in the bioimage informatics platform Icy[61]. This protocol was established to minimize the impact of differences in staining intensities between individual samples. Each image consisted of three channels (DAPI, nuclei; 4-HNE, lipid peroxidation or 8-OHdG, DNA damage; CD11b, infiltrating neutrophils and monocytes). In a first step, the whole tissue area was segmented using the combined intensities from all three channels. In a next step a threshold was applied to create a segmentation of red pulp containing CD11b^{hi} cells (cells with high CD11b levels). The threshold value was set using Huang's method, which minimizes fuzziness[62] to avoid over-segmentation of noisy regions, especially at segmentation borders. Next, the CD11b^{hi} area was subtracted from the whole tissue area to create a segmentation of white pulp with little CD11b staining. To detect the proportion of 4-HNE^{hi} (or 8-OHdG^{hi}) pixels in the CD11b^{hi} and CD11b^{lo} (cells with low CD11b levels) regions, we used as threshold the sum of the mean 4-HNE signal over the entire tissue section plus three times the standard deviation. The staining index was then determined as the ratio of 4-HNE^{hi} pixel proportions in CD11b^{hi} over CD11b^{lo} regions. As a much simpler alternative, we also used a simple threshold of 100 across all samples, which gave similar results.

Flow cytometry. Spleen homogenates were prepared for flow cytometry as described in ref. 9. Relevant spectral parameters of 10,000–50,000 *Salmonella* were recorded in a FACS Fortessa II equipped with 488 and 561 nm lasers (Becton Dickinson), using thresholds on sideward and forward scatter to exclude electronic noise (channels: green fluorescent protein (GFP), excitation 488 nm, emission 502–525 nm; mCherry, excitation 561 nm, emission 604–628 nm; yellow autofluorescence channel, excitation 488 nm, emission 573–613 nm; infrared autofluorescence channel, excitation 561 nm, emission 750–810 nm). Data processing was performed with FlowJo and FCS Express.

Data availability. The data that support the findings of this study are available from the corresponding author upon request.

Received 10 May 2016; accepted 13 December 2016; published 23 January 2017

References

1. Klebanoff, S. J., Kettle, A. J., Rosen, H., Winterbourn, C. C. & Nauseef, W. M. Myeloperoxidase: a front-line defender against phagocytosed microorganisms. *J. Leukoc. Biol.* **93,** 185–198 (2013).
2. Arnhold, J., Furtmüller, P. G., Regelsberger, G. & Obinger, C. Redox properties of the couple compound I/native enzyme of myeloperoxidase and eosinophil peroxidase. *Eur. J. Biochem.* **268,** 5142–5148 (2001).
3. Storkey, C., Davies, M. J. & Pattison, D. I. Reevaluation of the rate constants for the reaction of hypochlorous acid (HOCl) with cysteine, methionine, and peptide derivatives using a new competition kinetic approach. *Free Radic. Biol. Med.* **73,** 60–66 (2014).
4. Parker, H. & Winterbourn, C. C. Reactive oxidants and myeloperoxidase and their involvement in neutrophil extracellular traps. *Front. Immunol.* **3,** 424 (2013).
5. Metzler, K. D., Goosmann, C., Lubojemska, A., Zychlinsky, A. & Papayannopoulos, V. A myeloperoxidase-containing complex regulates neutrophil elastase release and actin dynamics during NETosis. *Cell Rep.* **8,** 883–896 (2014).
6. Davies, M. J., Hawkins, C. L., Pattison, D. I. & Rees, M. D. Mammalian heme peroxidases: from molecular mechanisms to health implications. *Antioxid. Redox Signal.* **10,** 1199–1234 (2008).
7. Ruggeri, R. B. *et al.* Discovery of 2-(6-(5-chloro-2-methoxyphenyl)-4-oxo-2-thioxo-3,4-dihydropyrimidin-1(2*H*)-yl)acet amide (PF-06282999): a highly selective mechanism-based myeloperoxidase inhibitor for the treatment of cardiovascular diseases. *J. Med. Chem.* **58,** 8513–8528 (2015).
8. Winterbourn, C. C., Hampton, M. B., Livesey, J. H. & Kettle, A. J. Modeling the reactions of superoxide and myeloperoxidase in the neutrophil phagosome: implications for microbial killing. *J. Biol. Chem.* **281,** 39860–39869 (2006).
9. Burton, N. A. *et al.* Disparate impact of oxidative host defenses determines the fate of *Salmonella* during systemic infection in mice. *Cell Host Microbe* **15,** 72–83 (2014).
10. Imlay, J. A. in *EcoSal* (eds Curtiss, R. *et al.*) Module 5.4.4 (ASM, 2009).
11. Seaver, L. C. & Imlay, J. A. Hydrogen peroxide fluxes and compartmentalization inside growing *Escherichia coli*. *J. Bacteriol.* **183,** 7182–7189 (2001).
12. Makino, N., Sasaki, K., Hashida, K. & Sakakura, Y. A metabolic model describing the H_2O_2 elimination by mammalian cells including H_2O_2 permeation through cytoplasmic and peroxisomal membranes: comparison with experimental data. *Biochim. Biophys. Acta* **1673,** 149–159 (2004).
13. Kundrat, P., Bauer, G., Jacob, P. & Friedland, W. Mechanistic modelling suggests that the size of preneoplastic lesions is limited by intercellular induction of apoptosis in oncogenically transformed cells. *Carcinogenesis* **33,** 253–259 (2012).
14. Green, J. N., Kettle, A. J. & Winterbourn, C. C. Protein chlorination in neutrophil phagosomes and correlation with bacterial killing. *Free Radic. Biol. Med.* **77,** 49–56 (2014).
15. Korshunov, S. S. & Imlay, J. A. A potential role for periplasmic superoxide dismutase in blocking the penetration of external superoxide into the cytosol of Gram-negative bacteria. *Mol. Microbiol.* **43,** 95–106 (2002).
16. Stroppolo, M. E. *et al.* Single mutation at the intersubunit interface confers extra efficiency to Cu,Zn superoxide dismutase. *FEBS Lett.* **483,** 17–20 (2000).
17. Bull, C. & Fee, J. A. Steady-state kinetic studies of superoxide dismutases: properties of the iron containing protein from *Escherichia coli*. *J. Am. Chem. Soc.* **107,** 3295–3304 (1985).
18. Park, S., You, X. & Imlay, J. A. Substantial DNA damage from submicromolar intracellular hydrogen peroxide detected in Hpx- mutants of *Escherichia coli*. *Proc. Natl Acad. Sci. USA* **102,** 9317–9322 (2005).
19. Winterbourn, C. C. Reconciling the chemistry and biology of reactive oxygen species. *Nat. Chem. Biol.* **4,** 278–286 (2008).
20. Benfeitas, R., Selvaggio, G., Antunes, F., Coelho, P. M. & Salvador, A. Hydrogen peroxide metabolism and sensing in human erythrocytes: a validated kinetic model and reappraisal of the role of peroxiredoxin II. *Free Radic. Biol. Med.* **74,** 35–49 (2014).
21. Nauseef, W. M., Metcalf, J. A. & Root, R. K. Role of myeloperoxidase in the respiratory burst of human neutrophils. *Blood* **61,** 483–492 (1983).
22. Gerber, C. E., Kuci, S., Zipfel, M., Niethammer, D. & Bruchelt, G. Phagocytic activity and oxidative burst of granulocytes in persons with myeloperoxidase deficiency. *Eur. J. Clin. Chem. Clin. Biochem.* **34,** 901–908 (1996).
23. Gross, S. *et al.* Bioluminescence imaging of myeloperoxidase activity *in vivo*. *Nat. Med.* **15,** 455–461 (2009).
24. Kettle, A. J., Gedye, C. A., Hampton, M. B. & Winterbourn, C. C. Inhibition of myeloperoxidase by benzoic acid hydrazides. *Biochem. J.* **308**(Pt 2), 559–563 (1995).
25. Flemmig, J., Remmler, J., Zschaler, J. & Arnhold, J. Detection of the halogenating activity of heme peroxidases in leukocytes by aminophenyl fluorescein. *Free Radic. Res.* **49,** 768–776 (2015).
26. Naegelen, I. *et al.* An essential role of syntaxin 3 protein for granule exocytosis and secretion of IL-1α, IL-1β, IL-12β, and CCL4 from differentiated HL-60 cells. *J. Leukoc. Biol.* **97,** 557–571 (2015).
27. Winterbourn, C. C., Kettle, A. J. & Hampton, M. B. Reactive oxygen species and neutrophil function. *Annu. Rev. Biochem.* **85,** 765–792 (2016).
28. Tsolis, R. M., Xavier, M. N., Santos, R. L. & Baumler, A. J. How to become a top model: the impact of animal experimentation on human *Salmonella* disease research. *Infect. Immun.* **79,** 1806–1814 (2011).
29. Conlan, J. W. Critical roles of neutrophils in host defense against experimental systemic infections of mice by *Listeria monocytogenes*, *Salmonella typhimurium*, and *Yersinia enterocolitica*. *Infect. Immun.* **65,** 630–635 (1997).

30. Vassiloyanakopoulos, A. P., Okamoto, S. & Fierer, J. The crucial role of polymorphonuclear leukocytes in resistance to *Salmonella* Dublin infections in genetically susceptible and resistant mice. *Proc. Natl Acad. Sci. USA* **95,** 7676–7681 (1998).
31. Cheminay, C., Chakravortty, D. & Hensel, M. Role of neutrophils in murine salmonellosis. *Infect. Immun.* **72,** 468–477 (2004).
32. Dejager, L., Pinheiro, I., Bogaert, P., Huys, L. & Libert, C. Role for neutrophils in host immune responses and genetic factors that modulate resistance to *Salmonella enterica* serovar typhimurium in the inbred mouse strain SPRET/Ei. *Infect. Immun.* **78,** 3848–3860 (2010).
33. Mastroeni, P. *et al.* Resistance and susceptibility to *Salmonella* infections lessons from mice and patients with immunodeficiencies. *Rev. Med. Microbiol.* **14,** 53–62 (2003).
34. Lee, C. *et al.* Redox regulation of OxyR requires specific disulfide bond formation involving a rapid kinetic reaction path. *Nat. Struct. Mol. Biol.* **11,** 1179–1185 (2004).
35. Aslund, F., Zheng, M., Beckwith, J. & Storz, G. Regulation of the OxyR transcription factor by hydrogen peroxide and the cellular thiol-disulfide status. *Proc. Natl Acad. Sci. USA* **96,** 6161–6165 (1999).
36. Swirski, F. K. *et al.* Myeloperoxidase-rich Ly-6C+ myeloid cells infiltrate allografts and contribute to an imaging signature of organ rejection in mice. *J. Clin. Invest.* **120,** 2627–2634 (2010).
37. Kremserova, S. *et al.* Lung neutrophilia in myeloperoxidase deficient mice during the course of acute pulmonary inflammation. *Oxid. Med. Cell Longev.* **2016,** 5219056 (2016).
38. Endo, D., Saito, T., Umeki, Y., Suzuki, K. & Aratani, Y. Myeloperoxidase negatively regulates the expression of proinflammatory cytokines and chemokines by zymosan-induced mouse neutrophils. *Inflamm. Res.* **65,** 151–159 (2016).
39. Brovkovych, V. *et al.* Augmented inducible nitric oxide synthase expression and increased NO production reduce sepsis-induced lung injury and mortality in myeloperoxidase-null mice. *Am. J. Physiol. Lung Cell Mol. Physiol.* **295,** L96–L103 (2008).
40. Homme, M., Tateno, N., Miura, N., Ohno, N. & Aratani, Y. Myeloperoxidase deficiency in mice exacerbates lung inflammation induced by nonviable *Candida albicans*. *Inflamm. Res.* **62,** 981–990 (2013).
41. Sugamata, R. *et al.* Contribution of neutrophil-derived myeloperoxidase in the early phase of fulminant acute respiratory distress syndrome induced by influenza virus infection. *Microbiol. Immunol.* **56,** 171–182 (2012).
42. Takeuchi, K. *et al.* Severe neutrophil-mediated lung inflammation in myeloperoxidase-deficient mice exposed to zymosan. *Inflamm. Res.* **61,** 197–205 (2012).
43. Brennan, M. L. *et al.* A tale of two controversies: defining both the role of peroxidases in nitrotyrosine formation *in vivo* using eosinophil peroxidase and myeloperoxidase-deficient mice, and the nature of peroxidase-generated reactive nitrogen species. *J. Biol. Chem.* **277,** 17415–17427 (2002).
44. Klinke, A. *et al.* Myeloperoxidase attracts neutrophils by physical forces. *Blood* **117,** 1350–1358 (2011).
45. Imlay, J. A. The molecular mechanisms and physiological consequences of oxidative stress: lessons from a model bacterium. *Nat. Rev. Microbiol.* **11,** 443–454 (2013).
46. Liou, G. Y. & Storz, P. Detecting reactive oxygen species by immunohistochemistry. *Methods Mol. Biol.* **1292,** 97–104 (2015).
47. Seki, S. *et al. In situ* detection of lipid peroxidation and oxidative DNA damage in non-alcoholic fatty liver diseases. *J. Hepatol.* **37,** 56–62 (2002).
48. Loft, S. & Poulsen, H. E. Cancer risk and oxidative DNA damage in man. *J. Mol. Med. (Berl.)* **74,** 297–312 (1996).
49. Finkel, T. & Holbrook, N. J. Oxidants, oxidative stress and the biology of ageing. *Nature* **408,** 239–247 (2000).
50. Lanza, F. Clinical manifestation of myeloperoxidase deficiency. *J. Mol. Med. (Berl.)* **76,** 676–681 (1998).
51. Yuzhalin, A. E. & Kutikhin, A. G. Common genetic variants in the myeloperoxidase and paraoxonase genes and the related cancer risk: a review. *J. Environ. Sci. Health C* **30,** 287–322 (2012).
52. Crimmins, E. M. & Finch, C. E. Infection, inflammation, height, and longevity. *Proc. Natl Acad. Sci. USA* **103,** 498–503 (2006).
53. Zhang, R. *et al.* Myeloperoxidase functions as a major enzymatic catalyst for initiation of lipid peroxidation at sites of inflammation. *J. Biol. Chem.* **277,** 46116–46122 (2002).
54. Kolaczkowska, E., Koziol, A., Plytycz, B. & Arnold, B. Inflammatory macrophages, and not only neutrophils, die by apoptosis during acute peritonitis. *Immunobiology* **215,** 492–504 (2010).
55. Grant, A. J. *et al.* Caspase-3-dependent phagocyte death during systemic *Salmonella enterica* serovar Typhimurium infection of mice. *Immunology* **125,** 28–37 (2008).
56. Branzk, N. *et al.* Neutrophils sense microbe size and selectively release neutrophil extracellular traps in response to large pathogens. *Nat. Immunol.* **15,** 1017–1025 (2014).
57. Kutter, D. *et al.* Consequences of total and subtotal myeloperoxidase deficiency: risk or benefit? *Acta Haematol.* **104,** 10–15 (2000).
58. Hjorth, R., Jonsson, A. K. & Vretblad, P. A rapid method for purification of human granulocytes using percoll. A comparison with dextran sedimentation. *J. Immunol. Methods* **43,** 95–101 (1981).
59. Hoiseth, S. K. & Stocker, B. A. Aromatic-dependent *Salmonella typhimurium* are non-virulent and effective as live vaccines. *Nature* **291,** 238–239 (1981).
60. Kroger, C. *et al.* The transcriptional landscape and small RNAs of *Salmonella enterica* serovar Typhimurium. *Proc. Natl Acad. Sci. USA* **109,** E1277–E1286 (2012).
61. de Chaumont, F. *et al.* Icy: an open bioimage informatics platform for extended reproducible research. *Nat. Methods* **9,** 690–696 (2012).
62. Huang, L.-K. & Wang, M.-J. J. Image thresholding by minimizing the measures of fuzziness. *Pattern Recognit.* **28,** 41–51 (1995).

Acknowledgements

The authors thank K. Ullrich and R. Kühl for taking blood from human donors, and thank all donors for blood donations. The authors thank I. Bartholomaeus and A. Martin for support with confocal microscopy. This study was supported in part by grants from the Swiss National Foundation (310030_156818 to D.B., PZ00P3_142403 to N.K. and PP00P3_144863 to M.R.) and the Gebert Rüf Foundation (GRS 058/14 to C.H., A.-V.B. and M.R.).

Author contributions

N.S., P.F., B.F., N.E., A.T.-P., J.L. and D.B. performed experiments and analysed the data. O.C. and D.B. wrote code and ran the computational models. A.-V.B., C.H. and M.R. recruited patients. N.S., P.F., W.-D.H., N.K. and D.B. designed experiments. N.S., P.F. and D.B. wrote the paper.

Additional information

Supplementary information is available for this paper.

Reprints and permissions information is available at www.nature.com/reprints.

Correspondence and requests for materials should be addressed to D.B.

How to cite this article: Schürmann, N. *et al.* Myeloperoxidase targets oxidative host attacks to *Salmonella* and prevents collateral tissue damage. *Nat. Microbiol.* **2,** 16268 (2017).

Competing interests

The authors declare no competing financial interests.

nature microbiology

SUPPLEMENTARY INFORMATION

VOLUME: 2 | ARTICLE NUMBER: 16268

In the format provided by the authors and unedited.

Myeloperoxidase targets oxidative host attacks to *Salmonella* and prevents collateral tissue damage

Nura Schürmann, Pascal Forrer, Olivier Casse, Jiagui Li, Boas Felmy, Anne-Valérie Burgener, Nikolaus Ehrenfeuchter, Wolf-Dietrich Hardt, Mike Recher, Christoph Hess, Astrid Tschan-Plessl, Nina Khanna and Dirk Bumann

Supplementary Information

Table of Contents

Supplementary Note

Computational model parameters

We build a diffusion-reaction model based on a previous neutrophil phagosome model[1] combined with experimental data on *Salmonella* protective enzyme expression as obtained by ex vivo proteomics[2], estimated bacterial ROS production[3,4], adjusted vacuole volume based on electron microscopy[5], and updated reaction kinetics and diffusion constants based on recent reports. Our combined model included four compartments (host cell cytosol, phagosome lumen, *Salmonella* periplasm, *Salmonella* cytosol), 8 small molecules, 10 host and bacterial enzymes, and 27 different reactions including generation and interconversion of various reactive oxygen species (ROS), their diffusion across the phagosomal membrane and the two *Salmonella* membranes, as well as ROS detoxification by *Salmonella* superoxide dismutases, catalases, and peroxidases with quantitative abundance data based on our *ex vivo* proteomics results[13].

Salmonella / phagosome geometry

Salmonella shape was approximated as a cylinder with a length of 2 µM and a diameter of 0.8 µM (ccdb.wishartlab.com/CCDB/intron_new.html). We assumed an outer membrane area of $5.8x10^{-12}$ m^2, an inner membrane area of $5.4x10^{-12}$ m^2, a periplasm volume of $5.7x10^{-17}$ l, and a cytoplasm volume of $8.3x10^{-16}$ l. The phagosomal membrane was assumed to enclose one single *Salmonella*[5]. The distance between phagosomal membrane and *Salmonella* outer membrane was set to 200 nm based on TEM images[5]. This yielded a phagosomal membrane area of $1.1x10^{-11}$ m^2, a total phagosome volume of $2.59x10^{-15}$ l and a phagosome lumen of $1.7x10^{-15}$ l (excluding the volume occupied by *Salmonella*).

Generation of reactive oxygen species

Salmonella was assumed to endogenously generate $O_2^{\cdot-}$ in periplasm and cytoplasm at rates of 3 µM s^{-1} and 5 µM s^{-1}, respectively[3]; and 10 µM s^{-1} H_2O_2 in the cytoplasm based on a total generation of 14 µM s^{-1} H_2O_2, which included 4 µM s^{-1} due to dismutation of endogenously generated $O_2^{\cdot-}$[4]. Neutrophil phagosomes were assumed to generate $O_2^{\cdot-}$ at rates of $5.2x10^{-3}$ mol l^{-1} s^{-1} in the phagosome lumen[1], and to contain 1 mM MPO (normal levels)[1]. Rates for the various reactions of MPO and chloride concentration (100 mM) were used as reported[1].

Membrane permeability for reactive oxygen species

For superoxide in the protonated form $HO_2^{\cdot}$, membrane permeability was set to $9x10^{-6}$ m s^{-1} for all three membranes (phagosomal membrane, *Salmonella* outer and inner membranes)[6], while the deprotonated form was assumed to permeate poorly (< 10^{-9} m s^{-1}) based on reported values for liposomes[6].

For H_2O_2, a membrane permeability of $3.2x10^{-5}$ m s^{-1} was assumed based on the reported permeability of intact *E. coli* ($1.6x10^{-5}$ m s^{-1}; two membranes)[7]. The phagosomal membrane was assumed to have the same permeability based on the range of reported values for mammalian membranes[8].

OCl^- was predicted to have a short reach (33 nm) based on phagosomal protein concentrations[1], reaction rate constants[9], and its diffusion coefficient[10]. This short reach prevented leakage of OCl^- through membranes.

Spontaneous dismutation of superoxide

Superoxide dismutation depends on its protonation state. The total dismutation rate is the sum of rates of two different mechanisms, (i) $HO_2^{\cdot} + O_2^{\cdot-} + H_2O \rightarrow H_2O_2 + O_2 + HO^-$ with a second order rate constant $k_{AB} = 8.5x10^7$ M^{-2} s^{-1}; (ii) $2\ HO_2^{\cdot} \rightarrow H_2O_2 + O_2$, $k_{AA} = 7.6x10^5$ M^{-2} s^{-1}. The relative proportions of $HO_2^{\cdot} + O_2^{\cdot-}$ were calculated based on its pKa of 4.88 [11,12]. We assumed pH 7.4 in the neutrophil phagosome lumen and *Salmonella* periplasm in macrophages.

Detoxification of reactive oxygen species by *Salmonella* enzymes

Absolute *Salmonella* in vivo enzyme copy numbers were obtained from our recent study[13]: SodCI, 39'800 ± 8'300 copies per *Salmonella* cell; SodCII, 370 ± 200; SodA, 4'000 ± 1'000; SodB, 10'200 ± 2'100; KatG, 2'600 ± 500; KatE and KatN, below detection limit; Tpx, 22'000 ± 4'000; AhpC, 15'200 ± 3'500; AhpF, 1'000 ± 400; TsaA, 21'700 ± 3'600.

We used the following kinetic parameters for these enzymes: SodCI, SodCII, $k_{cat}/K_M = 4x10^9$ $M^{-1}s^{-1}$ diffusion-limited[14]; SodA, SodB, $k_{cat}/K_M = 7x10^9$ $M^{-1}s^{-1}$ diffusion-limited[15]; KatG, k_{cat} = 14'000 s^{-1}, $K_M = 5.9$ mM[16]; Tpx, $k_{cat} = 76$ s^{-1}, $K_M = 1.7$ mM[17]; AhpC (and its paralog TsaA), k_{cat} = 55.1 s^{-1}, $K_M = 1.4$ µM[18]; AhpF, $k_{cat} = 25.5$ s^{-1}, $K_M = 14.3$ µM[18]).

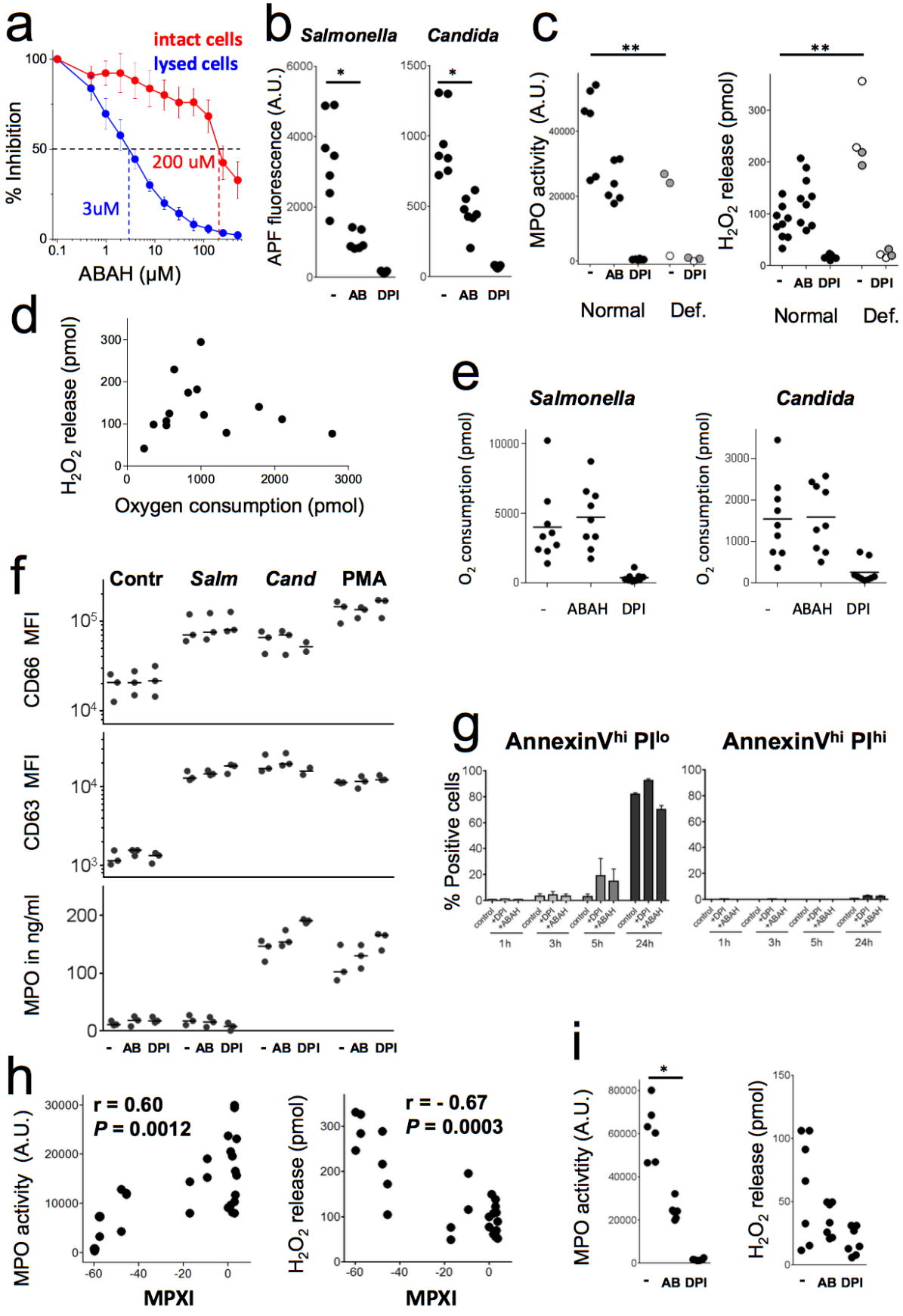
a
intact cells
lysed cells
200 uM
3uM
% Inhibition
ABAH (µM)
b
Salmonella
Candida
APF fluorescence (A.U.)
- AB DPI
c
MPO activity (A.U.)
H_2O_2 release (pmol)
Normal
Def.
d
H_2O_2 release (pmol)
Oxygen consumption (pmol)
e
Salmonella
Candida
O_2 consumption (pmol)
- ABAH DPI
f
Contr
Salm
Cand
PMA
CD66 MFI
CD63 MFI
MPO in ng/ml
g
AnnexinV^{hi} PI^{lo}
AnnexinV^{hi} PI^{hi}
% Positive cells
control
+DPI
+ABAH
1h
3h
5h
24h
h
r = 0.60
P = 0.0012
r = - 0.67
P = 0.0003
MPO activity (A.U.)
H_2O_2 release (pmol)
MPXI
i
MPO activity (A.U.)
H_2O_2 release (pmol)

Supplementary Figure 1: Reactive oxygen species generation and leakage of human neutrophils in vitro.

a, Inhibition of myeloperoxidase activity by ABAH in intact or lysed neutrophils. Data (means and standard deviations of six technical triplicates) from one representative experiment out of two are shown. The dotted lines indicate 50% activity and the corresponding ABAH concentrations for lysed or intact cells, respectively. **b**, MPO activity measured as APF oxidation in neutrophils from seven different normal donors after 60 min stimulation in presence/absence of the MPO inhibitor ABAH (AB) or the NADPH oxidase inhibitor DPI (Wilcoxon test; *, $P< 0.05$). **c**, MPO activity and H_2O_2 release of neutrophils from eight different normal donors (black circles), two partially deficient donors (grey), and two severely deficient donors (empty circles) during stimulation with *Candida* in presence/absence of the MPO inhibitor ABAH (AB) or the NADPH oxidase inhibitor DPI (Kruskal-Wallis multiple comparisons test; **, $P< 0.01$). **d**, Relationship between oxygen consumption and H_2O_2 release in neutrophils stimulated with heat-killed *Candida* for 75 min. Mean values of triplicate wells containing 100'000 neutrophils are shown. **e**, Impact of inhibiting myeloperoxidase with ABAH, or NADPH oxidase with DPI, on oxygen consumption rate after stimulation with heat-killed *Salmonella* and *Candida*. **f**, Impact of inhibitors on neutrophil degranulation. Cells from three different donors were stimulated with PBS (Contr), heat-killed *Salmonella* (*Salm*), *Candida* (*Cand*), or PMA for 75 min in presence/absence of the MPO inhibitor ABAH (AB) or the NADPH oxidase inhibitor DPI. Surface expression of degranulation markers CD63 and CD66 was measured by flow cytometry. MPO release to the extracellular medium was quantified using ELISA. Different stimuli triggered the three degranulation processes to a various degree, but all three assays demonstrated no impact of inhibitors ABAH and DPI on neutrophil degranulation. **g**, Impact of 500 µM ABAH and 10 µM DPI on neutrophil viability. The fraction of cells undergoing apoptosis [annexinV^{hi} propidium iodide $(PI)^{lo}$, left] and cells undergoing necrosis (annexinV^{hi} PI^{hi}, right) at various times after inhibitor addition is shown. Means and standard deviations for four donors measured in one experiment are shown. In all other experiments of this study, cells were exposed to these inhibitors for a maximum of 75 min. **h**, Relationship between donor mean peroxidase index (MPXI) and HOCl generation (left) or H_2O_2 release (right) after stimulation with live or heat-killed *Salmonella* (r, Spearman correlation coefficient). Each dot represents data for an individual human donor. **i**, MPO activity and H_2O_2 release of neutrophils from seven different normal donors during stimulation with 1 nM PMA in presence/absence of the MPO inhibitor ABAH (AB) or the NADPH oxidase inhibitor DPI (Wilcoxon test; *, $P< 0.05$).

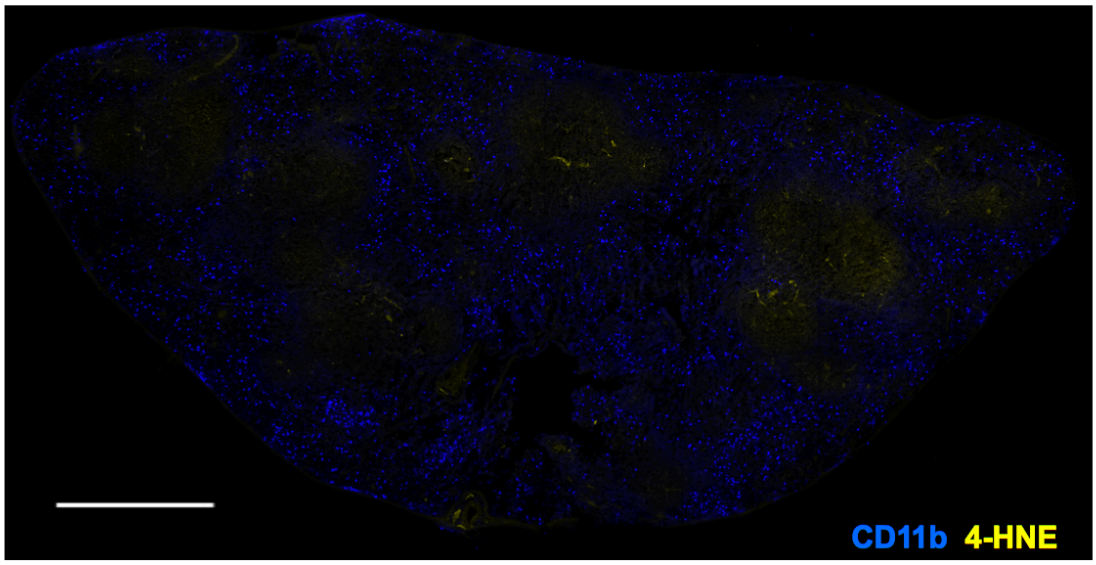

Supplementary Figure 2: Lipid peroxidation in uninfected spleen as detected by an antibody to 4-hydroxynonenal (4-HNE).

Representative micrograph of a spleen cross-section from one out of four uninfected MPO-deficient mice. CD11b^{hi} cells populate the red pulp. 4-HNE signals are undetectable in these areas, whereas some background staining is visible in the white pulp areas (which are negative for CD11b). The scale bar represents 500 µm.

Supplemental References

1 Winterbourn, C. C., Hampton, M. B., Livesey, J. H. & Kettle, A. J. Modeling the reactions of superoxide and myeloperoxidase in the neutrophil phagosome: implications for microbial killing. *J Biol Chem* **281**, 39860-39869 (2006).

2 Burton, N. A. *et al.* Disparate impact of oxidative host defenses determines the fate of Salmonella during systemic infection in mice. *Cell host & microbe* **15**, 72-83, doi:10.1016/j.chom.2013.12.006 (2014).

3 Imlay, J. A. in *EcoSal* (ed R. III.; Kaper Curtiss, J.B.; Squires, C.L.; Karp, P.D.; Neidhardt, F.C.; Slauch, J.M.) Ch. Modul 5.4.4, (ASM Press, 2009).

4 Seaver, L. C. & Imlay, J. A. Are respiratory enzymes the primary sources of intracellular hydrogen peroxide? *J Biol Chem* **279**, 48742-48750 (2004).

5 Beuzon, C. R. *et al.* Salmonella maintains the integrity of its intracellular vacuole through the action of SifA [published erratum appears in EMBO J 2000 Aug 1;19(15):4191]. *EMBO J.* **19**, 3235-3249 (2000).

6 Korshunov, S. S. & Imlay, J. A. A potential role for periplasmic superoxide dismutase in blocking the penetration of external superoxide into the cytosol of Gram-negative bacteria. *Mol Microbiol* **43**, 95-106 (2002).

7 Seaver, L. C. & Imlay, J. A. Hydrogen peroxide fluxes and compartmentalization inside growing Escherichia coli. *J Bacteriol* **183**, 7182-7189 (2001).

8 Makino, N., Sasaki, K., Hashida, K. & Sakakura, Y. A metabolic model describing the H2O2 elimination by mammalian cells including H2O2 permeation through cytoplasmic and peroxisomal membranes: comparison with experimental data. *Biochimica et biophysica acta* **1673**, 149-159, doi:10.1016/j.bbagen.2004.04.011 (2004).

9 Storkey, C., Davies, M. J. & Pattison, D. I. Reevaluation of the rate constants for the reaction of hypochlorous acid (HOCl) with cysteine, methionine, and peptide derivatives using a new competition kinetic approach. *Free radical biology & medicine* **73**, 60-66, doi:10.1016/j.freeradbiomed.2014.04.024 (2014).

10 Kundrat, P., Bauer, G., Jacob, P. & Friedland, W. Mechanistic modelling suggests that the size of preneoplastic lesions is limited by intercellular induction of apoptosis in oncogenically transformed cells. *Carcinogenesis* **33**, 253-259, doi:10.1093/carcin/bgr227 (2012).

11 Behar, D., Czapski, G., Rabani, J., Dorfman, L. M. & Schwarz, H. A. Acid dissociation constant and decay kinetics of the perhydroxyl radical. *The Journal of Physical Chemistry* **74**, 3209-3213, doi:10.1021/j100711a009 (1970).

12 Aurudi, R. L. R., A.B. Reactivity of HO_2/O^{-2} radicals in aqueous solution. *J Phys Chem Ref Data* **14**, 1041–1100 (1985).

13 Steeb, B. *et al.* Parallel exploitation of diverse host nutrients enhances salmonella virulence. *PLoS Pathog* **9**, e1003301 (2013).

14 Stroppolo, M. E. *et al.* Single mutation at the intersubunit interface confers extra efficiency to Cu,Zn superoxide dismutase. *FEBS Lett* **483**, 17-20 (2000).

15 Bull, C. & Fee, J. A. Steady-state kinetic studies of superoxide dismutases: properties of the iron containing protein from Escherichia coli. *Journal of the American Chemical Society* **107**, 3295-3304, doi:10.1021/ja00297a040 (1985).

16 Meir, E. & Yagil, E. Further characterization of the two catalases inEscherichia coli. *Current Microbiology* **12**, 315-319, doi:10.1007/bf01567889 (1985).

17 Baker, L. M. & Poole, L. B. Catalytic mechanism of thiol peroxidase from Escherichia coli. Sulfenic acid formation and overoxidation of essential CYS61. *J Biol Chem* **278**, 9203-9211 (2003).

18 Poole, L. B. Bacterial defenses against oxidants: mechanistic features of cysteine-based peroxidases and their flavoprotein reductases. *Arch Biochem Biophys* **433**, 240-254 (2005).

5.2 Antigen presenting cell-like neutrophils contribute to sepsis pathology and activate T-cell responses

Pascal Forrer[1], Matthias Kreuzaler[1], Claudia Stühler[1], Mauricio Rosas Ballina[2], Julien Roux[3], Jiagui Li[2], Christoph Schmutz[2], David Burckhardt[1], Fabian Franzeck[1,6], Matthias Gunzer[5], Daniela Finke[1], Alexander Schmidt[4], Dirk Bumann[2], Nina Khanna[1,6] *

[1]Department Biomedicine and University Hospital Basel, University of Basel, [2]Focal Area Infection Biology, Biozentrum, University of Basel, [3]Bioinformatics Core Facility, Department Biomedicine and University Hospital Basel, University of Basel, [4]Proteomics Core Facility, Biozentrum, University of Basel, CH-4056 Basel, [5]Institut für Experimentelle Immunologie und Bildgebung IMCES, University of Duisburg-Essen, D-45117 Essen, [6] Division of Infectious Diseases and Hospital Epidemiology, University Hospital of Basel.

* Corresponding author

Manuscript is ready for submission.

Statement of my work:

Design of experiments, Performance of experiments, Analysis of data, Recruitment of patients and healthy volunteers, Writing the paper.

Figure 1 (all); Figure 2 (Fig. 2A; Fig. 2B; Fig. 2C; Fig. 2E); Figure 3 (all); Figure 4 (all); Figure 5 (Fig. 5A; Figure 5B; Fig. 5E; Fig. 5F)

Note: The following part contains the whole manuscript.

Antigen presenting cell-like neutrophils contribute to sepsis pathology and activate T-cell responses

Pascal Forrer[1‡], Matthias Kreuzaler[1], Claudia Stühler[1], Mauricio Rosas Ballina[2], Julien Roux[3], Jiagui Li[2], Christoph Schmutz[2], David Burckhardt[1], Fabian Franzeck[1,6], Matthias Gunzer[5], Daniela Finke[1], Alexander Schmidt[4], Dirk Bumann[2], Nina Khanna[1,6] *

[1]Department Biomedicine and University Hospital Basel, University of Basel, [2]Focal Area Infection Biology, Biozentrum, University of Basel, [3]Bioinformatics Core Facility, Department Biomedicine and University Hospital Basel, University of Basel, [4]Proteomics Core Facility, Biozentrum, University of Basel, CH-4056 Basel, [5]Institut für Experimentelle Immunologie und Bildgebung IMCES, University of Duisburg-Essen, D-45117 Essen, [6] Division of Infectious Diseases and Hospital Epidemiology, University Hospital of Basel.

Correspondence and requests for materials should be addressed to nina.khanna@usb.ch.

Nina Khanna

Petersgraben 4

CH-4031 Basel

Phone: +41 61 328 7325

5.2.1 Abstract/ Summary

Sepsis is a detrimental disease manifested as dysregulated host immunity upon infection. Despite the unambiguous involvement of neutrophils in this fatal disease, there are very limited data about the molecular signaling mechanisms, phenotype and function in human neutrophils in sepsis. Here, we systematically elaborated the role of neutrophils in the inflammatory phase of sepsis to understand the aberrant neutrophil immune response. By using a large-scale proteomics and flow cytometry approach, we identified an antigen-presenting cell (APC)-like phenotype in neutrophils with major histocompatibility complex (MHC) class II molecule expression. These APC-like neutrophils could be induced by pro-inflammatory cytokines such as granulocyte-macrophage colony-stimulating factor (GM-CSF) and interferon-γ (IFN-γ) and were capable to activate T-cell clones upon antigen presentation. GM-CSF-stimulated neutrophils reorganized a complex network of phosphoproteins which in turn led to the activation of three major signaling pathways, the Janus kinase- signal transducer and activator of transcription (JAK-STAT), the mitogen-activated protein kinase (MAPK) and the phosphoinositide 3-kinase (PI3K)-Akt-mechanistic target of rapamycin (mTOR) pathways. The overrepresented MAPK kinase activity and the central JAK1/2 kinase orchestrated the downstream protein phosphorylation cascade, leading to the formation of the MHC class II enhanceosome via cAMP response element-binding protein 1 (CREB1) phosphorylation and class II major histocompatibility complex transactivator (CIITA) induction. In a mouse model of systemic salmonellosis, we could demonstrate the presence of APC-like neutrophils *in vivo*. These data show that neutrophil immune cell function in sepsis is highly versatile and goes far beyond simple pathogen destruction.

5.2.2 Introduction

Sepsis is the host inflammatory response to severe, life-threatening infections with the manifestation of organ dysfunction [164]. Sepsis imposes a detrimental global disease associated with high mortality and morbidity [165]. The global incidence is estimated up to 50 million annually [167], with estimated deaths up to 5.3 million [168]. Recently, the World Health Organization has recognized sepsis as a global health priority and implemented strategies to reduce this fatal disease [166]. Current medical treatment options are vastly limited and there is a high unmet medical need globally for new therapies [169].

Despite huge progress in the basic understanding of the pathophysiology of sepsis, the imbalances in the host immune system leading to sepsis are incompletely understood [170,171]. Host immunity in sepsis is disturbed in a paradox way, involving excessive inflammation, followed by immune suppression and an overall failure to return to normal immune homeostasis [168]. Metabolic reprogramming in immune cells raising aberrant immune responses is an emerging concept in sepsis [172].

Neutrophils as first line defense against invading pathogens play an explicit role to recognize, phagocytose and kill pathogens in sepsis. Pathogen elimination is crucially dependent on neutrophil recruitment to the site of infection [5]. Beside those beneficial neutrophil responses, neutrophils can contribute to the development of multiple organ failure in sepsis [190], most likely by aberrant regulation of NETosis [199]. Therefore, the precise orchestration of neutrophil immune responses is indispensable for a good outcome in sepsis.

Several studies have observed that circulating neutrophil cell counts are abnormally high and neutrophil lifespan is prolonged in sepsis [191]. Moreover, chemotactic activity seems to be reduced and neutrophil migration to the site of infection is impaired [191,192]. Recently, there are some rare reports supporting a role of atypical antigen-presenting cell (APC)-like neutrophils in sepsis [209]. Davey *et al.* found an APC-like phenotype of circulating neutrophils in acute human sepsis with increased levels of APC-associated molecules (CD86, CD64 and CD40), a phenotype that can be induced by unconventional T cells *in vitro* [210]. Delano *et al.* identified an immature Gr-1^{+}/ CD11b^{+} population in a murine mouse model of polymicrobial sepsis, which contributed to sepsis-induced T-cell suppression and T_H2 polarization [202]. Nevertheless, it is largely unknown how these APC-like neutrophils contribute in the pathophysiology of sepsis and which signaling mechanisms lead to an APC-like neutrophil phenotype. Moreover, the impact of neutrophils during septic immune responses are incompletely understood, mostly limited to a descriptive design and lack in a systematic analysis [191].

Novel approaches to elaborate the role of neutrophils in sepsis are urgently needed and a systematic understanding of the inflammatory, dysregulated immune response will have crucial implications for the development of new therapeutic approaches in sepsis. The purpose of the study was to characterize the phenotype, function and signaling mechanisms in neutrophils in the inflammatory phase of sepsis.

5.2.3 Research highlights

- This report systematically elaborated the role of human neutrophils in the inflammatory phase of sepsis to understand the aberrant immunological neutrophil response in this fatal disease.
- We could demonstrate with a proteomics approach and flow cytometry that human neutrophils in sepsis within a pro-inflammatory milieu are shifting into a novel APC-like phenotype with elevated MHC class I and *de novo* induced MHC class II molecule expression.
- MHC class I and MHC class II expression on human neutrophils could be induced by pro-inflammatory cytokines GM-CSF (for MHC class II) and IFN-γ (for MHC class I and MHC class II) after 48h in culture and were capable to activate T-cell clones upon peptide stimulation.
- GM-CSF stimulation in neutrophils alters the phosphorylation of a complex network of proteins involved in 3 major signaling pathways, the JAK-STAT, the MAPK and the PI3K-Akt-mTOR pathways, with overrepresented MAPK kinase activity and a central JAK1/2 kinase orchestrating the broad downstream protein phosphorylation. Moreover, we could link GM-CSF signaling to the formation of the MHC class II enhanceosome via CREB1 phosphorylation at serine 133.
- We could demonstrate that the MAPK-p38-MSK1-CREB1 signaling cascade contributes to *de novo* MHC class II induction in neutrophils and the MHC class II transactivator CIITA is highly expressed after 4h stimulation with GM-CSF *in vitro*, in agreement with experimental data for IFN-γ-stimulated, non-constitutive MHC class II expression in human vascular endothelial cells and macrophages.
- In a mouse model of systemic salmonellosis that mimics important aspects of human typhoid fever, we confirmed the presence of APC-like neutrophils *in vivo*, strongly supporting the results found in human sepsis.

5.2.4 Results

Neutrophils mimic APC-like phenotype in patients with sepsis

Neutrophils from 34 sepsis patients and healthy controls, matched for age (74 years versus 76 years; N=23,10; P>0.05; Fig. S1A) and body mass index (25.3 kg/m^2 versus 25.5 kg/m^2; N=18,10; P>0.05; Fig. S1B), were investigated. Baseline characteristics are listed in Table 1. In accordance with literature[165,191,220], we found significantly increased absolute numbers of circulating neutrophils and decreased reactive oxygen species (ROS) production in response to bacterial and fungal stimuli in sepsis patients compared to healthy controls (74 x 10^6 cells versus 41.1 x 10^6 cells in total per 15ml blood; N=21,10; P<0.01; Fig. 1A, Fig. S1D). Neutrophils viability was 99% in both, healthy controls and sepsis patients (Fig. S1C). Moreover, sepsis patients showed a significantly higher neutrophils-to-lymphocyte ratio (NLR, Fig. S1E), an inflammation marker and potential predictor for poor disease outcome [221]. In a systematic proteomics approach, we identified in total 2204 peptides with mass spectrometry, of these 380 peptides were significantly changed in sepsis (Fig. 1B, 317 peptides upregulated, 63 downregulated, p-value < 0.02). Metacore Enriched Pathway Analysis identified antigen presentation by MHC class I and II as strongly enriched in patients with sepsis (*Antigen presentation by MHC class I,* p-value = 10^{-9}; *Antigen presentation by MHC class I: Cross-presentation,* p-value = 10^{-6}; *Antigen presentation by MHC class II*, p-value = 10^{-2}; Fig. 1C, Fig. S1F). GO Enrichment Analysis of Processes and Molecular Functions confirmed antigen processing and presentation as highly enriched in sepsis (Fig. S1G; Fig. S1H).

We identified 21 proteins involved in antigen presentation by MHC class I and II that were significantly changed upon sepsis (Fig. 1D, threshold set at p-value < 0.02, ratio cut off (log2) > 0.6, and Fig. S1I). We identified three strongly upregulated MHC class I proteins (1B42, 1B73, 1B45), five endoplasmic reticulum-to-golgi peptides (SC23A, RB27A, HYOU1, SC24D, VAMP3), one molecule in the TAP complex (TAP1), one aminopeptidase (ERAP1), tapasin (TPSN), calreticulin (CALR), one protein of the 26S proteasome complex (PSD12) and two proteins of the 20S core proteasome complex (PSB2, PSB4), all contributing to antigen processing and presentation by MHC class I and MHC class II molecules to the adaptive immune system [222-224] (Fig. 1E, Fig. S1J). These data strongly suggested that neutrophils might have acquired antigen presentation capacity in sepsis. To verify the proteomics data, we elaborated surface expression of MHC class I and II on neutrophils with flow cytometry. Surface staining for HLA-A, -B, -C confirmed a 1.57-fold increase in MHC class I levels (MFI_{sepsis} = 35304, $MFI_{control}$ = 22418, Fig. 1F) and *de novo* induction of MHC class II expression (0.93% and 4.11% HLA-DR/ -DP/ -DQ$^+$ PMN in controls and sepsis patients, respectively, Fig. 1G) on neutrophils in sepsis. Additionally,

increased surface expression of single HLA-DR and the invariant chain Li (CD74) strongly supported *de novo* MHC class II induction in sepsis (Fig. S1K).

Since sepsis is considered to be a heterogeneous, inflammatory host response to an infection [165,168], we analyzed blood serum samples from patients and controls for their particular inflammatory cytokine signature. Interleukin-6 (IL-6), granulocyte-macrophage colony-stimulating factor (GM-CSF), interferon-gamma (IFN-γ), monocyte chemotactic protein 1 (MCP-1, also known as CCL2), and interleukin-18 (IL-18) were significantly elevated in plasma samples from sepsis patients (Fig. 1H), whereas interleukin-8 (IL-8), interleukin-1beta (IL-1β), interleukin-17 (IL-17A), interleukin-23 (IL-23), interleukin-10 (IL-10), tumor necrosis factor- alpha (TNF-α) were not changed and interleukin-12 (IL-12) and interleukin-33 (IL-33) were not detectable (below standard curve range) (Fig S1L).

Taken together, we could demonstrate with a large-scale proteomics approach and flow cytometry that human neutrophils in sepsis are modulated to APC-like phenotype with elevated MHC class I and *de novo* induced MHC class II expression. Moreover, neutrophils in sepsis are in a cytokine-rich, pro-inflammatory environment with high levels of IL-6, GM-CSF, IFN-γ, MCP-1 and IL-18.

GM-CSF and IFN-γ induce APC-like phenotype in human neutrophils *in vitro,* reduce neutrophil apoptosis and stimulate T-cell clones upon antigen presentation

Next, we investigated the capability of those cytokines with increased levels in sepsis to induce APC-like phenotype in human neutrophils. IFN-γ was able to upregulate HLA-A, -B, -C on neutrophil surface after 24h of cultivation (Fig. S2A, top; mRNA level for *HLA-B* and *B2M* in Fig. S2A, bottom). GM-CSF and IFN-γ were able to induce *de novo* HLA-DR/ -DP/- DQ expression after 48 hours of incubation, whereas IL-6 and IL-18 had no effect on MHC class I or II expression (Fig. 2A-C). In parallel, we found that GM-CSF and IFN-γ prolonged neutrophil survival (Fig. 2A, upper panel and Fig. S2B). To clarify whether *de novo* HLA-DR/ -DP/- DQ expression is not only the consequence from prolonged neutrophil survival, we used a low-dose, effective Pan-Caspase inhibitor q.OPh [225] (Fig. S2E) to reduce neutrophil apoptosis *in vitro* (Fig. 2A-C, Fig. S2A-C). The Caspase inhibitor q.OPh reduced the extrinsic (via Caspase-8, Caspase-3) and intrinsic Caspase (via Caspase-9, Caspase-3)-mediated cell death pathway (Fig. S2D), but did neither affect *de novo* HLA-DR/ -DP/- DQ expression nor HLA-A, -B, -C induction on human neutrophils (Fig. 2B, Fig. S2A). *De novo* induction of HLA-DR and CD74 (Li) by GM-CSF and IFN-γ stimulation was further confirmed on RNA level (Fig. 2E).

Previous reports described an APC-like phenotype mostly in immature neutrophil populations [157]. To determine if mature neutrophils are able to develop an APC-like phenotype, we visualized single cells by Image Stream X. The HLA-DR/ -DP/- DQ molecule co-localizes with surface marker CD66b (Fig. 2D). Notably, HLA-DR/ -DP/- DQ^+ neutrophils had segmented nuclei morphology, indicating that neutrophils expressing APC-like molecules are mature [226] (Fig. 2D, gating strategy for Image Stream X in Fig. S2F, higher magnification in Fig. 2F).

Next, we wanted to know whether HLA-DR^+ neutrophils are capable of antigen presentation to an autologous peptide-specific $CD4^+$ T-cell clone *in vitro*. For that reason, we stimulated neutrophils with GM-CSF and IFN-γ for 48 hours, pulsed them with a specific peptide and measured $CD4^+$ T-cell activation by intracellular cytokine staining for IFN-γ and TNF-α [227] (Fig. 2G, middle and right panel). Autologous dendritic cells (DCs) were used as a positive control. Although our data show that APC-like neutrophils are capable to present peptides and activate $CD4^+$ T cells *in vitro*, it is still a minor effect compared to professional APCs such as DCs.

Together, these data show that the pro-inflammatory cytokines GM-CSF and IFN-γ can reduce neutrophil apoptosis *in vitro* and are able to induce *de novo* expression of MHC class II on mature neutrophils after 48h in culture (Fig. S2G). Moreover, these cytokine-primed APC-like neutrophils are able to induce autologous $CD4^+$ T-cell activation *in vitro*.

GM-CSF signaling leads to the activation of JAK-STAT, MAPK p38 and Akt- mTOR signaling pathways and phosphorylation of transcription factor CREB1

Next, we wondered which signaling pathways are responsible for cytokine-induced MHC class II expression on neutrophils. Since the IFN-γ signaling pathway associated with MHC class II induction is well described in human vascular endothelial cells and macrophages [143,228], we focused on GM-CSF-induced MHC class II expression. Previous studies have already shown that GM-CSF signaling in neutrophils affects diverse cellular processes such as survival, proliferation, differentiation and ROS production [229]. For that reason, we used a label-free quantitative phosphoproteomics strategy and analyzed phosphorylation by liquid chromatography-tandem mass spectrometry, as previously described [230] (Fig. 3A). In human neutrophils stimulated *in vitro* for 30 minutes with GM-CSF, we detected 3579 phosphopeptides. 858 phosphopeptides showed significantly changed phosphorylation (n=466) or desphosphorylation (n=392) status (Fig. S3A-C, q-value < 0.05).

The majority of significant phosphorylation and dephosphorylation events were identified on serine and threonine residues (Fig. S3A). As a control, neutrophil stimulation with GM-CSF induced optimal STAT5 phosphorylation after 30 minutes *in vitro* (Fig. S3D). The phosphoproteomics data set revealed the induction of MAPK signaling, JAK-STAT and PI3K-Akt-mTOR signaling pathways after GM-CSF stimulation *in vitro* (Fig. 3B), in agreement with literature [231]. We confirmed the involvement of those 3 identified pathways by flow cytometry using phospho-STAT5 (pY694), phospho-mTOR (pS2448), phospho-Akt (pS473), and phospho-p38 (pT180/pY182) (Fig. 3D) and pharmacological inhibition to JAK1/2 (Ruxolitinib), PDK-1 (BX-745), Akt (MK-2206) and mTORC1/2 (PP242). JAK1/2 inhibition with Ruxolitinib at non-toxic concentrations (data not shown) led to full inhibition of STAT5, mTOR, Akt and p38 phosphorylation in human neutrophils (Fig. 3E). To identify overrepresented phosphorylation motifs in the phosphoproteome, we applied the motif extraction by Motif-X algorithm [232,233]. We found ten distinctive motif sequences with central serine phosphorylation (Fig. 3C, left, q-value < 0.05), including the motifs SP, RXXS, PXSP, RXS, and RXRXXS. By using an experimentally verified kinase prediction tool collecting phosphorylation sites from PhosphoELM and SwissProt (RegPhos 1.0, www.regphos-mbc.nctu.edu.tw [234]) and using extensive literature research, we predicted MAPK signaling as predominantly represented (JNK, p38, ERK signaling for SP motif [234]; RSKs, MSK1/2 for RXXS motif [230,235]; MEK/ ERK2 signaling for PXSP motif [235,236,237]), whereas Akt (or AGC kinase family for RXRXXS [230]) signaling was less prominent (Fig. 3C).

We further identified an important candidate linking GM-CSF signaling to APC-like phenotype, the cyclic AMP response element-binding protein1 (CREB1) [143,238] (Fig. 3B). CREB1 phosphorylation is an essential part in the formation of the MHC class II enhanceosome, consequently leading to the induction of MHC class II gene expression [239].

Taken together, these results show that GM-CSF stimulation in neutrophils alters the phosphorylation of a complex network of proteins involved in 3 major signaling pathways, the JAK-STAT, the MAPK and the PI3K-Akt-mTOR pathways (Fig. S3E), with overrepresented MAPK kinase activity and a central JAK1/2 kinase orchestrating the broad downstream protein phosphorylation. Moreover, we could link GM-CSF signaling to the potential formation of the MHC class II enhanceosome via CREB1 phosphorylation at serine 133.

Targeting the MHC class II enhanceosome in human neutrophils

Next, we aimed to identify the responsible kinase for CREB1 phosphorylation at residue Ser133 in neutrophils. Potential candidates for CREB1 phosphorylation are the kinases mitogen- and stress-activated protein kinase-1 (MSK1), p90 ribosomal S6 kinase ($pp90^{RSK}$), Akt and protein kinase A (PKA). Using pharmacological inhibitors specifically targeting these kinases, we could demonstrate that only MSK1 inhibition significantly reduces CREB1 phosphorylation (Fig. 4A, right; representative example for CREB1 phosphorylation at Ser133, Fig. 4A, left; Fig. S4A). Again, JAK1/2 inhibition led to the full inhibition of CREB1 phosphorylation, in agreement with our previous finding that JAK 1/2 is not only necessary for the JAK-STAT pathway, but also involved in the MAPK and the PI3K-Akt-mTOR signaling pathways (Fig. 3E).

Next, we investigated the link of CREB1 phosphorylation with the induction of *de novo* MHC class II expression in neutrophils. Pre-treatment with various, non-toxic concentrations of CREB1-CBP protein interaction inhibitor [240] and consecutive stimulation with GM-CSF for 48h showed a dose-dependent reduction up to 70% in HLA-DR/ -DP/ -DQ surface expression on neutrophils (Representative example, Fig. 4D, left; Summary in Fig. 4D, right), whereas CREB1 on a transcriptional level was not affected by GM-CSF stimulation (Fig. 4C). Secondly, pharmacological inhibitors to JAK1/2, p38 and MSK1, but not to MEK1/2 and ERK, inhibited HLA-DR/ -DP/ -DQ surface expression on neutrophils (Fig. 4E), strongly supporting the role of MAPK-p38-MSK1-CREB1 signaling axis as driver for *de novo* MHC class II induction on neutrophils.

In addition to CREB1 phosphorylation [239], the transcriptional control of MHC class II gene expression is tightly regulated in cell types such as human endothelial cells and monocytes-macrophages by another 3 key factors (reviewed in [143]), namely the MHC class II transactivator CIITA [241,242], NFY [243] and the RFX complex (composed of RFX5 [244], RFXAP [245] and RFXANK[246]. Therefore, we investigated whether *de novo* MHC class II expression in neutrophils uses a similar mechanism. We tested *CIITA* mRNA levels 4h, 24h and 48h after GM-CSF stimulation and found a 100-fold *CIITA* upregulation after 4h, with a gradual decrease over time (Fig. 4B). *CIITA* induction could be fully blocked using a JAK1/2 inhibitor (Fig. S4B), again accentuating the central role of JAK1/2 signaling for MHC class II induction in neutrophils. However, *NFYa*, *RFXank* and *CREB* mRNA levels were not affected by GM-CSF stimulation (Fig. 4C), in agreement with literature that stresses CIITA as the master transcriptional regulator of the MHC class II enhanceosome [143,242]. To summarize, we could demonstrate that GM-CSF-induced *de novo* expression of MHC class II on neutrophils is mediated by the same MHC class II enhanceosome that also regulates IFN-γ-induced, non-constitutive MHC class II expression in human vascular endothelial cells and macrophages [228].

GM-CSF-induced MHC class II induction is mediated by a MAPK-p38-MSK1-CREB1 signaling cascade and the MHC class II transactivator CIITA in a strictly JAK1/2 kinase-dependent manner (Fig. 4F).

Induction of APC-like neutrophils in a systemic *Salmonella* mouse model mimicking human typhoid fever

To investigate the relevance of APC-like neutrophils *in vivo*, we used a well-established mouse model of systemic salmonellosis [247,248]. To demonstrate the homology of this model to human sepsis, we compared the proteome data sets obtained from splenic neutrophils of mice infected with *Salmonella enterica* serovar Typhimurium with the proteome data sets from human sepsis patients. Splenic proteome analysis from sorted PMN ($CD11b^+$, $Ly6C^{Int}$, $Ly6G^+$) of infected mice compared to uninfected mice at day 4 post infection (Fig. S5A) identified 2223 peptides in total, of which 595 peptides were significantly changed upon *Salmonella* infection (Fig. S5B, 503 peptides upregulated, 92 downregulated, p-value < 0.03, fold change > 1.5). Comparable to the data obtained in sepsis patients, the analysis revealed a significant change in antigen processing and presentation pathways in infected mice (Fig. 5E; Fig. S5B-E). Comparison of the human and murine data sets in terms of common differential protein expression by using one-to-one orthologous homology information from the Ensembl database [249-251] identified in total 1157 orthologous proteins in humans and mice (Fig. 5F). 52 orthologous proteins were differentially expressed in both species during infection, most of them are linked to antigen presentation and processing pathways (FDR<0.05; Fig. S5F), clearly indicating that the systemic salmonellosis model is ideally suited to investigate APC-like neutrophils in a mouse model.

Next, we investigated the kinetics of neutrophil MHC class II induction during the course of infection in different organs, such as blood, bone marrow, spleen and liver. In the systemic *Salmonella* infection model, bacteria replicate early in spleen and liver and disseminate to the blood and bone marrow during the peak of infection at day 4 (Fig 5D). Interestingly, APC-like neutrophils ($CD45^+$/ $CD11b^+$/ $Ly6G^+$/ $Ly6C^{int}$) expressing MHC class II were present in all organs starting 2 days after infection and MHC class II expression did not directly correlate with bacterial load (Fig. 5C, splenic example dot plot in Fig. 5B).

In conclusion, these *in vivo* data substantiate the suitability of the systemic salmonellosis mouse model as appropriate model to study bacterial sepsis and confirm the induction of APC-like neutrophils during sepsis, revealing the vast heterogeneity and diversity of neutrophils under inflammatory conditions.

5.2.5 Discussion

Neutrophils in sepsis are believed to execute direct pathogen killing. In this study, we identified a subset of neutrophils with antigen-presenting properties during the hyperinflammatory phase of sepsis. These MHC class II$^+$ neutrophils can be induced by GM-CSF and IFN-γ via the formation of the MHC class II enhanceosome and are able to present antigens and activate antigen-specific T-cell clones. Furthermore, these findings could be confirmed in a mouse model of systemic *Salmonella* infection, where this APC-like neutrophil subset already appears after 2 days of infection with cellular protein changes involved in antigen processing and presentation. Thus, the role of neutrophils in sepsis seems to go beyond direct pathogen killing mechanisms and is pointing towards immunoregulatory functions in sepsis.

Moderate levels of MHC class II on neutrophils have been previously identified in human autoimmune diseases such as Wegener's granulomatosis [252,253] and rheumatoid arthritis [153]. However, it is controversially discussed whether similar mechanisms exist in the context of bacterial infections. In our study, we found that during the early phase of sepsis, neutrophils acquire antigen-presenting cell characteristics. Simultaneously high levels of IFN-γ and GM-CSF are detected in plasma of sepsis patients. This is in line with previous reports [148,252,254,255] that show that both cytokines GM-CSF and IFN-γ can induce *de novo* MHC class II transcription and surface expression on human neutrophils. Thus, we believe that the inflammatory conditions and not bacterial infection *per se* triggers the induction of APC-like neutrophils in sepsis.

While previous work has focused on proteomic changes of secreted proteins from *ex vivo* stimulated neutrophils with cytoB/fMLF from sepsis patients [256], this is to our knowledge the first study investigating comprehensively the proteomic changes in neutrophils from human and mouse sepsis. Despite patient heterogeneity, individual medical treatment and differences among species, the human neutrophil proteome in sepsis shares 36% of homologous protein regulation with the mouse neutrophil proteome in gram-negative infection (FDR < 0.05). Most of the identified proteins are linked to the cellular machinery involved in antigen presentation and processing.

Our work adds to a recent study showing that MHC class II and costimulatory molecules are induced in the presence of antigen and antigen-specific memory CD4$^+$ T cells [163]. Most likely, antigen-specific memory CD4$^+$ T-cell derived cytokines such as GM-CSF and IFN-γ induce the observed MHC class II expression on neutrophils *in vitro,* as we demonstrated in our study. Supporting this idea, we could observe that antigen-specific CD4$^+$ T cell clones produce large amounts of GM-CSF and IFN-γ upon activation [257].

However, it should be noted that all *in vitro* studies (including our group) have used high cytokine levels at non-physiological levels (ranging from 1-100 ng/ml) to induce APC-like phenotype. It remains speculative whether neutrophils *in vivo* encounter these somehow artificial conditions. Therefore, it would be relevant to measure local, heterogeneous cytokine concentration gradients among tissues and organs *in vivo*.

Among GM-CSF, IFN-γ and other cytokines [258], high levels of IL-3, a close family member of GM-CSF [259], has been recently linked to high mortality in human sepsis. The authors have showed that IL-3 potentiates acute inflammation and contributes majorly to the observed "cytokine storm" in the inflammatory phase of sepsis [176]. However, it is unclear from that study whether IL-3 also induces APC-like neutrophil phenotype and whether APC-like neutrophils contribute to the observed cytokine storm. Future studies might clarify this issue.

We further investigated signaling mechanisms that control *de novo* MHC class II expression in neutrophils. Previous studies could show that the control of *de novo* MHC class II expression is tightly regulated by several key factors (reviewed in [143]), namely the MHC class II transactivator CIITA [241,242], CREB1 [239], NFY [243] and the RFX complex (composed of RFX5 [244], RFXAP [245] and RFXANK[246]) and that genetic deficiencies in those key factors can cause severe pathologies such Bare Lymphocyte syndrome (BLS) [241] and lymphoid cancers [260]. However, since these studies on *de novo* MHC class II induction have been restricted to the IFN-γ signaling pathway in human vascular endothelial cells and macrophages [143,228], it is vastly unclear how GM-CSF-mediated signaling factors are related to the induction of MHC class II molecules in any cell type. In this study, we found that GM-CSF phosphorylates CREB1 at Ser133 *in vitro* and that CREB1-CBP protein interaction inhibition strongly decreases *de novo* HLA-DR/ -DP/- DQ expression on neutrophil surface. Further, we could demonstrate that GM-CSF-mediated signaling leads to the induction of *CIITA* mRNA transcription, whereas *NFY* and *RFX* levels are not affected. Conclusively, our data highlight for the first time a major role of GM-CSF-induced CREB1 phosphorylation and CIITA induction in APC-like neutrophils.

Furthermore, it is known that CREB1 is a substrate for various cellular kinases [261] such as MSK1 [262], pp90^{RSK} (or RSK2) [263], Akt [264], PKA [265] and MAPKAP-2 [266]. By using pharmacological inhibitors specifically targeting these kinases, we demonstrated that MSK1 inhibition significantly reduces CREB1 phosphorylation, whereas the other inhibitors targeting pp90^{RSK}, Akt and PKA did not affect CREB1 phosphorylation. We therefore strongly support the role of MAPK-p38-MSK1-CREB1 signaling axis as driver for *de novo* MHC class II induction on human neutrophils. Another group has shown that LPS or TNF-stimulated human neutrophils use the same p38-MSK1-CREB1 axis to produce cytokines [267].

Therefore, we postulate that CREB1 is an important transcription factor that regulates a vast repertoire of immune responses in neutrophils in inflammation.

In the present study, we were able to demonstrate that JAK1/2 inhibition at non-toxic concentrations leads to full inhibition of GM-CSF-mediated STAT5, mTOR, Akt, p38 and CREB1 phosphorylation in human neutrophils, rendering JAK1/2 an interesting drug target in neutrophils to cease a huge variety of signaling pathways at once (Abstract online by Lopez et al., Blood 2017 130:4805), inclusive those signaling events leading to APC-like phenotype. So far, the clinical use of JAK1/2 inhibitors is approved in patients suffering from myelofibrosis and rheumatoid arthritis and they are currently in the clinical development targeting several indications such as graft-versus-host-disease, pancreatic cancer, and myeloproliferative diseases (www.clinicaltrials.gov, recently reviewed by [268]). It remains to be elucidated whether JAK1/2 inhibitors may be useful as a treatment option during the course of sepsis.

HLA-DR/ -DP/- DQ surface molecule expression on neutrophils co-localizes with CD66b, a specific marker consistently expressed on human neutrophil surface independent of the cell location, level of activation and disease state [269]. Interestingly, nuclear stainings revealed that those HLA-DR/ -DP/- DQ^+ neutrophils show a segmented nuclei morphology, classically known for mature neutrophils [226]. This finding is contrary to a report showing "APC-like hybrid tumor-associated neutrophils (TANs)" in early stage lung cancer that exhibit characteristics of neutrophils and antigen-presenting cells with a round, immature cell morphology [157]. These discrepancies in relation to nuclear morphology could be partially explained by the various factors involved in extravasation and the local tumor microenvironment that may influence neutrophil nuclear phenotype.

Neutrophils are limited in lifespan and difficult to cultivate *ex vivo* [22,270]. We could clearly identify a trade-off situation between neutrophil apoptosis and *de novo* HLA-DR/ -DP/- DQ expression over time. Both, GM-CSF and IFN-γ have the capacity to reduce neutrophil apoptosis *in vitro* [20,21]. Therefore, it is unclear whether *de novo* HLA-DR/ -DP/- DQ expression is the logical consequence of prolonged neutrophil survival in this *in vitro* system. For that reason, we used a low-dose, effective Pan-Caspase inhibitor q.OPh [225] to reduce neutrophil apoptosis *in vitro.* The Caspase inhibitor q.OPh reduces the extrinsic and intrinsic Caspase-mediated cell death pathway, but does not affect *de novo* HLA-DR/ -DP/- DQ expression on human neutrophils. Conclusively, we assume that apoptosis progression and *de novo* induction of MHC class II are two distinguished, intrinsic programs in neutrophils. Moreover, the substantial reduction of neutrophil apoptosis by using Pan-Caspase inhibitor q.OPh is an indispensable tool to avoid unspecific contamination and binding in experimental procedures such as RNA isolation and T-cell activation assays *in vitro*.

Classical APCs such as DCs and macrophages orchestrate adaptive immune response by T-cell activation. Our data show that APC-like neutrophils are capable to present peptides and activate autologous $CD4^+$ T cell clones *in vitro*. However, T-cell activation by APC-like neutrophils is moderate compared to professional APCs such as DCs, in agreement with Vono *et al* [163]. By the fact that we were not able to induce $CD4^+$ T-cell proliferation *in vitro* (data not shown), it remains speculative how precisely APC-like neutrophils regulate adaptive immune responses *in vivo* and how they effectively contribute to infection control. Further experiments using neutrophil-specific conditional knockout mice defective in MHC class II could help to unravel this fundamental question in future experiments.

In conclusion, this comprehensive analysis of neutrophil immunity in sepsis reveals that neutrophils are not only simple foot soldiers that kill pathogens, but also express features of atypical APCs when they are exposed to a GM-CSF and IFN-γ-rich cytokine environment. Despite the ability to induce T-cell responses *in vitro* by APC-like neutrophils, their precise role in infection *in vivo* needs to be clarified, whether they act as friend or foe. Moreover, the MAPK-p38-MSK1-CREB1 axis drives atypical APC-like neutrophil phenotype and targeting this particular pathway could have crucial impact in the development of new therapies in sepsis.

5.2.6 Methods

Patients and healthy volunteers

The single-center prospective clinical study was performed at the University Hospital Basel, Switzerland. In total, 34 participants with confirmed gram-negative bacteremia (2 or more diagnostic criteria for systemic inflammatory response syndrome (SIRS) [271] plus confirmed presence of gram-negative bacteria in blood culture, n=24) and healthy controls (n=10) matching for age and body mass index were recruited between June and November of 2016. Exclusion criteria for patients and controls were pregnancy and lipid disorders. One patient was excluded due to technical reasons (P6). The study was approved by the ethical committee Nordwest- and Zentralschweiz (BASEC Project ID: 2016-00676) and was in agreement with the Declaration of Helsinki and Good Clinical Practice (GCP) Guidelines.

Patient severity was determined according to the recommendations of the Third International Consensus Definitions for Sepsis and Septic Shock (Sepsis-3) [272]. Namely, patients with bacteremia/ infection that fulfilled 2 or more criteria of the quick Sequential Organ Failure Assessment (qSOFA) score were considered to possibly have sepsis (i.e. bacteremia plus organ dysfunction). Patients with bacteremia receiving vasopressor therapy required to maintain mean arterial pressure above 65 mmHg and lactate levels >2 mmol/L despite adequate fluid resuscitation were considered to have septic shock. Peripheral blood was drawn within 24h of confirmed bacteremia. Plasma was obtained by centrifugation (10min, 1'600 x g).

Human PMN isolation

Human PMN were isolated as previously described [46,273]. In brief, human peripheral blood was collected in 7.5 ml polyethylene tubes containing 1.6 mg EDTA/ml blood (Sarsted), mixed with 3% Dextran (Pharmacia) / NaCl solution. The leukocyte-rich plasma was transferred to a discontinuous Percoll gradient with 53% and 67% Percoll (GE Healthcare). Percoll Gradient centrifugation was performed for 30 min at 1400 rpm, 4°C, no braking. The visible ring containing PMN fraction was collected and washed in 0.9% NaCl, resuspended in RPMI (Invitrogen Gibco) + 10% fetal bovine serum (FBS) respectively 10% human serum. Cells were counted with Türk solution and an automatic cell counter system ADAM (Digital Bio). Purity and viability was routinely >97% and >99%, respectively.

Pathogen cultures

Salmonella strains used in this study were derived from *Salmonella enterica* serovar Typhimurium *SL1344 hisG rpsL xyl* [274,275]. *Salmonella* were cultured at 37°C with aeration (200 rpm) in Lennox LB. *Salmonella* were grown to mid-log phase, washed twice in phosphate-buffered saline (PBS) used for *in vivo* experiments. Heat-inactivation was performed at 99°C for 15 min. Heat-inactivated *Salmonella* were opsonized in 10% human serum in PBS for 20 min at 37°C, washed with PBS, and diluted to MOI 200 for immediate use (heat-inactivated *Salmonella*).

Candida albicans SC5314 was grown overnight in yeast peptone dextrose (YPD, BD Difco) media at 37°C as previously described [46]. A subculture was inoculated 1:100 and grown to mid-log phase. *C. albicans* was washed twice with 0.9% NaCl and heat-inactivated at 95°C for 1h. *C. albicans* was opsonized in 10% human serum in PBS for 20 min at 37°C, washed with PBS and diluted to MOI 1 for immediate use.

Inhibitors and cytokines

Ruxolitinib (JAK1/2 inhibitor, Cat. No. S1378), PD98059 (MEK1 inhibitor, Cat. No. S1177), Trametinib (MEK1/2 inhibitor, Cat. No. S2673), Wortmannin (PI3K inhibitor, Cat. No. S2758), Neratinib (EGFR1/2 inhibitor, Cat. No. S2150), LY294002 (PI3K inhibitor, Cat. No. S1105), IPA-3 (PAK1 inhibitor, Cat. No. S7093), BX-795 (PDK-1 inhibitor, Cat. No. S1274), MK-2206 (Akt1/2/3 inhibitor, Cat. No. S1078), BI-D1870 (RSK1-4 inhibitor, Cat. No. S2843), PF-4708671 (S6K1 inhibitor, Cat. No. S2163), SB203580 (p38 MAPK inhibitor, Cat. No. S1076), SCH772984 (ERK1/2 inhibitor, Cat. No. S7101), H89 (PKA inhibitor, Cat. No. S1582), PP242 (mTORC1/2 inhibitor, Cat. No. S2218), Rapamycin (mTORC1 inhibitor, Cat. No. S1039), Atorvastatin (HMG-CoA Reductase inhibitor, Cat. No. S2077), Lovastatin (HMG-CoA Reductase inhibitor, Cat. No. S2061) were obtained from Selleckchem, SB747651A (MSK1 inhibitor, Cat. No. 4630) was obtained from Tocris, CAS 92-78-4 (CREB-CBP inhibitor, Cat. No. 217505) was obtained from Calbiochem. Human recombinant GM-CSF, IFN-γ, IL-6 and IL-18 were ordered by Peprotech.

Sample preparation for Proteomics (LC-MS) analysis

$5x10^5$ freshly isolated human neutrophils were used for proteomics analysis. Cells were washed twice with PBS (Sigma) and were lysed in 200 µl lysis buffer (2% sodium deoxycholate (SDC), 0.1 M ammoniumbicarbonate) using strong ultra-sonication (two cycles of sonication S3 for 10 seconds, Hielscher Ultrasonicator). Protein concentration

was determined by BCA assay (Thermo Fisher Scientific) using a small sample aliquot. 50µg of proteins were digested as described previously [276], reduced with 5 mM TCEP for 15 min at 95 °C and alkylated with 10 mM iodoacetamide for 30 min in the dark at 25 °C. After diluting samples with 100 mM ammonium bicarbonate buffer to a final DOC concentration of 1%, proteins were digested by incubation with sequencing-grade modified trypsin (1/50, w/w; Promega, Madison, Wisconsin) overnight at 37°C. Then, the samples were acidified with 2 M HCl to a final concentration of 50 mM, incubated for 15 min at 37 °C and the precipitated detergent removed by centrifugation at 10,000xg for 15 min. Subsequently, peptides were desalted on C18 reversed-phase spin columns according to the manufacturer's instructions (Microspin, Harvard Apparatus) and dried under vacuum.

TMT labeling and HpH-fractionation

The dried peptide samples were subsequently labeled with isobaric tag (TMT 10-plex, Thermo Fisher Scientific) according to the manufacturer's instructions. To control for ratio distortion during quantification, a peptide calibration mixture consisting of six digested standard proteins mixed in different amounts were added to each sample before TMT labeling as recently described [276]. After pooling the TMT labeled peptide samples, peptides were again desalted on C18 reversed-phase spin columns according to the manufacturer's instructions (Macrospin, Harvard Apparatus) and dried under vacuum. TMT-labeled peptides were fractionated by high-pH reversed phase separation using a XBridge Peptide BEH C18 column (3,5 µm, 130 Å, 1 mm x 150 mm, Waters) on an Agilent 1260 Infinity HPLC system. Peptides were loaded on column in buffer A (ammonium formate (20 mM, pH 10) in water) and eluted using a two-step linear gradient starting from 2% to 10% in 5 minutes and then to 50% (v/v) buffer B (90% acetonitrile / 10% ammonium formate (20 mM, pH 10) over 55 minutes at a flow rate of 42 µl/min. Elution of peptides was monitored with a UV detector (215 nm, 254 nm). A total of 36 fractions were collected, pooled into 12 fractions using a post-concatenation strategy as previously described [277], dried under vacuum and subjected to LC-MS/MS analysis.

Sample preparation for Phosphoproteomic Analysis

Samples were prepared as previously described [230]. In brief, for each condition, 10^8 neutrophils were stimulated for 30 minutes without or with GM-CSF. Next, the cells were put on ice and washed twice with ice-cold PBS. Samples were collected in urea solution (8M Urea (AppliChem, Darmstadt, Germany), 0.1M Ammoniumbicarbonate (Sigma, St. Louis, MO), 0.1% RapiGest (Waters, Milford, MA) in the presence of phosphatase inhibitor

1x PhosSTOP (Roche, Basel, Switzerland). Supernatants were collected and stored at -80°C for further processing. BCA Protein Assay (Pierce, Rockford, IL) was used to measure protein concentration.

Phosphopeptide Enrichment for Phosphoproteomics

2mg of total protein lysate was digested with trypsin, cleaned up using an C18 column and enriched for phosphorylated peptides using titanium dioxide beads as described [230]. After C18-cleanup, 1 µg of peptides were LC-MS analyzed as described below with the following changes; the normalized collision energy was set to 27%, the mass isolation window was set to 1.4 m/z. The acquired raw-files were imported into the Progenesis QI software (v2.0, Nonlinear Dynamics Limited), which was used to extract peptide precursor ion intensities across all samples applying the default parameters. The generated mgf-files were searched using MASCOT as above using the following search criteria: full tryptic specificity was required (cleavage after lysine or arginine residues, unless followed by proline); 3 missed cleavages were allowed; carbamidomethylation (C) was set as fixed modification; oxidation (M) and phosphorylation (STY) were applied as variable modifications; mass tolerance of 10 ppm (precursor) and 0.02 Da (fragments). The database search results were filtered using the ion score to set the false discovery rate (FDR) to 1% on the peptide and protein level, respectively, based on the number of reverse protein sequence hits in the datasets. The relative quantitative data obtained were normalized and statistically analyzed using our in-house script as above [276].

LC-MS/MS Analysis

The setup of the µRPLC-MS system was as described previously [276]. Chromatographic separation of peptides was carried out using an EASY nano-LC 1000 system (Thermo Fisher Scientific), equipped with a heated RP-HPLC column (75 µm x 37 cm) packed in-house with 1.9 µm C18 resin (Reprosil-AQ Pur, Dr. Maisch). Aliquots of 1 µg total peptides were analyzed per LC-MS/MS run using a linear gradient ranging from 95% solvent A (0.15% formic acid, 2% acetonitrile) and 5% solvent B (98% acetonitrile, 2% water, 0.15% formic acid) to 30% solvent B over 90 minutes at a flow rate of 200 nl/min. Mass spectrometry analysis was performed on Q-Exactive HF mass spectrometer equipped with a nanoelectrospray ion source (both Thermo Fisher Scientific). Each MS1 scan was followed by high-collision-dissociation (HCD) of the 10 most abundant precursor ions with dynamic exclusion for 20 seconds. Total cycle time was approximately 1 s. For MS1, 3e6 ions were accumulated in the Orbitrap cell over a maximum time of 100 ms and scanned at

a resolution of 120,000 FWHM (at 200 m/z). MS2 scans were acquired at a target setting of 1e5 ions, accumulation time of 100 ms and a resolution of 30,000 FWHM (at 200 m/z). Singly charged ions and ions with unassigned charge state were excluded from triggering MS2 events. The normalized collision energy was set to 35%, the mass isolation window was set to 1.1 m/z and one microscan was acquired for each spectrum.

Protein Quantification and Database Searching

The acquired raw-files were converted to the mascot generic file (mgf) format using the msconvert tool (part of ProteoWizard, version 3.0.4624 (2013-6-3)). Using the MASCOT algorithm (Matrix Science, Version 2.4.1), the mgf files were searched against a decoy database containing normal and reverse sequences of the predicted SwissProt entries of Homo sapiens (www.ebi.ac.uk, release date 2014/11/24), the six calibration mix proteins [276] and commonly observed contaminants (in total 84,610 sequences for Homo sapiens) generated using the SequenceReverser tool from the MaxQuant software (Version 1.0.13.13). The precursor ion tolerance was set to 10 ppm and fragment ion tolerance was set to 0.02 Da. The search criteria were set as follows: full tryptic specificity was required (cleavage after lysine or arginine residues unless followed by proline), 3 missed cleavages were allowed, carbamidomethylation (C), TMT6plex (K and peptide n-terminus) were set as fixed modification and oxidation (M) as a variable modification. Next, the database search results were imported to the Scaffold Q+ software (version 4.3.2, Proteome Software Inc., Portland, OR) and the protein false identification rate was set to 1% based on the number of decoy hits. Protein probabilities were assigned by the Protein Prophet program [278]. Proteins that contained similar peptides and could not be differentiated based on MS/MS analysis alone were grouped to satisfy the principles of parsimony. Proteins sharing significant peptide evidence were grouped into clusters. Acquired reporter ion intensities in the experiments were employed for automated quantification and statically analysis using a modified version of our in-house developed SafeQuant R script, v2.3 [276]. This analysis included adjustment of reporter ion intensities, global data normalization by equalizing the total reporter ion intensity across all channels, summation of reporter ion intensities per protein and channel, calculation of protein abundance ratios and testing for differential abundance using empirical Bayes moderated t-statistics. Finally, the calculated p-values were corrected for multiple testing using the Benjamini−Hochberg method.

Mouse Infections and Tissue Collection

All animal experiments were approved (license 2890, Kantonales Veterinäramt Basel) and performed according to local guidelines (Tierschutz-Verordnung, Basel) and the Swiss animal protection law (Tierschutz-Gesetz). C57BL/6J congenic mice were infected by tail vein injection of 1000 +/- 200 *Salmonella* in 100 µl PBS and euthanized days 1, 2, 3 or 4 post infection. Spleen, liver, blood and bone marrow was collected from each mouse and dissected into several pieces if needed. CFU counts were determined by plating.

Sample preparation for Salmonella-infected host proteomics

Spleen cells were carefully extracted mechanically by pressing spleens with two glass slides. The resulting cells were passed through 40-micron cell strainer (BD Falcon). Cell were then spun down and resuspended in cold red blood cell lysis buffer (Sigma) and incubated at room temperature for 5 minutes with gentle shaking. Cells were passed again through a cell strainer, washed once with PBS, and resuspended in FACS buffer (PBS, 0.5% BSA, 2mM EDTA) containing the following antibodies: CD11b-PE (clone M1/70, BD Biosciences), Ly6C-FITC (clone AL-21, BD Biosciences), Ly6G-APCCy7 (clone 1A8, Biolegend). Cells were incubated on ice for 30 minutes. Neutrophils ($CD11b^{+}$, $Ly6C^{Int}$, $Ly6G^{+}$) were sorted with a FACSAria (BD Biosciences) into Falcon tubes containing RPMI + 2% FCS. Neutrophils were washed once with cold PBS and pellets were kept at -80°C until further processing.

Comparison of human and mouse proteome

Human and mouse differential protein expression was compared using human-mouse homology information from the ENSEMBL database (release 90; http://aug2017.archive.ensembl.org/) [249]. The one-to-one orthologs between the two species were retrieved, along with their corresponding Entrez IDs, with the R package biomaRt (version 2.32) [279] from Bioconductor release 3.5 [280]. Only orthology relations annotated at the taxonomic level Euarchontoglires or Eutheria were retained. The merged human and mouse proteomics data set included in total 1157 orthologous proteins. The Venn diagram displaying shared differentially expressed proteins was drawn using the Bioconductor package limma (version 3.32) [281]. Significance level of both proteomic data were set at FDR > 0.05.

ROS production assay of human neutrophils

ROS production was measured using luminol-enhanced chemoluminescence, as previously described [46]. In brief, $2x10^5$ cells were incubated in RPMI+ 10% human serum for 1h at 37°C, 5% CO_2 without inhibitors, or with 10 µM DPI. Neutrophils were stimulated with opsonized *Salmonella* (MOI=100 and 200) or *Candida albicans* (MOI=2) in the presence of 10% human serum and 100 µM luminol (Fluka) in HBSS (Invitrogen, Gibco) containing 0.1% glucose (Braun). Chemiluminescence was measured at 5 min intervals at 37°C with a luminometer (Microlumat Plus, Berthold Technologies). Values were corrected based on unstimulated controls and initial time points.

Phosflow Assay with flow cytometry

p-Akt (pS473, BD Phosflow™, Cat. No 558434), p-mTOR (pS2448, BD Phosflow™, Cat. No 564242), p-p38 (pT180/pY182, BD Phosflow™, Cat. No 612595), p-STAT5 (pY694, BD Phosflow™, Cat. No 612598), and p-CREB (pS133, BD Phosflow™, Cat. No 558434) in human neutrophils were measured by flow cytometry using an adapted BD Phosflow™ protocol for human PBMCs. In brief, 500'000 PMN were pre-treated with inhibitors for 1h, washed twice, then stimulated with GM-CSF or PMA (Sigma, 10nM, as positive control) for 30min. The cells were fixed with 1x BD Phosflow™ Fix buffer I (BD, Cat. No. 557870) for 12 min at 37°C, then permeabilized using BD Phosflow™ Perm buffer III (Cat. No. 558050) on ice for 30 min, followed by indicated Phosflow™ antibody staining for another 1h at room temperature. Unspecific Fc receptor blocking (Human TruStain FcX™, Biolegend, Cat. No. 422301) and surface staining with FITC anti-human CD66b (Clone: G10F5, Biolegend) or APC anti-human CD66b (Clone: G10F5, Biolegend) for 1h was performed immediately before fixation for 30min. The stainings were initially performed with respective IgG isotype control (BD, Cat. No. 5577839. For data analysis, $CD66^+$ cells were initially gated to check SSC/ FSC position in FACS plot. Data were obtained using FACS CytoFlex (Beckman Coulter) and analyzed by using FlowJo v10.4.1.

Surface Molecule staining for flow cytometry

After PMN isolation or stimulation with cytokines, human neutrophils were washed twice in PBS to remove all cell debris and cytokines. To reduce unspecific antibody binding, neutrophils were incubated for 15min at room temperature in presence of human TruStain FcX™ Blocking solution (Biolegend, Catalog No.: 422302, 2µl/test) or mouse TruStain fcX™ (anti-mouse CD16/Cd32) blocking antibodies (Biolegend, Catalog No.:

101320, 2µl/test) followed by antibody staining for 30 minutes in the dark at 4°C. Samples were acquired with a BD Fortessa or Cytoflex (Beckman Coulter) flow cytometer. Data were analysed using FlowJo software, version v10.4.1. As a negative control, unstimulated sample or isotype control was used. Antibodies for PE anti-human HLA-DR/ -DP/ -DQ (Clone: REA332, Miltenyi), PE-Cy7 anti-human HLA-DR (Clone: Tü39, Biolegend), APC anti-human HLA-DR (Clone: L243, Biolegend), APC-Cy7 anti-human HLA-DR (Clone: L243, Biolegend), FITC anti-human CD66b (Clone: G10F5, Biolegend), APC anti-human CD66b (Clone: G10F5, Biolegend), APC anti-human CD74 (Clone: LN2, Biolegend), APC-Cy7 anti-human HLA-A, -B, -C (W6/32, Biolegend), FITC mouse isotype control IgM (Clone: MM-30, Biolegend), APC-Cy7 mouse isotype control IgG1 (Clone: MOPC-21, Biolegend), PE-Cy7 mouse isotype control IgG2a (Clone: MOPC-21, Biolegend), APC mouse isotype control IgG1 (Clone: MOPC-21, Biolegend), APC mouse isotype control IgG2a (Clone: MOPC-21, Biolegend), APC-Cy7 mouse isotype control IgG2a (Clone: MOPC-173, Biolegend), APC mouse isotype control IgG2a (Clone: MOPC-173, Biolegend) were used. Zombie UV Fixable Viability Kit (Biolegend), Alexa647 anti-mouse CD45 (Clone: 30-F11, Biolegend), PerCP/Cy5.5 anti-mouse CD11b (Clone: M1/70, Biolegend), APC/Cy7 anti-mouse CD11c (Clone: N418, Biolegend), BV650 anti-mouse Ly6G (Clone: 1A8, Biolegend), PE/Cy7 anti-mouse Ly6C (Clone: HK1.4, Biolegend), BV711 anti-mouse I-A/I-E (Clone: M5/114.152, Biolegend) were used.

CD4$^+$ T-cell clone activation *in vitro*

Antigen-specific CD4$^+$ T-cell clones for the *A. fumigatus* 15-mer antigen Crf1/p41 were generated and expanded using the rapid expansion protocol as previously described [282,283]. Mature dendritic cells were generated from autologous PBMC as previously published [257,284]. Autologous PMN were stimulated with GM-CSF (10 ng/ml) and IFN-γ (1 ng/ml) in the presence of Pan-Caspase q.OPh (3 µM) for 48h. T-cell stimulation was analyzed by intracellular cytokine staining as previously published [227,284]. Briefly, DCs and PMNs were pulsed with 1 µg/ml Crf1/p41 peptide at 37°C for 30min, then washed twice to remove unspecific antigen. DCs and PMNs were co-incubated with the CD4$^+$ T-cell clones (1x10^5 cells) in a ratio of 1:1 respectively 10:1 in RPMI with 5% human serum supplemented with q.OPh Pan-Caspase inhibitor (3 µM) at 37°C for 6h in the presence of Brefeldin A (10 µg/ml) for the last 5h. Cells were stained with Zombie Aqua Fixable Viability Dye (Biolegend, Cat. No. 423101), CD3-BrilliantViolet785 (Biolegend, Cat. No. 317330), CD4-BrilliantViolet650 (Biolegend, Cat. No. 317436), IFN-γ-APC (Biolegend Cat. No. 502512) and TNF-α-PE/Cy7 (Biolegend, Cat. No. 502930).

Caspase activity assay

FAM-FLICA Caspase-3/-7 Assay Kit (Cat. No. 93), FAM-FLICA Caspase-8 Assay Kit (Cat. No. 99), FAM-FLICA Caspase-9 Assay Kit (Cat. No. 912), and FAM-FLICA Poly Caspase Assay Kit (Cat. No. 91) were ordered from ImmunoChemistry Technologies. Reagents were dissolved in DMSO as indicated by manufacturer's instruction. 1x FLICA Caspase solution was added to 300'000 neutrophils/ condition in a volume of 100µl for 30min at 37°C, then washed twice with FACS buffer and analyzed for its fluorescence in FL-1 channel with a flow cytometer (Accuri C6, BD).

Caspase inhibition assay

Caspase inhibitors for Caspase-3, Caspase-6, Caspase-7, Caspase-8 and Caspase-9 were ordered from R&D (Sampler Pack, Cat. No. FMKSP01) and Pan-Caspase OPH inhibitor Q-VD (short q.OPh, R&D systems, Cat. No. OPH001). In brief, 100'000 neutrophils/ condition were pre-treated with Caspase inhibitors (final concentration = [10µM] for sampler pack inhibitors, final concentration = [3µM] for Pan-Caspase OPH inhibitor Q-VD) for 18h, then washed with FACS buffer and stained for propidium iodide (PI; 1:100) and Annexin V-APC (1:100) for 15 min at room temperature. Sample acquisition was done in between 2 hours by using FL-2 (PI) and FL-4 (APC) on Accuri C6 flow cytometer (BD).

Annexin V assay

Followed by antibody staining, the cells were washed and re-buffered in FACS buffer supplemented with 2.5mM $CaCl_2$, stained with Annexin V (1:100) for 15 min at room temperature and washed in FACS buffer. Sample acquisition was done in between 2 hours. BV421 Annexin V (Biolegend), APC Annexin V (Biolegend) and FITC Annexin V (Biolegend) were used.

Cytokine measurements in human plasma

Peripheral blood was drawn in 2.7ml polyethylene tubes (Sarsted), spun down at 1'600 x g for 10 min and plasma-rich supernatant (upper phase) was collected and stored at –80°C until further processing. Cytokines in plasma were measured using the customized human LEGENDplex™ multi-analyte flow assay kit (Biolegend) for IL-13, IL-2, GM-CSF, IL-9, IL-10, IFN-γ, TNF-α, IL-17A, IL-6, IL-4, IL-21, IL-2 and IL-17F, according to manufacturer's instructions.

ImageStreamX

$2x10^6$ cells were plated in a 96-well plate, followed by human TruStain FcX™ blocking for 15min at 4°C (Biolegend, Catalog No.: 422302) and antibody staining (HLA-DR/DP/DQ-PE, Miltenyi Biotec, No. 130-104-827 and CD66b-AlexaFluor647, Biolegend, No. 305110) for 30min in the dark at 4°C. Cells were fixed with Fixation buffer (Biolegend, No. 420801) for 20min at room temperature, permeabilized with Permeabilization Wash buffer (Biolegend, No. 421002) and stained with DAPI (final conc. 0.5µg/ml) for 5min at room temperature. Cells were resuspended in FACS buffer and acquired with ImageStream X Mark II Imaging Flow cytometer (EMD Millipore) at 60x magnification using the channels CH1 (brightfield), CH3 (HLA-DR/DP/DQ-PE), CH7 (DAPI) and CH11 (CD66b-AlexaFluor647).

mRNA determination and RT-PCR

Total RNA was extracted from $10x10^6$ human neutrophils at 4h, 24h and 48 of incubation by using the RNAeasy mini kit (Qiagen, Cat. No. 74104) according to manufacturer's instructions, with a second RNA purification step to optimize RNA yield and purity [285]. RNA concentration was measured with NanoDrop (Thermo Fisher Scientific), and purity was determined with the ratio 260nm/280nm method. cDNA synthesis was performed with the Omniscript RT kit (Qiagen, Cat. No. 2051119). mRNA expression was measured by real-time PCR using the FastStart Universal SYBR Green Master (Roche, Cat. No. 04 913 850 001). The deltadelta Ct method [286] was used to obtain the relative mRNA expression using *GAPDH* and *B2M* as internal controls (HK) [287]. Samples were run in technical triplicates. Results are shown as fold change relative to unstimulated and internal control. The following primers were used: *CIITA* (forward: CTG AAG GAT GTG GAA GAC CTG GGA AAG C, reverse: GTC CCC GAT CTT GTT CTC ACT C), *B2M* (forward: ACT GAA TTC ACC CCC ACT GA, reverse: CCT CCA TGA TGC TGC TTA CA), *HLA-DRA* (forward: GAG TTT GAT GCT CCA AGC CCT CTC CCA, reverse: CAG AGG CCC CCT GCG TTC TGC TGC ATT), *CD74* (forward: CAC CTG CTC CAG AAT GCT G, reverse: CAG TTC CAG TGA CTC TTT CG), *RFX5* (forward: GTG TTT ATG ATG CCT ATC GGA AGT, reverse: TCC TCC TTA TGC CAC TGT AGC), *CREB* (forward: ATG GAA TCT GGA GCC GAG AA, reverse: GTG GCT GGG CTT GAA CTG), *RFXANK* (forward: TGA GAC CGT TCG CTT CCT, reverse: GTC CCT CCA TTC CAA TCA TAG ATG), *NFYa* (forward: GCC AGG CAA TGT GGT CAA, reverse: GCT TCT TCA TCG GCT TGG TT), *GAPDH* (forward: AAG TAT GAC AAC AGC CTC AAG AT, reverse: CAT GAG TCC TTC CAC GAT ACC), *NLRC5* (forward: GAG AGT GGA CCT GGA GAA GA, reverse: GCG GAT GAC TTG GAT GCT A), *HLA-B* (forward: TGA GAT GGG AGC CGT CTT, reverse: CAC GCA GCC TGA GAG TAG).

Statistical analysis

Comparisons between unpaired groups with a nonparametric distribution were made using the Mann-Whitney test. Comparisons between paired groups with a nonparametric distribution were made using Wilcoxon matched-pairs signed rank test. P values < 0.05 were considered statistically significant. Statistical analysis was performed with GraphPad Prism 7 software.

Data availability

The data that support the findings of this study are available from the corresponding author upon request. Proteomics data will be uploaded upon paper submission.

Correspondence and requests for materials should be addressed to N.K.

5.2.7 Acknowledgements

We thank K. Ullrich and R. Kühl for drawing blood from human donors and all donors for blood donations. We thank D. Gremmelmaier for the recruitment of healthy volunteers. We thank D. Labes and E. Trauneker for support with flow cytometry and sorting, and Nicolas Luginbühl for helping with neutrophil isolation. This study was supported in part by grants from Swiss National Foundation (PZ00P3_142403 to N.K., 310030_156818 to D.B.), the Bangerter-Rhyner foundation (to N.K.) and the Forschungsfonds Nachwuchsforschende (to M.K.)

5.2.8 Author contributions

P.F., M.K., C.S., M.R.B., J.L., D.B., A.S., D.B., and N.K. performed experiments and analyzed the data; P.F., F.F., and N.K. recruited patients and healthy volunteers; P.F., M.K., C.S., M.R.B., C.S., D.B, and N.K. designed experiments; J.R. and A.S. helped with data analysis; M.G. and D.F. provided mouse strains and reagents; and P.F. and N.K. wrote the paper.

5.2.9 Additional information

Supplementary information is available online. Reprints and permissions information is available online at XY.

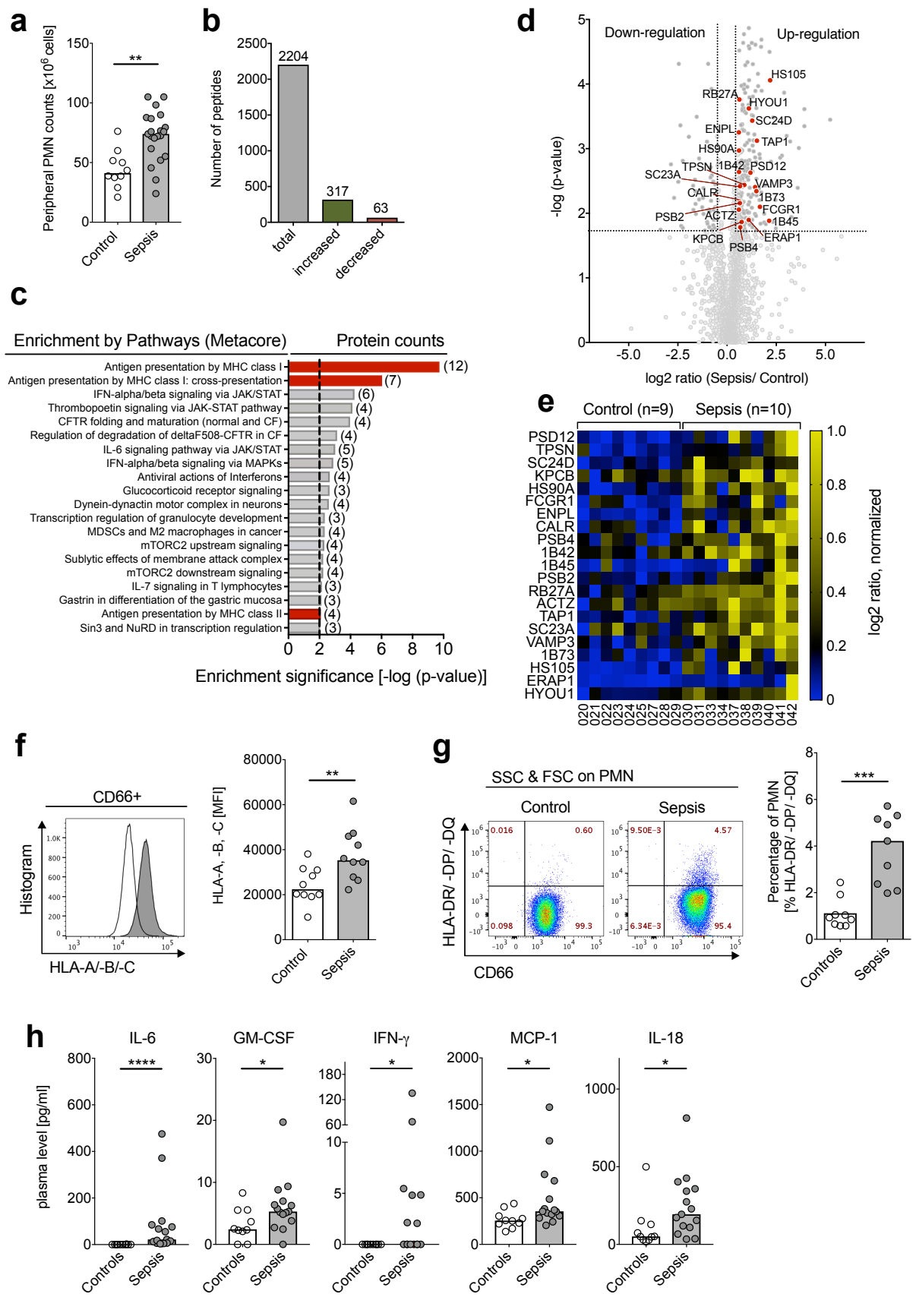
a
Peripheral PMN counts [x10^6 cells]
150
100
50
0
**
Control
Sepsis
b
Number of peptides
2500
2000
1500
1000
500
0
2204
317
63
total
increased
decreased
c
Enrichment by Pathways (Metacore)
Protein counts
Antigen presentation by MHC class I (12)
Antigen presentation by MHC class I: cross-presentation (7)
IFN-alpha/beta signaling via JAK/STAT (6)
Thrombopoetin signaling via JAK-STAT pathway (4)
CFTR folding and maturation (normal and CF) (4)
Regulation of degradation of deltaF508-CFTR in CF (4)
IL-6 signaling pathway via JAK/STAT (5)
IFN-alpha/beta signaling via MAPKs (5)
Antiviral actions of Interferons (4)
Glucocorticoid receptor signaling (3)
Dynein-dynactin motor complex in neurons (4)
Transcription regulation of granulocyte development (3)
MDSCs and M2 macrophages in cancer (4)
mTORC2 upstream signaling (4)
Sublytic effects of membrane attack complex (4)
mTORC2 downstream signaling (4)
IL-7 signaling in T lymphocytes (3)
Gastrin in differentiation of the gastric mucosa (3)
Antigen presentation by MHC class II (4)
Sin3 and NuRD in transcription regulation (3)
0 2 4 6 8 10
Enrichment significance [-log (p-value)]
d
Down-regulation
Up-regulation
-log (p-value)
5
4
3
2
1
0
HS105
RB27A
HYOU1
SC24D
ENPL
TAP1
HS90A
TPSN
1B42
PSD12
SC23A
VAMP3
CALR
1B73
FCGR1
PSB2
ACTZ
1B45
KPCB
ERAP1
PSB4
-5.0 -2.5 0.0 2.5 5.0
log2 ratio (Sepsis/ Control)
e
Control (n=9)
Sepsis (n=10)
PSD12
TPSN
SC24D
KPCB
HS90A
FCGR1
ENPL
CALR
PSB4
1B42
1B45
PSB2
RB27A
ACTZ
TAP1
SC23A
VAMP3
1B73
HS105
ERAP1
HYOU1
020 021 022 023 024 025 027 028 029 030 031 033 034 037 038 039 040 041 042
1.0
0.8
0.6
0.4
0.2
0
log2 ratio, normalized
f
CD66+
Histogram
HLA-A/-B/-C
HLA-A, -B, -C [MFI]
80000
60000
40000
20000
0
**
Control
Sepsis
g
SSC & FSC on PMN
Control
Sepsis
HLA-DR/ -DP/ -DQ
CD66
0.016
0.60
0.098
99.3
9.50E-3
4.57
6.34E-3
95.4
Percentage of PMN [% HLA-DR/ -DP/ -DQ]
8
6
4
2
0
***
Controls
Sepsis
h
IL-6
GM-CSF
IFN-γ
MCP-1
IL-18
plasma level [pg/ml]
800
600
400
200
0
****
30
20
10
0
*
180
120
60
10
5
0
*
2000
1500
1000
500
0
*
1000
500
0
*
Controls
Sepsis

Fig. 1: Human neutrophils in sepsis show APC-like phenotype.

a, Human peripheral blood-derived neutrophil counts (PMN, in $x10^6$ cells) of control (n=10) and sepsis patients (n=23), counted with ADAM automated cell counter system. All values are shown as medians (Mann-Whitney test; **, P< 0.01).

b, Number of peptides (n=2204) identified by human neutrophil proteomics from control (n=9) and sepsis patients (n=10) with significant increased (n=317) and decreased (n=63) peptide levels. Significance threshold was set at P-value < 0.02.

c, Enriched pathways from proteomics analysis on human neutrophils from control (n=9) and sepsis patients (n=10), using Metacore Enrichment by Pathway Maps. P-value of proteomics data was set < 0.05, threshold = 0, listed are the top 20 hits with an enrichment significance of P-value < 0.01. Identified protein counts are indicated in brackets. Red bars highlight *Antigen Presentation and processing by MHC class I and MHC class II* as highly changed pathways in sepsis.

d, Volcano dot plot from proteomics analysis on human neutrophils from control (n=9) and sepsis patients (n=10). Highlighted proteins (red dots) are associated with *Antigen presentation and processing by MHC class I and II*, significance threshold (dotted line) was set at P-value < 0.02 and fold change ≤ 1.5 cut-off in order of P-value.

e, Heat map of proteins involved in *Antigen presentation and processing by MHC class I and II* in human neutrophils from control (n=9) and sepsis patients (n=10), shown on an individual level with log2 ratio, normalized (0-1, blue to yellow). Significance threshold was set at P-value < 0.02 and fold change ≤ 1.5 cut-off in order of P-value. Protein names are used according to entry names in UniProt database (www.uniprot.org).

f, Representative histogram of HLA-A, -B, -C surface expression (Mean Fluorescence Intensity) on human neutrophils of control (white) and sepsis patient (grey), measured with flow cytometry and summarized for control (n=10) and sepsis patients (n=10). All values are shown as medians (Mann-Whitney test; **, P < 0.01).

g, Representative scatter dot plot of CD66b and HLA-DR/ -DP/ -DQ surface expression on human neutrophils of control (left panel) and sepsis patient (right panel), measured with flow cytometry and summarized for control (n=9) and sepsis patients (n=9). Red numbers are highlighting percentage of population. All values are shown as medians (Mann-Whitney test; ***, P < 0.001).

h, Plasma cytokine concentration for IL-6, GM-CSF, IFN-γ, MCP-1 and IL-18 of control (n=10) and sepsis patients (n=17). Concentrations are indicated in [pg/ml] and interpolated to a non-linear standard curve fit. All values are shown as medians (Mann-Whitney test; *, P< 0.05; ****, P< 0.0001).

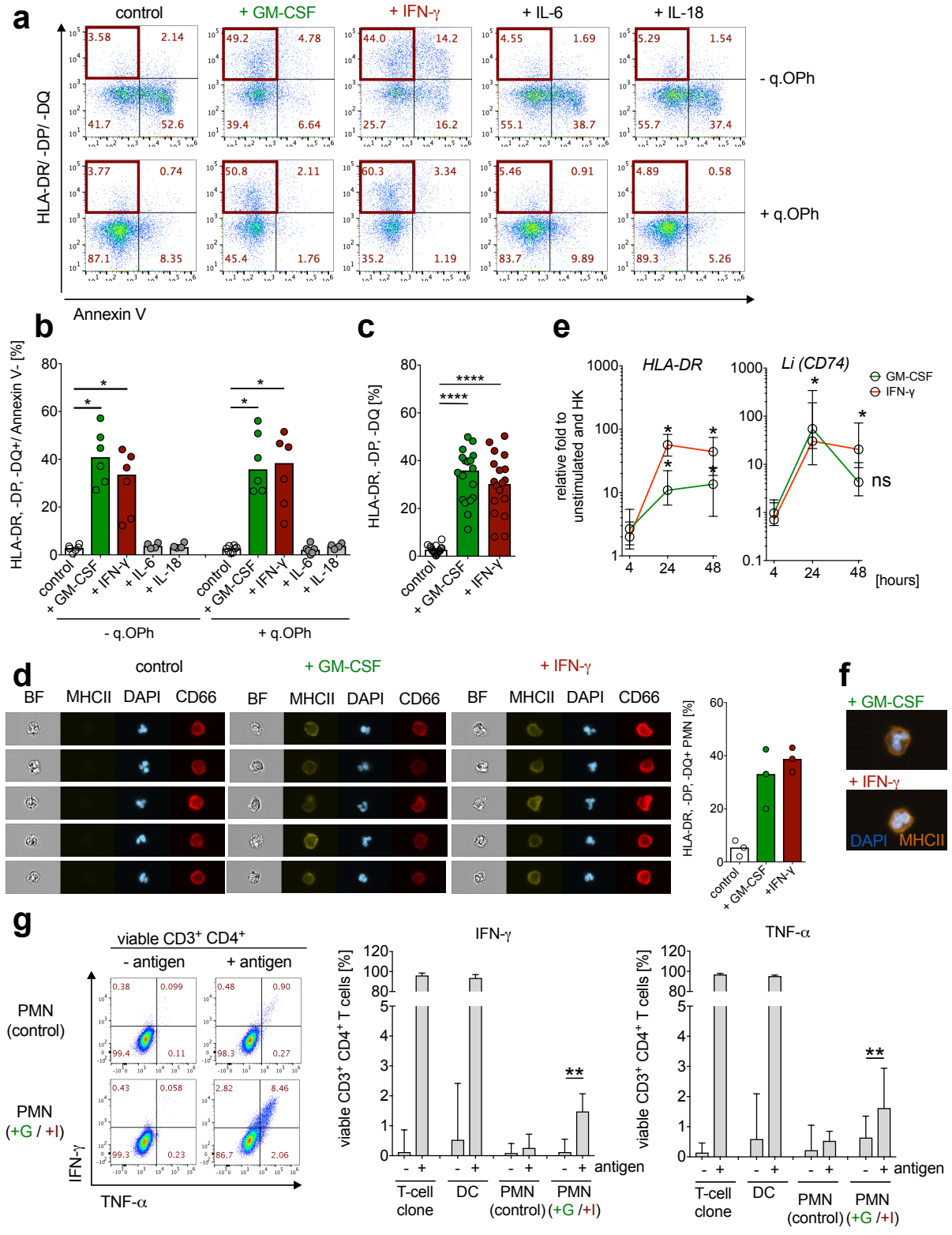
a
control
+ GM-CSF
+ IFN-γ
+ IL-6
+ IL-18
- q.OPh
+ q.OPh
HLA-DR/ -DP/ -DQ
Annexin V
b
HLA-DR, -DP, -DQ+/ Annexin V- [%]
control
+ GM-CSF
+ IFN-γ
+ IL-6
+ IL-18
- q.OPh
+ q.OPh
c
HLA-DR, -DP, -DQ [%]
e
HLA-DR
Li (CD74)
GM-CSF
IFN-γ
relative fold to unstimulated and HK
ns
[hours]
d
control
+ GM-CSF
+ IFN-γ
BF
MHCII
DAPI
CD66
HLA-DR, -DP, -DQ+ PMN [%]
f
+ GM-CSF
+ IFN-γ
DAPI
MHCII
g
viable CD3+ CD4+
- antigen
+ antigen
PMN (control)
PMN (+G / +I)
IFN-γ
TNF-α
IFN-γ
TNF-α
viable CD3+ CD4+ T cells [%]
antigen
T-cell clone
DC
PMN (control)
PMN (+G /+I)

Fig. 2: IFN-γ and GM-CSF induce APC-like neutrophil phenotype *in vitro*.

a, Representative scatter dot plot of HLA-DR/ -DP/ -DQ and Annexin V surface expression on human neutrophils (CD66b+ cells) after stimulation with human recombinant GM-CSF (10 ng/ml), IFN-γ (10 ng/ml), IL-6 (10 ng/ml) and IL-18 (10 ng/ml) for 48h, pre-incubated -/ + Pan-Caspase inhibitor q.OPh (3µM) for 1h, measured with flow cytometry. Red squares are highlighting the percentage of HLA-DR/ -DP/ -DQ+ /Annexin V- population.

b, Percentage of HLA-DR/ -DP/ -DQ+ /Annexin V- neutrophils after pre-incubation with -/ + Pan-Caspase inhibitor q.OPh (3µM) and stimulation with human recombinant GM-CSF (10 ng/ml), IFN-γ (10 ng/ml), IL-6 (10 ng/ml) and IL-18 (10 ng/ml) for 48h. All values are shown as medians (n=6; Mann-Whitney test; *, P< 0.05).

c, Percentage of HLA-DR/ -DP/ -DQ+ /Annexin V- neutrophils after pre-incubation with -/ + Pan-Caspase inhibitor q.OPh (3µM) and stimulation with human recombinant GM-CSF (10 ng/ml) and IFN-γ (10 ng/ml) for 48h. All values are shown as medians (n=18; Mann-Whitney test; ****, P< 0.0001).

d, Representative example of *de novo* MHC class II (HLA-DR/ -DP/ -DQ) surface molecule expression on neutrophils after stimulation with human recombinant GM-CSF (10 ng/ml) and IFN-γ (10 ng/ml) for 48h, measured with Image Stream X (left) and summarized (right, n= 3). DAPI was used for nuclear staining and CD66b as surface expression marker. BF, Bright field.

e, *HLA-DR* and *Li* (CD74) mRNA expression after stimulation with human recombinant GM-CSF (10 ng/ml) and IFN-γ (10 ng/ml) for 4, 24 and 48h. Values are shown as relative fold change to unstimulated control and internal control (housekeeping genes, HK). All values are shown as medians (n=6; Mann-Whitney test; *, P< 0.05; ns, not significant).

f, Representative overlay of *de novo* MHC class II (HLA-DR/ -DP/ -DQ, orange) surface molecule expression on neutrophils after stimulation with human recombinant GM-CSF (10 ng/ml) and IFN-γ (10 ng/ml) for 48h, measured by Image Stream X at 60x magnification. DAPI (blue) was used for nuclear staining and CD66b as surface expression marker.

g, Intracellular cytokine staining for IFN-γ and TNF-α-activated viable CD3+ CD4+ T cells, co-incubated with and without antigen-pulsed PMN (control, ratio 1:10) and cytokine-stimulated PMN (recombinant GM-CSF, 10 ng/ml; recombinant IFN-γ, 1 ng/ml, ratio 1:10) for 6 hours. Representative scatter dot plot (left) and summarized in percentage for IFN-γ (middle) and TNF-α (right). As a positive control, autologous dendritic cells (DCs, 1:1 ratio) and T-cell clones alone were used. All values are shown as medians with interquartile ranges (n=11; n=6 for positive control with DCs; Wilcoxon signed rank test; **, P< 0.01).

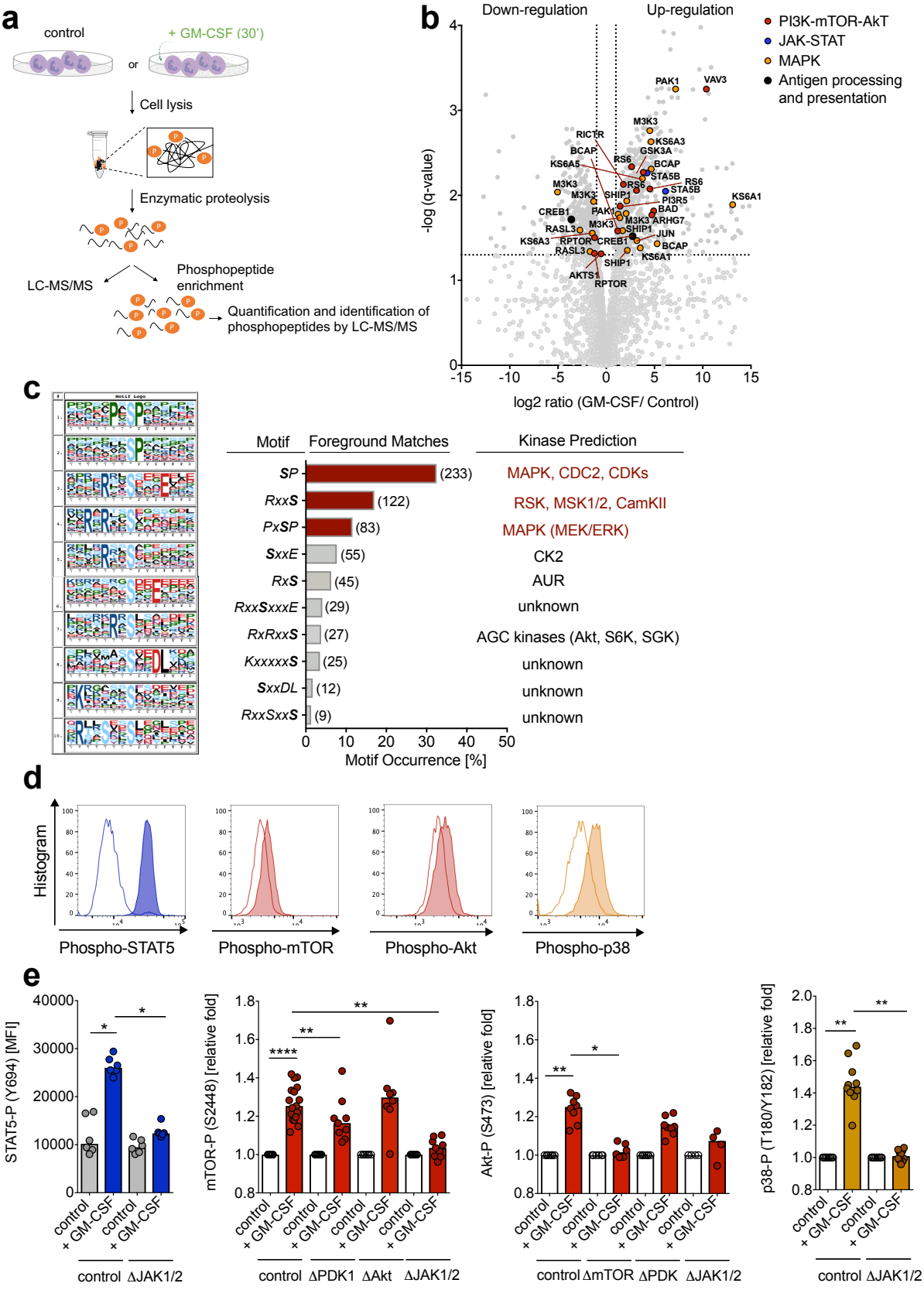
a
control
+ GM-CSF (30')
or
Cell lysis
Enzymatic proteolysis
LC-MS/MS
Phosphopeptide enrichment
Quantification and identification of phosphopeptides by LC-MS/MS
b
Down-regulation
Up-regulation
PI3K-mTOR-AkT
JAK-STAT
MAPK
Antigen processing and presentation
-log (q-value)
log2 ratio (GM-CSF/ Control)
c
Motif
Foreground Matches
Kinase Prediction
SP (233) MAPK, CDC2, CDKs
RxxS (122) RSK, MSK1/2, CamKII
PxSP (83) MAPK (MEK/ERK)
SxxE (55) CK2
RxS (45) AUR
RxxSxxxE (29) unknown
RxRxxS (27) AGC kinases (Akt, S6K, SGK)
KxxxxxS (25) unknown
SxxDL (12) unknown
RxxSxxS (9) unknown
Motif Occurrence [%]
d
Histogram
Phospho-STAT5
Phospho-mTOR
Phospho-Akt
Phospho-p38
e
STAT5-P (Y694) [MFI]
mTOR-P (S2448) [relative fold]
Akt-P (S473) [relative fold]
p38-P (T180/Y182) [relative fold]
control
+ GM-CSF
control ΔJAK1/2
control ΔPDK1 ΔAkt ΔJAK1/2
control ΔmTOR ΔPDK ΔJAK1/2

Fig. 3: GM-CSF signaling leads to the activation of JAK-STAT, MAPK p38 and Akt-mTOR signaling pathways and phosphorylation of transcription factor CREB1.

a, Visualization of phosphoproteomics experimental procedure. Neutrophils (10^8 cells each condition) were unstimulated or stimulated with GM-CSF (10 ng/ml) for 30min and then collected for further processing.

b, Volcano dot plot of detected phosphopeptide changes (n=3579) after stimulation with GM-CSF for 30min. Significance threshold was set at q-value < 0.05 and fold change ≤ 2 cut-off in order of P-value. Phosphopeptides belonging to PI3K-Akt-mTOR signaling were shown in red, phosphopeptides belonging to JAK-STAT signaling were shown in blue, and phosphopeptides belonging to MAPK signaling were shown in orange. Phosphopeptides directly linked to *Antigen presentation and processing* were indicated in black.

c, Overrepresented phosphorylation motifs after stimulation with GM-CSF for 30min. The overrepresented phosphorylation motifs were extracted with *MOTIF-X software tool*, V1.2. Ten distinct motifs were identified with significance < 0.000035 (p-value < 0.01), peptide width of 15 and occurrence of 5 (left). Putative kinases responsible for the phosphorylation of the ten observed, significant motifs are indicated (right, in red). Putative kinases were predicted using PhosphoELM, SwissProt (RegPhos 1.0, www.regphos-mbc.nctu.edu.tw) and extensive literature research.

d, Representative histograms for STAT5- (Y694), mTOR- (S2448), Akt- (S473), and p38- (T180/Y182) phosphorylation after GM-CSF stimulation for 30min by using PhosFlow antibodies for flow cytometry. Unstimulated control is shown in white, GM-CSF stimulation is shown shaded.

e, Quantification of flow cytometry data as shown in d, with absolute values in MFI (mean fluorescence intensity) or relative values in fold changes to control. Inhibitors Ruxolitinib (ΔJAK1/2 inhibitor, final conc. = 3μM), BX-795 (ΔPDK1 inhibitor, final conc. = 10μM), MK-2206 (ΔAkt1/2/3 inhibitor, final conc. = 10μM), and PP242 (ΔmTORC1/2 inhibitor, final conc. = 5μM) were used (n = 4-17; Wilcoxon signed rank test, ****, P< 0.0001; **, P< 0.01; *, P< 0.05).

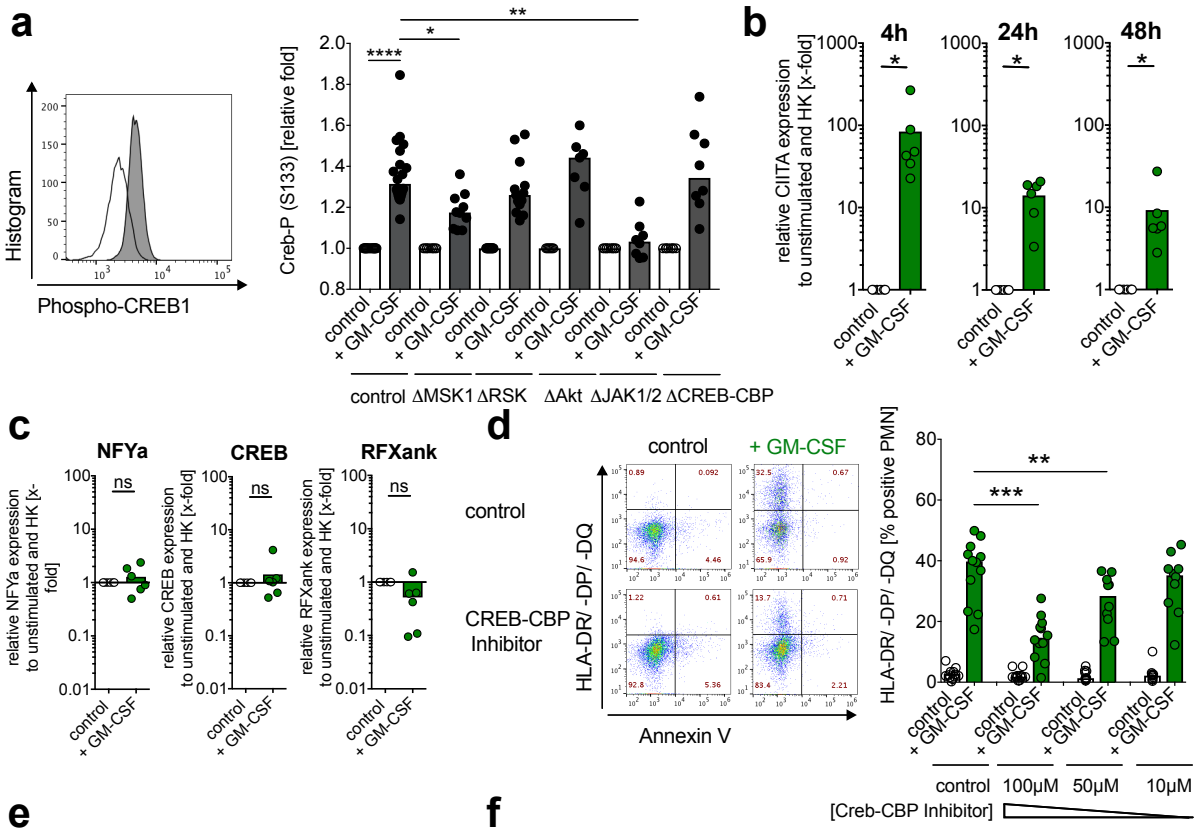
a
Histogram
Phospho-CREB1
Creb-P (S133) [relative fold]
control + GM-CSF
control ΔMSK1 ΔRSK ΔAkt ΔJAK1/2 ΔCREB-CBP
b
relative CIITA expression to unstimulated and HK [x-fold]
4h
24h
48h
c
NFYa
CREB
RFXank
relative NFYa expression to unstimulated and HK [x-fold]
relative CREB expression to unstimulated and HK [x-fold]
relative RFXank expression to unstimulated and HK [x-fold]
ns
d
control
+ GM-CSF
CREB-CBP Inhibitor
HLA-DR/ -DP/ -DQ
Annexin V
HLA-DR/ -DP/ -DQ [% positive PMN]
control 100μM 50μM 10μM
[Creb-CBP Inhibitor]
e
HLA-DR/ -DP/ -DQ [% positive PMN]
control ΔJAK1/2 Δp38 ΔMSK1 ΔMEK ΔERK
f
GM-CSF receptor
JAK1/2
MHC class II
plasma membrane
cytoplasm
p38-MSK1-MAPK signaling
JAK/ STAT signaling
STAT5
p38
MSK1
CIITA
CBP
Pol II
RFX
CREB1
NFY
nucleus
De novo transcription
HLA-DR, HLA-DM, II
GAS site promotor binding
MHC class II enhanceosome formation
MHC class II gene induction + antigen processing

Fig. 4: Targeting the MHC class II enhanceosome in human neutrophils.

a, Representative histogram for CREB1 phosphorylation (S133) after GM-CSF stimulation (grey) compared to unstimulated (white) for 30min by using PhosFlow antibody for flow cytometry. Quantification of flow cytometry data are shown with relative fold changes to control. Inhibitors Ruxolitinib (ΔJAK1/2 inhibitor, final conc. = 3μM), SB 747651 A (ΔMSK1 inhibitor, final conc. = 10μM), BI-D1870 (ΔRSK1-4 inhibitor, final conc. = 10μM), and MK-2206 (ΔAkt1/2/3 inhibitor, final conc. = 10μM), CAS 92-78-4 (ΔCREB-CBP interaction inhibitor, final conc. = 50μM) were used (n = 2-12; Wilcoxon signed rank test, ****, *P*< 0.0001; **, *P*< 0.01; *, *P*< 0.05).

b, *CIITA* mRNA expression after stimulation with human recombinant GM-CSF (10 ng/ml) for 4, 24 and 48h. Values are shown as relative fold change to unstimulated control and internal control (housekeeping genes, HK). All values are shown as medians (n=6; Wilcoxon signed rank test; *, P< 0.05).

c, *NFYa, CREB* and *RFXank* mRNA expression after stimulation with human recombinant GM-CSF (10 ng/ml) for 4h. Values are shown as relative fold change to unstimulated control and internal control (housekeeping genes, HK). All values are shown as medians (n=6; Wilcoxon signed rank test; ns, not significant).

d, Representative scatter dot plot of HLA-DR/ -DP/ -DQ and Annexin V surface expression on human neutrophils ($CD66b^+$ cells) after stimulation with human recombinant GM-CSF (10 ng/ml) for 48h, pre-treatment with CAS 92-78-4 (ΔCREB-CBP interaction inhibitor, final conc. = 50μM). Red labels are indicating the percentage of population. Pan-Caspase inhibitor q.OPh (3μM) was used for all conditions. Percentage of HLA-DR/ -DP/ $-DQ^+$ /Annexin V^- neutrophils after pre-incubation with/ without CAS 92-78-4 inhibitor (ΔCREB-CBP interaction inhibitor, final conc. = 25, 50 and 100μM) and stimulation with human recombinant GM-CSF (10 ng/ml) for 48h. All values are shown as medians (n=10-12; Wilcoxon signed rank test; ***, *P*< 0.001; **, *P*< 0.01).

e, Percentage of HLA-DR/ -DP/ $-DQ^+$ /Annexin V^- neutrophils after pre-incubation with/ without inhibitors Ruxolitinib (ΔJAK1/2 inhibitor, final conc. = 3μM), SB203580 (Δp38 inhibitor, final conc. = 10μM), SB 747651 A (ΔMSK1 inhibitor, final conc. = 10μM), Trametinib (ΔMEK1/2 inhibitor, final conc. = 10μM), and SCH772984 (ΔERK1/2 inhibitor, final conc. = 5μM), and stimulation with human recombinant GM-CSF (10 ng/ml) for 48h. All values are shown as medians (n=2-20; Wilcoxon signed rank test; ***, *P*< 0.001; **, *P*< 0.01).

f, Human neutrophil signaling cascade leading to *de novo* MHC class II induction after stimulation with GM-CSF. JAK1/2, Janus Kinase 1 and 2; STAT5, Signal Transducer and Activator of Transcription 5; Y694, Tyrosine phosphorylation site at residue 694; CIITA, MHC class II transactivator; p38, p38 mitogen-activated protein kinase; MSK1, Mitogen- and stress-activated protein kinase-1; RFX, Regulatory factor X; CREB1, cAMP responsive element binding protein 1; Pol II; Polymerase II; CBP, CREB-binding protein; HLA-DR, HLA-DM, Li, MHC class II genes.

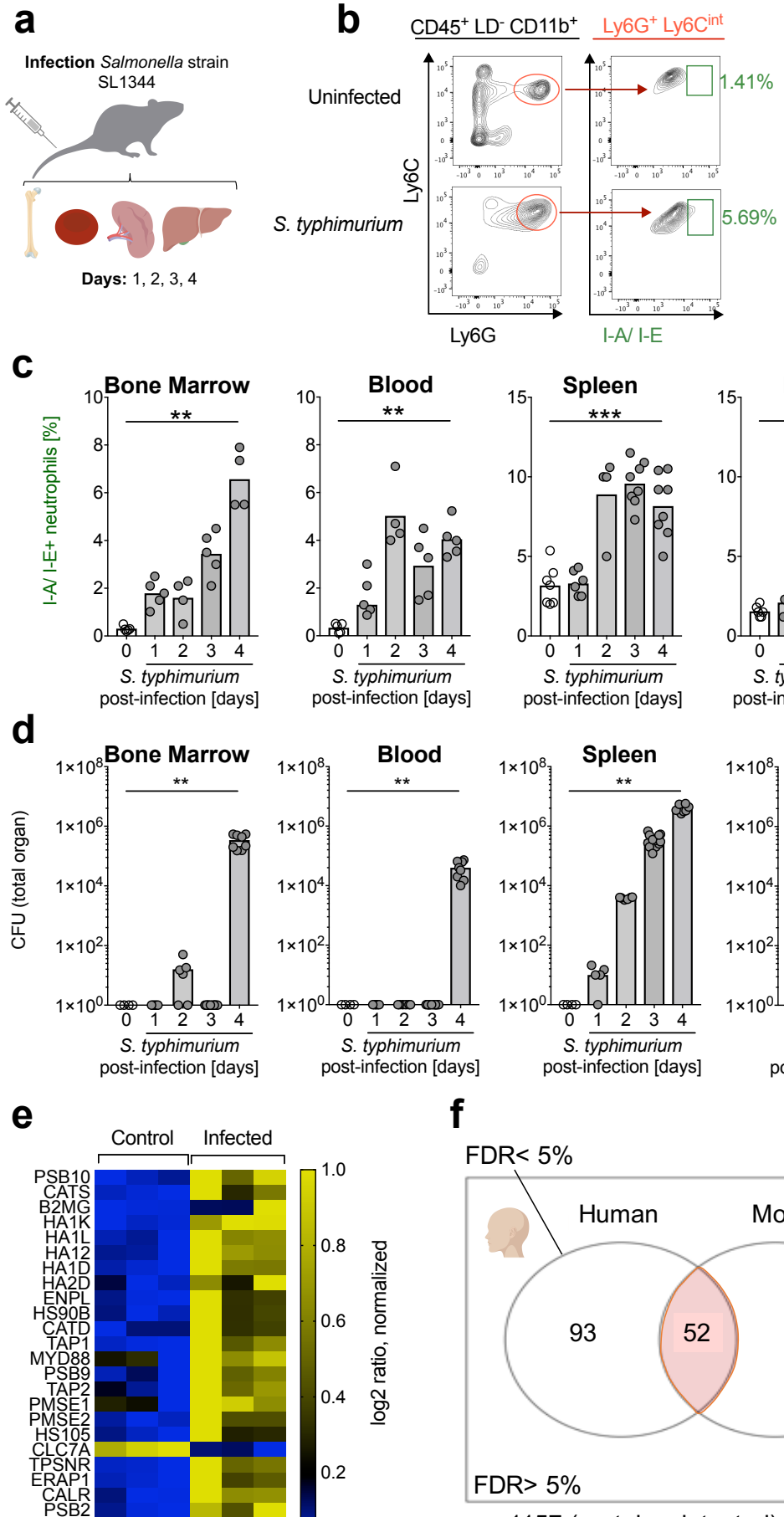
a
Infection Salmonella strain SL1344
Days: 1, 2, 3, 4
b
CD45+ LD- CD11b+
Ly6G+ Ly6Cint
Uninfected
S. typhimurium
1.41%
5.69%
Ly6C
Ly6G
I-A/ I-E
c
Bone Marrow
Blood
Spleen
Liver
I-A/ I-E+ neutrophils [%]
S. typhimurium post-infection [days]
d
CFU (total organ)
e
Control
Infected
PSB10
CATS
B2MG
HA1K
HA1L
HA12
HA1D
HA2D
ENPL
HS90B
CATD
TAP1
MYD88
PSB9
TAP2
PMSE1
PMSE2
HS105
CLC7A
TPSNR
ERAP1
CALR
PSB2
TPSN
CATZ
log2 ratio, normalized
f
FDR< 5%
Human
Mouse
93
52
199
813
FDR> 5%
n= 1157 (proteins detected)

Fig. 5: Induction of APC-like neutrophils in a systemic *Salmonella* mouse model mimicking human typhoid fever.

a, Overview of experimental *Salmonella enterica* serovar Typhimurium *SL1344* infection procedure in wildtype C57BL/6 mice. Bone marrow, blood, spleen and liver were collected at day 1, day 2, day 3 and day 4.

b, Representative scatter density plot of splenic Ly6C and Ly6G from viable $CD45^+$ $CD11b^+$ population, uninfected or infected with *Salmonella enterica* serovar Typhimurium *SL1344* at day 3. I-A/ I-E expression on $Ly6G^+$/ $Ly6C^{dim}$ cells is indicated in percentage (green). LD, live/dead marker.

c, I-A/ $I\text{-}E^+$ cells (in percent) from $Ly6G^+$/ $Ly6C^{dim}$ population in bone marrow, blood, spleen and liver over day 1, day 2, day 3 and day 4 of *Salmonella enterica* serovar Typhimurium *SL1344* infection are shown. All values are shown as means (n=4-8; Mann-Whitney test; ***, $P< 0.001$; **, $P< 0.01$).

d, CFU per total organ from bone marrow, blood, spleen and liver over day 1, day 2, day 3 and day 4 of *Salmonella enterica* serovar Typhimurium *SL1344* infection are shownon a logarithmic scale. All values are shown as means (n=4-8; Mann-Whitney test; **, $P< 0.01$).

e, Heat map of proteins involved in *Antigen presentation and processing by MHC class I and II* in splenic, murine neutrophils from control (uninfected, 1-3) and infected with *Salmonella enterica* serovar Typhimurium *SL1344* (4-6), shown on an individual level with log2 ratio, normalized (0-1, blue to yellow). Significance threshold was set at *P-value* < 0.03 and fold change ≤ 1.5 cut-off in order of *P-value*. Protein names are used according to entry names in UniProt database (www.uniprot.org).

f, The Venn diagram is showing the comparison of the proteome data sets from isolated splenic murine neutrophils infected with *Salmonella enterica* serovar Typhimurium at day 4 and the human peripheral blood derived neutrophils in sepsis in terms of common differential protein expression by using one-to-one orthologous homology information. In total identified orthologous proteins (n=1157) in humans and mice were indicated below. Differentially expressed, orthologous proteins in humans and mice are indicated in red (n=52, FDR<0.05).

Table 1: Clinical characteristics of patients and controls

	Patients (n=23)	**Controls (n=10)**
Demographic characteristics		
Age, years (median, IQR)	74 (69-85)	76 (69-83)
Male (n, %)	13 (57)	6 (60)
BMI (median, IQR)	25.3 (20.8-27.5)	25.5 (23.5-32.0)
Infection type		
Urinary tract (n, %)	17 (74)	-
Pulmonary (n, %)	2 (8.7)	-
Intestinal (n, %)	4 (17.3)	-
Bacterial species		
Escherichia coli (n, %)	17 (74)	-
Pseudomonas aeruginosa (n, %)	2 (8.7)	-
Klebsiella oxytoca (n, %)	1 (4.3)	-
Klebsiella pneumonia (n, %)	1 (4.3)	-
Serratia marcescens (n, %)	1 (4.3)	-
Proteus mirabilis (n, %)	1 (4.3)	-
Severity*		
Infection	21 (91.3)	-
Sepsis	2 (8.7)	-
Septic shock	0 (0)	-
Neutrophil-to-Lymphocyte ratio (median, interquartile range)	6.7 (5.1-17.2)	1.9 (1.3-3.0)
C-reactive protein** (median, IQR)	144.8 (118.4-271.8)	-
Pro-Calcitonin*** (median, IQR)	0.6 (0.28-37.0)	-
Outcome (d30 mortality) (n, %)	1 (4.3)	0 (0)

* Sepsis-3 definition with qSOFA score after (Singer *et al.*, JAMA 2016)

** CRP is measured in mg/L. Normal values are below 10mg/L.

*** Pro-Calcitonin is measured in ng/ml. Normal values are below 0.5 ng/ml.

IQR= interquartile range

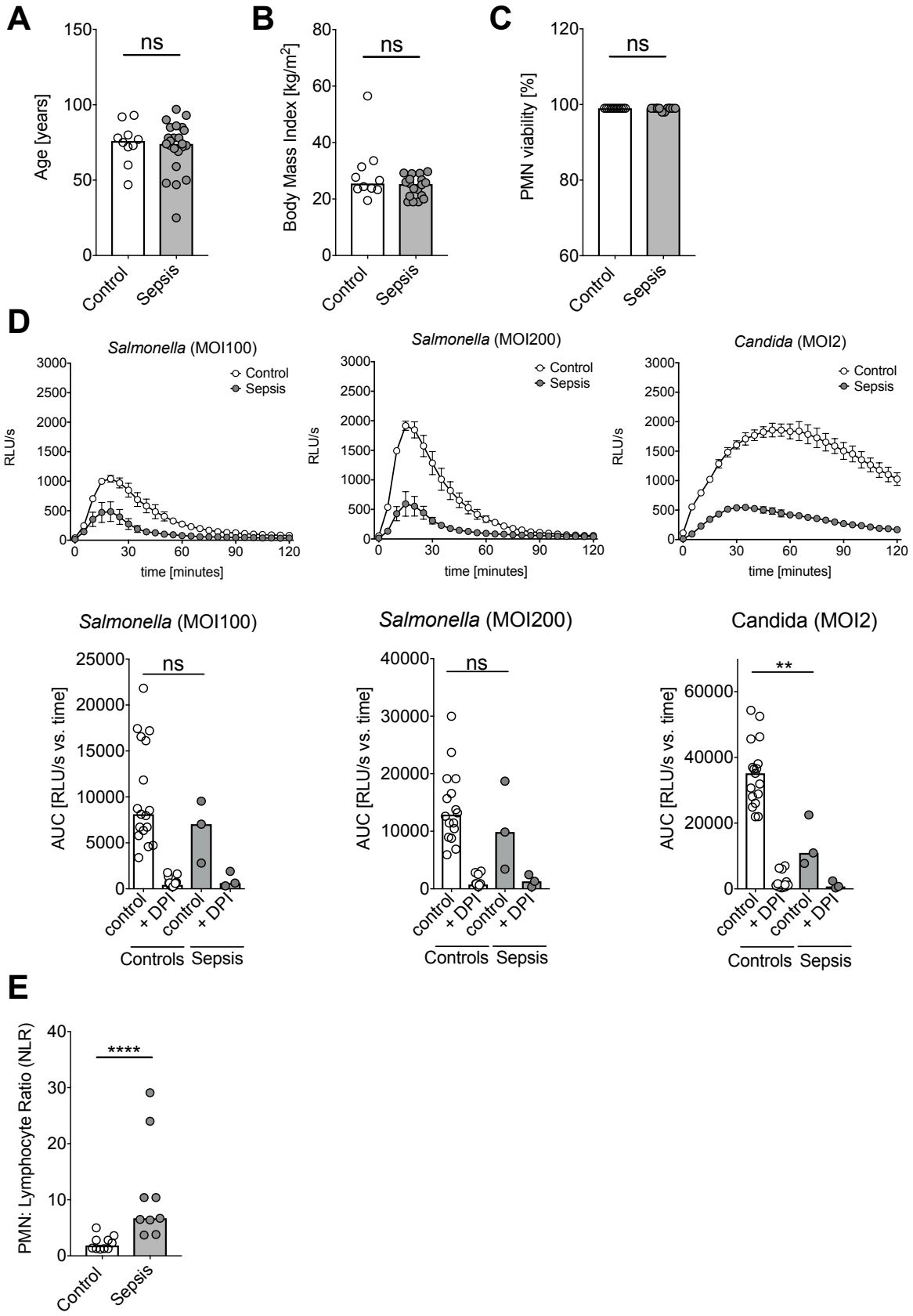
A
Age [years]
ns
Control
Sepsis
B
Body Mass Index [kg/m2]
ns
Control
Sepsis
C
PMN viability [%]
ns
Control
Sepsis
D
Salmonella (MOI100)
Salmonella (MOI200)
Candida (MOI2)
Control
Sepsis
RLU/s
time [minutes]
Salmonella (MOI100)
Salmonella (MOI200)
Candida (MOI2)
AUC [RLU/s vs. time]
ns
ns
**
control
+ DPI
Controls
Sepsis
E
PMN: Lymphocyte Ratio (NLR)
****
Control
Sepsis

F

Antigen presentation by MHC class I

Uniprot ID	Protein	Fold Change (log2)	q-value
P14625	Endoplasmin (ENPL_HUMAN)	0.6	0.005
P07900	Heat Shock Protein HSP 90-alpha (HS90A_HUMAN)	0.61	0.008
P30480	HLA class I histocompatibility antigen, B-42 alpha chain (1B42_HUMAN)	0.61	0.013
Q31612	HLA class I histocompatibility antigen, B-73 alpha chain (1B73_HUMAN)	1.49	0.020
P30483	HLA class I histocompatibility antigen, B-45 alpha chain (1B45_HUMAN)	2.14	0.038
P27797	Calreticulin (CALR_HUMAN)	0.63	0.025
Q03518	Antigen peptide transporter 1 (TAP1_HUMAN)	1.52	0.007
Q15436	Protein Transport Protein Sec23A (SC23A_HUMAN)	0.66	0.017
P49721	Proteasome subunit Beta type 2 (PSB2_HUMAN)	0.65	0.026
Q9NZ08	Endoplasmatic reticulum aminopeptidase 1 (ERAP1_HUMAN)	1.10	0.037
O15533	Tapasin (TPSN_HUMAN)	0.88	0.017
Q92598	Heat shock protein 105 kDa (HS105_HUMAN)	2.19	0.002

Antigen presentation by MHC class I: Cross-presentation

Uniprot ID	Protein	Fold Change (log2)	q-value
P14625	Endoplasmin (ENPL_HUMAN)	0.6	0.005
P07900	Heat Shock Protein HSP 90-alpha (HS90A_HUMAN)	0.61	0.008
O15533	Tapasin (TPSN_HUMAN)	0.88	0.017
P51159	Ras-related protein Rab-27A (RB27A_HUMAN)	0.63	0.002
Q9Y4L1	Hypoxia up-regulated protein 1 (HYOU1_HUMAN)	1.11	0.003
P12314	High affinity immunoglobulin gamma Fc receptor I (FCGR1_HUMAN)	1.67	0.028
Q92598	Heat shock protein 105 kDa (HS105_HUMAN)	2.19	0.002

Antigen presentation by MHC class II

Uniprot ID	Protein	Fold Change (log2)	q-value
P14625	Endoplasmin (ENPL_HUMAN)	0.6	0.005
P07900	Heat Shock Protein HSP 90-alpha (HS90A_HUMAN)	0.61	0.008
P05771	Protein Kinase C beta type (KPCB_HUMAN)	0.74	0.039
P61163	Alpha-centractin (ACTZ_HUMAN)	0.6	0.029

G

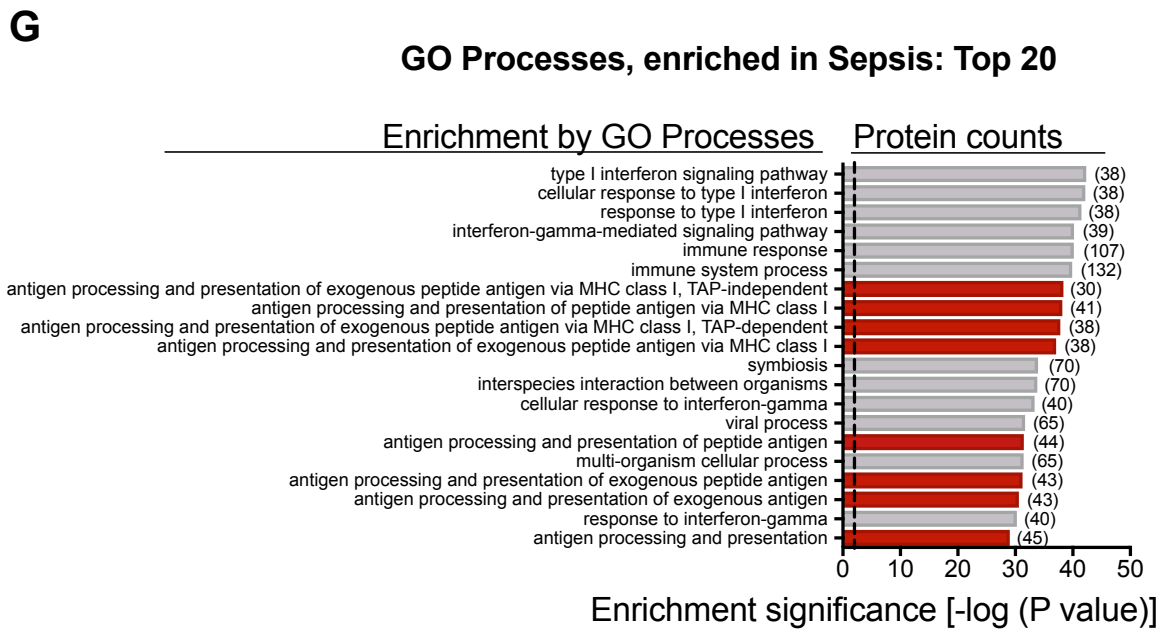
GO Processes, enriched in Sepsis: Top 20
Enrichment by GO Processes
Protein counts
type I interferon signaling pathway (38)
cellular response to type I interferon (38)
response to type I interferon (38)
interferon-gamma-mediated signaling pathway (39)
immune response (107)
immune system process (132)
antigen processing and presentation of exogenous peptide antigen via MHC class I, TAP-independent (30)
antigen processing and presentation of peptide antigen via MHC class I (41)
antigen processing and presentation of exogenous peptide antigen via MHC class I, TAP-dependent (38)
antigen processing and presentation of exogenous peptide antigen via MHC class I (38)
symbiosis (70)
interspecies interaction between organisms (70)
cellular response to interferon-gamma (40)
viral process (65)
antigen processing and presentation of peptide antigen (44)
multi-organism cellular process (65)
antigen processing and presentation of exogenous peptide antigen (43)
antigen processing and presentation of exogenous antigen (43)
response to interferon-gamma (40)
antigen processing and presentation (45)
0 10 20 30 40 50
Enrichment significance [-log (P value)]

H

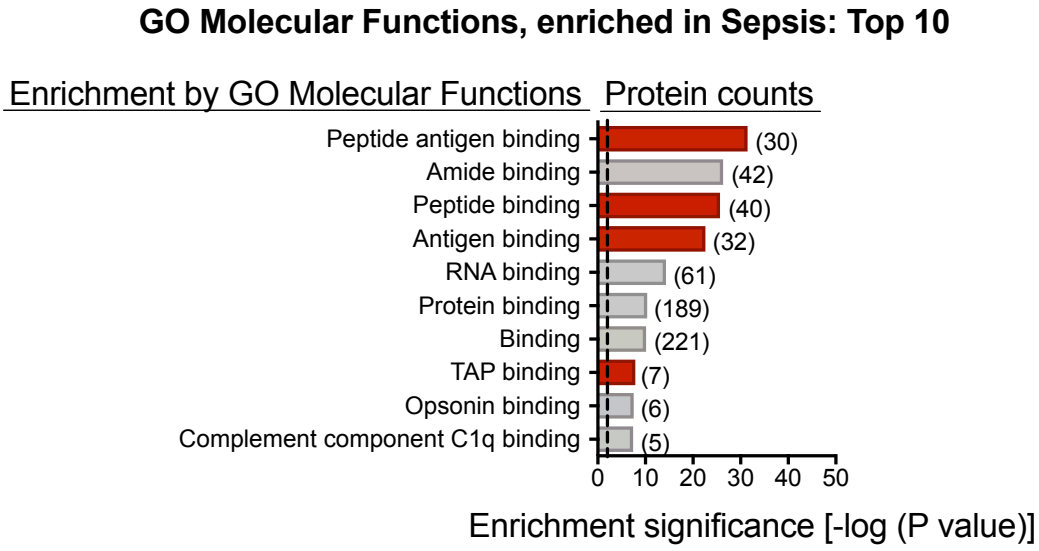
GO Molecular Functions, enriched in Sepsis: Top 10
Enrichment by GO Molecular Functions
Protein counts
Peptide antigen binding (30)
Amide binding (42)
Peptide binding (40)
Antigen binding (32)
RNA binding (61)
Protein binding (189)
Binding (221)
TAP binding (7)
Opsonin binding (6)
Complement component C1q binding (5)
0 10 20 30 40 50
Enrichment significance [-log (P value)]

I

Antigen presentation by MHC class I and MHC class II

Uniprot ID	Protein	Fold Change (log2)	q-value
P14625	Endoplasmin (ENPL_HUMAN)	0.6	0.005
P07900	Heat Shock Protein HSP 90-alpha (HS90A_HUMAN)	0.61	0.008
Q92598	Heat shock protein 105 kDa (HS105_HUMAN)	2.19	0.002
P30480	HLA class I histocompatibility antigen, B-42 alpha chain (1B42_HUMAN)	0.61	0.013
Q31612	HLA class I histocompatibility antigen, B-73 alpha chain (1B73_HUMAN)	1.49	0.020
P30483	HLA class I histocompatibility antigen, B-45 alpha chain (1B45_HUMAN)	2.14	0.038
P27797	Calreticulin (CALR_HUMAN)	0.63	0.025
Q03518	Antigen peptide transporter 1 (TAP1_HUMAN)	1.52	0.007
Q15436	Protein Transport Protein Sec23A (SC23A_HUMAN)	0.66	0.017
Q9NZ08	Endoplasmatic reticulum aminopeptidase 1 (ERAP1_HUMAN)	1.10	0.037
O15533	Tapasin (TPSN_HUMAN)	0.88	0.017
P51159	Ras-related protein Rab-27A (RB27A_HUMAN)	0.63	0.002
Q9Y4L1	Hypoxia up-regulated protein 1 (HYOU1_HUMAN)	1.11	0.003
P12314	High affinity immunoglobulin gamma Fc receptor I (FCGR1_HUMAN)	1.67	0.028
P05771	Protein Kinase C beta type (KPCB_HUMAN)	0.74	0.039
P61163	Alpha-centractin (ACTZ_HUMAN)	0.6	0.029
Q15836	Vesicle-associated membrane protein 3 (VAMP3_HUMAN)	1.43	0.018
O94855	Protein transport protein Sec24D (SC24D_HUMAN)	1.28	0.004
O00232	26S Proteasome non-ATPase regulatory subunit 12 (PSD12_HUMAN)	1.19	0.013
P49721	Proteasome subunit beta type-2 (PSB2_HUMAN)	0.65	0.026
P28070	Proteasome subunit beta type-4 (PSB4_HUMAN)	0.67	0.044

J

MHC class I

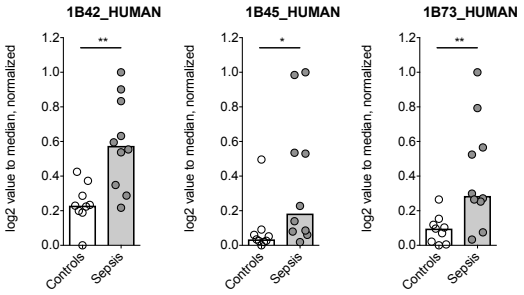

ER-to-Golgi

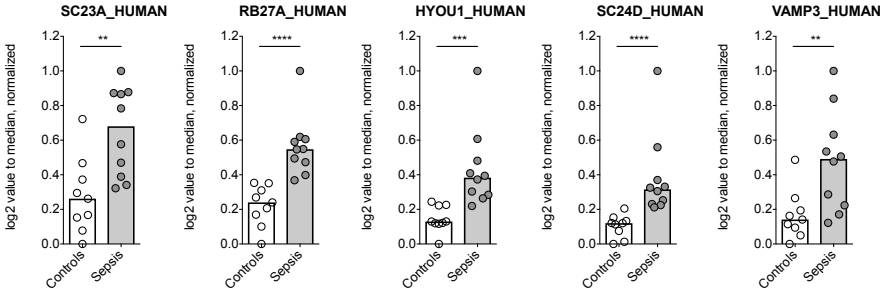

ER-associated degradation

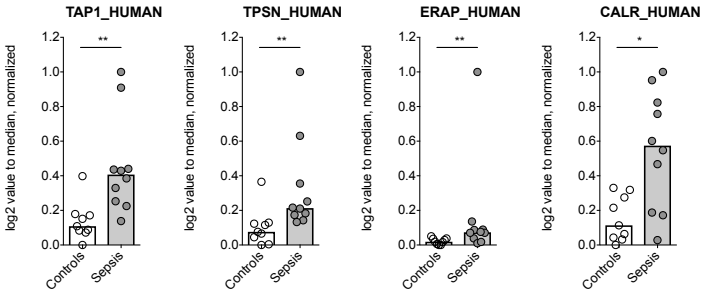

20S + 26S Proteasome complex

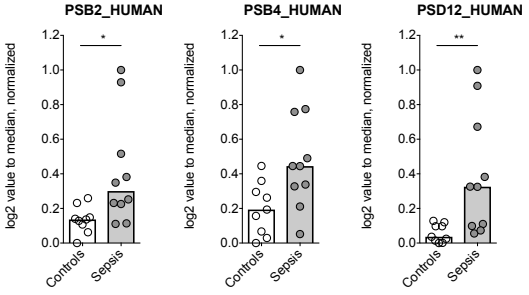

K

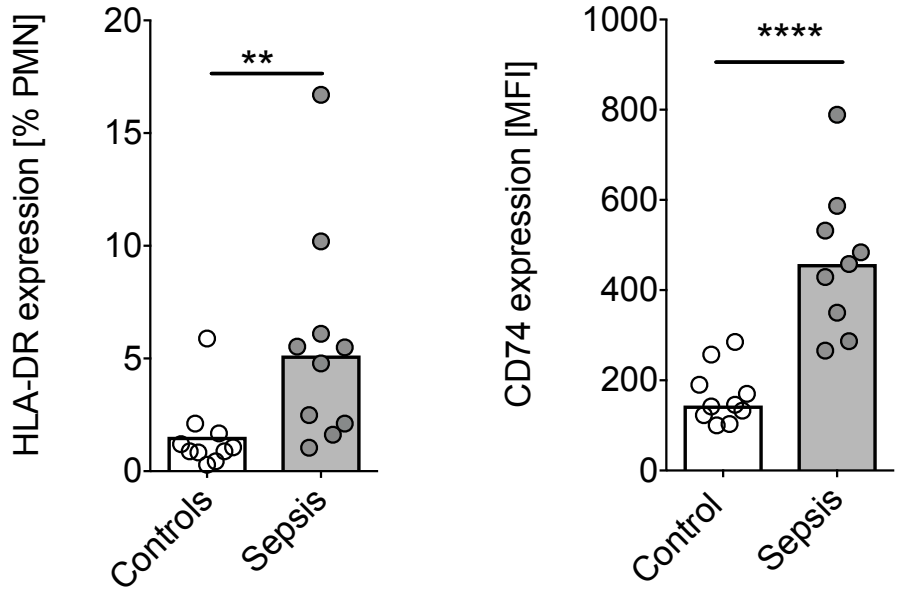
HLA-DR expression [% PMN]
20
15
10
5
0
**
Controls
Sepsis
CD74 expression [MFI]
1000
800
600
400
200
0
****
Control
Sepsis

L

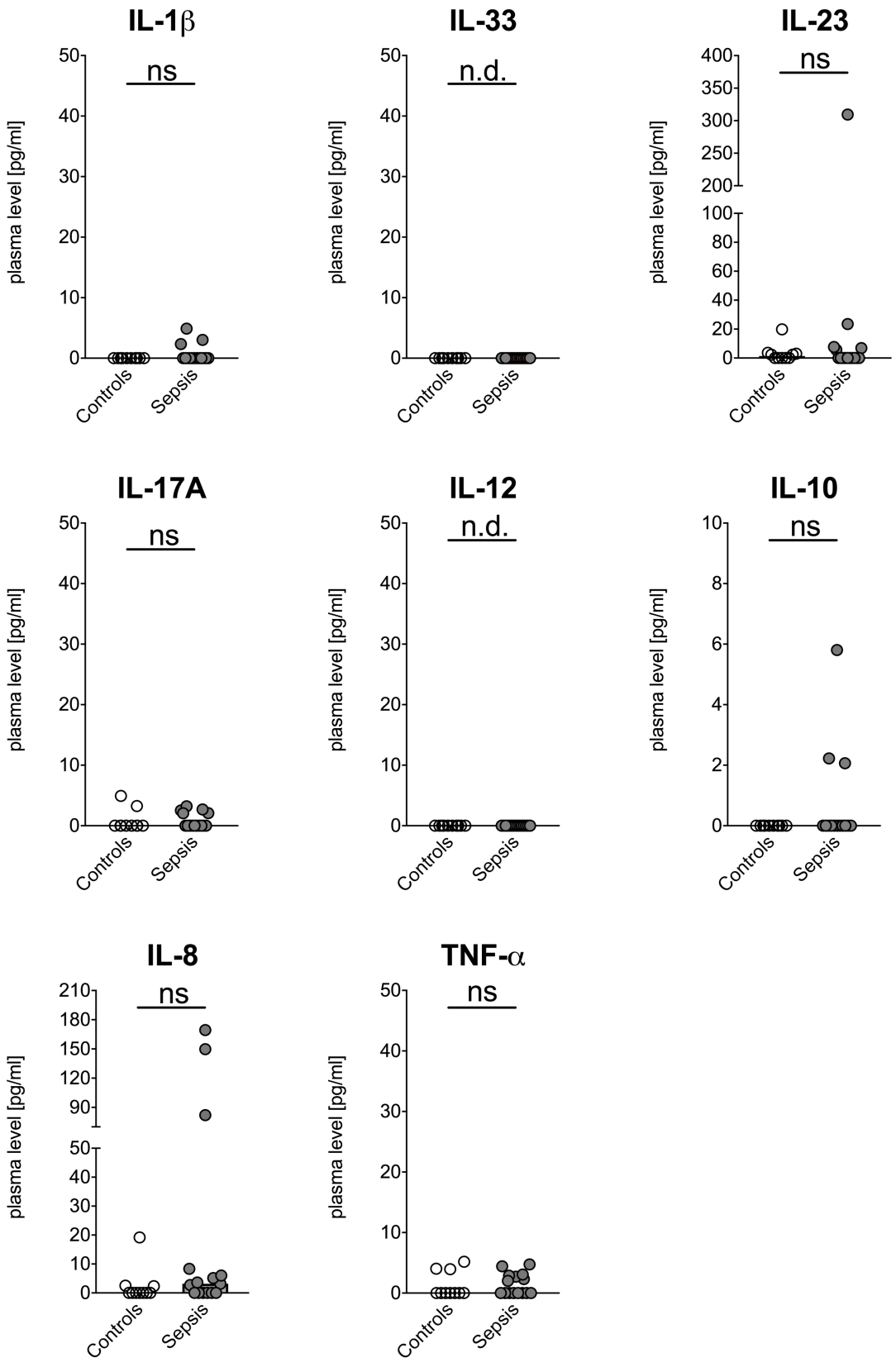
IL-1β
ns
IL-33
n.d.
IL-23
ns
IL-17A
ns
IL-12
n.d.
IL-10
ns
IL-8
ns
TNF-α
ns
plasma level [pg/ml]
Controls
Sepsis

Fig. S1: Neutrophils mimic APC-like phenotype in sepsis.

a, Age in years for controls and sepsis patients. All values are shown as medians (n= 9 for controls, n= 23 for sepsis; Mann-Whitney test; ns, not significant).

b, Body Mass Index in kg/m2 for controls and sepsis patients. All values are shown as medians (n= 10 for controls, n= 18 for sepsis; Mann-Whitney test; ns, not significant).

c, Polymorphonuclear cells (PMN) viability in percentage, measured with ADAM cell counter system. Viability was measured with ADAM Automated Cell Counter using Propidium Iodide (PI) staining. All values are shown as medians (n= 10 for controls, n= 12 for sepsis; Mann-Whitney test; ns, not significant).

d, **top** Representative kinetics of ROS production (RLU/s detection over 2 hours) in response to *in vitro Salmonella* (MOI100, MOI200) and *Candida* stimulation (MOI2) for control and sepsis patient. Means and standard deviations of three technical replicas are shown.

buttom Summary for control and sepsis patients. DPI as control was used (NADPH oxidase inhibitor, 10µM). All values are shown as medians (n= 18 for controls, n= 3 for sepsis; Mann-Whitney test; **, *P*< 0.01; ns, not significant).

e, PMN-to-lymphocyte ratio (NLR) as an index for severity of disease. NLR was measured in whole blood with flow cytometry using CD66+ / CD3+ antibodies. All values are shown as medians (n= 9 for controls, n= 12 for sepsis; Mann-Whitney test; ***, *P*< 0.001).

f, **top** List of significant protein changes involved in *Antigen presentation by MHC class I* from proteomics data analysis (n= 9 for controls, n= 10 for sepsis). Significance threshold was set at P-value < 0.02 and fold change ≤ 1.5 cut-off in order of P-value. Uniprot ID, Protein name (and gene name), Fold change (log2) and q-value are listed.

middle List of significant protein changes involved in *Antigen presentation by MHC class I: Cross-presentation* from proteomics data analysis (n= 9 for controls, n= 10 for sepsis). Significance threshold was set at P-value < 0.02 and fold change ≤ 1.5 cut-off in order of P-value. Uniprot ID, Protein name (and gene name), Fold change (log2) and q-value are listed.

below List of significant protein changes involved in *Antigen presentation by MHC class II* from proteomics data analysis (n= 9 for controls, n= 10 for sepsis). Significance threshold was set at P-value < 0.02 and fold change ≤ 1.5 cut-off in order of P-value. Uniprot ID, Protein name (and gene name), Fold change (log2) and q-value are listed.

g, Gene Ontology (GO) Process Enrichment from proteomics analysis on human neutrophils from control (n= 9) and sepsis patients (n= 10), using Metacore Enrichment by GO Processes. P-value of proteomics data was set < 0.05, threshold = 0, listed are the top 20 hits with an enrichment significance of P-value < 0.01. Identified protein counts are indicated in brackets. Red bars highlight Processes involved in *Antigen processing and presentation* in sepsis.

h, Gene Ontology (GO) Molecular Functions Enrichment from proteomics analysis on human neutrophils from control (n= 9) and sepsis patients (n= 10), using Metacore Enrichment by GO Molecular Functions. P-value of proteomics data was set < 0.05, threshold = 0, listed are the top 10 hits with an enrichment significance of P-value < 0.01. Identified protein counts are indicated in brackets. Red bars highlight Molecular Functions involved in *Antigen processing and presentation* in sepsis, such as Peptide Antigen Binding, Peptide Binding, Antigen binding, and TAP binding.

i, List of significant protein changes involved in *Antigen presentation by MHC class I and II* from proteomics analysis on human neutrophils (n= 9 for controls, n= 10 for sepsis). Significance threshold was set at P-value < 0.02 and fold change ≤ 1.5 cut-off in order of P-value. Uniprot ID, Protein name (and gene name), Fold change (log2) and q-value are listed. Target proteins were identified by using Metacore software analysis, Uniprot database (www.uniprot.org) and extensive literature research.

j, List of significant, identified protein changes involved in *Antigen presentation and processing by MHC class I and II* in human neutrophils from control (n= 9) and sepsis patients (n= 10), shown on an individual level with log2 ratio, normalized (0-1) and grouped according to cellular localizations. Significance threshold was set at P-value < 0.02 and fold change ≤ 1.5 cut-off in order of P-value. Protein names are used according to entry names in UniProt database (www.uniprot.org). All values are shown as medians (Mann-Whitney test; ****, P< 0.0001; **, P< 0.001; **, P< 0.01; *, P< 0.05).

k, HLA-DR and CD74 (Li) surface expression on human neutrophils of control and sepsis patients, measured with flow cytometry. Data are shown as Mean Fluorescence Intensity (MFI) and Percentage. All values are shown as medians (n= 10 for controls; n= 10 for sepsis; Mann-Whitney test; ****, $P < 0.0001$; **, $P < 0.01$).

l, Plasma cytokine concentration for IL-1β, IL-33, IL-23, IL-17A, IL-12, IL-10, IL-8 and TNF-α of control (n= 10) and sepsis patients (n= 17). Concentrations are indicated in [pg/ml]. All values are shown as medians (Mann-Whitney test; ns, not significant; n.d., not determined, out of standard curve range).

A

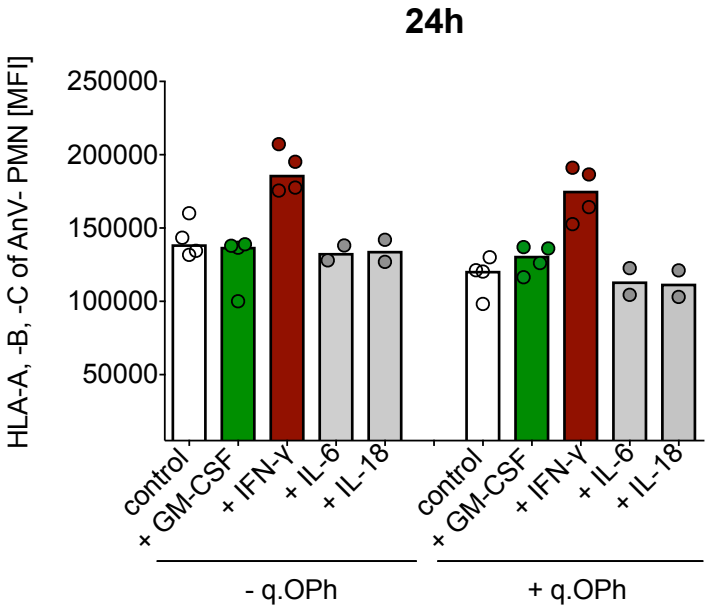
24h
HLA-A, -B, -C of AnV- PMN [MFI]
250000
200000
150000
100000
50000
control
+ GM-CSF
+ IFN-γ
+ IL-6
+ IL-18
control
+ GM-CSF
+ IFN-γ
+ IL-6
+ IL-18
- q.OPh
+ q.OPh

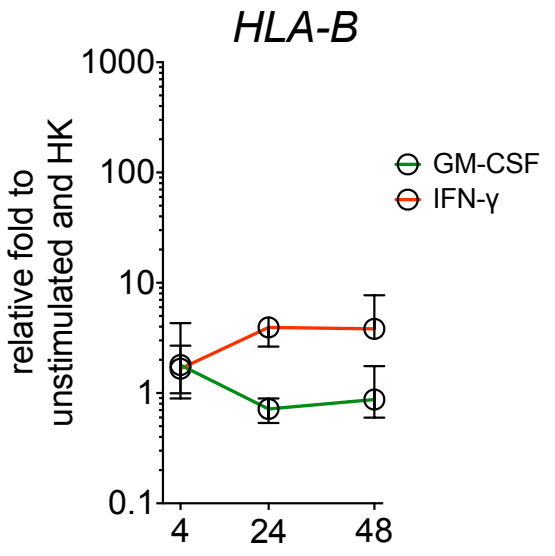
HLA-B
relative fold to unstimulated and HK
1000
100
10
1
0.1
4
24
48
GM-CSF
IFN-γ

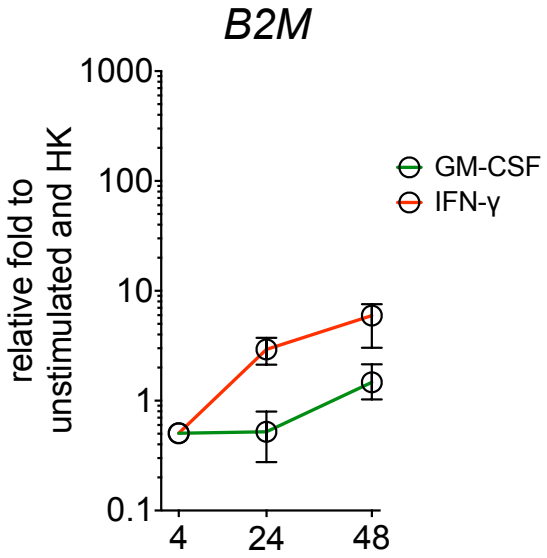
B2M
relative fold to unstimulated and HK
1000
100
10
1
0.1
4
24
48
GM-CSF
IFN-γ

B

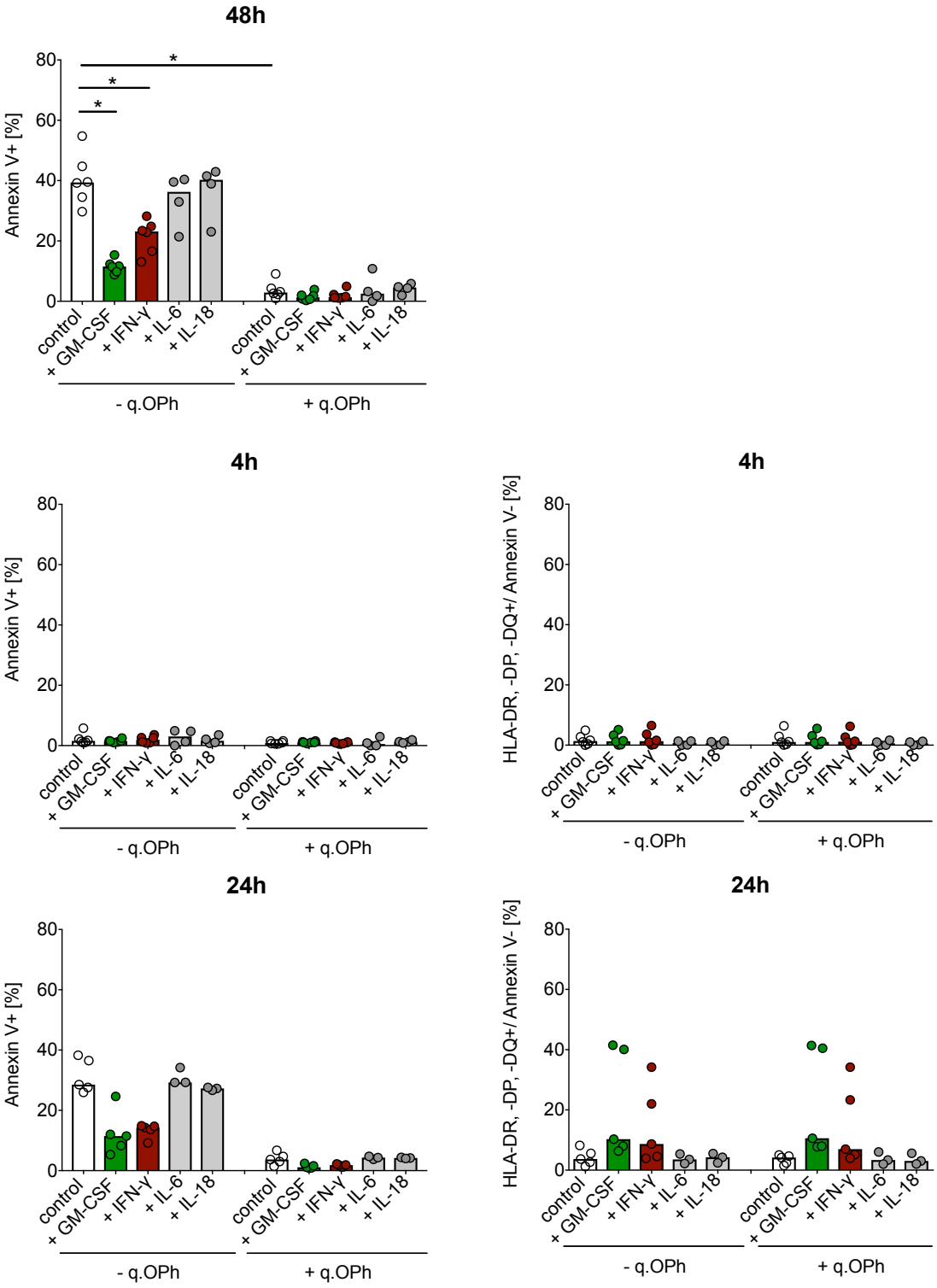
48h
4h
4h
24h
24h
Annexin V+ [%]
HLA-DR, -DP, -DQ+/ Annexin V- [%]
control
+ GM-CSF
+ IFN-γ
+ IL-6
+ IL-18
- q.OPh
+ q.OPh
*

C

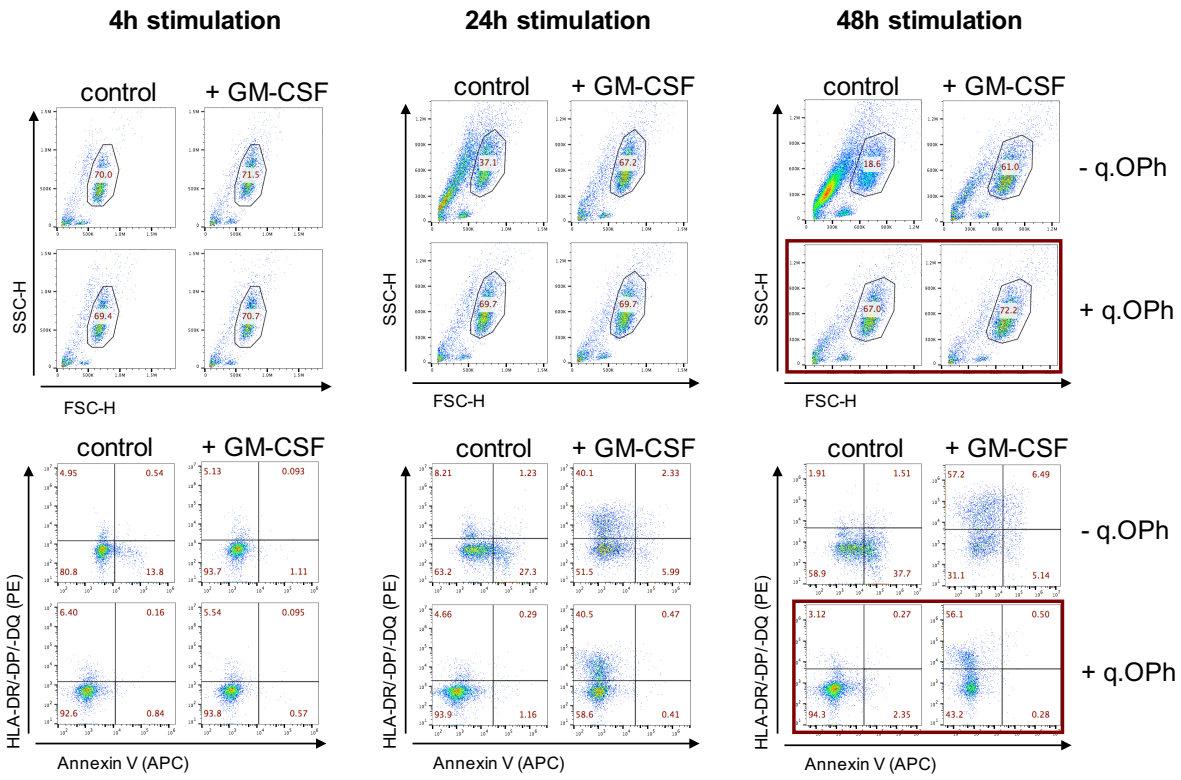
4h stimulation
24h stimulation
48h stimulation
control
+ GM-CSF
- q.OPh
+ q.OPh
SSC-H
FSC-H
HLA-DR/-DP/-DQ (PE)
Annexin V (APC)

D

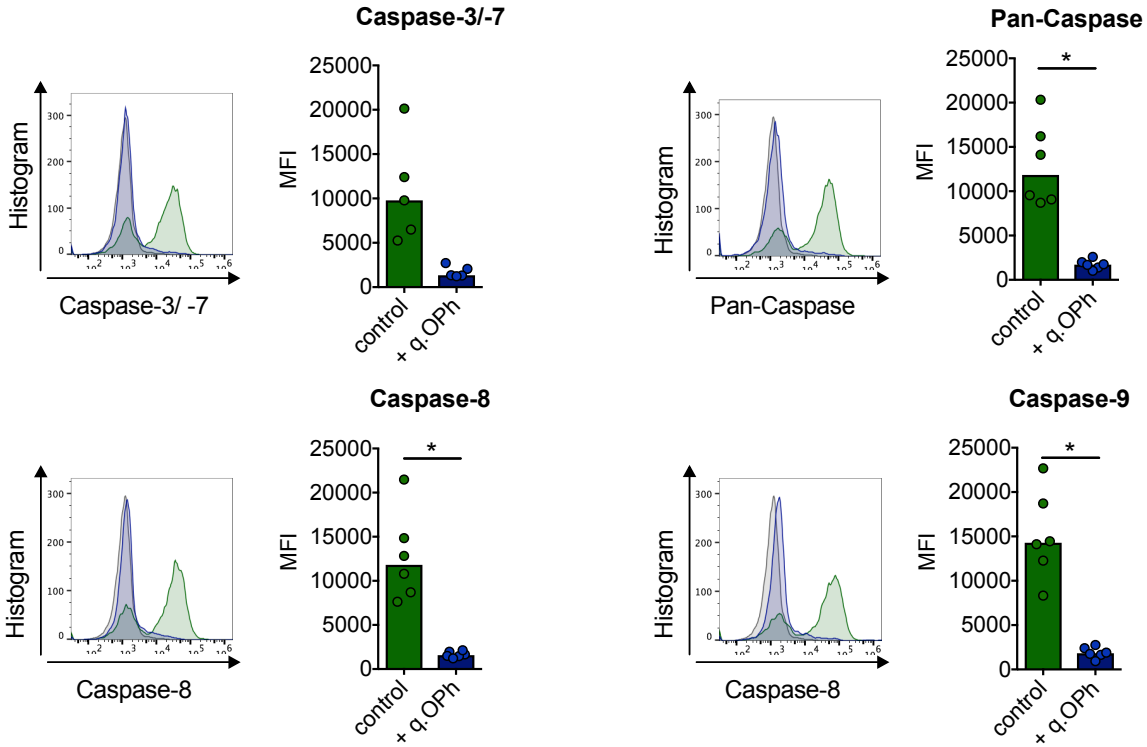
Caspase-3/-7
Histogram
Caspase-3/ -7
MFI
25000
20000
15000
10000
5000
0
control
+ q.OPh
Pan-Caspase
Histogram
Pan-Caspase
MFI
*
control
+ q.OPh
Caspase-8
Histogram
Caspase-8
MFI
*
control
+ q.OPh
Caspase-9
Histogram
Caspase-8
MFI
*
control
+ q.OPh

E

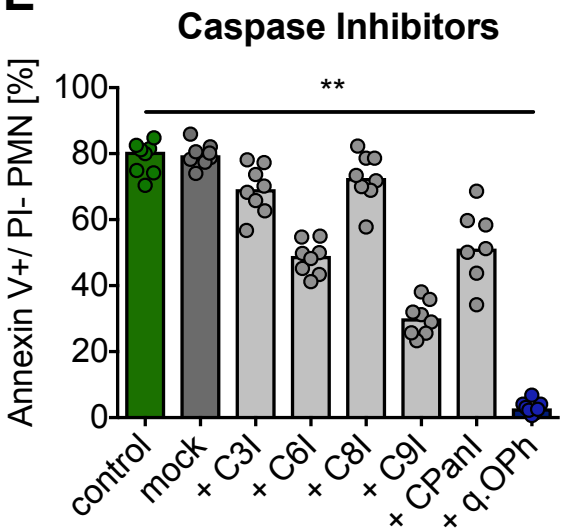
Caspase Inhibitors
Annexin V+/ PI- PMN [%]
**
100
80
60
40
20
0
control
mock
+ C3I
+ C6I
+ C8I
+ C9I
+ CPanI
+ q.OPh

F

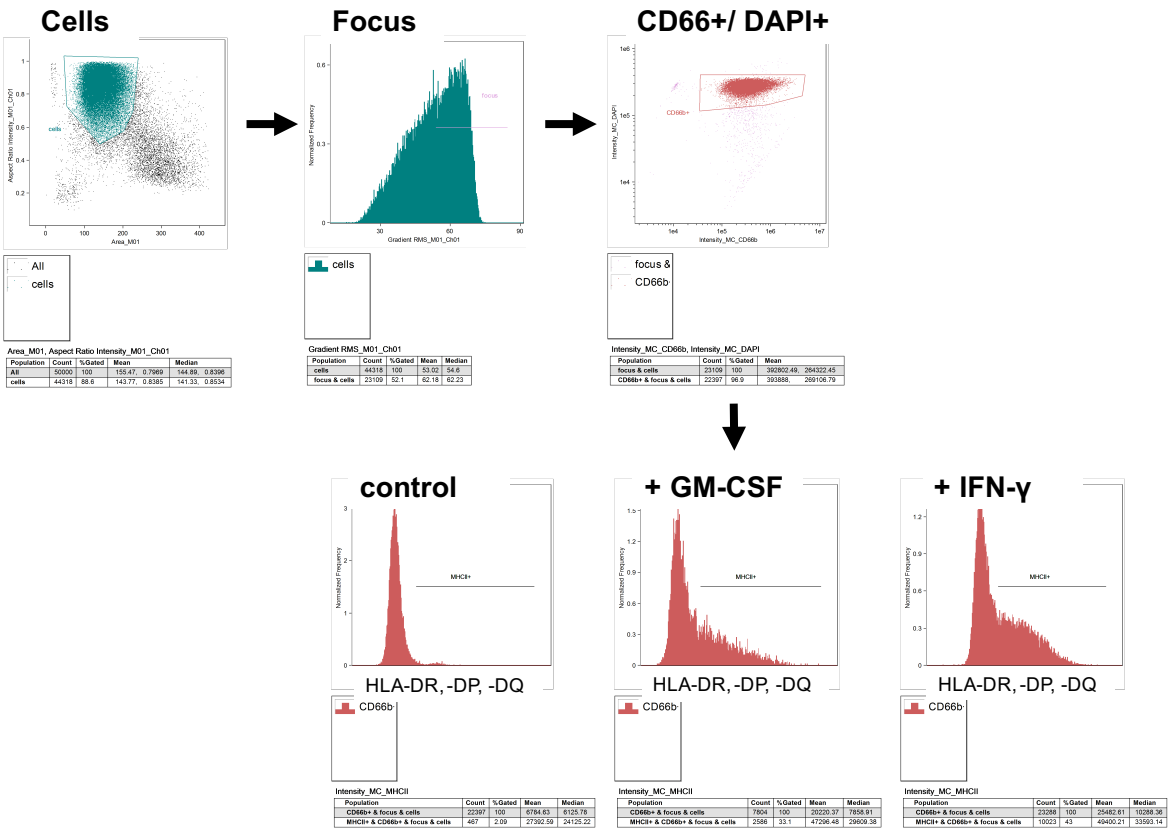

Area_M01, Aspect Ratio Intensity_M01_Ch01

Population	Count	%Gated	Mean		Median	
All	50000	100	155.47,	0.7969	144.89,	0.8396
cells	44318	88.6	143.77,	0.8385	141.33,	0.8534

Gradient RMS_M01_Ch01

Population	Count	%Gated	Mean	Median
cells	44318	100	53.02	54.6
focus & cells	23109	52.1	62.18	62.23

Intensity_MC_CD66b, Intensity_MC_DAPI

Population	Count	%Gated	Mean	
focus & cells	23109	100	392802.49,	264322.45
CD66b+ & focus & cells	22397	96.9	393888,	269106.79

Intensity_MC_MHCII

Population	Count	%Gated	Mean	Median
CD66b+ & focus & cells	22397	100	6784.63	6125.78
MHCII+ & CD66b+ & focus & cells	467	2.09	27392.59	24125.22

Intensity_MC_MHCII

Population	Count	%Gated	Mean	Median
CD66b+ & focus & cells	7804	100	20220.37	7858.91
MHCII+ & CD66b+ & focus & cells	2586	33.1	47296.48	29609.38

Intensity_MC_MHCII

Population	Count	%Gated	Mean	Median
CD66b+ & focus & cells	23288	100	25482.61	10288.36
MHCII+ & CD66b+ & focus & cells	10023	43	49400.21	33593.14

G

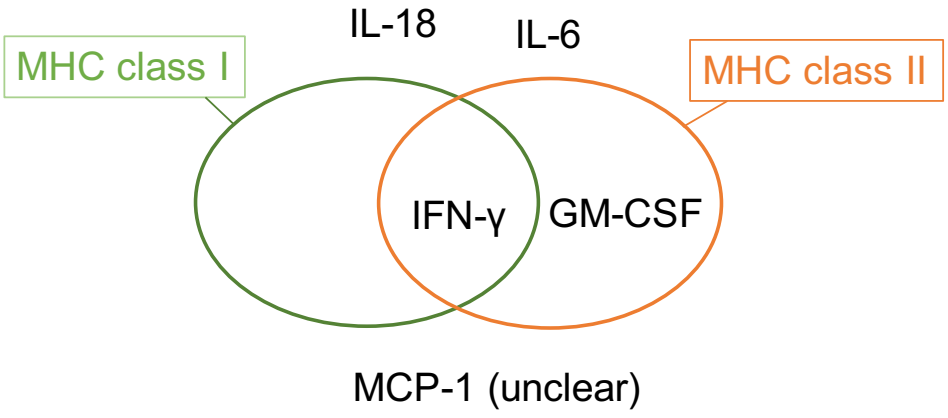

Fig. S2: GM-CSF and IFN-γ induce APC-like phenotype in human neutrophils *in vitro* and reduce neutrophil apoptosis.

a, **top** HLA-A, -B, -C expression (MFI) of viable (Annexin V-) neutrophils was measured after stimulation with human recombinant GM-CSF (10 ng/ml), IFN-γ (10 ng/ml), IL-6 (10 ng/ml) and IL-18 (10 ng/ml) for 24h, pre-incubated with/ without Pan-Caspase inhibitor q.OPh (3μM), measured with flow cytometry. All values are shown as medians (n=2-4).

bottom HLA-B and B2M mRNA expression after stimulation with human recombinant GM-CSF (10 ng/ml) and IFN-γ (10 ng/ml) for 4, 24 and 48h. Values are shown as relative fold change to unstimulated control and internal control (housekeeping gene, HK). All values are shown as medians (n=6).

b, Apoptotic neutrophils (Annexin V+) were shown after stimulation with human recombinant GM-CSF (10 ng/ml), IFN-γ (10 ng/ml), IL-6 (10 ng/ml) and IL-18 (10 ng/ml) for 4h, 24h and 48h, pre-incubated with/ without Pan-Caspase inhibitor q.OPh (3μM), measured with flow cytometry. All values are shown as medians (n=3-6). Percentage of HLA-DR/ -DP/ -DQ+ /Annexin V- neutrophils on human neutrophils (CD66b+ cells) after stimulation with human recombinant GM-CSF (10 ng/ml), IFN-γ (10 ng/ml), IL-6 (10 ng/ml) and IL-18 (10 ng/ml) for 4h and 24h, pre-incubated with/ without Pan-Caspase inhibitor q.OPh (3μM), measured with flow cytometry. All values are shown as medians (n=3-6).

c, Representative scatter dot plots of HLA-DR/ -DP/ -DQ and Annexin V surface expression on human neutrophils after stimulation with human recombinant GM-CSF (10 ng/ml) for 4h, 24h and 48h, pre-incubated -/ + Pan-Caspase inhibitor q.OPh (3μM), measured with flow cytometry. SSC-H and FSC-H plot demonstrate the increasing rate of neutrophils apoptosis (controls) *in vitro* without Pan-Caspase inhibitor q.OPh addition. HLA-DR/ -DP/ -DQ and Annexin V plots underline the increasing rate of neutrophils apoptosis (controls) *in vitro* without Pan-Caspase inhibitor q.OPh addition, despite strict gating conditions. Red squares are highlighting the beneficial effect of Pan-Caspase inhibitor q.OPh addition for neutrophil survival.

d, Caspase-3/-7, Caspase-8, Caspase-9 and Pan-Caspase activity in human neutrophils was measured with FAM FLICA™ Caspase kit. Neutrophils were pre-incubated without (green) and with Pan-Caspase inhibitor q.OPh (blue, 3μM) for 48h, and Caspase activity measured with flow cytometry. Unstained, untreated control is indicated in grey. All MFI values are shown as medians (n=5-6; Wilcoxon signed rank test; **, $P < 0.01$; *, $P < 0.05$).

e, Neutrophils were pre-incubated without (green), mock control (DMSO, 1:100, dark grey), and selective Caspase inhibitors for Caspase-3 (C3I), Caspase-6 (C6I), Caspase-8 (C8I), Caspase-9 (C9I), Pan-Caspase (CPanI), and with Pan-Caspase inhibitor q.OPh (blue, 3μM) for 48h, and apoptosis was determined with flow cytometry (Annexin V+/PI- cells). All percentages of Annexin V+/PI- cells are shown as medians (n=8; Wilcoxon signed rank test; **, $P < 0.01$).

f, Gating strategy of a representative example of *de novo* MHC class II (HLA-DR/ -DP/ -DQ) surface molecule expression on neutrophils after stimulation with human recombinant GM-CSF (10 ng/ml)

respectively IFN-γ (10 ng/ml) for 48h, measured by Image Stream X. The cell population gate was defined by the Aspect Ratio Intensity and Area, the focus was set at Gradient RMS levels > 50. Human neutrophils were identified as CD66+/DAPI+ cells. MHC class II expression levels were measured by HLA-DR/-DP/-DQ expression.

g, Schematic overview of cytokine-induced MHC class I and MHC class II induction in human neutrophils *in vitro*. GM-CSF induces *de novo* MHC class II after 48h, whereas MHC class I expression is unaffected. IFN-γ induces both, MHC class I and MHC class II expression after 24h and 48h, respectively. IL-18 and IL-6 neither induce MHC class I nor MHC class II expression on neutrophils *in vitro*.

A

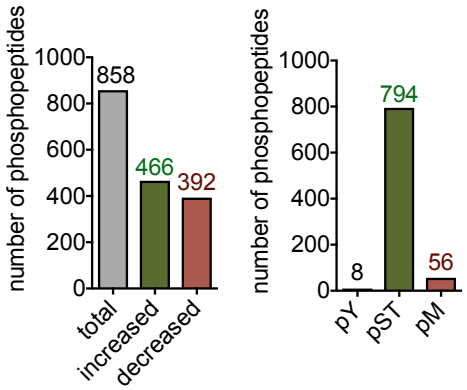

Total detected phosphopeptides: 3579
Total detected phosphoproteins: 1328

B

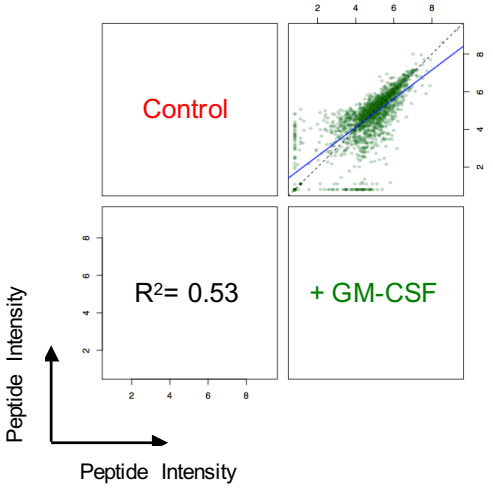

C

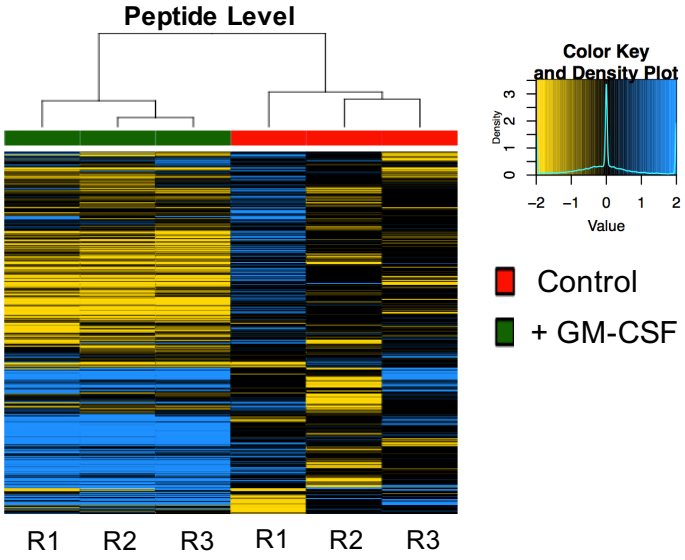

D

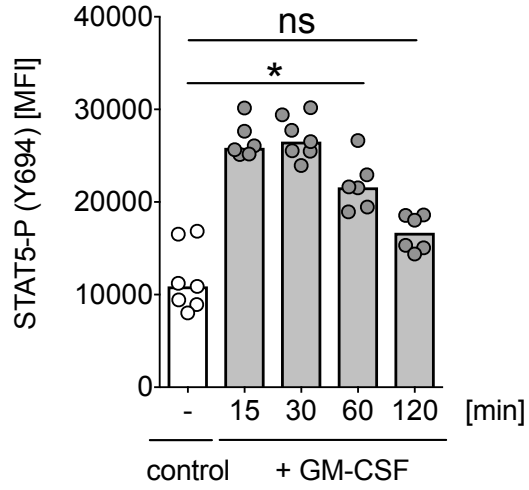
STAT5-P (Y694) [MFI]
40000
30000
20000
10000
0
ns
*
-
15
30
60
120
[min]
control
+ GM-CSF

E

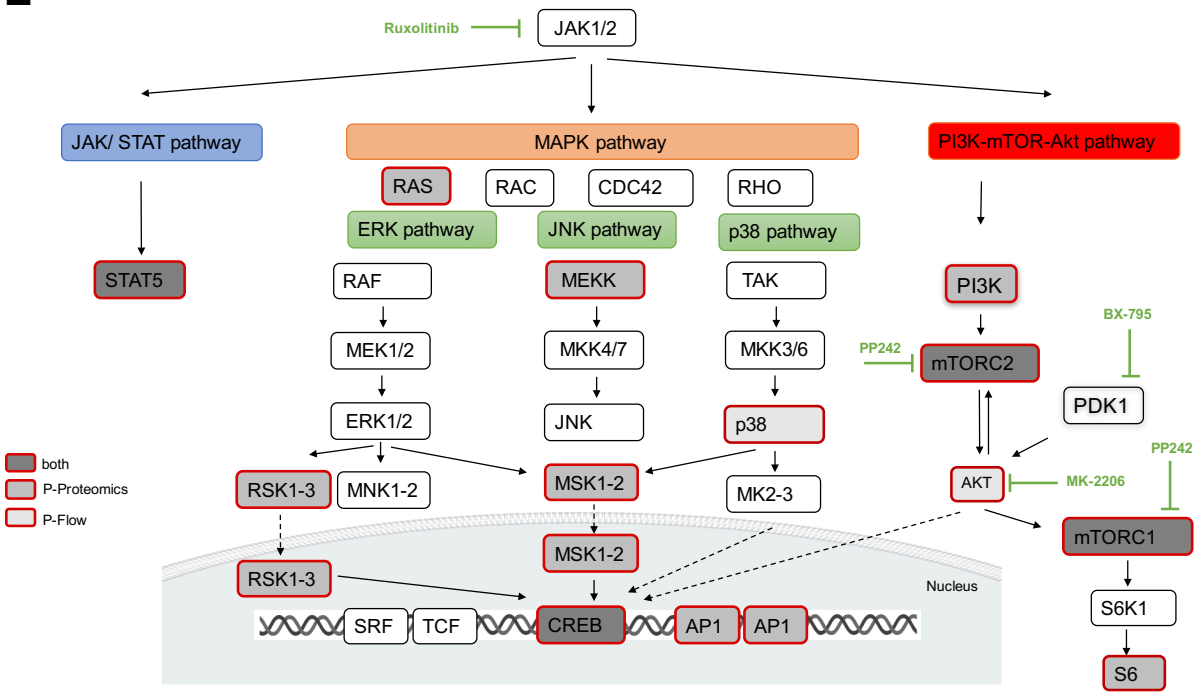
Ruxolitinib
JAK1/2
JAK/ STAT pathway
MAPK pathway
PI3K-mTOR-Akt pathway
RAS
RAC
CDC42
RHO
ERK pathway
JNK pathway
p38 pathway
STAT5
RAF
MEKK
TAK
PI3K
BX-795
MEK1/2
MKK4/7
MKK3/6
PP242
mTORC2
PDK1
ERK1/2
JNK
p38
both
P-Proteomics
P-Flow
RSK1-3
MNK1-2
MSK1-2
MK2-3
AKT
MK-2206
PP242
mTORC1
MSK1-2
RSK1-3
Nucleus
SRF
TCF
CREB
AP1
AP1
S6K1
S6

Fig. S3: GM-CSF signaling leads to the activation of JAK-STAT, MAPK p38 and mTOR-AKT signaling pathways and phosphorylation of transcription factor CREB1.

a, 3579 phosphopeptides were detected in human neutrophils after stimulation with GM-CSF for 30min, belonging to 1328 phosphoproteins. Phosphoproteomics data were performed in three biological replica each condition. 858 significant phosphopeptide changes were identified, whereas 466 phosphopeptides were increased and 392 phosphopeptides were decreased upon GM-CSF stimulation. Significance threshold was set at q-value < 0.05 and fold change ≤ 2 cut-off in order of P-value. The majority of significantly changed phosphopeptides contain a serine/threonine residue phosphorylation (pST, n=794), whereas tyrosine residue phosphorylation (pY, n=8) and oxidation (pM, n=56) were minor.

b, Squared Pearson correlation coefficient R^2 of integrated peptide feature intensities between GM-CSF stimulation and control is 0.53.

c, Hierarchical clustering of log10 abundance ratios of changed phosphopeptides for three biological replica R1-R3 each condition (GM-CSF stimulation, green; control, red).

d, Temporal dynamics of STAT5 phosphorylation (Y694) after GM-CSF stimulation for 15, 30, 60 and 120 min, measured by using PhosFlow antibodies for flow cytometry. Unstimulated control is shown in white, GM-CSF stimulation is shown shaded. Quantification of flow cytometry data with absolute values in MFI (mean fluorescence intensity). All values are shown as medians (n = 6; Wilcoxon signed rank test, *, P< 0.05; ns, not significant).

e, Overview of hierarchical signaling phosphorylation events in human neutrophils upon GM-CSF stimulation *in vitro*. Proteins from the phosphoproteome of GM-CSF stimulated neutrophils are surrounded in red and filled in average-grey, additionally confirmed phosphoproteins by PhosFlow were surrounded in red and filled in dark-grey. Single confirmation of phosphoproteins by PhosFlow were were surrounded in red and filled in light-grey. JAK1/2 inhibition by Ruxolitinib inhibits all three different pathways. Figure was drawn with the help of Biorendor software (www.biorender.io). JAK1/2, Janus Kinase 1 and 2; STAT5, Signal Transducer and Activator of Transcription 5; p38, p38 mitogen-activated protein kinase; MSK1, Mitogen- and stress-activated protein kinase-1; PI3K, Phosphoinositide-3-kinase; mTOR, mechanistic Target of Rapamycin; S6K1, p70 ribosomal S6 kinase 1; AP1, Activator protein-1; RSK, p90 ribosomal S6 kinase; JNK, C-Jun-N-terminal kinase; RAS, Rat sarcoma protein; RAC, Rho family of GTPases; CDC42, Cell division control protein 42; TAK, Tat-associated kinase; MEKK, MAP kinase kinase kinase; MEK, kinase of MAP kinase; MKK, Mitogen-activated protein kinase kinase; ERK, Extracellular-signal regulated kinase; MK, Mitogen-activated protein kinase 2.

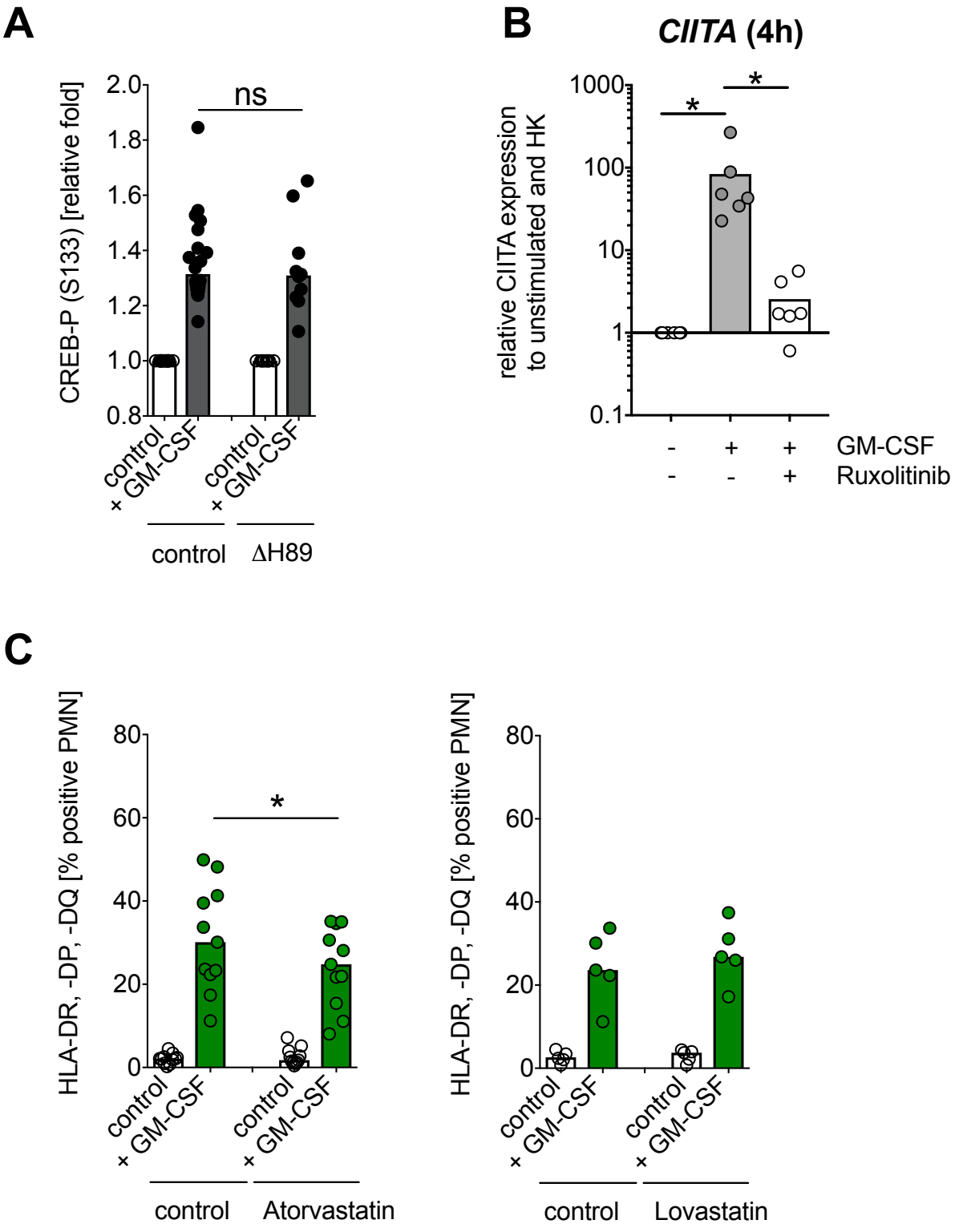
A
CREB-P (S133) [relative fold]
2.0
1.8
1.6
1.4
1.2
1.0
0.8
ns
control
× GM-CSF
control
× GM-CSF
control
ΔH89
B
CIITA (4h)
relative CIITA expression
to unstimulated and HK
1000
100
10
1
0.1
*
*
- + + GM-CSF
- - + Ruxolitinib
C
HLA-DR, -DP, -DQ [% positive PMN]
80
60
40
20
0
*
control
× GM-CSF
control
× GM-CSF
control
Atorvastatin
HLA-DR, -DP, -DQ [% positive PMN]
80
60
40
20
0
control
× GM-CSF
control
× GM-CSF
control
Lovastatin

Fig. S4: Targeting the MHC class II enhanceosome in human neutrophils.

a, CREB1 phosphorylation at Ser133 in upon GM-CSF stimulation for 30min, pre-treated with inhibitor H89 (PKA inhibitor, final conc. = 10µM), was quantified with flow cytometry. Data are shown with relative fold changes to control (n = 10-18; Wilcoxon signed rank test; ns, not significant).

b, *CIITA* mRNA expression after stimulation with human recombinant GM-CSF (10 ng/ml) for 4h, pretreated with Ruxolitinib (ΔJAK1/2 inhibitor, final conc. = 3µM) for 1h. Values are shown as relative fold change to unstimulated control and internal control (housekeeping genes, HK). All values are shown as medians (n=6; Wilcoxon signed rank test; *, P< 0.05).

c, Percentage of HLA-DR/ -DP/ -DQ+ /Annexin V- neutrophils after pre-incubation with/ without Atorvastatin (ΔHMG-CoA reductase inhibitor, final conc. = 50µM), and Lovastatin (ΔHMG-CoA reductase inhibitor, final conc. = 50µM), stimulated with human recombinant GM-CSF (10 ng/ml) for 48h. All values are shown as medians (n=11 for Atorvastatin, n=5 for Lovastatin; Wilcoxon signed rank test; *, P< 0.05).

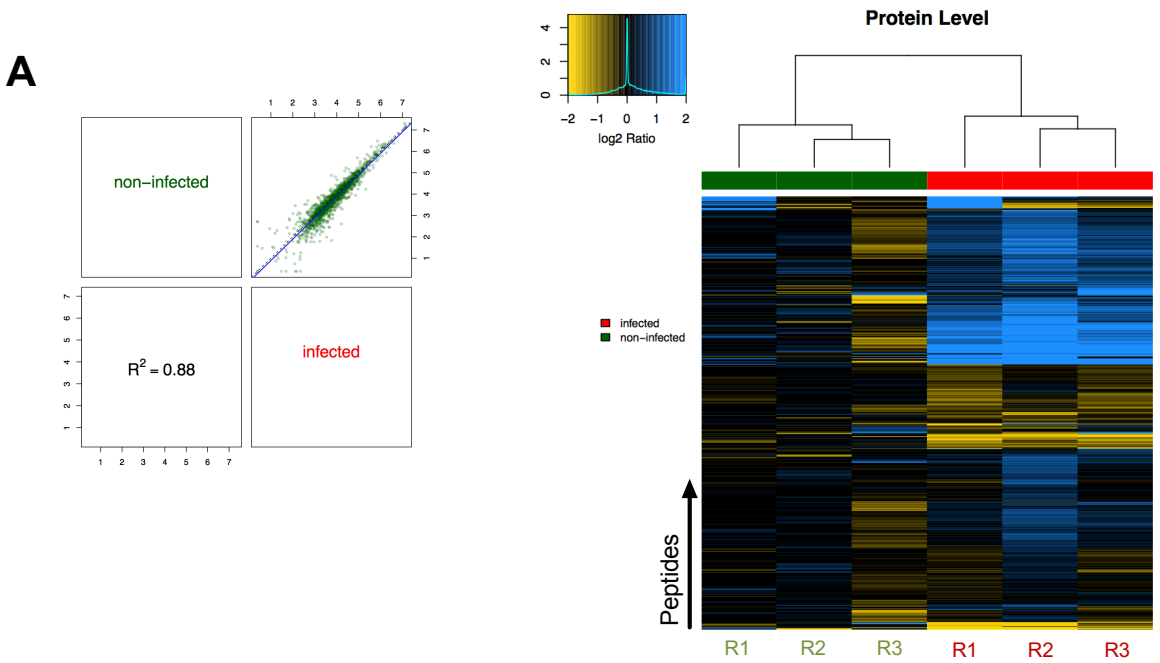
A
non−infected
infected
R^2 = 0.88
log2 Ratio
Protein Level
infected
non−infected
Peptides
R1
R2
R3
R1
R2
R3

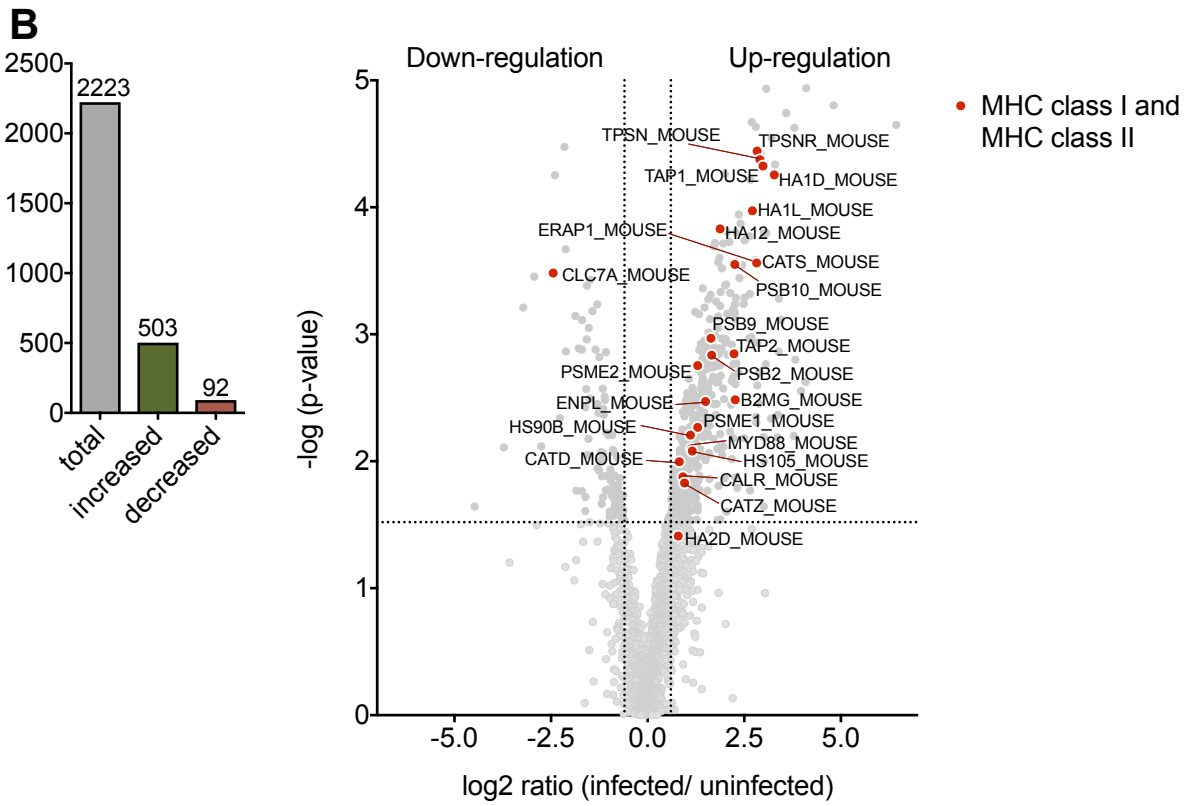
B
2223
503
92
total
increased
decreased
Down-regulation
Up-regulation
-log (p-value)
log2 ratio (infected/ uninfected)
TPSN_MOUSE
TPSNR_MOUSE
TAP1_MOUSE
HA1D_MOUSE
HA1L_MOUSE
ERAP1_MOUSE
HA12_MOUSE
CATS_MOUSE
CLC7A_MOUSE
PSB10_MOUSE
PSB9_MOUSE
TAP2_MOUSE
PSME2_MOUSE
PSB2_MOUSE
ENPL_MOUSE
B2MG_MOUSE
HS90B_MOUSE
PSME1_MOUSE
MYD88_MOUSE
CATD_MOUSE
HS105_MOUSE
CALR_MOUSE
CATZ_MOUSE
HA2D_MOUSE
MHC class I and
MHC class II

C

Pathways, enriched in systemic *Salmonella* infection, d04: Top 20

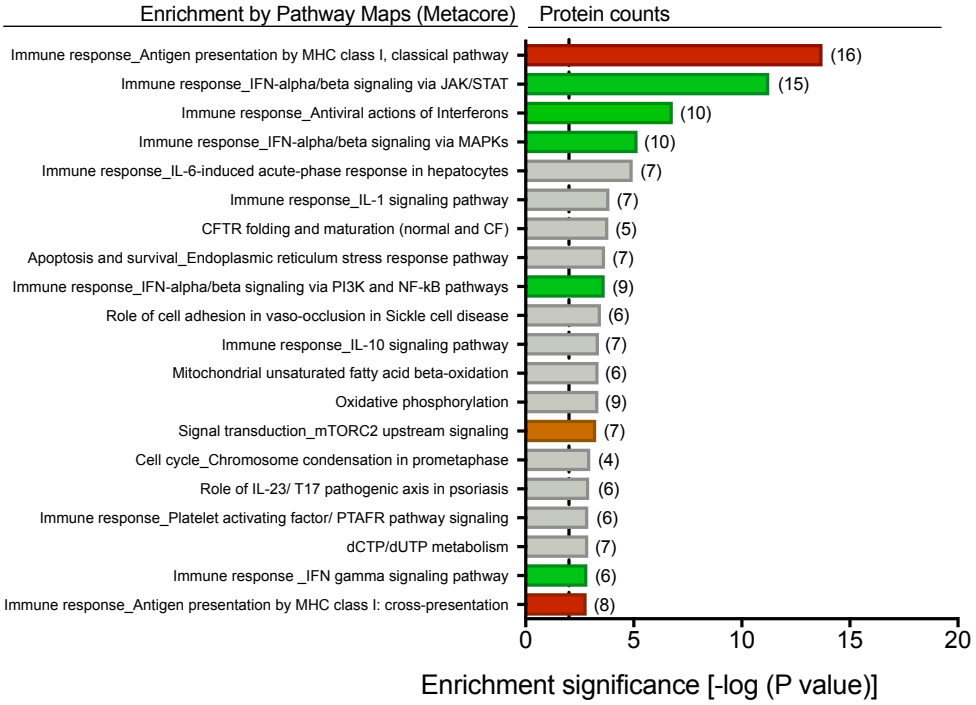

Classification based on Metacore software, P value< 0.05, T=0

D

GO Molecular Functions, enriched in systemic *Salmonella* infection, d04: 13 out of Top 50

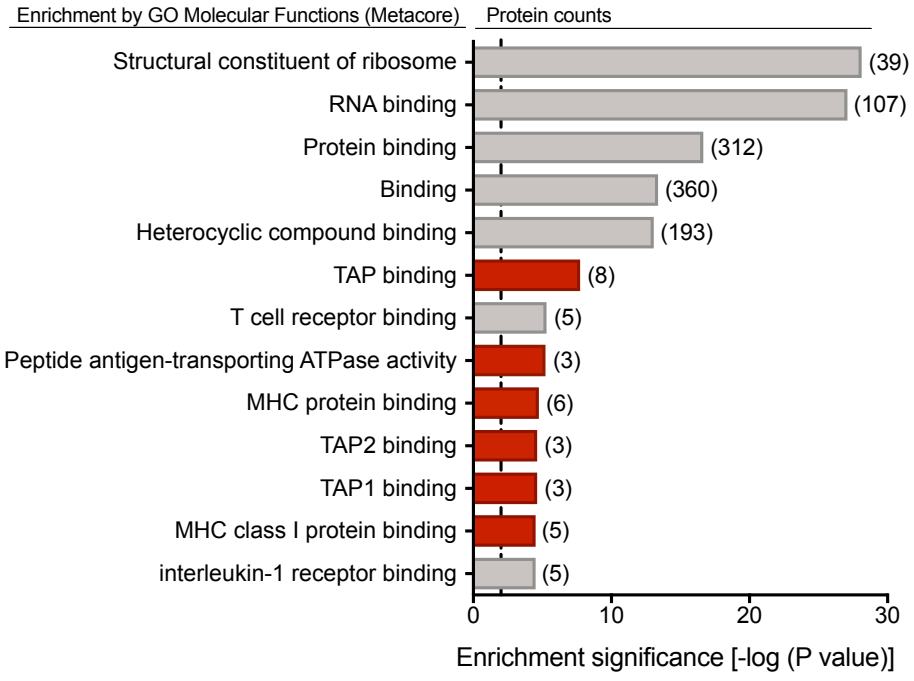

Classification based on Metacore software, P value< 0.05, T>1

E

Antigen presentation by MHC class I and MHC class II (n=25)

Uniprot ID	Protein	Fold Change (log2)	P-value
P04223	H-2 class I histocompatibility antigen, K-K alpha chain (HA1K_MOUSE)	3.78	0.000
P01902	H-2 class I histocompatibility antigen, K-D alpha chain (HA1D_MOUSE)	3.27	0.000
P01897	H-2 class I histocompatibility antigen, L-D alpha chain (HA1L_MOUSE)	2.71	0.000
P01900	H-2 class I histocompatibility antigen, D-D alpha chain (HA12_MOUSE)	1.87	0.000
P04228	H-2 class II histocompatibility antigen, A-D alpha chain (HA2D_MOUSE)	0.79	0.039*
P01887	Beta-2-microglobulin (B2MG_MOUSE)	2.26	0.003
P97371	Proteasome activator complex subunit 1 (PMSE1_MOUSE)	1.29	0.005
P97372	Proteasome activator complex subunit 2 (PMSE2_MOUSE)	1.29	0.002
Q9R1P3	Proteasome subunit beta type-2 (PSB2_MOUSE)	1.66	0.001
P28076	Proteasome subunit beta type-9 (PSB9_MOUSE)	1.64	0.001
O35955	Proteasome subunit beta type-10 (PSB10_MOUSE)	2.25	0.000
P21958	Antigen peptide transporter 1 (TAP1_MOUSE)	2.98	0.000
P36371	Antigen peptide transporter 2 (TAP2_MOUSE)	2.23	0.001
Q9R233	Tapasin (TPSN_MOUSE)	2.91	0.000
Q8VD31	Tapasin-related protein (TPSNR_MOUSE)	2.83	0.000
P08113	Endoplasmin (ENPL_MOUSE)	1.49	0.003
Q9EQH2	Endoplasmic reticulum aminopeptidase 1 (ERAP1_MOUSE)	2.26	0.000
P14211	Calreticulin (CALR_MOUSE)	0.91	0.013
P11499	Heat shock protein HSP 90-beta (HS90B_MOUSE)	1.10	0.006
P22366	Myeloid differentiation primary response protein MyD88 (MyD88_MOUSE)	1.13	0.008
Q61699	Heat shock protein 105 kDa (HS105_MOUSE)	1.15	0.008
Q6QLQ4	C-type lectin domain family 7 member A, Synoyme: Dectin-1 (CLC7A_MOUSE)	-2.4	0.000
O70370	Cathepsin S (CATS_MOUSE)	2.82	0.000
P18242	Cathepsin D (CATD_MOUSE)	0.82	0.010
Q9WUU7	Cathepsin Z (CATZ_MOUSE)	0.95	0.015

F

Gene ID (_MOUSE or _HUMAN)	Protein Name	Regulation HUMAN	Regulation MOUSE	Function
RL5	60S ribomal protein L5	Up	Up	Ribosome
RPN1	Dolichyl-diphphooligaccharide–protein glycyltransferase subunit 1	Up	Up	
SSRA	Translocon-associated protein subunit alpha	Up	Up	
PACS1	Phphofurin acidic cluster sorting protein 1	Down	Down	
MLEC	Malectin	Up	Up	
ETFA	Electron transfer flavoprotein subunit alpha, mitochondrial	Up	Up	Mitochodrion
ACADM	Medium-chain specific acyl-CoA dehydrogenase, mitochondrial	Up	Up	Mitochodrion
ARSB	Arylsulfatase B	Down	Up	
HYOU1	Hypoxia up-regulated protein 1	Up	Up	Antigen processing and presentation
CASP1	Caspase-1	Up	Up	Interferon Signaling
CAMP	Cathelin-related antimicrobial peptide	Down	Down	
COX41	Cytochrome c oxidase subunit 4 isoform 1, mitochondrial	Up	Up	Mitochondrion/ Apoptose
ACSL1	Long-chain-fatty-acid–CoA ligase 1	Up	Up	
DHB4	Peroxisomal multifunctional enzyme type 2	Up	Up	
HS105	Heat shock protein 105 kDa	Up	Up	Antigen processing and presentation
ELAV1	ELAV-like protein 1	Up	Up	
IFIT2	Interferon-induced protein with tetratricopeptide repeats 2	Up	Up	Interferon Signaling
STT3A	Dolichyl-diphphooligaccharide–protein glycyltransferase subunit STT3A	Up	Up	
LCP2	Lymphocyte cytolic protein 2	Up	Up	
PDIA1	Protein disulfide-isomerase	Up	Up	
PADI4	Protein-arginine deiminase type-4	Down	Down	
PROP	Properdin	Down	Down	
PPT1	Palmitoyl-protein thioesterase 1	Up	Up	
PSB4	Proteasome subunit beta type-4	Up	Up	Antigen processing and presentation
RL30	60S ribomal protein L30	Up	Up	Ribosome
RS18	40S ribomal protein S18	Up	Up	Ribosome
TAP1	Antigen peptide transporter 1	Up	Up	Antigen processing and presentation
TPSN	Tapasin	Up	Up	Antigen processing and presentation
CKAP4	Cytkeleton-associated protein 4	Up	Up	
TIAR	Nucleolysin TIAR	Up	Up	
ENPL	Endoplasmin	Up	Up	Antigen processing and presentation
GBP5	Guanylate-binding protein 5	Up	Up	Interferon Signaling
PTBP3	Polypyrimidine tract-binding protein 3	Up	Up	
EFTU	Elongation factor Tu, mitochondrial	Up	Up	
OAS3	2'-5'-oligoadenylate synthase 3	Up	Up	Interferon Signaling
PSB2	Proteasome subunit beta type-2	Up	Up	Antigen processing and presentation
AAK1	AP2-associated protein kinase 1	Up	Up	
PAR14	Poly [ADP-ribe] polymerase 14	Up	Up	
SND1	Staphylococcal nuclease domain-containing protein 1	Up	Up	
NAMPT	Nicotinamide phphoribyltransferase	Up	Up	
NIBAN	Protein Niban	Up	Down	
NMI	N-myc-interactor	Up	Up	
EF1D	Elongation factor 1-delta	Up	Up	Ribosome
RS20	40S ribomal protein S20	Up	Up	Ribosome
TMCO1	Transmembrane and coiled-coil domain-containing protein 1	Up	Up	
PDIA6	Protein disulfide-isomerase A6	Up	Up	
RS25	40S ribomal protein S25	Up	Up	Ribosome
CKAP5	Cytkeleton-associated protein 5	Up	Up	
MBOA7	Lysophpholipid acyltransferase 7	Up	Up	
MVP	Major vault protein	Up	Up	
ERAP1	Endoplasmic reticulum aminopeptidase 1	Up	Up	Antigen processing and presentation
RRBP1	Ribome-binding protein 1	Up	Up	Ribosome
LRC59	Leucine-rich repeat-containing protein 59	Up	Up	

Fig. S5: Induction of APC-like neutrophils in a systemic *Salmonella* mouse model mimicking human typhoid fever.

a, **left** Squared Pearson correlation coefficient R^2 of integrated peptide feature intensities between non-infected and *Salmonella enterica* serovar Typhimurium *SL1344* infected splenic neutrophils at day 4 is 0.88.

right Hierarchical clustering of log2 abundance ratios of changed peptides for three biological replica R1-R3 each condition (non-infected, green; infected, red).

b, **left** Number of peptides (n=2223) identified by murine neutrophil proteomics from non-infected (n=3) and *Salmonella enterica* serovar Typhimurium *SL1344* infected splenic neutrophils (n=3) at day 4 with significant increased (n=503) and decreased (n=92) peptide levels. Significance threshold was set at P-value < 0.03.

right Volcano dot plot from murine neutrophil proteomics from non-infected (n=3) and *Salmonella enterica* serovar Typhimurium *SL1344* infected splenic neutrophils (n=3) at day 4. Highlighted proteins (red dots) are associated with *Antigen presentation and processing by MHC class I and II*, significance threshold (dotted line) was set at P-value < 0.03 and fold change ≤ 1.5 cut-off in order of P-value.

c, Enriched pathways using murine neutrophil proteomics from non-infected (n=3) and *Salmonella enterica* serovar Typhimurium *SL1344* infected splenic neutrophils (n=3) at day 4, using Metacore Enrichment by Pathway Maps. P-value of proteomics data was set < 0.05, threshold = 0, listed are the top 20 hits with an enrichment significance of P-value < 0.01. Identified protein counts are indicated in brackets. Red bars highlight *Antigen Presentation and processing by MHC class I and MHC class II* as highly changed pathways upon *Salmonella enterica* serovar Typhimurium *SL1344* infection.

d, Gene Ontology (GO) Molecular Functions Enrichment using murine neutrophil proteomics from non-infected (n=3) and *Salmonella enterica* serovar Typhimurium *SL1344* infected splenic neutrophils (n=3) at day 4, using Metacore Enrichment by GO Molecular Functions. P-value of proteomics data was set < 0.05, threshold > 1, listed are the top 10 hits with an enrichment significance of P-value < 0.01. Identified protein counts are indicated in brackets. Red bars highlight Molecular Functions involved in *Antigen processing and presentation* upon *Salmonella enterica* serovar Typhimurium *SL1344* infection, such as TAP binding, Peptide antigen-transporting ATPase activity, MHC protein binding, TAP2 binding, TAP1 binding, and MHC class I protein binding.

e, List of significant protein changes involved in *Antigen presentation by MHC class I and II* from proteomics data analysis (n=3 for non-infected, n= 3 for infected). Significance threshold was set at P-value < 0.03 and fold change ≤ 1.5 cut-off in order of P-value. Uniprot ID, Protein name (and gene name), Fold change (log2) and P-value are listed.

f, List of significantly differentially expressed, orthologous proteins by comparing the proteome data sets from isolated splenic murine neutrophils infected with *Salmonella enterica* serovar Typhimurium at day 4 and the human peripheral blood derived neutrophils in sepsis (n=52, FDR< 0.05). Gene ID, protein

name, regulation in human and mice and function are listed. Around 15% of those identified proteins are involved in antigen processing and presentation (n=8).

5.3 Immune Reconstitution After Allogeneic Hematopoietic Stem Cell Transplantation and Association with Occurrence and Outcome of Invasive Aspergillosis

Stuehler C[1], Kuenzli E[2], Jaeger VK[3], Baettig V[2], Ferracin F[1], Rajacic Z[1], Kaiser D[1], Bernardini C[1], **Forrer P**[1], Weisser M[2], Elzi L[2], Battegay M[2], Halter J[4], Passweg J[4], Khanna N[1,2] *

[1]Infection Biology Laboratory, Department of Biomedicine; [2]Division of Infectious Diseases and Hospital Epidemiology, Department of Clinical Research; [3]Department of Rheumatology; [4]Division of Hematology, University Hospital of Basel, Switzerland.

* Corresponding author

Manuscript has been published in The Journal of Infectious Diseases, 2015; 212:959-67

DOI: 10.1093/infdis/jiv143

Statement of my work:

Design of experiments

ROS production assays + Analysis (partly contributed to Fig. 2A; Fig. 4A; Fig. 5A, but Fig. 6 is not shown in the paper).

Note: The following part contains only the abstract and the figures to which I contributed in this manuscript. The contribution of my work is the establishment and optimization of the chemiluminescence-enhanced ROS production assay and the finding that isolated neutrophils have to be processed as soon as possible because of cellular apoptosis.

5.3.1 Abstract/ Summary

Invasive aspergillosis (IA) remains a leading cause of morbidity and mortality in patients receiving allogeneic hematopoietic stem cell transplantation (HSCT). This infection occurs either early posttransplantation during neutropenia or late due to graft-versus-host disease (GVHD) and the required immunosuppressive treatment.

Antifungal prophylaxis or treatment in high-risk patients is often ineffective due to impaired host immunity and is furthermore associated with drug interactions, emergence of resistant fungi, toxicity, and high costs. Immune surrogate markers such as $CD4^+$ cell counts in human immunodeficiency virus–infected individuals and cytomegalovirus (CMV)–specific cell-mediated immunity in solid organ transplantation to guide treatment have not been established for patients with IA.

Innate immune cells, including macrophages and polymorphonuclear cells (PMNs), are key players to control fungal invasion. PMNs possess an array of effector functions involving reactive oxygen species (ROS)–dependent and independent killing mechanisms.

T cells, particularly $CD4^+$ memory T cells, specific for different Aspergillus antigens can be detected in the peripheral blood of healthy individuals and HSCT recipients. In general, T helper (T_H)1 and potentially T_H17 cytokines are considered to confer protective immunity against Aspergillus, whereas T_H2 responses are deleterious. Furthermore, recent studies suggest that natural killer (NK) cells are crucial for fungal clearance.

So far, specific reconstitution of antifungal immune responses in patients after HSCT with and without IA has not been investigated in detail. The purpose of this study was to prospectively follow patients after HSCT and to obtain comprehensive data on immune reconstitution and the functionality of PMNs, NK cells, different TH subsets, and $CD8^+$ T cells in order to characterize susceptibility of these patients to IA and to identify possible biomarkers to guide antifungal treatment.

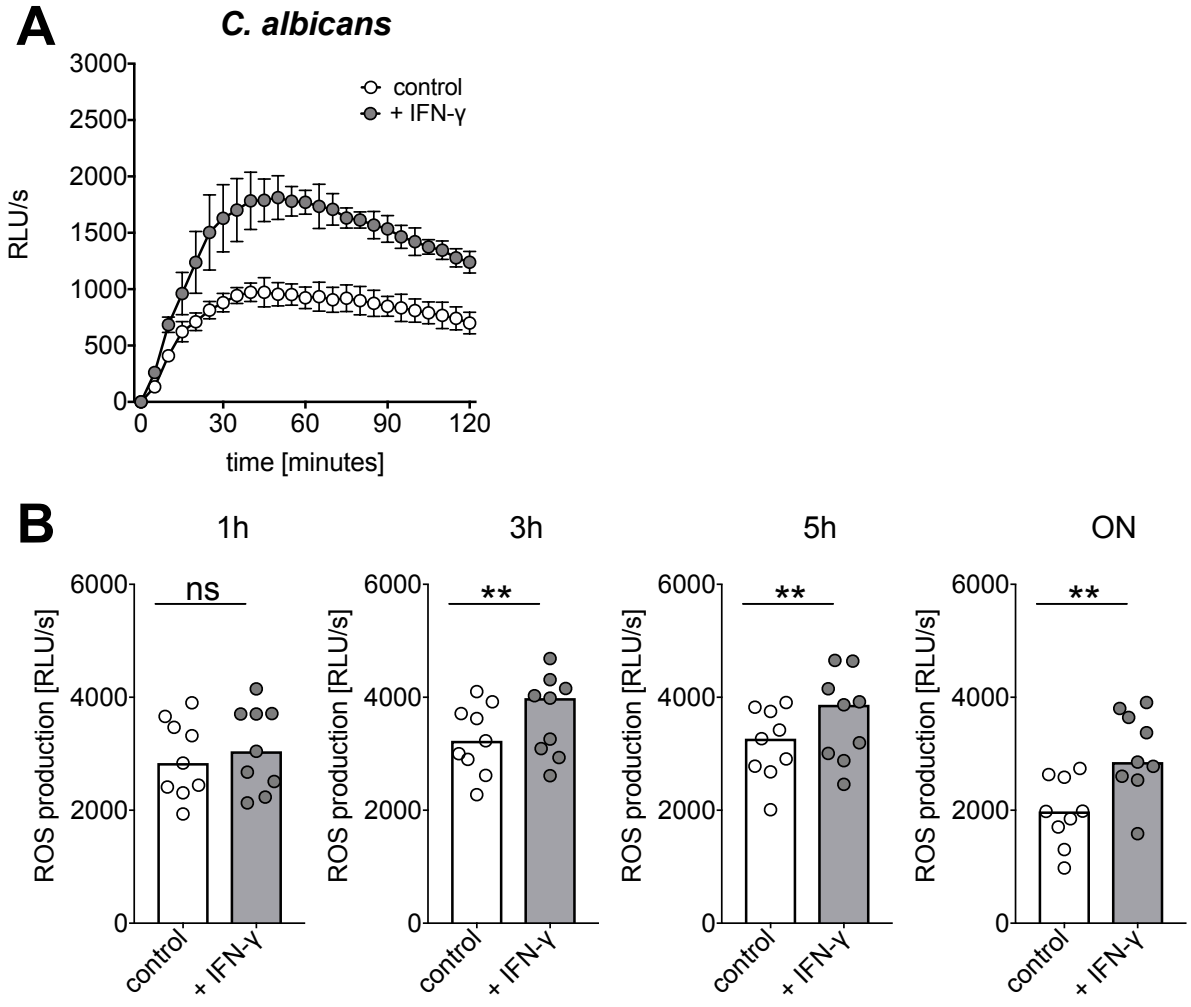

Fig. 6: IFN-γ enhances ROS production in response to *C. albicans* in healthy individuals.
A, Example plot for ROS production (RLU/s) by PMNs after stimulation with heat-inactivated C. albicans yeasts with and without IFN-γ priming for 3h. Data are shown in triplicates for *C. albicans* yeast stimulation over 120 min. **B**, Maximun release of ROS (RLU/s) by PMNs after stimulation with heat-inactivated *C. albicans* yeasts with and without IFN-γ priming for 1h, 3h, 5h and overnight (ON). RLU, relative light unit. All values are shown as medians (n=9; Wilcoxon signed rank test; **, $P< 0.01$).

5.4 Fatty acid oxidation modulates ROS and cytokine production by Ly6C^{hi} inflammatory monocytes in sepsis

Mauricio Rosas-Ballina[1]*, Nura Schürmann[1], **Pascal Forrer[2]**, Beatrice Claudi[1], Olivier Cunrath[1], Thomas Bock[3], Janine Zankl[4], Alexander Schmidt[3], Nina Khanna[2,5], Giuseppe Danilo Norata[6], Dirk Bumann[1]*.

[1] Focal Area Infection Biology, Biozentrum, University of Basel, 4056 Basel, Switzerland; [2] Infection Biology Laboratory, Department of Biomedicine, University of Basel, 4031 Basel, Switzerland; [3] Proteomics Core Facility, Biozentrum, University of Basel, Switzerland; [4] Flow Cytometry Core Facility, Biozentrum, University of Basel, Switzerland; [5] Division of Infectious Diseases and Hospital Epidemiology, Department of Clinical Research, University Hospital of Basel, 4031 Basel, Switzerland; [6] Department of Pharmacological and Biomolecular Sciences, University of Milan, Italy.

* Corresponding authors

Manuscript is ready for submission.

Statement of my work:

Design of experiments, Performing experiments, Data analysis.

Responsible clinical study manager; Writing patient study protocol; Submission of study-related documents to Ethics Committee EKNZ; Patient recruitment and coding; Immune cell isolation (Fig. 4A; Fig. 5A)

Note: The following part contains only the abstract to which I contributed in this manuscript. The contribution of my work is the planning, conducting and execution of the clinical study BASEC 2016-00676.

5.4.1 Abstract/ Summary

Systemic and cellular metabolic derangements are known components of the dysregulated host response to infection. However, how systemic lipid metabolism integrates with immune cell function to mediate phagocyte pro-inflammatory function in sepsis remains to be explored. Here we show that mice infected with *Salmonella* course with a pro-atherogenic state defined by increased low-density lipoprotein (LDL)-cholesterol plasma levels accompanied by neutral lipid accumulation in circulating and spleen inflammatory monocytes and neutrophils. Surprisingly, spleen inflammatory monocytes from septic mice had a pro-inflammatory phenotype with elevated ROS levels, and increased TNF and IL-1β mRNA levels despite a higher oxygen consumption rate driven by mitochondrial fatty acid oxidation, a metabolic feature of M2 anti-inflammatory activation *in vitro*. Further, a single dose of the beta-oxidation inhibitor etomoxir to septic mice increased neutral lipid and reduced total cellular ROS, TNF, and IL-1β levels in spleen inflammatory monocytes but worsened disease progression due to off-target effects on liver. Finally, monocytes from patients with gram-negative bacteremia contained higher neutral lipid content compared to age-, gender-, and body mass index-matched controls while *ex vivo* treatment with etomoxir reduced ROS levels in monocytes of patients and controls. Our results unravel a lipid metabolic program in sepsis common to atherosclerosis and put forth targeted inhibition of fatty acid oxidation in monocytes as a therapeutic approach against sepsis.

6 Discussion

Pathogen clearance in infectious diseases strongly depends on efficient innate and adaptive immune responses. We showed that “simple foot soldier” neutrophils are important for host defense against bacterial and fungal pathogens. With the help of two key enzymes, the NADPH oxidase and MPO, neutrophils are able to produce large amounts of ROS that are important for pathogen destruction. However, excessive ROS can also cause detrimental damage in host tissues. We showed that MPO has a protective role in the host by scavenging diffusible H_2O_2 at the *Salmonella* surface and converting it into highly reactive HOCl within a short reach. Hence, MPO confines potential harmful molecules to the pathogen microenvironment without causing collateral host tissue damage.

Neutrophils as “versatile commanders” are unambiguously involved in the pathogenesis of sepsis, the dysregulated host response to infection. We identified a subset of APC-like neutrophils with MHC class II molecule expression, which could be induced under inflammatory conditions. We could show that the MHC class II enhanceosome is responsible for the subsequent MHC class II expression on neutrophils and that targeting JAK1/2 kinase could be a promising therapeutic approach in sepsis to reach cellular homeostasis. Overall, we conclude that infectious disease control implies a specialized, but versatile immune system with diverse neutrophil functionality.

6.1 Neutrophils as simple foot soldiers of immunity in infectious diseases

Neutrophils are potent phagocytic cells that efficiently eradicate pathogens by using oxidative and non-oxidative killing mechanisms. The oxidative killing mechanism is strongly dependent on two key enzymes, the NADPH oxidase and MPO. Together, they produce large amounts of ROS that are lethal for pathogens. Previous reports could clearly demonstrate that NADPH oxidase deficiency leads to high pathogen load in organs in a mouse model of *Salmonellosis* and impaired *Salmonella* killing by neutrophils and inflammatory monocytes compared to wildtype mice [288]. However, the role of MPO in systemic *Salmonella* infection is entirely unclear. It is known that MPO converts almost all O_2^- or H_2O_2 into highly toxic hypohalous acids (OCl^-, OBr^-, OF^- or OI^-) with predominant HOCl production. HOCl is a highly reactive oxidant with potent antimicrobial efficacy [49] in somehow artificial cell culture systems. *In vivo*, data from both individuals and mice with MPO deficiency in infections were inconclusive. For that reason, we combined a computational modelling approach based on *in vivo* and *in vitro* data to elucidate the role of ROS and MPO in *Salmonella* infection.

Our data showed that during *Salmonella* infection, MPO co-localized mainly to deceased pathogen surface *in vivo*. This finding is strongly supporting the direct contribution of the MPO-mediated product HOCl in *Salmonella* killing. On the contrary, our data from MPO deficient mice revealed only slightly elevated levels of pathogen tissue load compared to wildtype mice, supporting the idea of compensatory MPO-independent killing mechanisms *in vivo* with other ROS release than HOCl or enhanced non-oxidative killing mechanisms. In our model, we implemented published data from a computational model of oxidative bursts in neutrophil phagosomes [66] with *in vivo* data from ROS defense in *Salmonella enterica* serovar Typhimurium [288]. We predicted that H_2O_2 levels accumulate in the *Salmonella* cytosol up to 15 µM in the absence of MPO. Lethality threshold was estimated around 2 µM [289], as reported by another group showing similar H_2O_2-induced lethality concentrations in *E. coli* [290]. Nevertheless, our data are contrary to the results found by Winterbourne *et al.* [66] They proposed an intraphagosomal accumulation of non-lethal levels of H_2O_2 up to 30 µM in the absence of MPO. Despite these discrepancies, our data clearly showed that *Salmonella* are eradicated either by MPO-derived HOCl if MPO is present or that *Salmonella* is killed by high, lethal levels of H_2O_2 in the absence of MPO.

MPO is it the most abundant granule protein in neutrophils [291], synthesised in daily amounts of hundreds of milligrams [49]. If MPO has a redundant function in pathogen killing, why does the cell invest high costs to produce it? We postulated that MPO has an important function in mitigating collateral tissue damage during oxidative stress exposure. In general, ROS production during antimicrobial host defense bears an enormous potential to damage host tissues. Therefore, precision guidance of ROS fluxes towards the pathogen is indispensable. MPO converts diffusible long-lived H_2O_2 into highly reactive, toxic and locally confined HOCl at the pathogen surface. Our computational model data could predict that the less MPO available in the phagosome, the less HOCl production and the higher the H_2O_2 accumulation in the neutrophil phagosome. Since the buffering capacity of the cell is limited to some extent, H_2O_2 leakage out of the phagosome and out of the host cell occurs at substantial rates. Our results are opposite to Winterbourne *et al.* They suggested that H_2O_2 leakage out of the cell can be scavenged by neutrophil protection mechanisms such as glutathion peroxidases [66], which is supported by the fact that neutrophils are known to be the most resistant cell type against exogenous H_2O_2 [292]. However, this assumption is based on *in vitro* studies using MPO-deficient neutrophils that did not reveal increased accumulation of H_2O_2, but elevated levels of O_2^- in neutrophils during the first few minutes of oxidative burst [293]. Thus, we re-examined this question by using pharmacological MPO inhibition and MPO deficient human neutrophils with longer stimulation time and specific assays to detect O_2^- production, H_2O_2 release, MPO activity and HOCl production. We could confirm our predicted computational modelling data by

showing that MPO deficient neutrophils release higher levels of H_2O_2, and not O_2^-, during oxidative bursts with experimental *in vitro* data. Moreover, our *in vivo* experiments with MPO deficient mice infected with *Salmonella* showed elevated levels of H_2O_2 in tissues and oxidative damage of lipids and DNA. In summary, we strongly assume that upon *Salmonella* infection, the pharmacological MPO inhibition and MPO deficiency in neutrophils leads to massive accumulation of H_2O_2 in the phagosome and subsequent H_2O_2 release to the extracellular space, without deficits in intracellular pathogen killing, but with collateral tissue damage.

Some reports could show that MPO deficiency *in vivo* results in enhanced chemokine expression and additional neutrophil recruitment in several mouse models [294-297]. Hence, increased oxidative tissue damage in MPO deficient mice could result from increased neutrophil recruitment producing higher ROS levels *in sum* rather than H_2O_2 leakage into the extracellular space *per se*. However, our tissue staining for CD11b (marker for inflammatory cells) and Ly6G (neutrophils) demonstrated similar immune cell recruitment in MPO deficient and wildtype animals *in vivo*. In agreement, human whole blood differentiation plots from healthy and MPO deficient individuals showed similar leukocyte cell counts. We conclude that in our chosen *in vivo* model system, there is no apparent neutrophil recruitment amplification loop.

Unfortunately, we were not able to show elevated H_2O_2-mediated tissue damage with pharmacologically inhibited MPO in stimulated, human neutrophils, co-cultivated with three different cells types (Jurkat T cells, L292 mouse fibroblasts and autologous PBMCs). We tested for different time points of co-incubation, several stimuli (*Candida*, *Salmonella* and PMA) with various MOI, various target cell numbers, various effector-to-target cell ratios and different media with/without supplements *in vitro*. Although we could induce tissue damage/ toxicity by using very high and somehow artificial levels of H_2O_2 (in range of mM) *in vitro*, in agreement with reports that showed rather high doses of H_2O_2 required for bacterial killing [298] and tissue damage, respectively [299-301]. Most of these studies using high doses referred to bolus injections of H_2O_2 into the medium (of which only a fraction penetrates into the bacterial cytosol and this fraction is further reduced by potent *Salmonella* detoxification mechanisms). Moreover, commonly used and non-physiological bolus injections of high amounts of H_2O_2 are much less effective in killing compared to continuous H_2O_2 exposure because they block metabolism and limit toxic Fenton reaction, rendering bacteria much less vulnerable to oxidative damage [290].

Recently, Reber *et al.* showed that neutrophils contribute to host protection by limiting LPS-induced inflammation in a MPO-dependent manner [302]. They speculate that anomalous ROS generation, namely H_2O_2 production, could contribute to exacerbated systemic

inflammation in MPO-deficient mice. However, it is unaddressed whether H_2O_2-induced systemic inflammation directly induces lipid peroxidation and DNA damage or vice versa. Furthermore, our *in vivo Salmonella* infection model did not show visible differences in terms of excessive inflammation and improved survival between MPO-deficient and wildtype mice.

Conclusively, we propose that MPO confines the lethal ROS fluxes locally to pathogens and ensures oxidative stress compartmentalized inside neutrophils phagosomes. With this elegant self-protective mechanism, inflammatory collateral tissue damage during *Salmonella* infection is lowered as good as possible and the primary objective, pathogen destruction, is even so executed as desired.

6.2 Neutrophils as versatile commanders of immunity in infectious diseases

Please find an extended discussion in the results section of the thesis under “APC-like neutrophils contribute to sepsis pathology and activate T-cell responses”.

7 Outlook

7.1 Neutrophils as simple foot soldiers of immunity in infectious diseases

We could demonstrate that neutrophils use their most abundant granule protein, MPO, to confine lethal oxidative stress into phagosomes during antimicrobial attack. This self-protective mechanism reduces collateral host tissue damage during *Salmonella* infection and supports efficient pathogen clearance.

To understand the MPO-mediated host tissue damage in in a systemic *Salmonella* infection mouse model

A recent report has complemented the concept of MPO-mediated host protection by limiting LPS-induced inflammation [302]. It would be interesting to know whether H_2O_2 - induced systemic inflammation induces lipid peroxidation and DNA damage or vice versa. Therefore, future experiments could investigate the temporal tissue cytokine profile around DNA damage and lipid peroxidation lesions, respectively. Moreover, it would be of interest to identify the local influence of aberrant H_2O_2 levels on bystander immune cells in the regulation of antimicrobial and inflammatory immune responses in MPO-deficient mice.

To understand the epidemiology of human MPO deficiency and monitor the clinical indications associated with MPO deficiency

Epidemiological studies on MPO deficiency are scarce. As we discussed in our paper, early studies have reported an increased cancer incidence in patients with complete MPO deficiency [58]. Our findings from MPO-deficient mice in a systemic *Salmonella* infection model showed collateral tissue damage with high lipid peroxidation and DNA oxidation. Thus, our data support the possibility that individuals with full MPO deficiency might have an increased risk to develop cancer if continuously exposed to pathogens. However, repeated human infections in immunocompetent individuals in industrialized countries are rare nowadays [303]. Thus, lifetime impact of MPO deficiency in infectious diseases is potentially underestimated. It would be interesting to classify human MPO deficiency as a global primary immunodeficiency with the aim to monitor the prevalence of MPO deficiency across different countries, to differentiate partial from full MPO deficiency and associate those MPO levels with clinical indications such as cancer, recurrent infectious disease complications and cardiovascular diseases. Future work will be needed to fully assess the impact of the MPO-mediated protective mechanism in humans and mice.

7.2 Neutrophils as versatile commanders of immunity in infectious diseases

To understand the dysregulated immunity in neutrophils, monocytes and lymphocytes during the hyperinflammatory and immunosuppressive phase in human sepsis

In our work, we could demonstrate that human neutrophils show an APC-like phenotype with elevated MHC class I and *de novo* induced MHC class II expression in the *pro-inflammatory phase* of sepsis. It would be interesting to extend the study design to identify immune-metabolic changes in neutrophils, monocytes and lymphocytes during the *immunosuppressive phase* of sepsis to get a comprehensive overview of dysregulated immunity during sepsis. For these reasons, we will consider to amend the study protocol in agreement with the responsible Ethics Committee. This research project will be a translational, single center, unblinded, case-control study project with five consecutive blood drawing events (day 0, day 2-3, day 5-7, day 10-14 and before discharge from hospital) aiming at identifying immune-metabolic changes in host immunity during hyperinflammatory phase (day 0) and immunosuppressive phase (day 5-7) in patients suffering from gram-negative sepsis compared to healthy, age-matched (+/- 5 years) and gender-matched control group. Plasma samples will be analyzed for total cholesterol, triacylglycerol, free fatty acids, apolipoprotein (apo)-B, and apo-AI levels to identify lipid metabolic changes. Plasma cytokine levels will be determined with Human Custom Inflammation Panel Kits for IL-1β, IFN-α, IFN-γ, TNF-α, GM-CSF, IL-6, IL-8 (CXCL8), IL-10, IL-12p70, IL-17A, IL-18, IL-23, and IL-33. Neutrophils, monocytes, and lymphocytes will be characterized in greater detail. Neutrophils and monocytes will be used to identify MHC class I and II, costimulatory molecules and activation marker (multi-color flow cytometry for HLA-DR, HLA-DR/DP/DQ, Li, CD80, CD86, CD40, HLA-A/B/C, CD83, CD54, CD11c, CXCR4, CD62L, CD14, CD66b, CD11b, PD-1L), quantitative proteomics (liquid chromatography-tandem mass spectrometry) and for oxygen consumption rate analysis (Seahorse cell metabolism analyzers). Monocytes will be used for total RNA isolation. Lymphocytes will be analyzed for phenotype (CD3, CD4, CD8, CD56, CD16, CD19), for T-cell subsets (CD3, CD4, FoxP3, CD127 and CD25), T-cell cytokine response after stimulation with anti-CD3/CD28 (IFN-γ, IL-4, IL-10, IL-2, GM-CSF and TNF-α production), T-cell cytotoxicity (Perforin, Granzyme B, Granulysin), T-cell proliferation (CFSE staining) and T-cell exhaustion (PD-1, TIM-3, CTLA-4). In order to determine neutral lipid content, leukocytes will be stained with the fluorescent dye LipidTox. For determination of reactive oxygen species levels, another set of samples will be stained with the fluorescent dye CellRox.

Moreover, one could extend the study arms to severity classes such as *Bacteremia*, *Sepsis* and *Septic Shock* with arms sizes of n=20. Results from such a study might provide insights into the pathogenesis of sepsis and identify immunological biomarkers, which could contribute to the development of novel therapeutic approaches for the treatment of this potentially lethal disease.

To understand the dynamic phosphoproteome signaling in human neutrophils after priming with GM-CSF and IFN-γ and pharmacological inhibition with ruxolitinib (JAK1/2 inhibitor)

Our results showed that GM-CSF stimulation in neutrophils alters the phosphorylation of a complex network of proteins involved in 3 major signaling pathways, the JAK-STAT, the MAPK and the PI3K-Akt-mTOR pathways with overrepresented MAPK kinase activity and a central JAK1/2 kinase orchestrating the broad downstream protein phosphorylation. However, we only considered neutrophils priming with GM-CSF after 30 minutes of stimulation. It would be very interesting to test dynamic phosphoproteome changes upon GM-CSF and IFN-γ priming, as previously shown for insulin signalling in adipocytes [305], and elaborate differences and connections of protein phosphorylation networks among these two cytokines. Moreover, it would be interesting to figure out the central role of JAK1/2 kinase-mediated protein phosphorylation in neutrophils upon GM-CSF priming by using inhibitors selective against JAK1/2 kinase (Ruxolitinib) and a large systems-level proteomics approach.

To understand the physiological relevance of APC-like neutrophils in a systemic *Salmonella* infection mouse model

Our *in vivo* data substantiate the suitability of the systemic salmonellosis mouse model as appropriate model to study bacterial sepsis and confirm the induction of APC-like neutrophils during sepsis, reflecting the vast heterogeneity and diversity of neutrophils under inflammatory conditions. However, there remains a major open question: What is the physiological relevance of APC-like neutrophils in systemic *Salmonella* infection?

To answer this question, we are aiming to generate a novel transgenic mouse strain with neutrophil-restricted deficiencies in MHC class II. Thus, we will cross *MHCclassII*^{fl} mice (provided by Prof. Dr. Daniela Finke group [306]) to the *Catchup* mouse (*C57BL/6-Ly6g(tm2621(Cre-tdTomato)Arte*), generated by Prof. Dr. Matthias Gunzer group [307]) with the help of Cre/loxP recombination system and gene targeting, which should show target-oriented deletions in neutrophils for MHC class II. Other conceivable approaches such as using neutrophil-depleting agents [142,308] or neutrophil-depleting systems [302] cannot properly answer this key question.

It is known that neutrophil-depleted mice are more susceptible to *Salmonella* infection than wildtype mice [308] and these mice show impaired *Salmonella* killing by neutrophils. However, neutrophil depletion approaches are not targeting MHC class II$^+$ neutrophils in particular and other potent antimicrobial neutrophil effector functions such as phagocytosis, ROS production, degranulation, NETosis and cytokine production are biasing the interpretation of the experimental data.

Moreover, mice deficient in MHC class II are affecting all APCs and suffer from severe immunodeficiency [143] and using *MHC classII*^{fl} mice crossing to mice expressing Cre under control of the murine lysozyme M gene promotor (LysM^{Cre} mice) will target MHC class II expression of all myeloid lineage cells, such as monocytes, macrophages and neutrophils [309]. Recently described, even brain neurons of the central nervous system could be affected by this cell type-unspecific system [310]. I conclude that crossing *MHCclassII*^{fl} mice to the *Catchup* mouse with the help of Cre/loxP recombination system will be the best approach to elaborate the physiological relevance of APC-like neutrophils in *Salmonella* mouse infection models.

To understand the interplay between APC-like neutrophils and T-cell responses in a systemic *Salmonella* infection mouse model

To answer the question, whether APC-like neutrophils activate or suppress T-cell responses in *Salmonella* infections, we will use the help from the transgenic mice above. Previous studies from other groups have shown that APC-like neutrophils are able to present OVA peptide to OVA-specific T cells and induce T-cell activation and proliferation [160,162]. As the *Salmonella* mouse model induces a robust CD4$^+$ T_H1 response [311], this model is well suited to investigate the interaction of MHC class II positive neutrophils with CD4$^+$ T cells *in vivo* in the context of a complex bacterial infection.

So far, our experiments were performed in C57BL/6 mice infected i.v. with *Salmonella* strains derived from *Salmonella enterica* serovar Typhimurium *SL1344 hisG rpsL xyl* [274,275]. However, since mice infected with wildtype *Salmonella enterica* serovar Typhimurium strain *SL1344* succumb to this infection model within a few days and adaptive T-cell responses typically peak 7-15 days after initial antigen stimulation [304], we will optimize the mouse infection model. It has been shown by other groups, that vaccination of mice with attenuated *Salmonella* strains (SL1344ΔaroA[312]) will lead to a long-lasting T-cell memory and protection against re-challenge with wildtype *Salmonella enterica* serovar Typhimurium strain *SL1344*[313,314]. Thus, we hypothesize that during the secondary response to *Salmonella enterica* serovar Typhimurium strain *SL1344*, APC-like neutrophils in infected tissues might be involved in activation or suppression of tissue-resident *Salmonella*-specific

memory T cells generated during the primary infection with *Salmonella enterica* serovar Typhimurium strain *SL1344* ΔaroA. To test this hypothesis, we plan to rechallenge mice previously infected with attenuated *Salmonella enterica* serovar Typhimurium strain SL1344ΔaroA for 40 days later with wildtype *Salmonella enterica* serovar Typhimurium strain *SL1344* and we will analyse the immune cell infiltrates for APC-like neutrophils (CD11b+, Ly6G+, Ly6C+, I-A/I-E+) and memory T cells (CD3, CD4, CD44, CD62, CCR7, intracellular IFN-γ, TNF-α, GM-CSF and IL-2[315]) by flow cytometry. To determine the course of T-cell activation over time, we will analyse T-cell activation surface markers (CD69, CD11a, CD49d, CD44, CD62L, CD29, CD54) at different time points during the experiments. For those time points and organs that show the best conditions, namely the presence of APC-like neutrophils as well as T-cell activation, we will visualize a potential co-localization of APC-like neutrophils and $CD4^+$ T-cells by immunohistochemistry. We further plan to isolate APC-like neutrophils from single cell suspensions of different organs of infected mice by fluorescence activated cell sorting and to test *ex vivo* if these cells are able to trigger T-cell responses (CD69, CD11a, CD49d, CD44, CD62L, CD29, CD54, CFSE staining) of isolated peripheral blood T cells from uninfected mice.

To understand the selective influence of GM-CSF and IFN-γ on APC-like neutrophil induction in a systemic *Salmonella* infection mouse model

We could show that the pro-inflammatory cytokines GM-CSF and IFN-γ can induce *de novo* expression of MHC class II on mature neutrophils *in vitro*. However, it would be interesting to test those findings in the *Salmonella* mouse model *in vivo*. IFN-γ- deficient [316,317] and GM-CSF-deficient mice [318] are more susceptible to *Salmonella* infection than wildtype mice and *in vivo* treatment with a blocking anti-IFN-γ antibody leads to impaired *Salmonella* killing by neutrophils [288,319]. However, to assess neutrophil-selective GM-CSF and IFN-γ receptor signalling in context of *de novo* MHC class II expression in systemic *Salmonella enterica* serovar Typhimurium infection, it would be interesting to generate transgenic mouse strains with neutrophil-restricted deficiencies in GM-CSF- and IFN-γ receptors. We plan to cross *CSF2rb*^{fl} mice (provided by Prof. Dr. Burkhard Becher group [320]) to the *Catchup* mouse (*C57BL/6-Ly6g(tm2621(Cre-tdTomato)Arte*), generated by Prof. Dr. Matthias Gunzer group [307]) with the help of Cre/loxP recombination system and gene targeting, which should show target-oriented deletions in neutrophils for GM-CSF receptor. Moreover, we want to cross the *Ifngr1*^{tm1} mice (provided by Prof. Dr. Daniel Pinschewer) to the *Catchup* mouse to delete target-oriented in neutrophils for IFN-γ receptor. We expect that these breedings will lead to mice with normal neutrophil numbers in the periphery, but lack in receptors for GM-CSF and IFN-γ respectively [307,320].

We will regularly perform breeding maintenance (PCR analysis for all mouse strains to confirm

the genetic construct *C57BL/6-Ly6g(tm2621(Cre-tdTomato)Arte, CSF2rb^{fl,}*, *Ifngr1^{tm1}*) as well as target-oriented breeding (PCR analysis for newly constructed mouse strains *C57BL/6-Ly6g(tm2621(Cre-tdTomato)Arte x CSF2rb^{fl,}* and *Ly6g(tm2621(Cre-tdTomato)Arte x Ifngr1^{tm1}*), genotyping and testing for IFN-γ- and GM-CSF receptor expression on neutrophils with Ly6G (or tdTomato^{+} cells or alternative gating approach for neutrophils according to literature [307]), Ly6C, CD11b for flow cytometry and PCR analysis for *Ifngr1* and *gsf2rb*. Moreover, we will test the novel transgenic strains for abnormalities of circulating monocyte and neutrophil numbers. With the help of transgenic mouse strains with neutrophil-restricted deficiencies in GM-CSF- and IFN-γ receptors, we could finally elaborate the role of GM-CSF- and IFN-γ specifically on neutrophils in terms of MHC class II induction *in vivo.*

To understand the classical neutrophil effector functions in APC-like neutrophils in a systemic *Salmonella* infection mouse model

We would like to test other important neutrophil effector functions such as ROS production and pathogen killing *in vivo*, as previously shown by co-workers [46,288], in the transgenic mouse strain with neutrophil-restricted deficiencies in MHC class II in response to systemic *Salmonella* infection. To determine whether APC-like neutrophils in the mouse model show impairments in their antimicrobial capacity we will use *Salmonella* reporter strains [288] which allow *in situ* visualization of the neutrophil/pathogen interaction by immunohistochemistry and *ex vivo* analysis by fluorescence activated cell sorting. To determine whether APC-like neutrophils are still able to effectively release ROS *in situ* and *ex vivo*, we will use a H_2O_2 *Salmonella* biosensor construct to report ROS exposure in tissue together with neutrophil markers CD11b, Ly6G and I-A/I-E. The H_2O_2 *Salmonella* biosensor construct *pkatGp-gfp* was previously described [46,288]. To determine whether APC-like neutrophils are still able to effectively kill *Salmonella in vivo* and *ex vivo*, we will use a *Salmonella* RFP reporter strain (*Salmonella enterica* serovar Typhimurium *SL1344 sifBp::mCherry* [288]) together with antibodies against bacterial LPS and antibodies against the neutrophil markers CD11b, Ly6G and I-A/I-E to assess whether residing *Salmonella* within MHC class II^{+} and MHC class II^{-} neutrophils are viable (RFP^{+}LPS^{+}) or dead (RFP^{-}LPS^{+}).

To elaborate the proteome changes of APC-like neutrophils compared to classical neutrophils in a systemic *Salmonella* infection mouse model

We demonstrated the presence of APC-like neutrophils *in vivo* in a well-established mouse model of systemic salmonellosis [247,248] by using proteome data sets obtained from splenic neutrophils of mice infected with *Salmonella enterica* serovar Typhimurium. However, it would be of great interest to identify proteome changes in MHC class II^{+} and MHC class II^{-} neutrophils.

We will isolate MHC class II^+ and MHC class II^- neutrophils from single cell suspensions of *Salmonella*- infected organs by fluorescence activated cell sorting and analyse the organ-specific neutrophil proteome.

8 Conclusion

Together, these data showed that infectious disease control implies a specialized and highly versatile immune system with diverse neutrophil functionality. We showed that “simple foot soldier” neutrophils are important for host defense against bacterial and fungal pathogens by producing large amounts of ROS. MPO, one of the key enzymes in ROS production, has a protective role in the host by scavenging diffusible H_2O_2 at the *Salmonella* surface and converting it into highly reactive HOCl, which leads to both effective pathogen destruction and minimal collateral host tissue damage (Fig. 5).

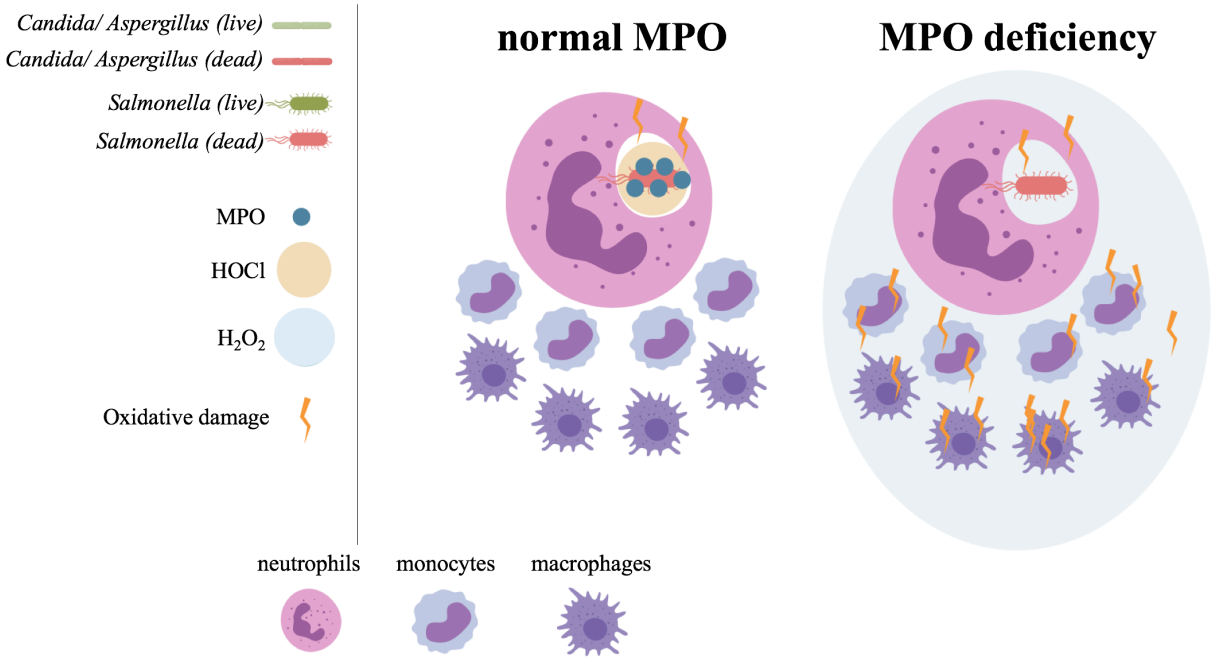

Fig. 5: The role of neutrophils as simple foot soldiers of immunity in infectious diseases.

Neutrophils as “versatile commanders” are unambiguously involved in the pathogenesis of sepsis, the dysregulated host response to infection. We could show that under inflammatory conditions, the MHC class II enhanceosome is responsible for the subsequent MHC class II expression on neutrophils, ultimately leading to T-cell activation. Targeting JAK1/2 kinase in neutrophils could be a promising therapeutic approach in sepsis. Overall, the immunological function of neutrophils in infectious diseases is highly versatile and goes far beyond simple pathogen destruction (Fig. 6).

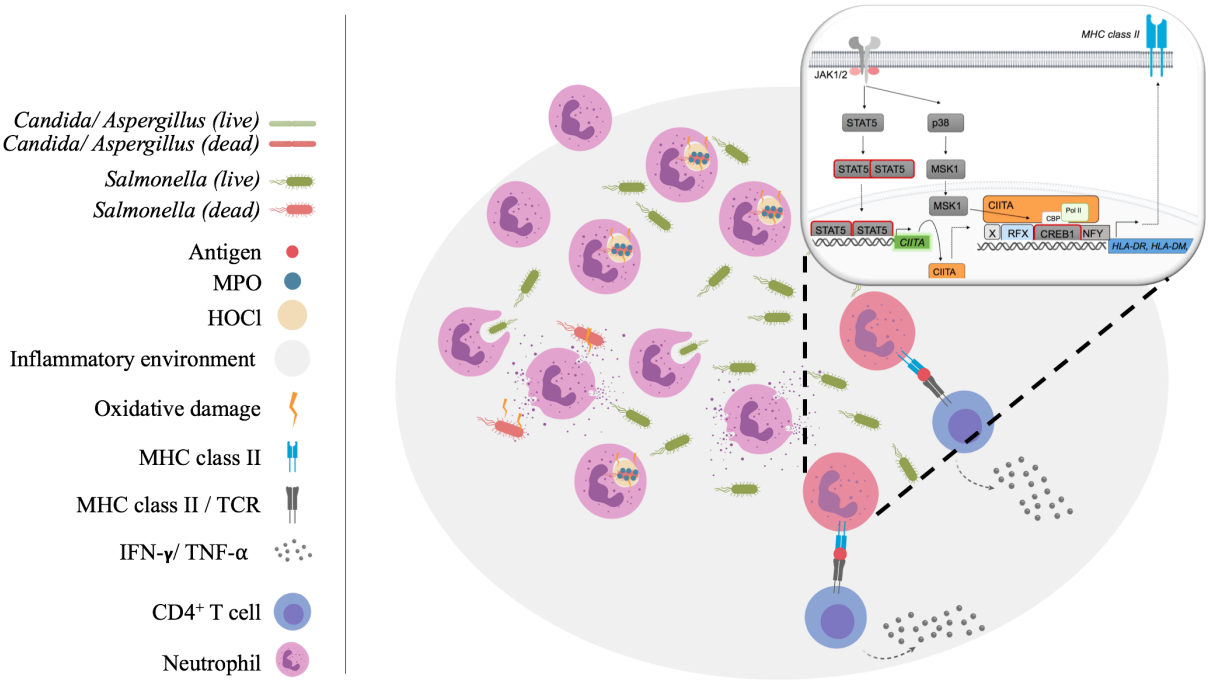

Fig. 6: The role of neutrophils as versatile commanders of immunity in infectious diseases.

9 References

1 Mantovani, A., Cassatella, M. A., Costantini, C. & Jaillon, S. Neutrophils in the activation and regulation of innate and adaptive immunity. *Nat Rev Immunol* **11**, 519-531, doi:10.1038/nri3024 (2011).

2 Borregaard, N. Neutrophils, from marrow to microbes. *Immunity* **33**, 657-670, doi:10.1016/j.immuni.2010.11.011 (2010).

3 Coffelt, S. B., Wellenstein, M. D. & de Visser, K. E. Neutrophils in cancer: neutral no more. *Nat Rev Cancer* **16**, 431-446, doi:10.1038/nrc.2016.52 (2016).

4 Athens, J. W. *et al.* Leukokinetic studies. IV. The total blood, circulating and marginal granulocyte pools and the granulocyte turnover rate in normal subjects. *The Journal of clinical investigation* **40**, 989-995, doi:10.1172/jci104338 (1961).

5 Kolaczkowska, E. & Kubes, P. Neutrophil recruitment and function in health and inflammation. *Nat Rev Immunol* **13**, 159-175, doi:10.1038/nri3399 (2013).

6 Nathan, C. Neutrophils and immunity: challenges and opportunities. *Nature reviews. Immunology* **6**, 173-182, doi:10.1038/nri1785 (2006).

7 Hurst, J. K. What really happens in the neutrophil phagosome? *Free Radic Biol Med* **53**, 508-520, doi:10.1016/j.freeradbiomed.2012.05.008 (2012).

8 Cohen, J. J., Duke, R. C., Fadok, V. A. & Sellins, K. S. Apoptosis and programmed cell death in immunity. *Annual review of immunology* **10**, 267-293, doi:10.1146/annurev.iy.10.040192.001411 (1992).

9 Savill, J. Apoptosis in resolution of inflammation. *Journal of leukocyte biology* **61**, 375-380 (1997).

10 Gamberale, R., Giordano, M., Trevani, A. S., Andonegui, G. & Geffner, J. R. Modulation of human neutrophil apoptosis by immune complexes. *Journal of immunology (Baltimore, Md. : 1950)* **161**, 3666-3674 (1998).

11 DeLeo, F. R. Modulation of phagocyte apoptosis by bacterial pathogens. *Apoptosis : an international journal on programmed cell death* **9**, 399-413, doi:10.1023/B:APPT.0000031448.64969.fa (2004).

12 Yoshiie, K., Kim, H. Y., Mott, J. & Rikihisa, Y. Intracellular infection by the human granulocytic ehrlichiosis agent inhibits human neutrophil apoptosis. *Infection and immunity* **68**, 1125-1133 (2000).

13 van Zandbergen, G. *et al.* Chlamydia pneumoniae multiply in neutrophil granulocytes and delay their spontaneous apoptosis. *Journal of immunology (Baltimore, Md. : 1950)* **172**, 1768-1776 (2004).

14 Colotta, F., Re, F., Polentarutti, N., Sozzani, S. & Mantovani, A. Modulation of granulocyte survival and programmed cell death by cytokines and bacterial products. *Blood* **80**, 2012-2020 (1992).

15 Kobayashi, S. D., Voyich, J. M., Braughton, K. R. & DeLeo, F. R. Down-regulation of proinflammatory capacity during apoptosis in human polymorphonuclear leukocytes. *Journal of immunology (Baltimore, Md. : 1950)* **170**, 3357-3368 (2003).

16 Galli, S. J., Borregaard, N. & Wynn, T. A. Phenotypic and functional plasticity of cells of innate immunity: macrophages, mast cells and neutrophils. *Nat Immunol* **12**, 1035-1044, doi:10.1038/ni.2109 (2011).

17 Pillay, J. *et al.* In vivo labeling with 2H2O reveals a human neutrophil lifespan of 5.4 days. *Blood* **116**, 625-627, doi:10.1182/blood-2010-01-259028 (2010).

18 Tofts, P. S., Chevassut, T., Cutajar, M., Dowell, N. G. & Peters, A. M. Doubts concerning the recently reported human neutrophil lifespan of 5.4 days. *Blood* **117**, 6050-6052; author reply 6053-6054, doi:10.1182/blood-2010-10-310532 (2011).

19 Li, K. W., Turner, S. M., Emson, C. L., Hellerstein, M. K. & Dale, D. C. Deuterium and neutrophil kinetics. *Blood* **117**, 6052-6053; author reply 6053-6054, doi:10.1182/blood-2010-12-322271 (2011).

20 Bhatnagar, N. *et al.* Cytokine-activated NK cells inhibit PMN apoptosis and preserve their functional capacity. *Blood* **116**, 1308-1316, doi:10.1182/blood-2010-01-264903 (2010).

21 Costantini, C. *et al.* Neutrophil activation and survival are modulated by interaction with NK cells. *Int Immunol* **22**, 827-838, doi:10.1093/intimm/dxq434 (2010).

22 Summers, C. *et al.* Neutrophil kinetics in health and disease. *Trends Immunol* **31**, 318-324, doi:10.1016/j.it.2010.05.006 (2010).

23 Schmeling, D. J. *et al.* Chemotaxigenesis by cell surface components of Staphylococcus aureus. *Infection and immunity* **26**, 57-63 (1979).

24 Lawrence, M. B. & Springer, T. A. Leukocytes roll on a selectin at physiologic flow rates: distinction from and prerequisite for adhesion through integrins. *Cell* **65**, 859-873 (1991).

25 Tedder, T. F., Penta, A. C., Levine, H. B. & Freedman, A. S. Expression of the human leukocyte adhesion molecule, LAM1. Identity with the TQ1 and Leu-8 differentiation antigens. *Journal of immunology (Baltimore, Md. : 1950)* **144**, 532-540 (1990).

26 Foreman, K. E. *et al.* C5a-induced expression of P-selectin in endothelial cells. *The Journal of clinical investigation* **94**, 1147-1155, doi:10.1172/jci117430 (1994).

27 Moore, K. L. *et al.* P-selectin glycoprotein ligand-1 mediates rolling of human neutrophils on P-selectin. *The Journal of cell biology* **128**, 661-671 (1995).

28 von Andrian, U. H. *et al.* Two-step model of leukocyte-endothelial cell interaction in inflammation: distinct roles for LECAM-1 and the leukocyte beta 2 integrins in vivo. *Proceedings of the National Academy of Sciences of the United States of America* **88**, 7538-7542 (1991).

29 Muller, W. A., Weigl, S. A., Deng, X. & Phillips, D. M. PECAM-1 is required for transendothelial migration of leukocytes. *The Journal of experimental medicine* **178**, 449-460 (1993).

30 Diamond, M. S. *et al.* ICAM-1 (CD54): a counter-receptor for Mac-1 (CD11b/CD18). *The Journal of cell biology* **111**, 3129-3139 (1990).

31 Khan, A. I. *et al.* Role of CD44 and hyaluronan in neutrophil recruitment. *Journal of immunology (Baltimore, Md. : 1950)* **173**, 7594-7601 (2004).

32 Cooper, D., Lindberg, F. P., Gamble, J. R., Brown, E. J. & Vadas, M. A. Transendothelial migration of neutrophils involves integrin-associated protein (CD47). *Proceedings of the National Academy of Sciences of the United States of America* **92**, 3978-3982 (1995).

33 O'Neill, L. A., Golenbock, D. & Bowie, A. G. The history of Toll-like receptors - redefining innate immunity. *Nature reviews. Immunology* **13**, 453-460, doi:10.1038/nri3446 (2013).

34 Hayashi, F., Means, T. K. & Luster, A. D. Toll-like receptors stimulate human neutrophil function. *Blood* **102**, 2660-2669, doi:10.1182/blood-2003-04-1078 (2003).

35 Rabellino, E. M., Ross, G. D. & Polley, M. J. Membrane receptors of mouse leukocytes. I. Two types of complement receptors for different regions of C3. *Journal of immunology (Baltimore, Md. : 1950)* **120**, 879-885 (1978).

36 Mobberley-Schuman, P. S. & Weiss, A. A. Influence of CR3 (CD11b/CD18) expression on phagocytosis of Bordetella pertussis by human neutrophils. *Infection and immunity* **73**, 7317-7323, doi:10.1128/iai.73.11.7317-7323.2005 (2005).

37 Myones, B. L., Dalzell, J. G., Hogg, N. & Ross, G. D. Neutrophil and monocyte cell surface p150,95 has iC3b-receptor (CR4) activity resembling CR3. *The Journal of clinical investigation* **82**, 640-651, doi:10.1172/jci113643 (1988).

38 Mantovani, B. Different roles of IgG and complement receptors in phagocytosis by polymorphonuclear leukocytes. *Journal of immunology (Baltimore, Md. : 1950)* **115**, 15-17 (1975).

39 Gounni, A. S. *et al.* Human neutrophils express the high-affinity receptor for immunoglobulin E (Fc epsilon RI): role in asthma. *FASEB journal : official publication of the Federation of American Societies for Experimental Biology* **15**, 940-949 (2001).

40 Albrechtsen, M., Yeaman, G. R. & Kerr, M. A. Characterization of the IgA receptor from human polymorphonuclear leucocytes. *Immunology* **64**, 201-205 (1988).

41 Quinn, M. T. & Gauss, K. A. Structure and regulation of the neutrophil respiratory burst oxidase: comparison with nonphagocyte oxidases. *Journal of leukocyte biology* **76**, 760-781, doi:10.1189/jlb.0404216 (2004).

42 Volpp, B. D., Nauseef, W. M. & Clark, R. A. Two cytosolic neutrophil oxidase components absent in autosomal chronic granulomatous disease. *Science (New York, N.Y.)* **242**, 1295-1297 (1988).

43 Wientjes, F. B., Hsuan, J. J., Totty, N. F. & Segal, A. W. p40phox, a third cytosolic component of the activation complex of the NADPH oxidase to contain src homology 3 domains. *The Biochemical journal* **296 (Pt 3)**, 557-561 (1993).

44 Lomax, K. J., Leto, T. L., Nunoi, H., Gallin, J. I. & Malech, H. L. Recombinant 47-kilodalton cytosol factor restores NADPH oxidase in chronic granulomatous disease. *Science (New York, N.Y.)* **245**, 409-412 (1989).

45 DeLeo, F. R., Allen, L. A., Apicella, M. & Nauseef, W. M. NADPH oxidase activation and assembly during phagocytosis. *Journal of immunology (Baltimore, Md. : 1950)* **163**, 6732-6740 (1999).

46 Schurmann, N. *et al.* Myeloperoxidase targets oxidative host attacks to Salmonella and prevents collateral tissue damage. *Nat Microbiol* **2**, 16268, doi:10.1038/nmicrobiol.2016.268 (2017).

47 Segal, A. W. How neutrophils kill microbes. *Annu Rev Immunol* **23**, 197-223, doi:10.1146/annurev.immunol.23.021704.115653 (2005).

48 Cech, P. & Lehrer, R. I. Phagolysosomal pH of human neutrophils. *Blood* **63**, 88-95 (1984).

49 Klebanoff, S. J., Kettle, A. J., Rosen, H., Winterbourn, C. C. & Nauseef, W. M. Myeloperoxidase: a front-line defender against phagocytosed microorganisms. *J Leukoc Biol* **93**, 185-198, doi:10.1189/jlb.0712349 (2013).

50 Rosen, H. & Klebanoff, S. J. Bactericidal activity of a superoxide anion-generating system. A model for the polymorphonuclear leukocyte. *The Journal of experimental medicine* **149**, 27-39 (1979).

51 Segal, B. H., Leto, T. L., Gallin, J. I., Malech, H. L. & Holland, S. M. Genetic, biochemical, and clinical features of chronic granulomatous disease. *Medicine* **79**, 170-200 (2000).

52 Winkelstein, J. A. *et al.* Chronic granulomatous disease. Report on a national registry of 368 patients. *Medicine* **79**, 155-169 (2000).

53 Johnston, R. B., Jr. & Baehner, R. L. Improvement of leukocyte bactericidal activity in chronic granulomatous disease. *Blood* **35**, 350-355 (1970).

54 Kutter, D. Prevalence of myeloperoxidase deficiency: population studies using Bayer-Technicon automated hematology. *J Mol Med (Berl)* **76**, 669-675 (1998).

55 Marchetti, C., Patriarca, P., Solero, G. P., Baralle, F. E. & Romano, M. Genetic characterization of myeloperoxidase deficiency in Italy. *Hum Mutat* **23**, 496-505, doi:10.1002/humu.20027 (2004).

56 Nunoi, H., Kohi, F., Kajiwara, H. & Suzuki, K. Prevalence of inherited myeloperoxidase deficiency in Japan. *Microbiol Immunol* **47**, 527-531 (2003).

57 Kitahara, M., Eyre, H. J., Simonian, Y., Atkin, C. L. & Hasstedt, S. J. Hereditary myeloperoxidase deficiency. *Blood* **57**, 888-893 (1981).

58 Lanza, F. Clinical manifestation of myeloperoxidase deficiency. *J Mol Med (Berl)* **76**, 676-681 (1998).

59 Parry, M. F. *et al.* Myeloperoxidase deficiency: prevalence and clinical significance. *Ann Intern Med* **95**, 293-301 (1981).

60 Kutter, D. *et al.* Consequences of total and subtotal myeloperoxidase deficiency: risk or benefit ? *Acta Haematol* **104**, 10-15, doi:10.1159/000041062 (2000).

61 Patiroglu, T., Eke Gungor, H., Belohradsky, J. S., Unal, E. & Klein, C. Myeloperoxidase deficiency: the secret under the flag of unstained cell. *Turk J Haematol* **30**, 232-233, doi:10.4274/Tjh.2012.0012 (2013).

62 van der Veen, B. S., de Winther, M. P. & Heeringa, P. Myeloperoxidase: molecular mechanisms of action and their relevance to human health and disease. *Antioxid Redox Signal* **11**, 2899-2937, doi:10.1089/ARS.2009.2538 (2009).

63 Metzler, K. D. *et al.* Myeloperoxidase is required for neutrophil extracellular trap formation: implications for innate immunity. *Blood* **117**, 953-959, doi:10.1182/blood-2010-06-290171 (2011).

64 Branzk, N. *et al.* Neutrophils sense microbe size and selectively release neutrophil extracellular traps in response to large pathogens. *Nat Immunol* **15**, 1017-1025, doi:10.1038/ni.2987 (2014).

65 Lehrer, R. I. & Cline, M. J. Leukocyte myeloperoxidase deficiency and disseminated candidiasis: the role of myeloperoxidase in resistance to Candida infection. *J Clin Invest* **48**, 1478-1488, doi:10.1172/JCI106114 (1969).

66 Winterbourn, C. C., Hampton, M. B., Livesey, J. H. & Kettle, A. J. Modeling the reactions of superoxide and myeloperoxidase in the neutrophil phagosome: implications for microbial killing. *J Biol Chem* **281**, 39860-39869, doi:10.1074/jbc.M605898200 (2006).

67 Keyer, K., Gort, A. S. & Imlay, J. A. Superoxide and the production of oxidative DNA damage. *J Bacteriol* **177**, 6782-6790 (1995).

68 Aratani, Y. *et al.* Differential host susceptibility to pulmonary infections with bacteria and fungi in mice deficient in myeloperoxidase. *J Infect Dis* **182**, 1276-1279, doi:10.1086/315843 (2000).

69 Aratani, Y. *et al.* Critical role of myeloperoxidase and nicotinamide adenine dinucleotide phosphate-oxidase in high-burden systemic infection of mice with Candida albicans. *J Infect Dis* **185**, 1833-1837, doi:10.1086/340635 (2002).

70 Hirche, T. O., Gaut, J. P., Heinecke, J. W. & Belaaouaj, A. Myeloperoxidase plays critical roles in killing Klebsiella pneumoniae and inactivating neutrophil elastase: effects on host defense. *J Immunol* **174**, 1557-1565 (2005).

71 Hirsch, J. G. & Cohn, Z. A. Degranulation of polymorphonuclear leucocytes following phagocytosis of microorganisms. *The Journal of experimental medicine* **112**, 1005-1014 (1960).

72 Pham, C. T. Neutrophil serine proteases: specific regulators of inflammation. *Nat Rev Immunol* **6**, 541-550, doi:10.1038/nri1841 (2006).

73 Brumell, J. H. *et al.* Subcellular distribution of docking/fusion proteins in neutrophils, secretory cells with multiple exocytic compartments. *Journal of immunology (Baltimore, Md. : 1950)* **155**, 5750-5759 (1995).

74 Mansfield, P. J., Hinkovska-Galcheva, V., Carey, S. S., Shayman, J. A. & Boxer, L. A. Regulation of polymorphonuclear leukocyte degranulation and oxidant production by ceramide through inhibition of phospholipase D. *Blood* **99**, 1434-1441 (2002).

75 Martin-Martin, B., Nabokina, S. M., Blasi, J., Lazo, P. A. & Mollinedo, F. Involvement of SNAP-23 and syntaxin 6 in human neutrophil exocytosis. *Blood* **96**, 2574-2583 (2000).

76 Mocsai, A. *et al.* Kinase pathways in chemoattractant-induced degranulation of neutrophils: the role of p38 mitogen-activated protein kinase activated by Src family kinases. *Journal of immunology (Baltimore, Md. : 1950)* **164**, 4321-4331 (2000).

77 Mocsai, A., Ruland, J. & Tybulewicz, V. L. The SYK tyrosine kinase: a crucial player in diverse biological functions. *Nature reviews. Immunology* **10**, 387-402, doi:10.1038/nri2765 (2010).

78 Faurschou, M. & Borregaard, N. Neutrophil granules and secretory vesicles in inflammation. *Microbes Infect* **5**, 1317-1327 (2003).

79 Ganz, T. Fatal attraction evaded. How pathogenic bacteria resist cationic polypeptides. *The Journal of experimental medicine* **193**, F31-34 (2001).

80 Rice, W. G. *et al.* Defensin-rich dense granules of human neutrophils. *Blood* **70**, 757-765 (1987).

81 Lehrer, R. I. Primate defensins. *Nature reviews. Microbiology* **2**, 727-738, doi:10.1038/nrmicro976 (2004).

82 Stoka, V., Turk, V. & Turk, B. Lysosomal cathepsins and their regulation in aging and neurodegeneration. *Ageing Res Rev* **32**, 22-37, doi:10.1016/j.arr.2016.04.010 (2016).

83 Reeves, E. P. *et al.* Killing activity of neutrophils is mediated through activation of proteases by K+ flux. *Nature* **416**, 291-297, doi:10.1038/416291a (2002).

84 Belaaouaj, A., Kim, K. S. & Shapiro, S. D. Degradation of outer membrane protein A in Escherichia coli killing by neutrophil elastase. *Science* **289**, 1185-1188 (2000).

85 Belaaouaj, A. *et al.* Mice lacking neutrophil elastase reveal impaired host defense against gram negative bacterial sepsis. *Nat Med* **4**, 615-618 (1998).

86 Weinrauch, Y., Drujan, D., Shapiro, S. D., Weiss, J. & Zychlinsky, A. Neutrophil elastase targets virulence factors of enterobacteria. *Nature* **417**, 91-94, doi:10.1038/417091a (2002).

87 Toomes, C. *et al.* Loss-of-function mutations in the cathepsin C gene result in periodontal disease and palmoplantar keratosis. *Nat Genet* **23**, 421-424, doi:10.1038/70525 (1999).

88 Pham, C. T., Ivanovich, J. L., Raptis, S. Z., Zehnbauer, B. & Ley, T. J. Papillon-Lefevre syndrome: correlating the molecular, cellular, and clinical consequences of cathepsin C/dipeptidyl peptidase I deficiency in humans. *J Immunol* **173**, 7277-7281 (2004).

89 Borregaard, N., Heiple, J. M., Simons, E. R. & Clark, R. A. Subcellular localization of the b-cytochrome component of the human neutrophil microbicidal oxidase: translocation during activation. *The Journal of cell biology* **97**, 52-61 (1983).

90 Ward, P. P. & Conneely, O. M. Lactoferrin: role in iron homeostasis and host defense against microbial infection. *Biometals : an international journal on the role of metal ions in biology, biochemistry, and medicine* **17**, 203-208 (2004).

91 Klebanoff, S. J. & Waltersdorph, A. M. Prooxidant activity of transferrin and lactoferrin. *The Journal of experimental medicine* **172**, 1293-1303 (1990).

92 Ragland, S. A. & Criss, A. K. From bacterial killing to immune modulation: Recent insights into the functions of lysozyme. *PLoS Pathog* **13**, e1006512, doi:10.1371/journal.ppat.1006512 (2017).

93 Ahluwalia, J. *et al.* The large-conductance Ca2+-activated K+ channel is essential for innate immunity. *Nature* **427**, 853-858, doi:10.1038/nature02356 (2004).

94 Vissers, M. C. & Winterbourn, C. C. Oxidative damage to fibronectin. I. The effects of the neutrophil myeloperoxidase system and HOCl. *Arch Biochem Biophys* **285**, 53-59 (1991).

95 Brinkmann, V. *et al.* Neutrophil extracellular traps kill bacteria. *Science* **303**, 1532-1535, doi:10.1126/science.1092385 (2004).

96 Lood, C. *et al.* Neutrophil extracellular traps enriched in oxidized mitochondrial DNA are interferogenic and contribute to lupus-like disease. *Nat Med* **22**, 146-153, doi:10.1038/nm.4027 (2016).

97 Urban, C. F., Reichard, U., Brinkmann, V. & Zychlinsky, A. Neutrophil extracellular traps capture and kill Candida albicans yeast and hyphal forms. *Cell Microbiol* **8**, 668-676, doi:10.1111/j.1462-5822.2005.00659.x (2006).

98 Saitoh, T. *et al.* Neutrophil extracellular traps mediate a host defense response to human immunodeficiency virus-1. *Cell Host Microbe* **12**, 109-116, doi:10.1016/j.chom.2012.05.015 (2012).

99 Abi Abdallah, D. S. *et al.* Toxoplasma gondii triggers release of human and mouse neutrophil extracellular traps. *Infect Immun* **80**, 768-777, doi:10.1128/IAI.05730-11 (2012).

100 Brinkmann, V. & Zychlinsky, A. Neutrophil extracellular traps: is immunity the second function of chromatin? *The Journal of cell biology* **198**, 773-783, doi:10.1083/jcb.201203170 (2012).

101 Papayannopoulos, V. Neutrophil extracellular traps in immunity and disease. *Nat Rev Immunol* **18**, 134-147, doi:10.1038/nri.2017.105 (2018).

102 Urban, C. F. *et al.* Neutrophil extracellular traps contain calprotectin, a cytosolic protein complex involved in host defense against Candida albicans. *PLoS Pathog* **5**, e1000639, doi:10.1371/journal.ppat.1000639 (2009).

103 Dwyer, M. *et al.* Cystic fibrosis sputum DNA has NETosis characteristics and neutrophil extracellular trap release is regulated by macrophage migration-inhibitory factor. *J Innate Immun* **6**, 765-779, doi:10.1159/000363242 (2014).

104 Fuchs, T. A. *et al.* Novel cell death program leads to neutrophil extracellular traps. *J Cell Biol* **176**, 231-241, doi:10.1083/jcb.200606027 (2007).

105 Papayannopoulos, V., Metzler, K. D., Hakkim, A. & Zychlinsky, A. Neutrophil elastase and myeloperoxidase regulate the formation of neutrophil extracellular traps. *J Cell Biol* **191**, 677-691, doi:10.1083/jcb.201006052 (2010).

106 Rohm, M. *et al.* NADPH oxidase promotes neutrophil extracellular trap formation in pulmonary aspergillosis. *Infect Immun* **82**, 1766-1777, doi:10.1128/IAI.00096-14 (2014).

107 Akk, A., Springer, L. E. & Pham, C. T. Neutrophil Extracellular Traps Enhance Early Inflammatory Response in Sendai Virus-Induced Asthma Phenotype. *Front Immunol* **7**, 325, doi:10.3389/fimmu.2016.00325 (2016).

108 Sorensen, O. E. *et al.* Papillon-Lefevre syndrome patient reveals species-dependent requirements for neutrophil defenses. *J Clin Invest* **124**, 4539-4548, doi:10.1172/JCI76009 (2014).

109 Roberts, H. *et al.* Characterization of neutrophil function in Papillon-Lefevre syndrome. *J Leukoc Biol* **100**, 433-444, doi:10.1189/jlb.5A1015-489R (2016).

110 Metzler, K. D., Goosmann, C., Lubojemska, A., Zychlinsky, A. & Papayannopoulos, V. A myeloperoxidase-containing complex regulates neutrophil elastase release and actin dynamics during NETosis. *Cell Rep* **8**, 883-896, doi:10.1016/j.celrep.2014.06.044 (2014).

111 Yipp, B. G. *et al.* Infection-induced NETosis is a dynamic process involving neutrophil multitasking in vivo. *Nature medicine* **18**, 1386-1393, doi:10.1038/nm.2847 (2012).

112 Peschel, A. & Hartl, D. Anuclear neutrophils keep hunting. *Nature medicine* **18**, 1336-1338, doi:10.1038/nm.2918 (2012).

113 Scapini, P. *et al.* The neutrophil as a cellular source of chemokines. *Immunological reviews* **177**, 195-203 (2000).

114 Cassatella, M. A. Neutrophil-derived proteins: selling cytokines by the pound. *Advances in immunology* **73**, 369-509 (1999).

115 Bennouna, S., Bliss, S. K., Curiel, T. J. & Denkers, E. Y. Cross-talk in the innate immune system: neutrophils instruct recruitment and activation of dendritic cells during microbial infection. *J Immunol* **171**, 6052-6058 (2003).

116 Bennouna, S. & Denkers, E. Y. Microbial antigen triggers rapid mobilization of TNF-alpha to the surface of mouse neutrophils transforming them into inducers of high-level dendritic cell TNF-alpha production. *J Immunol* **174**, 4845-4851 (2005).

117 van Gisbergen, K. P., Sanchez-Hernandez, M., Geijtenbeek, T. B. & van Kooyk, Y. Neutrophils mediate immune modulation of dendritic cells through glycosylation-dependent interactions between Mac-1 and DC-SIGN. *J Exp Med* **201**, 1281-1292, doi:10.1084/jem.20041276 (2005).

118 van Gisbergen, K. P., Ludwig, I. S., Geijtenbeek, T. B. & van Kooyk, Y. Interactions of DC-SIGN with Mac-1 and CEACAM1 regulate contact between dendritic cells and neutrophils. *FEBS Lett* **579**, 6159-6168, doi:10.1016/j.febslet.2005.09.089 (2005).

119 Maffia, P. C. *et al.* Neutrophil elastase converts human immature dendritic cells into transforming growth factor-beta1-secreting cells and reduces allostimulatory ability. *Am J Pathol* **171**, 928-937, doi:10.2353/ajpath.2007.061043 (2007).

120 Schuster, S., Hurrell, B. & Tacchini-Cottier, F. Crosstalk between neutrophils and dendritic cells: a context-dependent process. *J Leukoc Biol* **94**, 671-675, doi:10.1189/jlb.1012540 (2013).

121 Costantini, C. & Cassatella, M. A. The defensive alliance between neutrophils and NK cells as a novel arm of innate immunity. *J Leukoc Biol* **89**, 221-233, doi:10.1189/jlb.0510250 (2011).

122 Altznauer, F. *et al.* Inflammation-associated cell cycle-independent block of apoptosis by survivin in terminally differentiated neutrophils. *The Journal of experimental medicine* **199**, 1343-1354, doi:10.1084/jem.20032033 (2004).

123 Dibbert, B. *et al.* Cytokine-mediated Bax deficiency and consequent delayed neutrophil apoptosis: a general mechanism to accumulate effector cells in inflammation. *Proceedings of the National Academy of Sciences of the United States of America* **96**, 13330-13335 (1999).

124 Weinmann, P., Gaehtgens, P. & Walzog, B. Bcl-Xl- and Bax-alpha-mediated regulation of apoptosis of human neutrophils via caspase-3. *Blood* **93**, 3106-3115 (1999).

125 del Peso, L., Gonzalez-Garcia, M., Page, C., Herrera, R. & Nunez, G. Interleukin-3-induced phosphorylation of BAD through the protein kinase Akt. *Science* **278**, 687-689 (1997).

126 Cowburn, A. S., Cadwallader, K. A., Reed, B. J., Farahi, N. & Chilvers, E. R. Role of PI3-kinase-dependent Bad phosphorylation and altered transcription in cytokine-mediated neutrophil survival. *Blood* **100**, 2607-2616, doi:10.1182/blood-2001-11-0122 (2002).

127 Derouet, M., Thomas, L., Cross, A., Moots, R. J. & Edwards, S. W. Granulocyte macrophage colony-stimulating factor signaling and proteasome inhibition delay neutrophil apoptosis by increasing the stability of Mcl-1. *The Journal of biological chemistry* **279**, 26915-26921, doi:10.1074/jbc.M313875200 (2004).

128 Cassatella, M. A. *et al.* Interferon-activated neutrophils store a TNF-related apoptosis-inducing ligand (TRAIL/Apo-2 ligand) intracellular pool that is readily mobilizable following exposure to proinflammatory mediators. *Journal of leukocyte biology* **79**, 123-132, doi:10.1189/jlb.0805431 (2006).

129 Lum, J. J., Bren, G., McClure, R. & Badley, A. D. Elimination of senescent neutrophils by TNF-related apoptosis-inducing [corrected] ligand. *Journal of immunology (Baltimore, Md. : 1950)* **175**, 1232-1238 (2005).

130 Thewissen, M., Damoiseaux, J., van de Gaar, J. & Tervaert, J. W. Neutrophils and T cells: bidirectional effects and functional interferences. *Mol Immunol* **48**, 2094-2101, doi:10.1016/j.molimm.2011.07.006 (2011).

131 Munder, M. *et al.* Suppression of T-cell functions by human granulocyte arginase. *Blood* **108**, 1627-1634, doi:10.1182/blood-2006-11-010389 (2006).

132 Rotondo, R. *et al.* Exocytosis of azurophil and arginase 1-containing granules by activated polymorphonuclear neutrophils is required to inhibit T lymphocyte proliferation. *J Leukoc Biol* **89**, 721-727, doi:10.1189/jlb.1109737 (2011).

133 Cemerski, S., Cantagrel, A., Van Meerwijk, J. P. & Romagnoli, P. Reactive oxygen species differentially affect T cell receptor-signaling pathways. *J Biol Chem* **277**, 19585-19593, doi:10.1074/jbc.M111451200 (2002).

134 Pelletier, M. *et al.* Evidence for a cross-talk between human neutrophils and Th17 cells. *Blood* **115**, 335-343, doi:10.1182/blood-2009-04-216085 (2010).

135 Himmel, M. E. *et al.* Human CD4+ FOXP3+ regulatory T cells produce CXCL8 and recruit neutrophils. *Eur J Immunol* **41**, 306-312, doi:10.1002/eji.201040459 (2011).

136 Pelletier, M., Micheletti, A. & Cassatella, M. A. Modulation of human neutrophil survival and antigen expression by activated CD4+ and CD8+ T cells. *J Leukoc Biol* **88**, 1163-1170, doi:10.1189/jlb.0310172 (2010).

137 Abadie, V. *et al.* Neutrophils rapidly migrate via lymphatics after Mycobacterium bovis BCG intradermal vaccination and shuttle live bacilli to the draining lymph nodes. *Blood* **106**, 1843-1850, doi:10.1182/blood-2005-03-1281 (2005).

138 Chtanova, T. *et al.* Dynamics of neutrophil migration in lymph nodes during infection. *Immunity* **29**, 487-496, doi:10.1016/j.immuni.2008.07.012 (2008).

139 Duffy, D. *et al.* Neutrophils transport antigen from the dermis to the bone marrow, initiating a source of memory CD8+ T cells. *Immunity* **37**, 917-929, doi:10.1016/j.immuni.2012.07.015 (2012).

140 Beauvillain, C. *et al.* CCR7 is involved in the migration of neutrophils to lymph nodes. *Blood* **117**, 1196-1204, doi:10.1182/blood-2009-11-254490 (2011).

141 Yang, C. W., Strong, B. S., Miller, M. J. & Unanue, E. R. Neutrophils influence the level of antigen presentation during the immune response to protein antigens in adjuvants. *J Immunol* **185**, 2927-2934, doi:10.4049/jimmunol.1001289 (2010).

142 Hampton, H. R., Bailey, J., Tomura, M., Brink, R. & Chtanova, T. Microbe-dependent lymphatic migration of neutrophils modulates lymphocyte proliferation in lymph nodes. *Nat Commun* **6**, 7139, doi:10.1038/ncomms8139 (2015).

143 Reith, W., LeibundGut-Landmann, S. & Waldburger, J. M. Regulation of MHC class II gene expression by the class II transactivator. *Nat Rev Immunol* **5**, 793-806, doi:10.1038/nri1708 (2005).

144 Sokol, C. L. *et al.* Basophils function as antigen-presenting cells for an allergen-induced T helper type 2 response. *Nat Immunol* **10**, 713-720, doi:10.1038/ni.1738 (2009).

145 Perrigoue, J. G. *et al.* MHC class II-dependent basophil-CD4+ T cell interactions promote T(H)2 cytokine-dependent immunity. *Nat Immunol* **10**, 697-705, doi:10.1038/ni.1740 (2009).

146 Kambayashi, T. & Laufer, T. M. Atypical MHC class II-expressing antigen-presenting cells: can anything replace a dendritic cell? *Nat Rev Immunol* **14**, 719-730, doi:10.1038/nri3754 (2014).

147 Matsumoto, S., Takei, M., Moriyama, M. & Imanishi, H. Enhancement of Ia-like antigen expression by interferon-gamma in polymorphonuclear leukocytes. *Chem Pharm Bull (Tokyo)* **35**, 436-439 (1987).

148 Gosselin, E. J., Wardwell, K., Rigby, W. F. & Guyre, P. M. Induction of MHC class II on human polymorphonuclear neutrophils by granulocyte/macrophage colony-stimulating factor, IFN-gamma, and IL-3. *J Immunol* **151**, 1482-1490 (1993).

149 Fanger, N. A. *et al.* Activation of human T cells by major histocompatability complex class II expressing neutrophils: proliferation in the presence of superantigen, but not tetanus toxoid. *Blood* **89**, 4128-4135 (1997).

150 Iking-Konert, C. *et al.* Transdifferentiation of polymorphonuclear neutrophils: acquisition of CD83 and other functional characteristics of dendritic cells. *J Mol Med (Berl)* **79**, 464-474 (2001).

151 Reinisch, W. *et al.* In vivo induction of HLA-DR on human neutrophils in patients treated with interferon-gamma. *Blood* **87**, 3068 (1996).

152 Mudzinski, S. P. *et al.* Expression of HLA-DR (major histocompatibility complex class II) on neutrophils from patients treated with granulocyte-macrophage colony-stimulating factor for mobilization of stem cells. *Blood* **86**, 2452-2453 (1995).

153 Iking-Konert, C. *et al.* Transdifferentiation of polymorphonuclear neutrophils to dendritic-like cells at the site of inflammation in rheumatoid arthritis: evidence for activation by T cells. *Ann Rheum Dis* **64**, 1436-1442, doi:10.1136/ard.2004.034132 (2005).

154 Sandilands, G. P., McCrae, J., Hill, K., Perry, M. & Baxter, D. Major histocompatibility complex class II (DR) antigen and costimulatory molecules on in vitro and in vivo activated human polymorphonuclear neutrophils. *Immunology* **119**, 562-571, doi:10.1111/j.1365-2567.2006.02471.x (2006).

155 Cross, A., Bucknall, R. C., Cassatella, M. A., Edwards, S. W. & Moots, R. J. Synovial fluid neutrophils transcribe and express class II major histocompatibility complex molecules in rheumatoid arthritis. *Arthritis Rheum* **48**, 2796-2806, doi:10.1002/art.11253 (2003).

156 Davey, M. S. *et al.* Microbe-specific unconventional T cells induce human neutrophil differentiation into antigen cross-presenting cells. *J Immunol* **193**, 3704-3716, doi:10.4049/jimmunol.1401018 (2014).

157 Singhal, S. *et al.* Origin and Role of a Subset of Tumor-Associated Neutrophils with Antigen-Presenting Cell Features in Early-Stage Human Lung Cancer. *Cancer Cell* **30**, 120-135, doi:10.1016/j.ccell.2016.06.001 (2016).

158 Okuda, K., Neely, B. C. & David, C. S. Expression of H-2 and Ia antigens on mouse peritoneal neutrophils. *Transplantation* **28**, 354-356 (1979).

159 Okuda, K., Tani, K., Ishigatsubo, Y., Yokota, S. & David, C. S. Antigen-pulsed neutrophils bearing Ia antigens can induce T lymphocyte proliferative response to the syngeneic or semisyngeneic antigen-primed T lymphocytes. *Transplantation* **30**, 368-372 (1980).

160 Fitzgerald, J. E., Sonis, S. T., Rodrick, M. L. & Wilson, R. E. Interaction of Ia antigen-bearing polymorphonuclear leukocytes and murine splenocytes. *Inflammation* **7**, 25-33 (1983).

161 Abi Abdallah, D. S., Egan, C. E., Butcher, B. A. & Denkers, E. Y. Mouse neutrophils are professional antigen-presenting cells programmed to instruct Th1 and Th17 T-cell differentiation. *Int Immunol* **23**, 317-326, doi:10.1093/intimm/dxr007 (2011).

162 Ostanin, D. V. *et al.* Acquisition of antigen-presenting functions by neutrophils isolated from mice with chronic colitis. *J Immunol* **188**, 1491-1502, doi:10.4049/jimmunol.1102296 (2012).

163 Vono, M. *et al.* Neutrophils acquire the capacity for antigen presentation to memory CD4(+) T cells in vitro and ex vivo. *Blood* **129**, 1991-2001, doi:10.1182/blood-2016-10-744441 (2017).

164 Vincent, J. L., Opal, S. M., Marshall, J. C. & Tracey, K. J. Sepsis definitions: time for change. *Lancet* **381**, 774-775, doi:10.1016/S0140-6736(12)61815-7 (2013).

165 Hotchkiss, R. S., Monneret, G. & Payen, D. Sepsis-induced immunosuppression: from cellular dysfunctions to immunotherapy. *Nat Rev Immunol* **13**, 862-874, doi:10.1038/nri3552 (2013).

166 Reinhart, K. *et al.* Recognizing Sepsis as a Global Health Priority - A WHO Resolution. *N Engl J Med* **377**, 414-417, doi:10.1056/NEJMp1707170 (2017).

167 Fleischmann, C. *et al.* Assessment of Global Incidence and Mortality of Hospital-treated Sepsis. Current Estimates and Limitations. *Am J Respir Crit Care Med* **193**, 259-272, doi:10.1164/rccm.201504-0781OC (2016).

168 van der Poll, T., van de Veerdonk, F. L., Scicluna, B. P. & Netea, M. G. The immunopathology of sepsis and potential therapeutic targets. *Nat Rev Immunol* **17**, 407-420, doi:10.1038/nri.2017.36 (2017).

169 Hotchkiss, R. S., Monneret, G. & Payen, D. Immunosuppression in sepsis: a novel understanding of the disorder and a new therapeutic approach. *Lancet Infect Dis* **13**, 260-268, doi:10.1016/S1473-3099(13)70001-X (2013).

170 Rittirsch, D., Flierl, M. A. & Ward, P. A. Harmful molecular mechanisms in sepsis. *Nat Rev Immunol* **8**, 776-787, doi:10.1038/nri2402 (2008).

171 Hotchkiss, R. S. & Karl, I. E. The pathophysiology and treatment of sepsis. *N Engl J Med* **348**, 138-150, doi:10.1056/NEJMra021333 (2003).

172 Cheng, S. C. *et al.* Broad defects in the energy metabolism of leukocytes underlie immunoparalysis in sepsis. *Nat Immunol* **17**, 406-413, doi:10.1038/ni.3398 (2016).

173 Harrison, C. Sepsis: calming the cytokine storm. *Nat Rev Drug Discov* **9**, 360-361, doi:10.1038/nrd3162 (2010).

174 Hotchkiss, R. S. & Opal, S. Immunotherapy for sepsis--a new approach against an ancient foe. *N Engl J Med* **363**, 87-89, doi:10.1056/NEJMcibr1004371 (2010).

175 Boomer, J. S. *et al.* Immunosuppression in patients who die of sepsis and multiple organ failure. *JAMA* **306**, 2594-2605, doi:10.1001/jama.2011.1829 (2011).

176 Weber, G. F. *et al.* Interleukin-3 amplifies acute inflammation and is a potential therapeutic target in sepsis. *Science* **347**, 1260-1265, doi:10.1126/science.aaa4268 (2015).

177 Stearns-Kurosawa, D. J., Osuchowski, M. F., Valentine, C., Kurosawa, S. & Remick, D. G. The pathogenesis of sepsis. *Annu Rev Pathol* **6**, 19-48, doi:10.1146/annurev-pathol-011110-130327 (2011).

178 Angus, D. C. & van der Poll, T. Severe sepsis and septic shock. *N Engl J Med* **369**, 840-851, doi:10.1056/NEJMra1208623 (2013).

179 van Dissel, J. T., van Langevelde, P., Westendorp, R. G., Kwappenberg, K. & Frolich, M. Anti-inflammatory cytokine profile and mortality in febrile patients. *Lancet* **351**, 950-953, doi:10.1016/S0140-6736(05)60606-X (1998).

180 Ertel, W. *et al.* Downregulation of proinflammatory cytokine release in whole blood from septic patients. *Blood* **85**, 1341-1347 (1995).

181 Torgersen, C. *et al.* Macroscopic postmortem findings in 235 surgical intensive care patients with sepsis. *Anesth Analg* **108**, 1841-1847, doi:10.1213/ane.0b013e318195e11d (2009).

182 Otto, G. P. *et al.* The late phase of sepsis is characterized by an increased microbiological burden and death rate. *Crit Care* **15**, R183, doi:10.1186/cc10332 (2011).

183 Monneret, G. *et al.* The anti-inflammatory response dominates after septic shock: association of low monocyte HLA-DR expression and high interleukin-10 concentration. *Immunol Lett* **95**, 193-198, doi:10.1016/j.imlet.2004.07.009 (2004).

184 Lukaszewicz, A. C. *et al.* Monocytic HLA-DR expression in intensive care patients: interest for prognosis and secondary infection prediction. *Crit Care Med* **37**, 2746-2752, doi:10.1097/CCM.0b013e3181ab858a (2009).

185 Pastille, E. *et al.* Modulation of dendritic cell differentiation in the bone marrow mediates sustained immunosuppression after polymicrobial sepsis. *J Immunol* **186**, 977-986, doi:10.4049/jimmunol.1001147 (2011).

186 Cavaillon, J. M. & Adib-Conquy, M. Bench-to-bedside review: endotoxin tolerance as a model of leukocyte reprogramming in sepsis. *Crit Care* **10**, 233, doi:10.1186/cc5055 (2006).

187 Carson, W. F., Cavassani, K. A., Dou, Y. & Kunkel, S. L. Epigenetic regulation of immune cell functions during post-septic immunosuppression. *Epigenetics* **6**, 273-283 (2011).

188 Wenzel, R. P. & Edmond, M. B. Septic shock--evaluating another failed treatment. *N Engl J Med* **366**, 2122-2124, doi:10.1056/NEJMe1203412 (2012).

189 Xiao, W. *et al.* A genomic storm in critically injured humans. *J Exp Med* **208**, 2581-2590, doi:10.1084/jem.20111354 (2011).

190 Brown, K. A. *et al.* Neutrophils in development of multiple organ failure in sepsis. *Lancet* **368**, 157-169, doi:10.1016/S0140-6736(06)69005-3 (2006).

191 Kovach, M. A. & Standiford, T. J. The function of neutrophils in sepsis. *Curr Opin Infect Dis* **25**, 321-327, doi:10.1097/QCO.0b013e3283528c9b (2012).

192 Sonego, F. *et al.* Paradoxical Roles of the Neutrophil in Sepsis: Protective and Deleterious. *Front Immunol* **7**, 155, doi:10.3389/fimmu.2016.00155 (2016).

193 Cummings, C. J. *et al.* Expression and function of the chemokine receptors CXCR1 and CXCR2 in sepsis. *J Immunol* **162**, 2341-2346 (1999).

194 Chishti, A. D., Shenton, B. K., Kirby, J. A. & Baudouin, S. V. Neutrophil chemotaxis and receptor expression in clinical septic shock. *Intensive Care Med* **30**, 605-611, doi:10.1007/s00134-004-2175-y (2004).

195 Arraes, S. M. *et al.* Impaired neutrophil chemotaxis in sepsis associates with GRK expression and inhibition of actin assembly and tyrosine phosphorylation. *Blood* **108**, 2906-2913, doi:10.1182/blood-2006-05-024638 (2006).

196 Freitas, A. *et al.* IL-17 receptor signaling is required to control polymicrobial sepsis. *J Immunol* **182**, 7846-7854, doi:10.4049/jimmunol.0803039 (2009).

197 Tavares-Murta, B. M. *et al.* Failure of neutrophil chemotactic function in septic patients. *Crit Care Med* **30**, 1056-1061 (2002).

198 Alves-Filho, J. C. *et al.* Interleukin-33 attenuates sepsis by enhancing neutrophil influx to the site of infection. *Nat Med* **16**, 708-712, doi:10.1038/nm.2156 (2010).

199 Czaikoski, P. G. *et al.* Neutrophil Extracellular Traps Induce Organ Damage during Experimental and Clinical Sepsis. *PLoS One* **11**, e0148142, doi:10.1371/journal.pone.0148142 (2016).

200 Clark, S. R. *et al.* Platelet TLR4 activates neutrophil extracellular traps to ensnare bacteria in septic blood. *Nat Med* **13**, 463-469, doi:10.1038/nm1565 (2007).

201 Remijsen, Q. *et al.* Dying for a cause: NETosis, mechanisms behind an antimicrobial cell death modality. *Cell Death Differ* **18**, 581-588, doi:10.1038/cdd.2011.1 (2011).

202 Delano, M. J. *et al.* MyD88-dependent expansion of an immature GR-1(+)CD11b(+) population induces T cell suppression and Th2 polarization in sepsis. *J Exp Med* **204**, 1463-1474, doi:10.1084/jem.20062602 (2007).

203 Makarenkova, V. P., Bansal, V., Matta, B. M., Perez, L. A. & Ochoa, J. B. CD11b+/Gr-1+ myeloid suppressor cells cause T cell dysfunction after traumatic stress. *J Immunol* **176**, 2085-2094 (2006).

204 Janols, H. *et al.* A high frequency of MDSCs in sepsis patients, with the granulocytic subtype dominating in gram-positive cases. *J Leukoc Biol* **96**, 685-693, doi:10.1189/jlb.5HI0214-074R (2014).

205 Veglia, F., Perego, M. & Gabrilovich, D. Myeloid-derived suppressor cells coming of age. *Nat Immunol* **19**, 108-119, doi:10.1038/s41590-017-0022-x (2018).

206 Uhel, F. *et al.* Early Expansion of Circulating Granulocytic Myeloid-derived Suppressor Cells Predicts Development of Nosocomial Infections in Patients with Sepsis. *Am J Respir Crit Care Med* **196**, 315-327, doi:10.1164/rccm.201606-1143OC (2017).

207 Kasten, K. R., Muenzer, J. T. & Caldwell, C. C. Neutrophils are significant producers of IL-10 during sepsis. *Biochem Biophys Res Commun* **393**, 28-31, doi:10.1016/j.bbrc.2010.01.066 (2010).

208 Pillay, J. *et al.* A subset of neutrophils in human systemic inflammation inhibits T cell responses through Mac-1. *J Clin Invest* **122**, 327-336, doi:10.1172/JCI57990 (2012).

209 Delano, M. J. & Ward, P. A. Sepsis-induced immune dysfunction: can immune therapies reduce mortality? *J Clin Invest* **126**, 23-31, doi:10.1172/JCI82224 (2016).

210 Davey, M. S. *et al.* Microbe-specific unconventional T cells induce human neutrophil differentiation into antigen cross-presenting cells. *J Immunol* **193**, 3704-3716, doi:10.4049/jimmunol.1401018 (2014).

211 Leliefeld, P. H., Wessels, C. M., Leenen, L. P., Koenderman, L. & Pillay, J. The role of neutrophils in immune dysfunction during severe inflammation. *Crit Care* **20**, 73, doi:10.1186/s13054-016-1250-4 (2016).

212 Wang, J. F. *et al.* Up-regulation of programmed cell death 1 ligand 1 on neutrophils may be involved in sepsis-induced immunosuppression: an animal study and a prospective case-control study. *Anesthesiology* **122**, 852-863, doi:10.1097/ALN.0000000000000525 (2015).

213 Huang, X. *et al.* Identification of B7-H1 as a novel mediator of the innate immune/proinflammatory response as well as a possible myeloid cell prognostic biomarker in sepsis. *J Immunol* **192**, 1091-1099, doi:10.4049/jimmunol.1302252 (2014).

214 Venet, F. & Monneret, G. Advances in the understanding and treatment of sepsis-induced immunosuppression. *Nat Rev Nephrol* **14**, 121-137, doi:10.1038/nrneph.2017.165 (2018).

215 de Kleijn, S. *et al.* IFN-gamma-stimulated neutrophils suppress lymphocyte proliferation through expression of PD-L1. *PLoS One* **8**, e72249, doi:10.1371/journal.pone.0072249 (2013).

216 Wang, T. T. *et al.* Tumour-activated neutrophils in gastric cancer foster immune suppression and disease progression through GM-CSF-PD-L1 pathway. *Gut* **66**, 1900-1911, doi:10.1136/gutjnl-2016-313075 (2017).

217 Bankey, P. E. *et al.* Cytokine induced expression of programmed death ligands in human neutrophils. *Immunol Lett* **129**, 100-107, doi:10.1016/j.imlet.2010.01.006 (2010).

218 Patera, A. C. *et al.* Frontline Science: Defects in immune function in patients with sepsis are associated with PD-1 or PD-L1 expression and can be restored by antibodies targeting PD-1 or PD-L1. *J Leukoc Biol* **100**, 1239-1254, doi:10.1189/jlb.4HI0616-255R (2016).

219 Brahmamdam, P. *et al.* Delayed administration of anti-PD-1 antibody reverses immune dysfunction and improves survival during sepsis. *J Leukoc Biol* **88**, 233-240, doi:10.1189/jlb.0110037 (2010).

220 Drifte, G., Dunn-Siegrist, I., Tissieres, P. & Pugin, J. Innate immune functions of immature neutrophils in patients with sepsis and severe systemic inflammatory response syndrome. *Crit Care Med* **41**, 820-832, doi:10.1097/CCM.0b013e318274647d (2013).

221 Liu, X. *et al.* Prognostic Significance of Neutrophil-to-Lymphocyte Ratio in Patients with Sepsis: A Prospective Observational Study. *Mediators Inflamm* **2016**, 8191254, doi:10.1155/2016/8191254 (2016).

222 Hansen, T. H. & Bouvier, M. MHC class I antigen presentation: learning from viral evasion strategies. *Nat Rev Immunol* **9**, 503-513, doi:10.1038/nri2575 (2009).

223 Jensen, P. E. Recent advances in antigen processing and presentation. *Nat Immunol* **8**, 1041-1048, doi:10.1038/ni1516 (2007).

224 Vyas, J. M., Van der Veen, A. G. & Ploegh, H. L. The known unknowns of antigen processing and presentation. *Nat Rev Immunol* **8**, 607-618, doi:10.1038/nri2368 (2008).

225 Caserta, T. M., Smith, A. N., Gultice, A. D., Reedy, M. A. & Brown, T. L. Q-VD-OPh, a broad spectrum caspase inhibitor with potent antiapoptotic properties. *Apoptosis* **8**, 345-352 (2003).

226 Campbell, M. S., Lovell, M. A. & Gorbsky, G. J. Stability of nuclear segments in human neutrophils and evidence against a role for microfilaments or microtubules in their genesis during differentiation of HL60 myelocytes. *J Leukoc Biol* **58**, 659-666 (1995).

227 Khanna, N. *et al.* Generation of a multipathogen-specific T-cell product for adoptive immunotherapy based on activation-dependent expression of CD154. *Blood* **118**, 1121-1131, doi:10.1182/blood-2010-12-322610 (2011).

228 Kwak, B., Mulhaupt, F., Myit, S. & Mach, F. Statins as a newly recognized type of immunomodulator. *Nat Med* **6**, 1399-1402, doi:10.1038/82219 (2000).

229 Al-Shami, A., Mahanna, W. & Naccache, P. H. Granulocyte-macrophage colony-stimulating factor-activated signaling pathways in human neutrophils. Selective activation of Jak2, Stat3, and Stat5b. *J Biol Chem* **273**, 1058-1063 (1998).

230 Schmutz, C. *et al.* Systems-level overview of host protein phosphorylation during Shigella flexneri infection revealed by phosphoproteomics. *Mol Cell Proteomics* **12**, 2952-2968, doi:10.1074/mcp.M113.029918 (2013).

231 Hamilton, J. A. Colony-stimulating factors in inflammation and autoimmunity. *Nat Rev Immunol* **8**, 533-544, doi:10.1038/nri2356 (2008).

232 Schwartz, D. & Gygi, S. P. An iterative statistical approach to the identification of protein phosphorylation motifs from large-scale data sets. *Nat Biotechnol* **23**, 1391-1398, doi:10.1038/nbt1146 (2005).

233 Chou, M. F. & Schwartz, D. Biological sequence motif discovery using motif-x. *Curr Protoc Bioinformatics* **Chapter 13**, Unit 13 15-24, doi:10.1002/0471250953.bi1315s35 (2011).

234 Lee, T. Y., Bo-Kai Hsu, J., Chang, W. C. & Huang, H. D. RegPhos: a system to explore the protein kinase-substrate phosphorylation network in humans. *Nucleic Acids Res* **39**, D777-787, doi:10.1093/nar/gkq970 (2011).

235 Park, J. *et al.* RAS-MAPK-MSK1 pathway modulates ataxin 1 protein levels and toxicity in SCA1. *Nature* **498**, 325-331, doi:10.1038/nature12204 (2013).

236 Ubersax, J. A. & Ferrell, J. E., Jr. Mechanisms of specificity in protein phosphorylation. *Nat Rev Mol Cell Biol* **8**, 530-541, doi:10.1038/nrm2203 (2007).

237 Hutti, J. E. *et al.* A rapid method for determining protein kinase phosphorylation specificity. *Nat Methods* **1**, 27-29, doi:10.1038/nmeth708 (2004).

238 Kwon, E. M., Raines, M. A., Blenis, J. & Sakamoto, K. M. Granulocyte-macrophage colony-stimulating factor stimulation results in phosphorylation of cAMP response element-binding protein through activation of pp90RSK. *Blood* **95**, 2552-2558 (2000).

239 Moreno, C. S., Beresford, G. W., Louis-Plence, P., Morris, A. C. & Boss, J. M. CREB regulates MHC class II expression in a CIITA-dependent manner. *Immunity* **10**, 143-151 (1999).

240 Best, J. L. *et al.* Identification of small-molecule antagonists that inhibit an activator: coactivator interaction. *Proc Natl Acad Sci U S A* **101**, 17622-17627, doi:10.1073/pnas.0406374101 (2004).

241 Steimle, V., Otten, L. A., Zufferey, M. & Mach, B. Complementation cloning of an MHC class II transactivator mutated in hereditary MHC class II deficiency (or bare lymphocyte syndrome). *Cell* **75**, 135-146 (1993).

242 Harding, C. V. & Boom, W. H. Regulation of antigen presentation by Mycobacterium tuberculosis: a role for Toll-like receptors. *Nat Rev Microbiol* **8**, 296-307, doi:10.1038/nrmicro2321 (2010).

243 Mantovani, R. The molecular biology of the CCAAT-binding factor NF-Y. *Gene* **239**, 15-27 (1999).

244 Steimle, V. *et al.* A novel DNA-binding regulatory factor is mutated in primary MHC class II deficiency (bare lymphocyte syndrome). *Genes Dev* **9**, 1021-1032 (1995).

245 Durand, B. *et al.* RFXAP, a novel subunit of the RFX DNA binding complex is mutated in MHC class II deficiency. *EMBO J* **16**, 1045-1055, doi:10.1093/emboj/16.5.1045 (1997).

246 Masternak, K. *et al.* A gene encoding a novel RFX-associated transactivator is mutated in the majority of MHC class II deficiency patients. *Nat Genet* **20**, 273-277, doi:10.1038/3081 (1998).

247 Santos, R. L., Tsolis, R. M., Baumler, A. J., Smith, R., 3rd & Adams, L. G. Salmonella enterica serovar typhimurium induces cell death in bovine monocyte-derived macrophages by early sipB-dependent and delayed sipB-independent mechanisms. *Infect Immun* **69**, 2293-2301, doi:10.1128/IAI.69.4.2293-2301.2001 (2001).

248 Santos, R. L. *et al.* Salmonella-induced cell death is not required for enteritis in calves. *Infect Immun* **69**, 4610-4617, doi:10.1128/IAI.69.7.4610-4617.2001 (2001).

249 Zerbino, D. R. *et al.* Ensembl 2018. *Nucleic Acids Res* **46**, D754-D761, doi:10.1093/nar/gkx1098 (2018).

250 Durinck, S., Spellman, P. T., Birney, E. & Huber, W. Mapping identifiers for the integration of genomic datasets with the R/Bioconductor package biomaRt. *Nat Protoc* **4**, 1184-1191, doi:10.1038/nprot.2009.97 (2009).

251 Huber, W. *et al.* Orchestrating high-throughput genomic analysis with Bioconductor. *Nat Methods* **12**, 115-121, doi:10.1038/nmeth.3252 (2015).

252 Iking-Konert, C. *et al.* Polymorphonuclear neutrophils in Wegener's granulomatosis acquire characteristics of antigen presenting cells. *Kidney Int* **60**, 2247-2262, doi:10.1046/j.1523-1755.2001.00068.x (2001).

253 Mayadas, T. N., Cullere, X. & Lowell, C. A. The multifaceted functions of neutrophils. *Annu Rev Pathol* **9**, 181-218, doi:10.1146/annurev-pathol-020712-164023 (2014).

254 Smith, W. B. *et al.* Neutrophils activated by granulocyte-macrophage colony-stimulating factor express receptors for interleukin-3 which mediate class II expression. *Blood* **86**, 3938-3944 (1995).

255 Reinisch, W. *et al.* Donor dependent, interferon-gamma induced HLA-DR expression on human neutrophils in vivo. *Clin Exp Immunol* **133**, 476-484 (2003).

256 Malmstrom, E. *et al.* Targeted mass spectrometry analysis of neutrophil-derived proteins released during sepsis progression. *Thromb Haemost* **112**, 1230-1243, doi:10.1160/TH14-04-0312 (2014).

257 Stuehler, C. *et al.* Cross-protective TH1 immunity against Aspergillus fumigatus and Candida albicans. *Blood* **117**, 5881-5891, doi:10.1182/blood-2010-12-325084 (2011).

258 Gentile, L. F. *et al.* Is there value in plasma cytokine measurements in patients with severe trauma and sepsis? *Methods* **61**, 3-9, doi:10.1016/j.ymeth.2013.04.024 (2013).

259 Broughton, S. E. *et al.* The GM-CSF/IL-3/IL-5 cytokine receptor family: from ligand recognition to initiation of signaling. *Immunol Rev* **250**, 277-302, doi:10.1111/j.1600-065X.2012.01164.x (2012).

260 Steidl, C. *et al.* MHC class II transactivator CIITA is a recurrent gene fusion partner in lymphoid cancers. *Nature* **471**, 377-381, doi:10.1038/nature09754 (2011).

261 Mayr, B. & Montminy, M. Transcriptional regulation by the phosphorylation-dependent factor CREB. *Nat Rev Mol Cell Biol* **2**, 599-609, doi:10.1038/35085068 (2001).

262 Deak, M., Clifton, A. D., Lucocq, L. M. & Alessi, D. R. Mitogen- and stress-activated protein kinase-1 (MSK1) is directly activated by MAPK and SAPK2/p38, and may mediate activation of CREB. *EMBO J* **17**, 4426-4441, doi:10.1093/emboj/17.15.4426 (1998).

263 Xing, J., Ginty, D. D. & Greenberg, M. E. Coupling of the RAS-MAPK pathway to gene activation by RSK2, a growth factor-regulated CREB kinase. *Science* **273**, 959-963 (1996).

264 Du, K. & Montminy, M. CREB is a regulatory target for the protein kinase Akt/PKB. *J Biol Chem* **273**, 32377-32379 (1998).

265 Brindle, P., Linke, S. & Montminy, M. Protein-kinase-A-dependent activator in transcription factor CREB reveals new role for CREM repressors. *Nature* **364**, 821-824, doi:10.1038/364821a0 (1993).

266 Tan, Y. *et al.* FGF and stress regulate CREB and ATF-1 via a pathway involving p38 MAP kinase and MAPKAP kinase-2. *EMBO J* **15**, 4629-4642 (1996).

267 Mayer, T. Z. *et al.* The p38-MSK1 signaling cascade influences cytokine production through CREB and C/EBP factors in human neutrophils. *J Immunol* **191**, 4299-4307, doi:10.4049/jimmunol.1301117 (2013).

268 Winthrop, K. L. The emerging safety profile of JAK inhibitors in rheumatic disease. *Nat Rev Rheumatol* **13**, 234-243, doi:10.1038/nrrheum.2017.23 (2017).

269 Lakschevitz, F. S. *et al.* Identification of neutrophil surface marker changes in health and inflammation using high-throughput screening flow cytometry. *Exp Cell Res* **342**, 200-209, doi:10.1016/j.yexcr.2016.03.007 (2016).

270 Hu, Y. Isolation of human and mouse neutrophils ex vivo and in vitro. *Methods Mol Biol* **844**, 101-113, doi:10.1007/978-1-61779-527-5_7 (2012).

271 Bone, R. C. *et al.* Definitions for sepsis and organ failure and guidelines for the use of innovative therapies in sepsis. The ACCP/SCCM Consensus Conference Committee.

American College of Chest Physicians/Society of Critical Care Medicine. *Chest* **101**, 1644-1655 (1992).

272 Singer, M. *et al.* The Third International Consensus Definitions for Sepsis and Septic Shock (Sepsis-3). *JAMA* **315**, 801-810, doi:10.1001/jama.2016.0287 (2016).

273 Hjorth, R., Jonsson, A. K. & Vretblad, P. A rapid method for purification of human granulocytes using percoll. A comparison with dextran sedimentation. *J Immunol Methods* **43**, 95-101 (1981).

274 Hoiseth, S. K. & Stocker, B. A. Aromatic-dependent Salmonella typhimurium are non-virulent and effective as live vaccines. *Nature* **291**, 238-239 (1981).

275 Kroger, C. *et al.* The transcriptional landscape and small RNAs of Salmonella enterica serovar Typhimurium. *Proc Natl Acad Sci U S A* **109**, E1277-1286, doi:10.1073/pnas.1201061109 (2012).

276 Ahrne, E. *et al.* Evaluation and Improvement of Quantification Accuracy in Isobaric Mass Tag-Based Protein Quantification Experiments. *J Proteome Res* **15**, 2537-2547, doi:10.1021/acs.jproteome.6b00066 (2016).

277 Wang, Y. *et al.* Reversed-phase chromatography with multiple fraction concatenation strategy for proteome profiling of human MCF10A cells. *Proteomics* **11**, 2019-2026, doi:10.1002/pmic.201000722 (2011).

278 Nesvizhskii, A. I., Keller, A., Kolker, E. & Aebersold, R. A statistical model for identifying proteins by tandem mass spectrometry. *Anal Chem* **75**, 4646-4658 (2003).

279 Durinck, S., Spellman, P. T., Birney, E. & Huber, W. Mapping Identifiers for the Integration of Genomic Datasets with the R/Bioconductor package biomaRt. *Nature protocols* **4**, 1184-1191, doi:10.1038/nprot.2009.97 (2009).

280 Huber, W. *et al.* Orchestrating high-throughput genomic analysis with Bioconductor. *Nat Meth* **12**, 115-121, doi:10.1038/nmeth.3252 (2015).

281 Ritchie, M. E. *et al.* limma powers differential expression analyses for RNA-sequencing and microarray studies. *Nucleic Acids Res* **43**, e47, doi:10.1093/nar/gkv007 (2015).

282 Stuehler, C. *et al.* Multispecific Aspergillus T cells selected by CD137 or CD154 induce protective immune responses against the most relevant mold infections. *J Infect Dis* **211**, 1251-1261, doi:10.1093/infdis/jiu607 (2015).

283 Beck, O. *et al.* Generation of highly purified and functionally active human TH1 cells against Aspergillus fumigatus. *Blood* **107**, 2562-2569, doi:10.1182/blood-2005-04-1660 (2006).

284 Rauser, G. *et al.* Rapid generation of combined CMV-specific CD4+ and CD8+ T-cell lines for adoptive transfer into recipients of allogeneic stem cell transplants. *Blood* **103**, 3565-3572, doi:10.1182/blood-2003-09-3056 (2004).

285 Tamassia, N., Cassatella, M. A. & Bazzoni, F. Fast and accurate quantitative analysis of cytokine gene expression in human neutrophils. *Methods Mol Biol* **1124**, 451-467, doi:10.1007/978-1-62703-845-4_27 (2014).

286 Schmittgen, T. D. & Livak, K. J. Analyzing real-time PCR data by the comparative C(T) method. *Nat Protoc* **3**, 1101-1108 (2008).

287 Zhang, X., Ding, L. & Sandford, A. J. Selection of reference genes for gene expression studies in human neutrophils by real-time PCR. *BMC Mol Biol* **6**, 4, doi:10.1186/1471-2199-6-4 (2005).

288 Burton, N. A. *et al.* Disparate impact of oxidative host defenses determines the fate of Salmonella during systemic infection in mice. *Cell Host Microbe* **15**, 72-83, doi:10.1016/j.chom.2013.12.006 (2014).

289 Seaver, L. C. & Imlay, J. A. Hydrogen peroxide fluxes and compartmentalization inside growing Escherichia coli. *J Bacteriol* **183**, 7182-7189, doi:10.1128/JB.183.24.7182-7189.2001 (2001).

290 Park, S., You, X. & Imlay, J. A. Substantial DNA damage from submicromolar intracellular hydrogen peroxide detected in Hpx- mutants of Escherichia coli. *Proc Natl Acad Sci U S A* **102**, 9317-9322, doi:10.1073/pnas.0502051102 (2005).

291 Odobasic, D., Kitching, A. R. & Holdsworth, S. R. Neutrophil-Mediated Regulation of Innate and Adaptive Immunity: The Role of Myeloperoxidase. *J Immunol Res* **2016**, 2349817, doi:10.1155/2016/2349817 (2016).

292 Pietarinen-Runtti, P., Lakari, E., Raivio, K. O. & Kinnula, V. L. Expression of antioxidant enzymes in human inflammatory cells. *Am J Physiol Cell Physiol* **278**, C118-125, doi:10.1152/ajpcell.2000.278.1.C118 (2000).

293 Nauseef, W. M., Metcalf, J. A. & Root, R. K. Role of myeloperoxidase in the respiratory burst of human neutrophils. *Blood* **61**, 483-492 (1983).

294 Takeuchi, K. *et al.* Severe neutrophil-mediated lung inflammation in myeloperoxidase-deficient mice exposed to zymosan. *Inflamm Res* **61**, 197-205, doi:10.1007/s00011-011-0401-y (2012).

295 Homme, M., Tateno, N., Miura, N., Ohno, N. & Aratani, Y. Myeloperoxidase deficiency in mice exacerbates lung inflammation induced by nonviable Candida albicans. *Inflamm Res* **62**, 981-990, doi:10.1007/s00011-013-0656-6 (2013).

296 Tateno, N., Matsumoto, N., Motowaki, T., Suzuki, K. & Aratani, Y. Myeloperoxidase deficiency induces MIP-2 production via ERK activation in zymosan-stimulated mouse neutrophils. *Free Radic Res* **47**, 376-385, doi:10.3109/10715762.2013.778990 (2013).

297 Kremserova, S. *et al.* Lung Neutrophilia in Myeloperoxidase Deficient Mice during the Course of Acute Pulmonary Inflammation. *Oxid Med Cell Longev* **2016**, 5219056, doi:10.1155/2016/5219056 (2016).

298 Imlay, J. A. & Linn, S. Mutagenesis and stress responses induced in Escherichia coli by hydrogen peroxide. *J Bacteriol* **169**, 2967-2976 (1987).

299 Siddique, Y. H., Ara, G. & Afzal, M. Estimation of lipid peroxidation induced by hydrogen peroxide in cultured human lymphocytes. *Dose Response* **10**, 1-10, doi:10.2203/dose-response.10-002.Siddique (2012).

300 Gulden, M., Jess, A., Kammann, J., Maser, E. & Seibert, H. Cytotoxic potency of H2O2 in cell cultures: impact of cell concentration and exposure time. *Free Radic Biol Med* **49**, 1298-1305, doi:10.1016/j.freeradbiomed.2010.07.015 (2010).

301 Antunes, F. & Cadenas, E. Estimation of H2O2 gradients across biomembranes. *FEBS Lett* **475**, 121-126 (2000).

302 Reber, L. L. *et al.* Neutrophil myeloperoxidase diminishes the toxic effects and mortality induced by lipopolysaccharide. *J Exp Med* **214**, 1249-1258, doi:10.1084/jem.20161238 (2017).

303 Crimmins, E. M. & Finch, C. E. Infection, inflammation, height, and longevity. *Proc Natl Acad Sci U S A* **103**, 498-503, doi:10.1073/pnas.0501470103 (2006).

304 Pennock, N. D. *et al.* T cell responses: naive to memory and everything in between. *Adv Physiol Educ* **37**, 273-283, doi:10.1152/advan.00066.2013 (2013).

305 Humphrey, S. J. *et al.* Dynamic adipocyte phosphoproteome reveals that Akt directly regulates mTORC2. *Cell Metab* **17**, 1009-1020, doi:10.1016/j.cmet.2013.04.010 (2013).

306 Hashimoto, K., Joshi, S. K. & Koni, P. A. A conditional null allele of the major histocompatibility IA-beta chain gene. *Genesis* **32**, 152-153 (2002).

307 Hasenberg, A. *et al.* Catchup: a mouse model for imaging-based tracking and modulation of neutrophil granulocytes. *Nat Methods* **12**, 445-452, doi:10.1038/nmeth.3322 (2015).

308 Cheminay, C., Chakravortty, D. & Hensel, M. Role of neutrophils in murine salmonellosis. *Infect Immun* **72**, 468-477 (2004).

309 Clausen, B. E., Burkhardt, C., Reith, W., Renkawitz, R. & Forster, I. Conditional gene targeting in macrophages and granulocytes using LysMcre mice. *Transgenic Res* **8**, 265-277 (1999).

310 Orthgiess, J. *et al.* Neurons exhibit Lyz2 promoter activity in vivo: Implications for using LysM-Cre mice in myeloid cell research. *Eur J Immunol* **46**, 1529-1532, doi:10.1002/eji.201546108 (2016).

311 Mastroeni, P. Immunity to systemic Salmonella infections. *Curr Mol Med* **2**, 393-406 (2002).

312 Lim, C. H. *et al.* Independent bottlenecks characterize colonization of systemic compartments and gut lymphoid tissue by salmonella. *PLoS Pathog* **10**, e1004270, doi:10.1371/journal.ppat.1004270 (2014).

313 Kirby, A. C., Sundquist, M. & Wick, M. J. In vivo compartmentalization of functionally distinct, rapidly responsive antigen-specific T-cell populations in DNA-immunized or Salmonella enterica serovar Typhimurium-infected mice. *Infect Immun* **72**, 6390-6400, doi:10.1128/IAI.72.11.6390-6400.2004 (2004).

314 Srinivasan, A. *et al.* Innate immune activation of CD4 T cells in salmonella-infected mice is dependent on IL-18. *J Immunol* **178**, 6342-6349 (2007).

315 Henao-Tamayo, M. I. *et al.* Phenotypic definition of effector and memory T-lymphocyte subsets in mice chronically infected with Mycobacterium tuberculosis. *Clin Vaccine Immunol* **17**, 618-625, doi:10.1128/CVI.00368-09 (2010).

316 Bao, S., Beagley, K. W., France, M. P., Shen, J. & Husband, A. J. Interferon-gamma plays a critical role in intestinal immunity against Salmonella typhimurium infection. *Immunology* **99**, 464-472 (2000).

317 Kupz, A. *et al.* Contribution of Thy1+ NK cells to protective IFN-gamma production during Salmonella typhimurium infections. *Proc Natl Acad Sci U S A* **110**, 2252-2257, doi:10.1073/pnas.1222047110 (2013).

318 Coon, C., Beagley, K. W. & Bao, S. The role of granulocyte macrophage-colony stimulating factor in gastrointestinal immunity to salmonellosis. *Scand J Immunol* **70**, 106-115, doi:10.1111/j.1365-3083.2009.02279.x (2009).

319 Muotiala, A. & Makela, P. H. The role of IFN-gamma in murine Salmonella typhimurium infection. *Microb Pathog* **8**, 135-141 (1990).

320 Croxford, A. L. *et al.* The Cytokine GM-CSF Drives the Inflammatory Signature of CCR2+ Monocytes and Licenses Autoimmunity. *Immunity* **43**, 502-514, doi:10.1016/j.immuni.2015.08.010 (2015).

10 Acknowledgement

I would like to thank Nina for your great supervision over the last 4 years. You always encouraged me with your passion about translational research to combine clinical questions with scientific research approaches.

Thanks to my PhD committee members Dirk Bumann, Urs Jenal and Petr Broz for your huge contribution in all these research projects. Your scientific input was of major importance for me and gave me a lot to reflect about my ongoing projects. Dirk, I loved your enthusiasm, your creativity, your social personality and your sharp intellect. Sometimes I had the impression that when I am on the way there, you are already on the way back. Urs, I enjoyed your structured thinking and the fast decision making. Petr, your pedestrian way of thinking combined with your profound immunological background challenged me to revise and adapt research constructs in my head.

Thanks to the current and previous members of the Khanna lab, Egli lab and the Bumann lab. You were always very friendly and helped me to feel comfortable in performing the lab experiments. Thanks to David and Nicolas for your experimental help in the lab, thanks to Matthias for your animal work, thanks to Anne for your lab organization and thanks to Yaseen for being a good person sharing the PhD student life with all the ups and downs.

Special thanks go to Nura Schürmann. It was a great pleasure to work with you on the MPO project. I appreciated your efficient way of working and the discussions over lunch. Thanks to Mauricio Rosas Ballina for your smooth collaboration on the sepsis project, but also your scientific exchange and wise input. Thanks to Claudia Stühler for your overall contributions on my projects. You always gave me a broader perspective, new ideas and you often set the ground for milestone experiments. Thanks to Shephard Mpofu for mentoring me outside academia and giving me invaluable insights into clinical development in the pharmaceutical industry.

Last but not least, thanks to all collaborators on the MPO project (Olivier Casse, Jiagui Li, Boas Felmy, Anne-Valerie Burgener, Nikolaus Ehrenfeuchter, Wolf-Dietrich Hardt, Mike Recher, Christoph Hess, Astrid Tschan-Plessl) and the APC-like neutrophil project (Julien Roux, Jiagui Li, Christoph Schmutz, Fabian Franzeck, Matthias Gunzer and Daniela Finke). It would have been impossible to the reach the same research quality without you.

Many thanks to the Proteomics Core Facility at the Biozentrum (Alex, Emmanuelle, Thomas) and the Flowcytometry Core Facility at DBM (Emmanuel, Dany). You introduced me a lot into the particular methodology and helped me with the experimental design.

Most importantly, I would like to thank my beautiful wife Madeleine, my family and my friends who always supported me during the PhD and gave me the indispensable work-life balance.